# Development of a multi-electrode impedimetric biosensor: detection of pathogenic bacteria and mycotoxins

Marília Barreiros dos Santos

Universitat de Barcelona

**Tesis doctoral**

# Development of a multi-electrode impedimetric biosensor: detection of pathogenic bacteria and mycotoxins


Memoria presentada por

**Marília Barreiros dos Santos**

para optar al grado de **doctor en Nanociencias**

**Departament d'Electrònica**
Universitat de Barcelona

**Programa de doctorado de Nanociencias**
2009-2014

Tesis doctoral dirigida por: **Prof. Josep Samitier Martí**
**Prof. Vasco Teixeira**


Barcelona, 2014

*Dedicado a Vítor Ribeiro*

# Acknowledgements

Me gustaría expresar mi más profundo y sincero agradecimiento a todas las personas que, directamente o indirectamente, han colaborado para la realización de este trabajo y lo siento si me olvidé de agradecer a alguien.

Me gustaría empezar por agradecer a mis directores de tesis. Al Prof. Josep Samitier, muchas gracias por la disponibilidad, por el apoyo, incentivo y seguimiento de esta tesis. Por toda la confianza depositada en mí, por la oportunidad de trabajar en su grupo y por darme todas las condiciones necesarias para la realización de esta tesis. ¡Muchas gracias! Al Prof. Vasco Teixeira, co-director de esta investigación, muchas gracias por la oportunidad de trabajar con usted, por todo el apoyo e interés demostrado.

Me gustaría también agradecer al Christian Sporer, por toda la ayuda, dedicación, apoyo y conocimiento científico, y por estar siempre disponible cuando surgía alguna duda en el día a día. Muchísimas gracias por toda la paciencia que ha tenido conmigo y por los ánimos que me ha dado; sin duda siempre ha visto el lado positivo de las cosas. A Beatriz Prieto, mi enorme gratitud por toda la ayuda, consejos, apoyo y conocimiento científico que me has dado durante esta tesis, siempre disponible a enseñar y ayudar aunque tuvieras mucho trabajo. Profesionalmente y personalmente, fue realmente muy gratificante trabajar con una persona como tú. A Elena, muchas gracias por toda la ayuda, tanto con la tesis como con temas burocráticos, y por el buen humor en el día a día. A Anna Lagunas muchas gracias por los consejos y por hacer que las pausas para el café fueran mucho más divertidas. A Patrizia Iavicoli, gracias por el apoyo y consejos en el trabajo, así como tu compañerismo en el laboratorio. A Mateu quiero agradecerle por toda la

ayuda y consejos en mi último año y también por haberme hecho participe del *Journal Club* que tanto me ha aportado científicamente. A Juanjo, muchas gracias por organizar los múltiples eventos, por los ánimos, la compañía y las conversaciones (o ataques de locura) de tantas noches pasadas en el laboratorio. Muchas gracias también a los otros seniors y post-docs del grupo por la ayuda y el apoyo recibido a lo largo de estos años: Mónica Mir, Errachid, Nadia, Xavi Fernández, Toni Homs, Maria Bulman, Tommy y Margarita.

Como no podría dejar de ser, quiero agradecer a todos los estudiantes y técnicos del laboratorio, con quienes he pasado muy buenos momentos. Quiero agradecer a todos ellos por las conversaciones, risas y eventos sociales varios. Quiero agradecer sobre todo a todos aquellos que en los días más "grises" siempre tuvieran una sonrisa o unas palabras para decirme, ni que fuera, "*hoy estás fea!*". Sin duda una parte muy gratificante de esta tesis fue conocer personas como vosotros. A David Izquierdo, le agradezco por animarme y trabajar conmigo, y por toda la ayuda, dedicación y paciencia proporcionada en fabricar nuestros "niños". Sin mi técnico preferido, solo podría contar la mitad de esta historia, muchísimas gracias! A Miriam, muchas gracias por estar siempre disponible a ayudar, por tu simpatía y ánimos transmitidos. Fue muy bueno compartir estos años contigo. A las técnicas de electroquímica, Eva y Reyes, muchas gracias por la ayuda y por dar vidilla dentro y fuera del laboratorio de una manera tan especial. A la Coco, con quien empecé esta aventura de la tesis, mi enorme gratitud por todo, especialmente por el apoyo y ánimos en el trabajo y por hacerme sentir en casa mismo estando tan lejos. A Sabine, muchas gracias por los buenos momentos pasados; sabes que eres mi alemana preferida. A Elio, que en los pocos meses que pasó en el laboratorio, ha compartido parte del trabajo y actividades extra, muchas gracias por la ayuda y por hacer que esos meses

fueran *tan padre*! ¡¡¡Juan Pablo!!! Porque tantas veces te he llamado, muchas gracias por la infinita ayuda y paciencia. Ha sido muy divertido y gratificante pasar estos años contigo con tantas historias para contar. A Jordi, muchas gracias por la ayuda y por los consejos, para mi eres el mejor "master del universo". Muchas gracias a Marta por todo el apoyo y ayuda, pero sobretodo, gracias por tu forma de ser que hacía que el día a día fuera más divertido y agradable. Muchas gracias Maruxa por las conversaciones y las risas que siempre alegraban los días; sin duda eres única! A la otra gallega, Lorena, quiero darle las gracias por su compañerismo y buena disposición, y por toda la ayuda especialmente con el OWLS. A Sergio, compañero de potenciostato y luchas diarias, muchas gracias por toda la ayuda en el trabajo o fuera de él ayudándome a olvidar las frustraciones que se podrían tener. Muchas gracias también a Óscar por la ayuda que me ha dado especialmente con los "quesitos", y por animar el día con esa risa contagiosa que tiene. A José Luis, que tantas veces me facilitaba bacteria, muchas gracias por todo! Gracias también a los nuevos *elenos*, Vero, María y Albert, por los ánimos y por transmitir tan buen rollo. Muchas gracias también a los demás compañeros del laboratorio, Rosella, Wilmer, Boach, Sam, Javi, Juanma, Ivón, Patricia, Eli, Ernest, Luis y Gizem.

Muchas gracias a los miembros de la Plataforma de Nanotecnología, Raúl, Marina, Judith e Isa, por su profesionalidad y ayuda cuando fue necesaria. Gracias también al personal de administración del IBEC, INL y de la secretaria de física, por su ayuda, atención y disponibilidad siempre que los necesité. Me gustaría también agradecer al INL por la beca de doctorado y por la oportunidad de poder desarrollar este trabajo.

Quiero también dar las gracias a las personas involucradas en los proyectos MICROPLEX Y NANOMEDIAG, con quien he colaborado en esta investigación. Ha sido un placer trabajar con vosotros y quiero agradecerles

sus consejos y por la gran aportación científica que me han dado. Un especial agradecimiento a la Prof. Pilar Marco, Dr. Núria Pascual y Dr. Núria Sanvincens del IQAC/CSIC, por recibirme en su laboratorio, por toda la ayuda y las discusiones científicas. A Prof. António Juarez y Dr. Eduard Torrents del IBEC, muchas gracias por la disponibilidad, ayuda, discusión científica y por facilitarme las muestras de bacterias. Muchas gracias también a Maria Carmen Jaramillo por su atención, disponibilidad y ayuda en el cultivo de las bacterias. Al Prof. Fernando Albericio y Dr. Hortensia Rodríguez del IRB, muchas gracias por su colaboración en el tema de los péptidos antimicrobianos, por su disponibilidad y por facilitarme las muestras. Al Prof. José António Plaza del CNM muchas gracias por su colaboración y ayuda en la pasivación de los multi-electrodos. Quiero también agradecer a Sofia de la Universidade do Minho, por toda su ayuda y dedicación en la fabricación de los substratos de ITO. Muchas gracias por tu compañerismo y amistad.

I would like to express my gratitude to Prof. Jean Louis Marty from the IMAGES laboratory, for giving me the opportunity to work in his highly prestigious research group and for his scientific advices. My enormous gratitude to Dr. Cheng Yang for the knowledge exchange, the hours that we spent working and the ways to overcome difficulties which appeared. I also want to acknowledge my desk partners in Perpignan and to Cheng, Amina and Diana for the funny moments and companionship.

Un agradecimiento muy especial merece la comprensión, paciencia y el ánimo recibido de mi familia y amigos porque ellos son el pilar de mi vida. Muchas gracias a mi padre que siempre me ha ayudado a seguir mis sueños y ha contribuido para poder llegar donde llegué. Y a la pregunta que me hace en los últimos años de cuando dejo de estudiar, diría que es ahora. A mis hermanas, Eugénia y Edite, que siempre han estado a mi lado y me apoyaron, muchísimas gracias. Muchas gracias también al resto de mi familia que

siempre se preocuparon y me desearon lo mejor. Espero que todos estéis muy orgullosos de mí.

Como no podría dejar de ser, tengo que agradecer a los *Power Rangers*, Nelson, Diogo, Marina y Tiago, amigos desde hace mucho tiempo, que siempre me recibieran de brazos abiertos cuando volvía a Portugal. Muchas gracias por las cenas, conversaciones y risas que tanta energía me han aportado para volver a Barcelona. Muchas gracias también a Aida, por todo su apoyo y animo en esta fase.

También querría agradecer a Marisa y Claudia, por todos los cafés que tomamos que hacían que me sintiera como en Portugal mismo estando en Barcelona. Marisa, contigo he empezado esta aventura, muchas gracias por las conversaciones, por cuidar de mí y por los ánimos dados especialmente en esos días que todo parecía ir mal. Claudia, muchas gracias por los buenos momentos vividos y por hacerme ver Barcelona con otros ojos.

Me gustaría de expresar mi más profundo agradecimiento a David por toda su ayuda y ánimos; esta tesis y mi vida no sería lo mismo sin ti. Porque contigo las impedancias eran mucho más divertidas, porque has tenido una paciencia infinita, porque me has dado fuerza para acabar esta tesis, porque siempre has estado a mi lado de una manera u otra. Por todo esto y mucho más, muchísimas gracias!

# General index

# Figure and table index

# Tables

# Abbreviations

| | |
|---|---|
| **A** | Adenine |
| **Ab** | Antibody |
| **AEE** | 2-(2-aminoethoxy)ethanol |
| **AFM** | Atomic Force Microscopy |
| **ALP** | Alkaline phosphatase |
| **AMP** | Antimicrobial peptide |
| **BAT** | Biotinylated alkanethiol |
| **BSA** | Bovine serum albumin |
| **BW** | Bulk wave |
| **C** | Cytosine |
| **CCD** | Charge-coupled-device |
| **CFU** | Colony Forming Unit |
| **CPE** | Constant phase element |
| **CV** | Cyclic voltammetry |
| **DIEA** | N,N-diisopropylethylamine |
| **DNA** | Deoxyribonucleic acid |
| **DTSSP** | 3,3'-dithiobis[sulfosuccinimidylpropionate] |
| **E** | Potential |
| ***E. coli*** | *Escherichia coli* |
| **EDC** | 1-ethyl-3-(3-dimethylaminopropyl) carbodiimide |
| **EHEC** | Enterohemorrhagic *Escherichia coli* bacteria |
| **EIS** | Electrochemical Impedance Spectroscopy |
| **El** | Electrode |
| **ELISA** | Enzyme linked immune sorbent assays |
| **FITC** | Fluorescein isothiocyanate |
| **FLD** | Fluorescence detectors |
| **G** | Guanine |

| | |
|---|---|
| **HA** | Hyaluronic acid |
| **HPLC** | High-performance liquid chromatography |
| **HPLC-FD** | High performance liquid chromatography coupled with fluorescence detection |
| **HPR** | Horseradish peroxidise |
| **HUS** | Haemolytic uraemic syndrome |
| **Ig** | Immunoglobulin |
| **I** | Current |
| **ITO** | Indium tin oxide |
| **IUPAC** | International Union of Pure and Applied Chemistry |
| **LB** | Luria–Bertani |
| **LOD** | Limit of detection |
| **MAb** | Monoclonal antibody |
| **MCH** | 6-mercapto-1-hexanol |
| **MB** | Methylene blue |
| **ME** | Multi-electrode |
| **MHA** | 6-mercaptohexanoic acid |
| **MHDA** | 16-mercaptohexadecanoic acid |
| **MRSA** | Metaciclin-Resistant Staphylococcus aureus; |
| **MS** | Mass spectrometry |
| **MSSA** | Metaciclin-Sensitive Staphylococcus aureus |
| **MUA** | 11-mercaptoundecanoic acid |
| **NHS** | N-hydroxysuccinimide |
| **$NR_{ct}$** | Normalized charge transfer resistance |
| **OA** | OTA aptamer |
| **OTA** | Ochratoxin A |
| **OWLS** | Optical Waveguide Lightmode Spectroscopy |

| | |
|---|---|
| **PAb** | Polyclonal antibody |
| **PALM** | Photo-activated localization microscopy |
| **PANi** | Polyaniline |
| **PBS** | Phosphate buffered saline |
| **PCR** | Polymerase chain reaction |
| **PDMS** | Polydimethylsiloxane |
| **PEG** | Poly(ethylene glycol) |
| **PEG3-thiol** | Triethylene glycol mono-11-mercaptoundecyl ether |
| **PFP** | 2,3,4,5,6-pentafluorophenol |
| **PLL** | Poly(L-lysine) |
| **QCM** | Quartz crystal microbalance |
| **RIE** | Reactive ion etching |
| **RNA** | Ribonucleic acid |
| **RPM** | Revolutions per minute |
| **RSD** | Relative standard deviation |
| **RT** | Room temperature |
| **SA** | Stearic acid |
| **SAM** | Self-assembled monolayer |
| **SATA** | N-Succinimidyl S-acetylthioacetate |
| **SAW** | Surface acoustic wave |
| **S.D.** | standard deviation |
| **SELEX** | Systematic evolution of ligands by an exponential enrichment |
| **SEM** | Scanning electron microscope |
| **SMCC** | Succinimidyl 4-(N-maleimidomethyl)-cyclohexane-1-carboxylate |
| **SPR** | Surface Plasmon Resonance |

| | |
|---|---|
| ***S. typhimurium*** | *Salmonella typhimurium* |
| **STORM** | Stochastic optical reconstruction microscopy |
| **T** | Thymine |
| **TCEP** | Tris(2-carboxyethyl)phosphine hydrochloride |
| **TE** | Transverse electric |
| **TIRF** | Internal reflection fluorescence microscope |
| **TLC** | Thin-layer chromatography |
| **TLC-FD** | Thin-layer chromatography fluorescence detection |
| **TM** | Transverse magnetic |
| **TMB** | 3,3',5,5'-tetramethylbenzidine |
| **Tris** | Tris(hydroxymethyl)aminomethane |
| **Tween 20** | Polyoxyethylenesorbitan monolaurate |
| **USDA-FSIS** | United States Department of Agriculture-Food Safety and Inspection Service |
| **UV** | Ultraviolet |
| **WE** | Working electrode |
| **Z** | Impedance |

# **Chapter 1.** General introduction

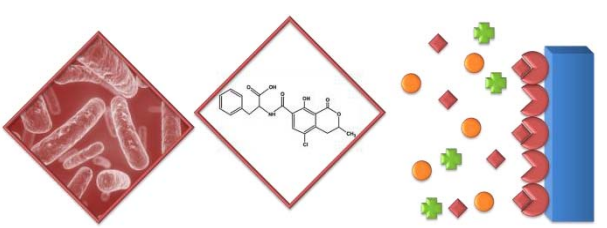

This chapter shows the general introduction and the main objectives of this thesis. We give an overview of biosensors, especially applied for pathogenic bacteria and mycotoxin detection, an important and challenging field of research. A general definition, classification and main applications of biosensors are first presented. Then, we describe the main bioreceptors and analytical methods used in this work and their application for specific pathogenic bacteria and mycotoxins detection. Finally, the motivation of the presented work and the need of developing novel approaches for pathogenic bacteria and mycotoxins detection is highlighted, and in particular, the importance of using multi-electrode platforms.

## Chapter index

## 1.1 Biosensors

Biosensors are versatile analytical tools of great importance because of their capability to resolve a potential large number of problems and challenges in diverse areas such as defence, homeland security, agricultures and food safety, environmental monitoring, medicine and pharmacology, among others [1]. They are expected to play an increasingly important role in the improvement of life quality that can be related with the control of diseases, food quality and safety, and quality of our environment [2]. For example, biosensor-based diagnostics might facilitate disease screening and improve the rates of earlier detection and attendant improved prognosis. Such technology may be extremely useful for enhancing health care delivery in the community setting and to underserved populations [3].

A biosensor is defined by the International Union of Pure and Applied Chemistry (IUPAC) as "*a device that uses specific biochemical reactions mediated by isolated enzymes, immunosystems, tissues, organelles, or whole cells to detect chemical compounds usually by electrical, thermal, or optical signals*" [4,5]. A schematic diagram of the parts comprising a typical biosensor is shown in Figure 1.

A biosensor consists of two main components: a bioreceptor or biorecognition element (Figure 1 (a)) and a transducer (Figure 1 (b)). The bioreceptor is generally an immobilized biological system or component that is able to specifically recognize the target analyte among many others (impurities). The transducer converts the corresponding biological responses into a measurable electrical signal. The amplifier in the biosensor (Figure 1 (c)) responds to the small input signal from the transducer and delivers a large output signal that contains the essential waveform features of the input

signal. The amplified signal is then processed by the signal processor (Figure 1 (d)) where it can later be stored, displayed and analysed (Figure 1 (e)). Biosensors can be applied to a large variety of samples including body fluids, food samples, cell cultures and environmental samples [6–8].

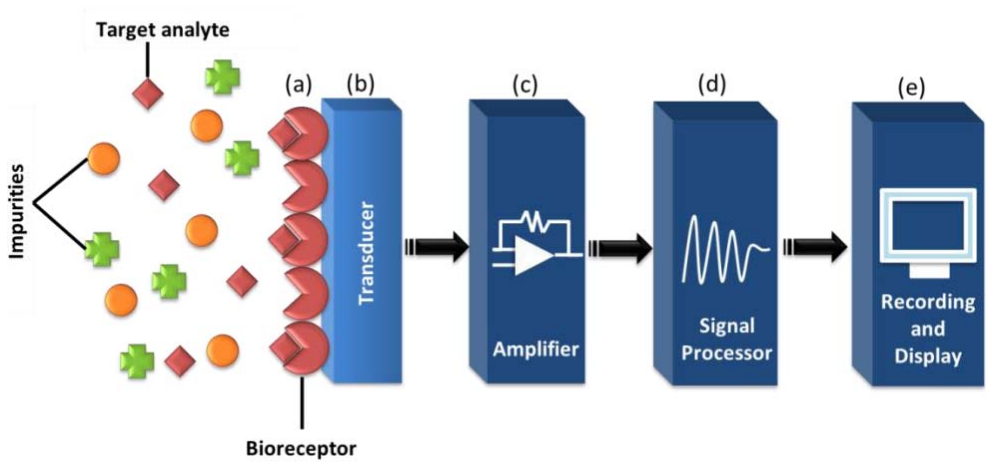


Figure 1. Schematic diagram of a biosensor, showing the different building blocks: (a) bioreceptor, (b) transducer, (c) amplifier, (d) signal processing and (e) recording and display.

In a successful biosensor, the biorecognition layer must be highly specific to the analyte and the reaction should be independent of physical parameters such as stirring, pH and temperature. The biosensor should be manageable and the response accurate, precise, reproducible and linear over the useful analytical range, without dilution or concentration. Additionally, it should be also free from electrical noise. The complete biosensor should be cheap, small, portable and capable of being used by unskilled operators. Finally, the biosensor selected to be used in clinical situations should be tiny, biocompatible and a non-invasive monitoring must be used [8,9].

The main components involved in biosensors (see Figure 1) are described in the following sections. Figure 2 shows some examples of these components and their relative sizes, ranging from the nanometric size of thiol molecules and DNA (deoxyribonucleic acid) probes up to the micrometric size of pathogens and transducers. The most common biorecognition elements and the principal transduction methods used are next described. One key step in the development of biosensors is the immobilization of the biological component at the transducer surface. Therefore, some surface modifications methodologies are also discussed. Finally, the principal applications of biosensors in the real word are presented.

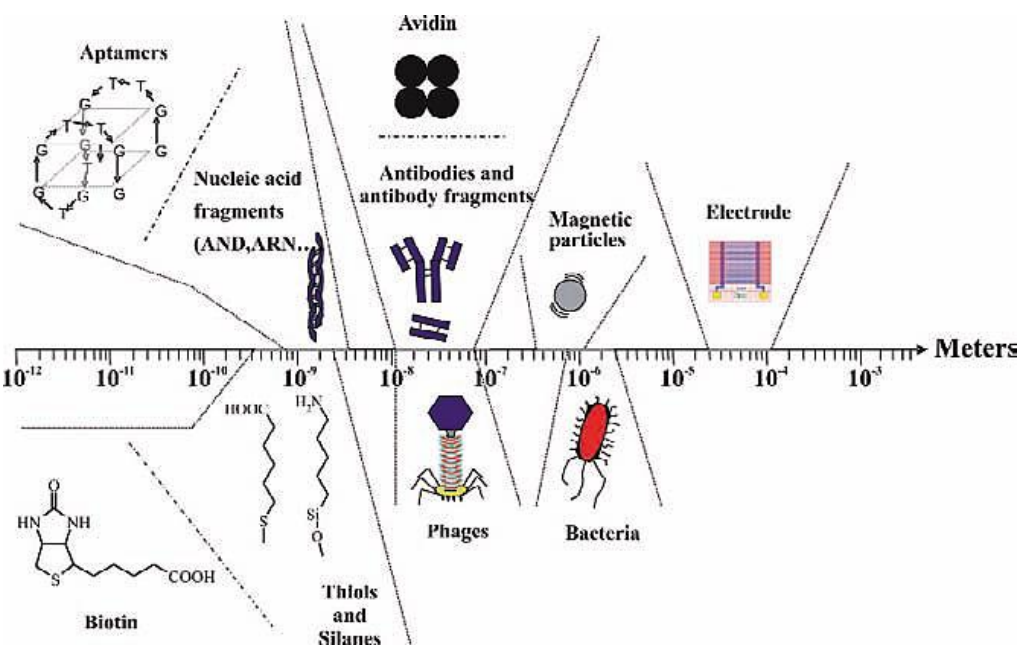


Figure 2. Relative sizes of various components typically used in biosensors [10].

### 1.1.1 Bioreceptors

A bioreceptor is a biological molecular specie or living biological system that utilizes a biochemical mechanism for recognition [11] (see Figure 1). Bioreceptors are the key to specificity for biosensor technologies and can generally be classified into five major categories as represented in Figure 3. The categories typically used in biosensors include antibody/antigen, enzymes, nucleic acids/DNA, and cellular structures/cells. However, other bioreceptors, such as biomimetic receptors, aptamers, peptides and bacteriophage, have been widely used in the last years [7,12,13].

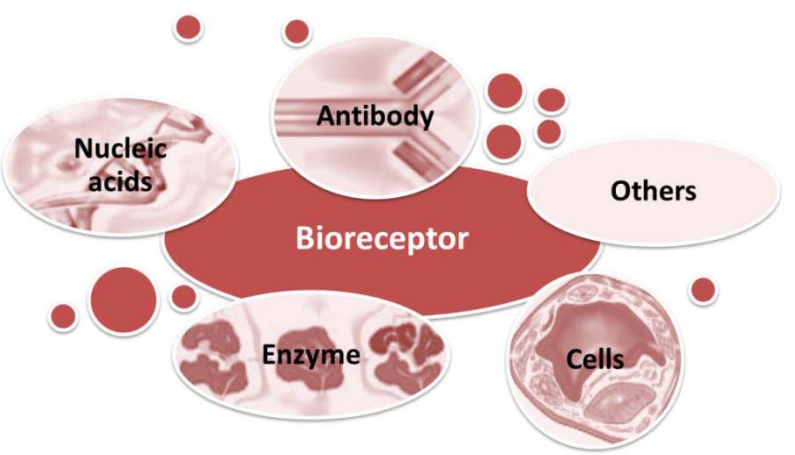


Figure 3: Major bioreceptors categories typically used in biosensors.

Next, an overview of the major bioreceptors used in this work is shown, including antibodies, enzymes, nucleic acids, aptamers and antimicrobial peptides (AMPs). This overview aims to give a broad picture of the different bioreceptors, their main advantages and disadvantages, and some applications.

#### *1.1.1.1 Antibody*

An antibody is a complex biomolecule, made up of hundreds of individual amino acids arranged in a highly ordered sequence [11]. Antibodies are a family of glycoproteins known as immunoglobulins (Ig). The basic functional unit of each antibody is an Ig monomer and the basic antibody structure is represented in Figure 4 (a) [10]. The Ig monomer is a "Y"-shaped molecule (~150 KDa) that consists of four polypeptide chains; two identical heavy chains and two identical light chains connected by disulphide bonds [14]. Each chain has a constant and variable part. The variable part is specific to the antigen that is bound with a corresponding antigen which is highly specific and selective [15].

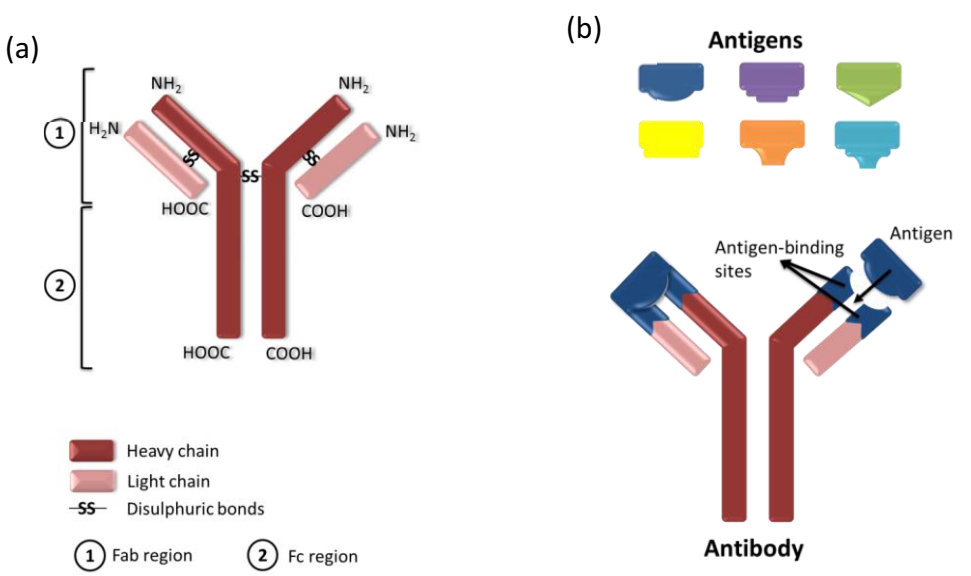


Figure 4. (a) The basic structure of an antibody. (b) Antigen–antibody *lock and key* fit (adapted from [7,13–15]).

Antibodies are the most widely used biorecognition elements because of the high specificity of the antibody-antigen binding. The way in which an

antigen and an antigen-specific antibody interact is similar to a *lock and key* fit (Figure 4 (b)). An antigen-specific antibody fits its unique antigen in a highly specific manner, so that the three-dimensional structures of antigen and antibody molecules are matching. Due to this three-dimensional shape fitting, and the diversity inherent in individual antibody make-up, it is possible to find an antibody that can recognize and bind to any one of a large variety of molecular shapes [7,13].

Antibodies may be polyclonal (PAb), monoclonal (MAb) or recombinant, depending on their selective properties and the way they are synthesized [16,17]. MAb provide the highest specificity, are homogeneous and available in a limitless supply, despite being time consuming and expensive to generate. PAbs are relatively easy to produce in a timely and cost-efficient way, and they are commonly used in approaches not demanding “excessively high” specificity [10,18].

Biosensors that use antibodies as recognition elements are termed *immunosensors*. They are usually used because antibodies are highly specific, versatile, and bind strongly and stably to the antigen. The main advantage of using antibodies as bio-recognition elements is their high sensitivity and selectivity, while some limitations are long-term stability and manufacturing costs (especially for multi-target biosensor applications where many ligands are needed) [3].

Antibodies recognize and bind to an analyte of interest, even in extremely small amounts, within a large number of other chemical substances. The antibodies can be immobilized onto a surface to specifically capture the antigens of interest. Antibody-antigen reactions are highly compatible with well-understood conjugation chemistries [19]. These properties of antibodies make the immunosensors a powerful analytical tool

to detect chemicals [20], biomolecules [21] and microorganisms [22,23], among others [14,24].

#### *1.1.1.2 Enzymes*

Enzymes are often chosen as bioreceptors based on their specific binding capabilities as well as their catalytic activity [11]. Analyte recognition is enabled through several possible mechanisms: (i) the enzyme converting the analyte into a product that is sensor-detectable, (ii) detecting enzyme inhibition or activation by the analyte, or (iii) monitoring modification of enzyme properties resulting from interaction with the analyte [25]. Though enzymes are one category of the biorecognition elements, they are mostly used to function as labels than the actual bioreceptor.

Enzymes offer the advantages of high sensitivity, possibility of direct visualization and long stability. But there are some disadvantages found when using enzymes as labels, which include multiple assay steps and the possibility of interference from endogenous enzymes. Many enzyme detection methods are visual, eliminating the need for expensive and complicated equipment [7].

The use of enzymes as labels has gained more popularity in immunoassay detection such as ELISA (Enzyme-Linked ImmunoSorbent Assay). There are three enzymes generally used in ELISA, the earliest was alkaline phosphatase, the most commonly used now is horseradish peroxidase (HRP) and the third is beta-galactosidase [26]. Since the development of the first biosensor (amperometric enzyme electrode for a glucose sensor [27]), enzyme-based biosensors have faced a massive growth in usage for various applications up to the present [28]. Enzyme-based

biosensors can be used to detect cholesterol [29], food safety and environmental monitoring [30], heavy metals [31] and also pesticides [32].

#### *1.1.1.3 Nucleic acids*

In nucleic acid bioreceptors the identification of a target analyte's nucleic acid is achieved by matching the complementary base pairs of adjacent strands (adenine to thymine *A*-*T* and cytosine to guanine *C*-*G*), forming a double helix of DNA though stable hydrogen bonds [25].

Biosensors based on nucleic acid as biorecognition element are simple, rapid, and inexpensive. Additionally, they are highly stable and easily reusable by thermal melting of the DNA duplex. Hundreds of compounds bind and interact with DNA. In addition, this biosensor possesses a remarkable specificity to provide analytical tools that can measure the presence of a single molecule species in a complex mixture. In contrast to enzyme or antibodies bioreceptors, nucleic acid recognition layers can be readily synthesized and regenerated.

DNA damage is one of the most important factors to be considered when nucleic acid bioreceptor are used. Detection of chemicals may cause irreversible damage to DNA by changing the structure of DNA and the base sequence, which in turn disturbs the DNA replication [7,15].

Applications of nucleic acids as recognition elements are numerous. The DNA based biosensors has potential applications in clinical diagnostics for virus and disease detection [33,34]. Additionally, DNA microarrays have been used for the profiling of gene expression, detection and characterization of pathogens and genotyping, among others [35,36].

#### *1.1.1.4 Aptamers*

Aptamers are single-stranded oligonucleotides of DNA or RNA (ribonucleic acid) sequences, usually 25–80 bases long [37]. They are produced by an *in vitro* selection process called *systematic evolution of ligands by an exponential enrichment* (SELEX), that identifies a monomer sequence that tightly binds the target from a large library of random sequences (Figure 5) [38,39].

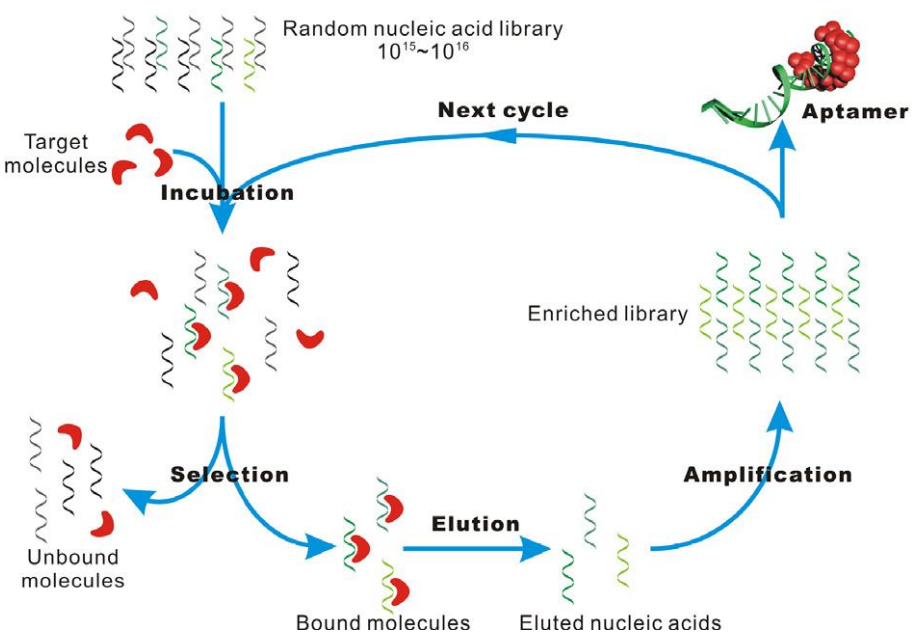


Figure 5. Scheme of the SELEX enrichment process. A random nucleic acid library is incubated with a target molecule, and unbound molecules are separated from bound molecules. Bound nucleic acids are eluted, amplified by polymerase chain reaction and serve as an enriched library for the next cycle [40].

Aptamers are small in size, chemically stable, cost effective and once selected, they can be synthesized with high reproducibility and purity from

commercial sources. Additionally, aptamer offer remarkable flexibility and convenience in the design of their structures [40]. In contrast with antibodies, aptamers are more stable and the biosensors using aptamers (termed *aptasensors*) can also be regenerated [39]. A common challenge facing the aptasensors is that they have the properties of nucleic acids (structural pleomorphic and chemical simplicity) which reduce the assay efficiency and also increase its production cost [15]. And so far, there are no standardized protocols available concerning the selection process, which is applicable without specific modifications of different targets [39].

Aptamers also present high versatility to being chemically modified by biotin, thiol or amino groups, allowing them to be immobilized on various solid supports [10]. They possess high recognition ability towards specific molecular targets ranging from small molecules to proteins and even cells [41]. Aptasensors applications include detection of biomarkers like thrombin [42], clinical testing of cancer related markers [43,44], and also detection of microorganisms and viruses [45].

#### *1.1.1.5 Antimicrobial peptides*

Antimicrobial peptides are small proteins with antimicrobial activity against bacteria and viruses. They are found throughout all kingdoms of life, serving as the first line of defense for the organism against microbial invasion. The peptides are mostly unstructured, and typically consist of 10−40 residues with a varied quantity of cationic residues distributed throughout [46]. Highly stable to adverse conditions, AMPs bind semi-selectively to microbial cell surfaces and exert their antimicrobial activity through membrane disruption [47].

The ease of synthesis and intrinsic stability of AMPs render them particularly interesting candidates for use as molecular recognition elements in biosensing platforms. AMPs are much more stable than typical globular proteins—explaining how they can be continually exposed to the natural environment—and are exceptionally efficient at fending off bacterial infection. The replacement of current antibody-based affinity probes with more stable and durable AMPs in biological sensors may thus help to increase the shelf life of current diagnostic platforms [48].

AMPs were successful used for whole bacterial cell detection [45–49]. Others authors have reported the use of immobilized peptide arrays for sensing and lipopolysaccharide molecules [46] and toxins [52].

### 1.1.2 Transducers

The transducer plays an important role in the detection process of a biosensor. Biosensors can also be classified based upon the transduction methods they employ, although there are new types of transducers constantly being developed for use in biosensors. Optical, electrochemical and mass-based transducers are given importance here since these are the most popular and common methods used (Figure 6) [7,53].

The three main classes contain many different subclasses and they can be categorized into two groups: *(i)* direct recognition and *(ii)* indirect detection biosensors. Direct detection biosensors utilize direct measurements of the phenomenon occurring during the biochemical reactions on a transducer surface and they do not require labelling for detection (i.e. label-free). Indirect detection sensors rely on secondary elements (labels) for

detection, such as enzymes and fluorescently tagged bioreceptors that enhance detection of a sandwich complex [3].

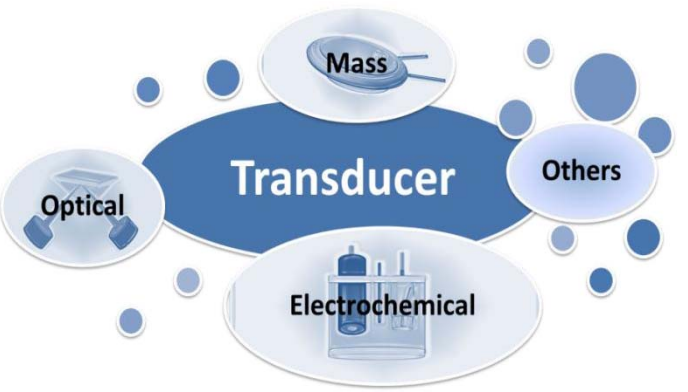


Figure 6. Major types of transducers used in biosensors.

Next, an overview of the major tranducers used in biosensor field is given. This overview aims to give a broad picture of the different transducers, applications, principal advantages and disadvantages. More details are given to the types of transducers used in this work.

#### *1.1.2.1 Optical-based biosensors*

Optical-based biosensors have been widely employed due to the many different types of existing spectroscopy measurements available (e.g. absorption, fluorescence, phosphorescence, Raman, refraction, dispersion spectrometry, etc.) with different spectrochemical properties recorded [11,13]. Optical biosensors are probably the most popular in bioanalysis, due to their selectivity and sensitivity. They have been developed for rapid detection of contaminants [54,55], toxins or drugs [56,57] and even for pathogenic bacteria [7,9,10,58]. Recently, fluorescence and surface plasmon

resonance-based methods have gained popularity because of their sensitivity [17]. Figure 7 shows some of the most common optical-based transducers used in the biosensors field and that will be used in this work.

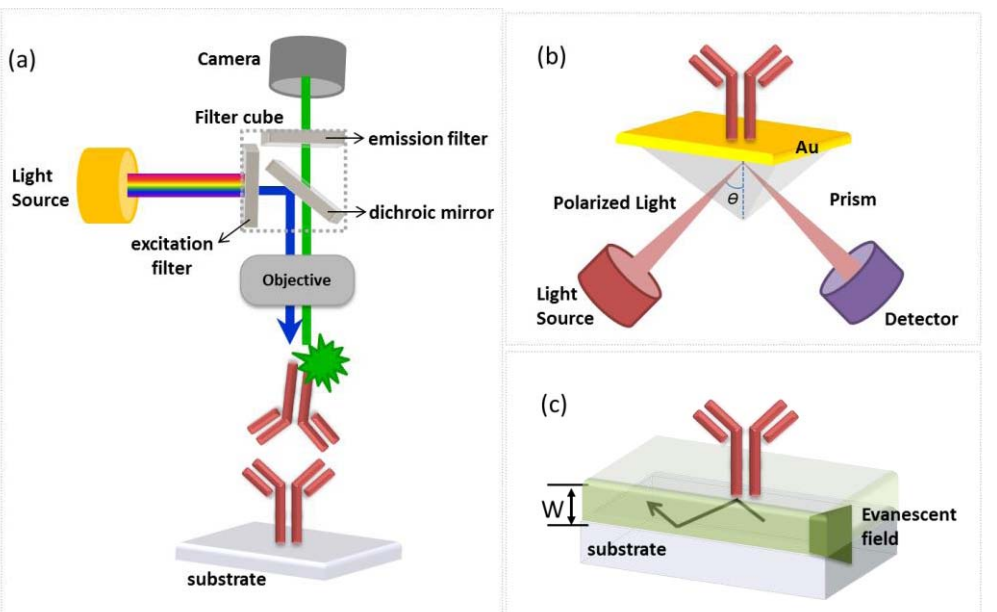


Figure 7. Major types of optical transducers used in biosensors. Schematic overview of surface-based optical detection platforms: (a) Fluorescence microscopy, (b) Surface Plasmon Resonance and (c) Optical Waveguide Lightmode Spectroscopy.

### Fluorescence microscopy

Fluorescence microscopy is a technique used to study specimens which can be made to fluoresce. The fluorescence microscope is based on the phenomenon that certain materials emit energy detectable as visible light when irradiated with light of a specific wavelength. The sample can either be fluorescing in its natural form like chlorophyll and some minerals, or the

specimen can be labeled specifically with a fluorescent molecule called *fluorophore* [59].

The typical components of a fluorescence microscope (Figure 7(a)) are the light source (xean arc or mercury-vapor lamp), the excitation filter, the dichroic mirror, and the emission filter. The objective is used both to illuminate and image the specimen. The light source sends full-spectrum light to the specimen via a fluorescence 'cube' that selectively illuminates the specimen with a wavelengths that excites a particular fluorophore. The cube has two filters, the dichroic mirror and the barrier filter, to prevent the exciting wavelengths from reaching the detector. The filters and the dichroic are chosen to match the spectral excitation and emission characteristics of the fluorophore used to label the specimen [60].

Fluorescence-based analysis remains one of the most popular detection methodologies, however issues such as the additional expense of labeling, dye photobleaching and instrumentation costs have driven the emergence of alternative label-free methods [53]. Most fluorescence microscopes in use are epifluorecence microscopes but more advanced microscopes and microscope techniques have been designed, such as the confocal microscope, the total internal reflection fluorescence microscope (TIRF) or a different set of super-resolution microscope techniques (stochastic optical reconstruction microscopy (STORM) or photo-activated localization microscopy (PALM)).

**Surface Plasmon Resonance (SPR)**

Surface Plasmon Resonance is a powerful technique to measure biomolecular interactions in real-time and label-free environment [54]. SPR-

based biosensors measure changes in the refractive index in the vicinity of the metal surface that will originate a change in the resonance angle [17,61].

A scheme showing the working principle of a SPR biosensor is presented in Figure 7(b). A sensor chip with a thin gold layer on the top is irradiated from the backside by *p*-polarized light (from a laser) via a hemispherical prism, and the light is reflected by the metal film acting as a mirror. The intensity of the reflected light can be monitored changing the angle of incidence, θ. The resulting plot is a curve showing that the intensity of the reflected light passes through a minimum. At this angle of incidence, the light will excite surface plasmons, inducing surface plasmon resonance and causing a dip in the intensity of the reflected light. The angle position of this minimum is determined by the properties of the gold-solution interface. Hence, adsorption phenomena and even reaction kinetics can be monitored using this sensitive technique [61].

In addition to the high sensitivity and temporal resolution offered by SPR, the main advantage of this technique is that labeling is not needed on target molecules. This has a direct impact on time and cost, as well as can avoid possible perturbations during the biorecognition studies due to this additional step. The main drawbacks of this technique lay in its complexity (specialized staff is required), high cost and large size of most currently available instruments [17,62].

**Optical Waveguide Lightmode Spectroscopy (OWLS)**

OWLS is a powerful method for monitoring the adsorption of macromolecules on a $Si_xTi_{(1-x)}O_2$ (where x=0,25±0,05) sensor surface known as *optical waveguide grating couple chip*. This grating serves to incouple light (He-Ne laser) into a planar optical waveguide in which the light is propagated,

generating an evanescent field (Figure 7(c)). This evanescent field is used to probe the optical properties of the solution in the vicinity of the surface. The changes in the refractive index allows the determination of layer thickness and coverage (or mass) of the adsorbed or bound material with ultra-high sensitivity [63,64].

OWLS technique measures the effective refractive index on the zero transverse electric (TE) and magnetic (TM) modes. Considering these values and assuming an optically uniform layer and a coefficient $d_n/d_c$ (defined below) of 0.182 g $cm^{-3}$, the mass of the adsorbed layer can be calculated using de Feijter's formula [65,66]:

$$M = d_A \frac{n_A - n_C}{d_n / d_c}$$

where $d_A$ is the thickness of the adsorbed layer, $n_a$ and $n_c$ the refractive index of the adsorbed molecules and the cover medium, respectively, and *dn/dc* is the refractive index increment of the media with the concentration of molecules [67].

The OWLS technique is highly sensitive (1 ng $cm^{-2}$) and allows the real time monitoring of macromolecular adsorption without the need for any labeling procedure [68]. Furthermore, OWLS could integrate an electrochemical flow cell (EC-OWLS) for electrochemical measurements. In this case, the sensor waveguide coated by typically a 10 nm of conductive indium tin oxide (ITO) layer is used as the working electrode [68,69]. A potential difference is applied between the ITO and Pt counter electrode, and the ITO potential is determined vs. an Ag/AgCl reference electrode.

### *1.1.2.2 Electrochemical based-biosensors*

Electrochemical-based sensors use an electrode as the transduction element and represent an important subclass of sensors [15]. Electrochemical biosensors can be classified into several categories such as amperometric, potentiometric and impedimetric based on the measured parameters such as current (*I*), potential (*E*) and impedance (*Z*), respectively (Figure 8) [17]. The electrochemical detection has several advantages such as low cost, ability to work with turbid samples and easy miniaturization. However, their sensitivity and selectivity can be slightly limited [7].

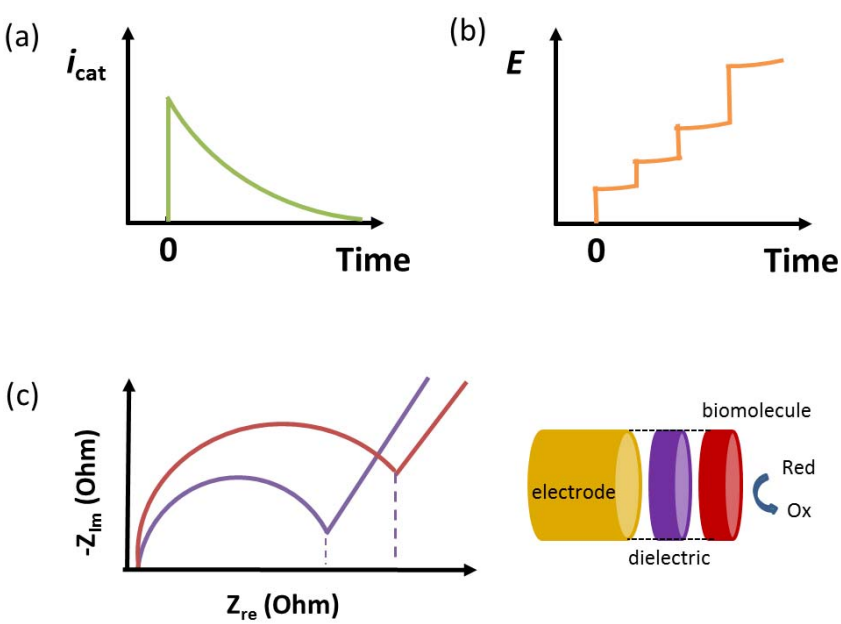


Figure 8. Schematic overview of electrochemical detection methods: (a) amperometry, (b) potentiometry and (e) electrochemical impedance spectroscopy, based on faradaic measurements (*right*).

Electrochemical sensing usually requires a reference electrode, a counter or auxiliary electrode and a working electrode, also known as the

sensing or redox electrode. The reference electrode, usually silver or silver chloride (Ag/AgCl), is kept at a fixed distance from the reaction site in order to maintain a known and stable potential. The working electrode, biofunctionalized with the bioreceptor, serves as the transduction element in the biochemical reaction. Finally, the counter or auxiliary electrode establishes a connection to the electrolytic solution so that a current can be applied to the working electrode. The working electrodes should be both conductive and chemically stable. Therefore, gold, platinum, carbon (e.g. graphite) and silicon compounds are commonly used, depending on the analyte [8,15,70].

We next describe in more detail the techniques described above, focusing on their working principle and their main advantages and drawbacks.

**Amperometric biosensors**

Amperometric sensors are based on the measurement of the current $i_{cat}$ as a function of time (Figure 8 (a)), resulting from the oxidation and reduction of an electroactive species in a biochemical reaction that mainly depends on the concentration of an analyte with a fixed potential [8,15]. The applied potential serves as the driving force for the electron transfer reaction, and the current produced is a direct measure of the rate of electron transfer [7]. In the case of biosensors, where direct electron exchange between the electrode and either the analyte or the biomolecule is not permitted, redox mediators are required. Redox mediators are small size compounds able to reversibly exchange electrons between both the sensor and the enzyme of choice (e.g., ferricyanide, osmium or ruthenium complexes, dyes, etc.)[17].

Despite the disadvantage of this often indirect sensing system, it is claimed that amperometric devices maintain sensitivity superior to potentiometric devices [8]. Amperometric biosensors have been widely used, but they show some drawbacks that limit their use. The presence of electroactive interference in the sample matrix can generate false current reading. There are various methods proposed to overcome this limitation such as sample dilution, coating the electrode with various polymers, changing the medium of analyte and/or adding a mediator [15].

**Potentiometric biosensors**

Potentiometry is the measurement of an electrical potential difference between two electrodes when the electrochemical cell current is zero. The two electrodes are known as the *indicator* and *reference* electrodes. The reference electrode is required to provide a constant half-cell potential. The indicator electrode develops a variable potential depending on the activity or concentration of a specific analyte in solution. The change in potential *E* is plotted as a function of time (Figure 8 (b)) and is related to analyte concentration in a logarithmic manner, allowing the detection of extremely small concentration changes [7,8].

Potentiometric biosensors rely on the use of an ion-selective electrode and ion-sensitive field effect transistor for obtaining the analytical information. The potentiometric transduction mechanism is very attractive for the operation of biosensors due to its selectivity, simplicity, rapidity, low cost and maintenance free measurement. However, the device is still less sensitive and often slower than amperometric biosensors [15].

**Electrochemical impedance spectroscopy biosensors**

Electrochemical impedance spectroscopy (EIS) is a well-suited technique for the detection of binding events on the transducer surface, as well as a valuable tool for characterizing surface modifications [71]. This versatile electrochemical tool, characterizes intrinsic electrical properties of any material or solution and its interface. The impedance *Z* of a system is generally determined by applying a voltage perturbation with small amplitude (10 mV amplitude or less) and detecting the current response. The impedance Z is the quotient of the voltage–time function V(t) and the resulting current–time function I(t):

$$\mathrm{Z} = \frac{\mathrm{V(t)}}{\mathrm{I(t)}} = \frac{\mathrm{V_0 sin(2\pi ft)}}{\mathrm{I_0 sin(2\pi ft + \phi)}} = \frac{1}{\mathrm{Y}} \quad (\omega = 2\pi f)$$

where $V_0$ and $I_0$ are the maximum voltage and current signals, respectively, $f$ is the frequency (angular frequency $\omega$), $t$ the time, ϕ the phase shift between the voltage–time and current–time functions, and $Y$ is the complex conductance or admittance.

The impedance is a complex value, since the current can differ not only in terms of the amplitude but it can also show a phase shift ϕ compared to the voltage–time function (Figure 9(a)). Thus, the value can be described either by the modulus $|Z|$ and the phase shift ϕ or alternatively, by the real part $Z_{Re}$ and the imaginary part $Z_{Im}$ of the impedance (Figure 9 (c)). Therefore the results of an impedance measurement can be illustrated in two different ways: using a *Bode plot* which plots $\log|Z|$ and ϕ as a function of log $\omega$ (or $f$) (Figure 9 (b)), or using a *Nyquist plot* which plots $Z_{Re}$ and $Z_{Im}$ ((Figure 8 (c) and Figure 9(c)) [70–72].

EIS approaches can be divided into those which are Faradaic and non-Faradaic, depending on whether there is a redox related charge transfer across the electrode interface during measurement. In faradaic EIS a redox species is alternately oxidized and reduced by the transfer of an electron to and from the metal electrode (Figure 8 (c), *right*). In non-Faradaic EIS, no such addition is made and there is no redox process. In the last case, the term *capacitive biosensor* is usually designated [38,70]. Faradaic EIS approaches are widely used in biosensors [73–75] and a typically redox probe is ferricyanide $[Fe(CN)_6]^{3-/4-}$ [38].

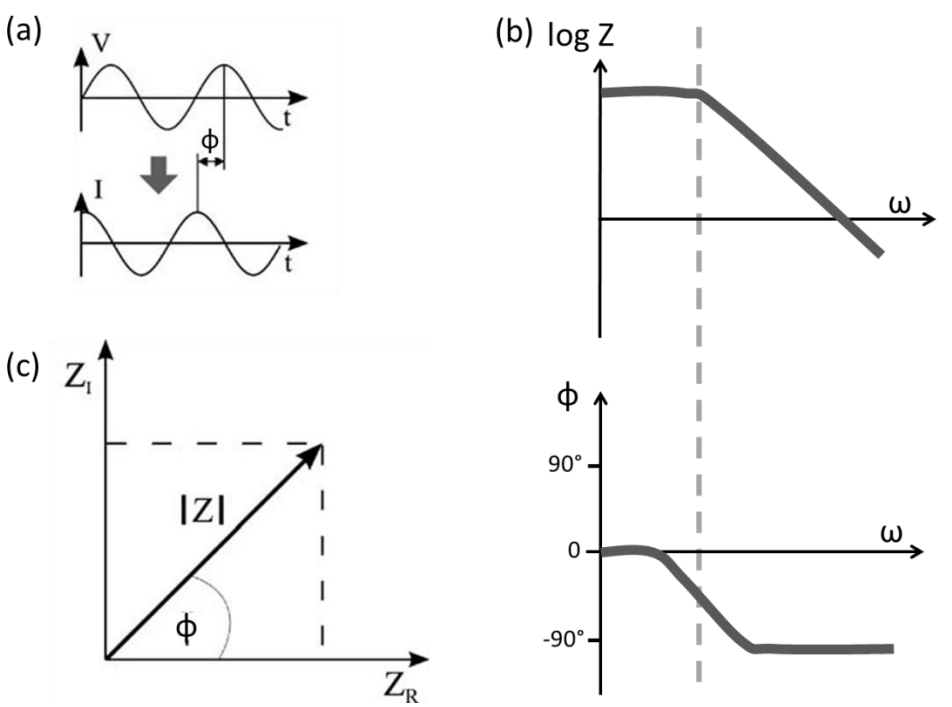


Figure 9. (a) Impedance is a complex value that is defined as the quotient of the voltage (time) and current(time) functions. It can be expressed as (b) the modulus |Z| and the phase angle ϕ (Bode plot) or it can be specified by (c) the real ($Z_R$) and the imaginary ($Z_I$) parts of the impedance (Nyquist plot) [70,71].

EIS data is commonly analyzed by fitting it to an *equivalent electrical circuit* model. This circuit represents the different physicochemical properties of the system, which commonly consists of resistances and capacitances. Equivalent circuits are used in order to approximate the experimental impedance data with these ideal or distributed impedance elements arranged in series and/or in parallel. The four elements usually used to describe the impedance behaviour are: ohmic resistance of the electrolyte, capacitance (double layer), constant phase element and Warburg impedance [10,38,70]. We next describe these four elements in more detail:

- **Electrolyte resistance.** The electrolyte resistance is often a significant factor in the impedance of an electrochemical cell that can be modelled as a simple impedance $Z=R_{sol}$ (see Figure 10(a)). The resistance of an ionic solution depends on the ionic concentration, type of ions, temperature and the geometry of the area in which current is carried.

- **Double layer capacitance.** An electrical double layer exists on the interface between an electrode and its surrounding electrolyte. This double layer is formed as ions from the solution "stick on" the electrode surface as a consequence of the polarization of the metal electrodes (see Figure 10(a)). The ions in the liquid media, having the opposite charge of that of the electrode, are attracted and surround the metal surface. These two charge distributions with opposite sign form the double layer that acts as a capacitor. The value of the double layer capacitance depends on many variables such as the electrode potential, temperature, ionic concentrations, types of ions, oxide layers, electrode roughness, impurity adsorption, etc.

- **Constant phase element**. Capacitors (*C*) in EIS experiments often do not behave ideally. Instead, they act like a constant phase element (*CPE*). The complex impedance of a *CPE* is given by $1/(j\omega A)^m$, where A is analogous to a capacitance, $\omega$ is the frequency expressed in rad/s, and $0.5<m<1$ ($m$=1 corresponds to a capacitor and $m$=0.5 corresponds to a Warburg element; $m$ for *C* modelling is typically between 0.85 and 0.98). This introduces a sub-90° phase shift, or equivalently a frequency-dependent resistor in addition to a pure capacitor.

- **Warburg impedance.** Diffusion can also create impedance called *Warburg* impedance, which depends on the frequency of the potential perturbation. At high frequencies (>Hz) the Warburg impedance is small since diffusing reactants do not have time to move very far. At low frequencies (<Hz), the reactants have time to diffuse farther, increasing the Warburg-impedance. On a Nyquist Plot the Warburg impedance appears as a diagonal line with a slope of 45° (see Figure 10). On a Bode Plot, the Warburg impedance exhibits a phase shift of 45°.

The most popular equivalent electrical circuit is the Randles circuit. It comprises the solution resistance $R_{sol}$, the charge transfer resistance $R_{ct}$, the double layer capacitance $C_{dl}$ and the Warburg impedance W. Figure 10 (a) shows the electrical double layer of a receptor modified electrode–electrolyte Interface associated with Randles equivalent circuit.

Nyquist plot shown in Figure 10 (b) commonly includes a semicircle region lying on the axis followed by a straight line. The semicircle portion (observed at higher frequencies) corresponds to the electron-transfer-limited process, while the straight line (characteristic of the low-frequency range) represents the diffusion-limited process. Such spectra can be used for extracting the electron transfer kinetics and diffusion characteristics. The

values for $R_{sol}$ and $R_{ct}$ can be easily determined. The diameter of the semicircle equals the electron transfer resistance. The intercepts of the semicircle with $Z_{re}$ axis correspond to those of $R_{sol}$. The double layer capacitance can be calculated from the frequency at the maximum of the semicircle ($\omega=2\pi f=1/R_{ct}C_{dl}$). Simply, $R_{sol}$ and $W$ represent the properties of the bulk solution and diffusion of the redox probe, neither being affected by target binding at the electrode surface. $R_{ct}$ and $C_{dl}$ are related to the dielectric and insulating features at the electrode–electrolyte interface, and can report directly and sensitively on any capture process.

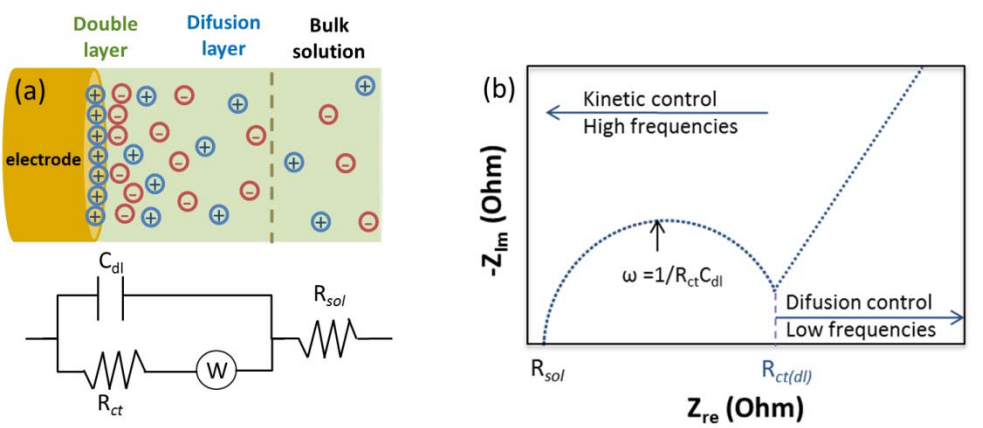


Figure 10. (a) The electrical double layer of a receptor modified electrode–electrolyte Interface (*on top*) and its associated Randles equivalent electrical circuit (*on bottom*). (b) Typical Nyquist plot resulting on a faradaic impedance spectrum.

EIS is a widely used technique for probing bioaffinity interactions at the surfaces and can be employed to investigate label-free detection of analytes via impedimetric transduction. Impedance biosensors have potential for simple, rapid, label-free, low-cost detection of biomolecules [7,70,71].

#### *1.1.2.3 Mass based biosensors*

Another form of transduction that has been used for biosensors is the measurement of small changes in mass. The principal means of mass analysis depends on the use of piezoelectric crystals, which can be made to vibrate at a specific frequency with the application of an electrical signal of a specific frequency. The frequency of oscillation is therefore dependent on the applied electrical frequency to the crystal as well as the mass of the crystal. Therefore, the frequency of oscillation of the crystal changes when the mass increases due to binding of chemicals. The resulting change can be measured electrically which can be used to determine the additional mass of the crystal [7,13].

Quartz is being used as a common piezoelectric material and the two types of mass-based sensors are bulk wave (BW) or quartz crystal microbalance (QCM) and surface acoustic wave (SAW) [7,12,76]. The advantages of using this type of transduction are real time monitoring, label-free detection and simplicity of use. However, there are also some important drawbacks such as lack of specificity and sensitivity as well as excessive interference [15].

### 1.1.3 Surfaces materials and modification methods

The design of sensor surfaces with oriented organizations of biomolecules is extremely important to obtain efficient biosensing devices. Nowadays, a wide variety of different materials and modification methods are used for the preparation of such surfaces. Depending on the measurement technique, surfaces need to fulfil specific requirements, such

as electrical conductivity (for electrochemical measurements) or transparency (for optical devices). Materials typically used include gold, silicon, silicon oxide, silicon nitride, graphite, glass carbon and Indium Tin Oxide (ITO), among others [8].

Gold is a suitable material for the chemistry attachment of many receptor classes, such as thiol coupling as well as by non-covalent coupling chemistries using biotin and streptavidin conjugate [77], although it is inert to many others chemistries. Additionally, gold is a very good material to be used as an electrode because of its relatively fast kinetics and it allows the formation of self-assembled monolayers (SAM) where biorecognition elements can be easily immobilized. Gold became the standard substrate for SAM formation because it is easy to obtain, manipulate and finally, it has bio-compatible characteristics [10].

Other commonly used materials include glass and oxide surfaces because of their very favourable optical characteristics. Among various semiconductor oxides, ITO has been considered as a very promising material for the characterization of biological systems. ITO surfaces are transparent (ideal for optical measurements), conductive and stable under physiological conditions. Biomolecules, including antibodies, antigens, and enzymes can be linked on the ITO surface through the formation of M+COO- covalent linkages (where M is indium or tin) between their free carboxyl groups and the abundant reactive hydroxyl groups (~12-13 OH groups $nm^{-2}$) [78,79].

The development of a biosensor requires the functionalization of the sensing surface in order to integrate the selected biorecognition elements. This is one of the most critical steps in biosensor development because biosensor performance (sensitivity, response time, dynamic range, and reproducibility) depends on how far the original properties of the bioreceptor are kept after its immobilization. Existing immobilization strategies include

adsorption (Figure 11 (a)), entrapment and encapsulation into polymers or membranes (Figure 11 (b) and (d), respectively), silanization and SAM formation coupled to biomolecule cross-binding or covalent bonding (Figure 11 (c)) [10,80].

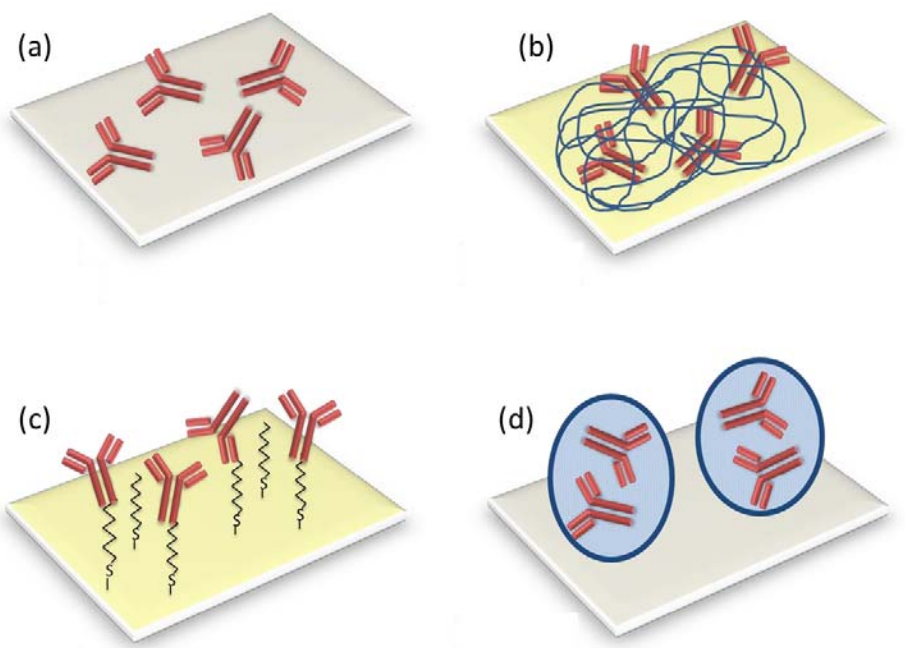


Figure 11. Different examples of biomolecule immobilization strategies: (a) adsorption, (b) entrapment, (c) cross-linking to a pre-assembled SAM, and (d) encapsulation (adapted from [10]).

The biorecognition element must be immobilized in a stable way, and its accessibility for the target molecule and its recognition ability must be ensured whatever the chosen strategy. In addition, the modified surface has to be inert and biocompatible, so that it does not affect the sample composition or integrity in any way; and it should also guarantee a constant

signal baseline. We next describe in more detail the different biomolecule immobilization strategies referred above.

#### *1.1.3.1 Adsorption*

Non-specific adsorption (Figure 11 (a)) is the easiest way to immobilize molecules on a physical substrate, and is based on the deposition of biomolecules on the surface, interacting in a completely random way. The driving forces may be initially hydrophobic or electrostatic, but protein adsorption is further stabilised by a combination of hydrophobic interactions, hydrogen bonding and/or Van der Waals forces, resulting in a behaviour highly dependent on each individual of protein-surface involved, and a highly stable product [72,81].

Adsorption on gold surfaces of proteins containing free $SH_2$ groups and/or S-S bonds, profits from the strong affinity of these functional groups for gold. Nevertheless, several reports demonstrate that antibodies perform better if immobilization is partly directed by reducing the interchain S-S bonds, generating free $SH_2$ groups, or using long-chain spacers prior to adsorption on gold [82,83]. As a consequence of adsorption, proteins may partly denature and thus lose structure and/or function [84]. Additionally, the adsorption process is difficult to control and the amount of protein adsorbed to most solid surfaces is usually below that which would correspond to a close-packed monolayer. Further, during the adsorption, the exposure of internal hydrophilic groups of proteins to hydrophobic surfaces causes a decrease in the activity and specificity of the protein/target interactions [10].

#### *1.1.3.2 Entrapment*

Biomolecules can be immobilized within organic or inorganic polymer matrices by entrapment during the matrix polymerization (Figure 11 (b)), without suffering any chemical modification that could affect their integrity. Confinement of proteins into small inert spaces contributes to stabilizing them by reducing unfolding and by shifting equilibrium between different configurations [85]. The main drawbacks associated with entrapment are the high concentrations of both monomer and biomolecule required, the biomolecule potential loss of structure and/or function following entrapment, the poor accessibility to certain target molecules, certain biomolecules' sensibility to the polymerization conditions and/or polymer components, and the lack of reproducibility between sensing surfaces [86].

#### *1.1.3.3 Microencapsulation*

Microencapsulation (Figure 11 (d)) involves the entrapment of molecules within micro/nano-capsules of different composition (particles, spheres, tubes, fibers, vesicles; made of hydrogel, polymer, carbon, silica, lipids, etc.) and formed by different strategies (via template moulding, polymerisation, self-assembly, emulsification, etc). Encapsulation, as entrapment has been reported to protect proteins from unfolding and degradation, ensuring longer activity times. On the other hand, microencapsulation requires relatively high biocomponent concentrations and generates longer response times compared to the case when the biocomponent is free in solution [10].

#### *1.1.3.4 Self-assembled monolayers*

Self-assembled monolayers (SAM) are crystalline chemisorbed organic single layers (typically of few nanometers) formed by spontaneous organization of thiolated molecules, generally on metal surfaces. They enable the formation of organic surfaces whose composition, structure, and properties can be varied rationally. The formation of these well-defined organic surfaces with useful and highly alterable chemical functionalities is made possible by the high affinity of sulphur for noble and coinage metals [87]. SAMs provide huge advantages for biosensor development as they are easy to prepare and functionalize in an ordinary chemistry laboratory. They can form on surfaces of any size and allow linking molecular-level structures to macroscopic interfacial phenomena. SAMs are often the basis for the subsequent immobilization of the recognition elements described previously. The possibilities are endless, since the functional groups provided by the SAM layer termination can be tailored to suit any particular requirement [72].

#### *1.1.3.5 Silanization*

Silanes have the general chemical composition formula $RSiX_3$, where R is an organofunctional group selected according to the desired surface properties; and X is a hydrolysable group, typically an alkoxy group (alkyl group linked to oxygen), which is capable of reacting with the substrate. Silanization of hydroxyl-terminated substrates is an effective and frequently used procedure for modification of chemical and physical properties of the substrate. Silanization is a SAM substitute for substrates such as silica, silicon, silicon oxide, silicon nitride, glass, cellulose, and metal oxide surfaces. Silanes

are normally hydrolysed at some stage in the coating process, allowing interaction with the substrate either via hydrogen or covalent bonds [10].

#### *1.1.3.6 The Biotin-(Strept)Avidin System*

This system is based on the natural strong binding of avidin with the small molecule biotin (also called vitamin H). This functional biotin group can be added to proteins, nucleic acids, and other molecules through well-known reactions. The biotin-avidin system is one of the most popular non-covalent conjugation methods and a very useful tool for targeting applications [88].

Another very similar protein to avidin is streptavidin and is often very used as it prevents non-specific bindings that are quite elevated with avidin due to its high isoelectric point and carbohydrate content. Both streptavidin and avidin can be conjugated to other proteins or labelled with various detection reagents without loss of biotin binding activity. One of the most advantageous features of this system is that although the affinity constant between avidin and biotin is rather high, the bonding is of non-covalent nature, which allows for multiple washing and re-use of the same sensing device. On the other hand, an important drawback is the high cost of the reagents involved.

#### *1.1.3.7 Chemical Conjugation*

The most commonly used strategy of chemical conjugation consists in cross-binding between carboxylic (-COOH) and amine groups (-$NH_2$) exploiting the EDC/NHS chemistry. The COOH group can be situated either on the termination of the SAM or on the (bio) component to be immobilized. The

use of glutaraldehyde allows the reaction of two amino groups. Thiols can be coupled to amino groups using heterofunctional cross-linkers such as succinimidyl 4-(N-maleimidomethyl)-cyclohexane-1-carboxylate (SMCC) or N-Succinimidyl S-acetylthioacetate (SATA). The polysaccharides present in some proteins can be oxidised with sodium periodate and later conjugated to amine or hydrazyde groups in the SAM by reductive amination. Hydroxyl groups on a SAM can be treated the same way [88]. In addition, the recognition element may also self-assemble. For example, a thiol-modified nucleic acid fragment (incorporating an –SH terminal group) will directly self-assemble on the metal surface.

### 1.1.4 Applications

Biosensors have several potential advantages over other biodetection methods, in particular increased assay speed and flexibility. Rapid and essentially real-time analysis can provide immediate interactive information to users. This speed of detection is an advantage in essentially all applications. Biosensors allow multi-target analyses, automation and reduced costs of testing.

The main applications of biosensors include medical (clinical, pharmaceutical and device manufacturing, and research) environmental (spill clean-up, monitoring and regulatory instances), public security (civil and military first responders as well as unattended monitoring) and food safety (food production, regulatory monitoring, and diagnosis of food poisoning) [3,5].

Rapid detection of pathogenic bacteria and mycotoxins is important for reducing foodborne illness. Biosensors can detect pathogens in a much

shorter time with sensitivity and selectivity comparable to the conventional methods. Since they are low-cost and high-throughput devices and do not require trained personnel, they can be used in future as stand-alone devices for on-site monitoring. Specific examples of pathogenic bacteria and mycotoxins detection using biosensors will be presented and discussed in further sections.

## 1.2 Detection of pathogenic bacteria

The detection of pathogenic bacteria is the key to prevention and identification of problems related to health and safety. Figure 12 (a) shows the areas of application in the field of pathogen detection. Taking account all research in this field, the three main areas are the food industry, water and environment quality control, and clinical diagnosis [17].

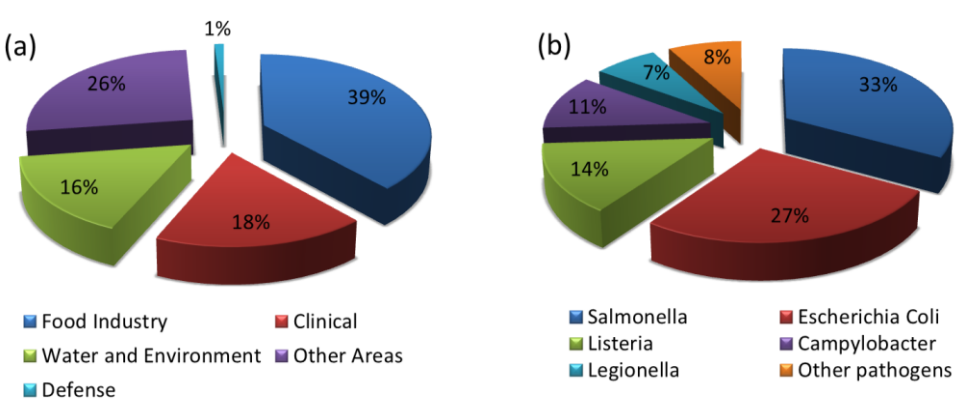


Figure 12. (a) Areas of interest for pathogen detection. (b) Reported methods, by microorganisms, for pathogen detection (adapted from [17]).

The most common foodborne infections are those caused by the bacteria *E. coli* O157:H7, *Salmonella*, *Listeria monocytogenes* and *Campylobacter jejuni* and by the *calicivirus*, also called *Norwalk viruses* (Figure 12 (b))[9]. Bacterial infections remain the leading cause of death in developing nations, accounting for an estimated 40% of deaths. Foodborne infections in the United States alone have been estimated to cause 76 million illnesses, more than 300000 hospitalizations and 5000 deaths [7,48,89].

The Recent *Salmonella* outbreak in 2007 affected consumers in 44 states of USA and was considered one of the largest case of foodborne disease. Pathogenic *Salmonella* are bacteria which cause salmonellosis. Humans usually become infected by eating food contaminated with animal faeces, especially raw and undercooked foods of animal origin, such as beef, poultry, milk, and eggs. Food may also become contaminated through cross-contamination and poor hygiene of food handlers. Infected persons develop diarrhoea, fever, and abdominal cramps between 12 and 72 hours after eating the contaminated food (infection doses: 15-20 organisms). In rare cases, the infection may spread to bloodstream and can cause death if left untreated [7].

Among the over 2000 serovars that have been identified and characterized, *S. enteritidis* and *Salmonella typhimurium* are epidemiologically the most important ones because they are the causative agent in 80% of all human infections reported world-wide [9]. It constitutes a major public health burden and represents a significant cost in many countries. Millions of human cases are reported worldwide every year and the disease results in thousands of deaths. For example, a large outbreak of gastroenteritis occurred in Catalonia in June 2002 with 1435 cases and 117 hospitalizations. Consumption of a hard pastry with vanilla cream was strongly associated with the illness [95].

The enterohemorrhagic *Escherichia coli* bacteria (EHEC) strains are also found to be responsible for serious foodborne outbreaks [7,91,92], as it has been recently reported in northern Europe [93,94]. The strain O157:H7 of *Escherichia coli* is considered to be one of the most dangerous foodborne pathogens [48]. *Escherichia coli* O157:H7 is a gram-negative rod-shaped bacterium that has been implicated in outbreaks of illness due to ingestion of meats, water and uncooked fruits and vegetables [95]. Ingestion of the bacteria causes severe and bloody diarrhoea and painful abdominal cramps. In some cases, a complication called haemolytic uraemic syndrome (HUS) can occur causing profuse bleeding and kidney failure [9].

It is estimated that there are about 73480 cases of infection and 61 deaths that occur in the United States each year caused by *E. coli* O157:H7 alone. Since the economic loss is so huge in terms of medical costs and product recalls caused by *E. coli* O157:H7, it is very important to rapidly detect and effectively control *E. coli* O157:H7 in food products [96].

Detection and control of EHEC pathogens, like the frequently found Shiga-like toxin producing *E. coli* serotype O157:H7, are very challenging problems in terms of their high virulence and the extremely low infectious dose required to cause disease (< 10 organisms) [7, 97–99]. The current policy of the United States Department of Agriculture-Food Safety and Inspection Service (USDA-FSIS) towards *E. coli* O157:H7 is zero tolerance. For example, the current limit of detection (LOD) by the approved USDA-FSIS method is 1 Colony Forming Units (CFU) per 65 g sample of meat [9].

### 1.2.1 Established methods in pathogen detection

Culture and colony counting methods, polymerase chain reaction (PCR) as well as immunology-based methods, are the most common tools used for pathogen detection (Figure 13).

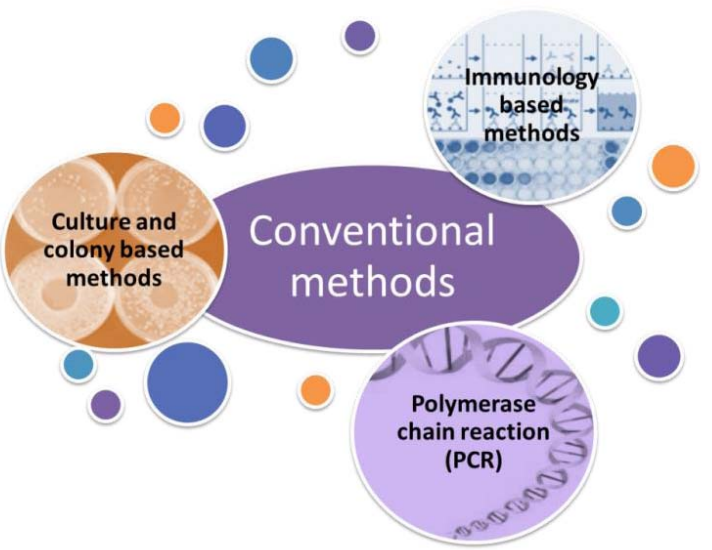


Figure 13. Major types of conventional methods used in pathogen detection.

So far, mainly microbiological methods have been applied for routine detection of bacteria. These methods include selective pre-enrichment steps using standard culture plates and a number of serological and biochemical tests for identification. These tests usually provide reliable and robust results (no false-positives); low detection limits and only viable cells are detected. However, they are very time-consuming (e.g. 18 h for *E. coli* detection) and are labour-intensive.

Other common tools for analysis of bacteria are based on biological recognition elements like nucleic acids and antibodies. Amplification of small

amounts of genetic material is performed by PCR. This technique is faster than plating techniques; it is very sensitive (10-$10^3$ CFU) and specific but often requires intensive sample pre-purification and skilled technical staff. Immunological methods like ELISA use specific antibody-antigen interactions for quantification. Herein the sensitivity of the method mainly depends on the affinity of the used antibodies. As a result, sample pre-concentration steps could become necessary for the detection of single cells. This makes these methods difficult to be used in many industrial applications, particularly for on-line or in-field detection of foodborne pathogens [95,96,100,101].

### 1.2.2 Biosensors for *E. coli* O157:H7 detection

As stated above, *Escherichia coli* O157:H7 is one of the main responsible for serious foodborne outbreaks (see section 1.2.1). Detection techniques based on biosensors are an interesting alternative to perform simple, sensitive, fast, selective and reliable measurements of these pathogenic bacteria, being at the same time cost-effective and applicable to real-time monitoring. *E. coli* has been detected using different bioreceptors (see section 1.1.1) including antibodies, AMPs, aptamers and DNA probes using as transducers optical, electrochemical and mass sensitive methods (see section 1.1.2). Table 1 shows a summary of some biosensors developed for the detection of pathogenic bacteria *E. coli* O157:H7 reported in literature according to the type of method, bioreceptor and assay used, and LOD obtained.

Table 1. Reported detection methods for pathogenic bacteria *E. coli*.

| Method | Bioreceptor | Assay type | Detection limit (CFU $mL^{-1}$) | Reference |
|---|---|---|---|---|
| Surface Plasmon Resonance | Antibody | Direct | $5\text{-}7\times 10^{7}$ | [103] |
| | Antibody | Indirect | $10^{5}$ | [104] |
| | Antibody | Indirect | $10^{4}$ | [105] |
| | Antibody | Direct | $10^{5}$ | [106] |
| | Antibody | Direct | $10^{2}$ - $10^{3}$ | [107] |
| Fluorescence microscopy | Antibody | Indirect | $10^{2}$ | [108] |
| | AMP | Direct | $1.6 \times 10^{5}$ | [47] |
| Quartz Crystal Microbalance | DNA | Indirect | $1.2 \times 10^{2}$ | [102] |
| | Antibody | Direct | $10^{3}$ | [109] |
| | Antibody | Indirect | 23 | [110] |
| Amperometry | Antibody | Indirect | 100 | [111] |
| | Antibody | Indirect | $6 \times 10^{2}$ | [113] |
| Potentiometry | Antibody | Indirect | $7 \times 10^{2}$ | [114] |
| | Antibody | Indirect | $10^{1}$ | [115] |
| Electrochemical Impedance Spectroscopy | Antibody | Indirect | $6 \times 10^{3}$ | [116] |
| | Antibody | Direct | $10^{6}$ | [79] |
| | Antibody | Direct | 10 | [77] |
| | Antibody | Direct | $1\times10^{3}$ | [117] |
| | AMP | Direct | $10^{3}$ | [48] |

Most of these works are based on antibody bioreceptors but other works though describe the use of further biorecognition elements. As an example, nucleic acid-based biosensors have been reported by many researchers for the detection of food pathogen like *E. coli* O157:H7 due to

their wide range of physical, chemical and biological activities [102]. AMP (magainin I) has also been used as a bioreceptor for *Escherichia coli* O157:H7 detection. As a second example, an array-based biosensor was developed by Kulagina et al [47] using AMP and fluorescence microscopy as a detection technique. Similarly, Manoor *et al* [48] developed a label-free electronic biosensor based on AMP magainin I with interdigitated microelectrode arrays for the sensitive and selective detection of pathogenic bacteria via impedance spectroscopy.

A wide variety of immunosensors have been described for the detection of *E. coli* (see Table 1). Among all of them, QCM allows the detection of bacteria using probes modified with immobilized antibodies [109,110]. Limits of detection in the order of $10^3$ CFU $mL^{-1}$ were reported [109].

SPR has also been successfully applied for the detection of pathogenic bacteria by means of immunoreactions [103–107] (see Table 1). Using a sandwich antibody assay, Taylor *et al* [105] reported a limit of detection of $\sim 10^4$ CFU $mL^{-1}$ in PBS for each of the four pathogens, *E. coli* O157:H7, *Listeria monocytogenes*, *Campylobacter jejuni*, and *S. typhimurium*. The limit of detection was not perturbed for none of the four pathogens when they were simultaneously present in apple juice matrix. Choi and Oh [108] used fluorescence microscopy for the detection of *E. coli* O157:H7 and reported a LOD of $10^2$ CFU $mL^{-1}$.

Optical-based techniques possibly provide good sensitivity, but they are expensive and complicated. As mentioned earlier, electrochemical biosensors have received particular attention in biomedical and environmental fields during the last years due to their multiple advantages, such as fast response, low cost, mass production and capability of miniaturization. Electrochemical methods such as amperometry and

potentiometry have been widely used for the detection of *E. coli* O157:H7 (see Table 1). Many researchers have reported amperometric detection of *E. coli* [111–113] with limits of detection of $1.6\times10^{1}$ to $6\times10^{2}$ CFU $mL^{-1}$. Limits of detection between 10 and $7\times10^{2}$ CFU $mL^{-1}$ were also obtained with potentiometry [114,115].

Several examples of impedimetric immunosensors for the detection of *E. coli* O157:H7 can be found in literature. EIS based sensors are particularly attractive because allow label-free detection with high sensitivity [118] (see section 1.1.2). Yang *et al* achieved LOD of $6\times10^{3}$ CFU $mL^{-1}$ for a label system [116] and $1\times10^{6}$ CFU $mL^{-1}$ for a label-free interdigitated array microelectrode [79]. Zhang *et al* [119] obtained lower LOD ($4.2\times10^{3}$ CFU $mL^{-1}$) using a similar approach. Other groups such Geng *et al* [117] used covalent immobilization on a gold electrode and found a LOD of $1\times10^{3}$ CFU $mL^{-1}$. The lowest LOD (10 CFU $mL^{-1}$) was reported by Maalouf *et al* [77], using a biotynilated polyclonal antibody linked to a mixed SAM on gold electrode through biotin-neutravidin interaction.

Impedimetric biosensors have been used to monitor foodborne pathogenic bacteria for many years. Compared to the other methods, they have several main advantages. They are label-free that simplifies the assembly process and lowers the cost. They are rapid and the detection time is generally less than 30 min with detection limits as low as those obtained with SPR and ELISA. Results are reproducible when the bio-recognition elements are immobilized on the electrode using strong chemical bonds such as SAM immobilization method, which reduces the cost of use. Additionally, impedance device miniaturization have been proved to be very successful in maximizing the impedance signal, minimizing the volume of testing sample, increasing sensitivity, and saving assay time. Other advantages of smaller scale approach are: the possibility of mass production and reduced unit costs,

the performance of multi-analyte analysis is enabled in the same device, which also shortens analysis time, and due to the tiny sample volumes needed, these devices provide more safety and they are more environmentally friendly.

Although the impedimetric biosensors have many advantages, they still have some limits. Further efforts should be devoted to developing commercial products in the area of impedimetric biosensors for foodborne pathogenic bacteria detection, which will require improved stability, reduced volume, increased sensitivity and lowered costs. In order to become attractive, they first need to show that their capability of reaching at least the same (ideally lower) detection levels as traditional techniques (between 10 and 100 CFU $mL^{-1}$) and the required limit of detection for bacterial analysis in food or clinical samples since the infectious doses of *E. coli* O157:H7 are lower than 10 cells [7,97]. In addition, it must be capable to detect pathogens in very low sample concentrations and it must be suitable for *in situ* real-time monitoring as well. Such a technique of detecting pathogens would offer a great commercial advantage to food processing and food manufacturing sector. And multiplexing analysis could be provided to the sensor by using a multi-electrodes system.

## 1.3 Detection of mycotoxins

Similar to pathogenic bacteria, the presence of mycotoxins in food is also a serious concern since it may compromise food safety. A toxin can be defined as a substance that is synthesised by a plant species, an animal, or by microorganisms, that is harmful to another organism. Mycotoxins are small (MW ~700 g/mol), toxic chemical products formed as secondary metabolites

by few fungal species that readily colonise crops and contaminate them with toxins in the field or after harvest. *Ochratoxins* and *Aflatoxins* are mycotoxins of major significance and hence there has been significant research on broad range of analytical and detection techniques that could be useful and practical [120].

Ochratoxins are a small group of chemically related toxic fungal metabolites (mycotoxins), produced by certain molds of the genera *Aspergillus* and *Penicillium*, growing on a wide range of raw food commodities. Some ochratoxins are potent toxins and their presence in food is undesirable [121]. Figure 14 shows the chemical structure of major types of ochratoxins. The ochratoxins are pentaketides made up of dihydro-isocoumarin linked to ß-phenylalanine. The most important and most toxic ochratoxin found naturally in food is ochratoxin A (OTA). From all the rest, only ochratoxin B is also found in food, which is rare and much less toxic. Other structurally related ochratoxins include ochratoxin C and α. These have been isolated from fungal cultures, but are not normally found in food [121]. In this section we will focus specifically on OTA due to its impact in food safety and public health protection.

OTA is a potent nephrotoxin and causes both acute and chronic effects in the kidneys of all mammalian species tested. OTA is also genotoxic (damages DNA) and teratogenic (damages the foetus) and is considered a probable carcinogen, causing renal carcinoma and other cancers in a number of animal species, although the mechanism for this is uncertain [122].

OTA has been found in a large variety of commodities: cereals, beans, dried fruits, coffee, beer, wine and meat fed with contaminated fodder. Limits vary according to the commodity, but range from 2-10 μg/kg. For example, the limit for dried vine fruits is 10 μg/kg, in torrefied coffee beans the maximum level for OTA is up to 5 μg/kg and 10 μg/kg in instant coffee.

The limit for unprocessed cereals is 5.0 µg/kg, but for processed cereal products intended for direct human consumption is 3.0 µg/kg body weight [124]. There is also a limit of 0.50 µg/kg for OTA in processed cereal-based foods for infants and young children [122].

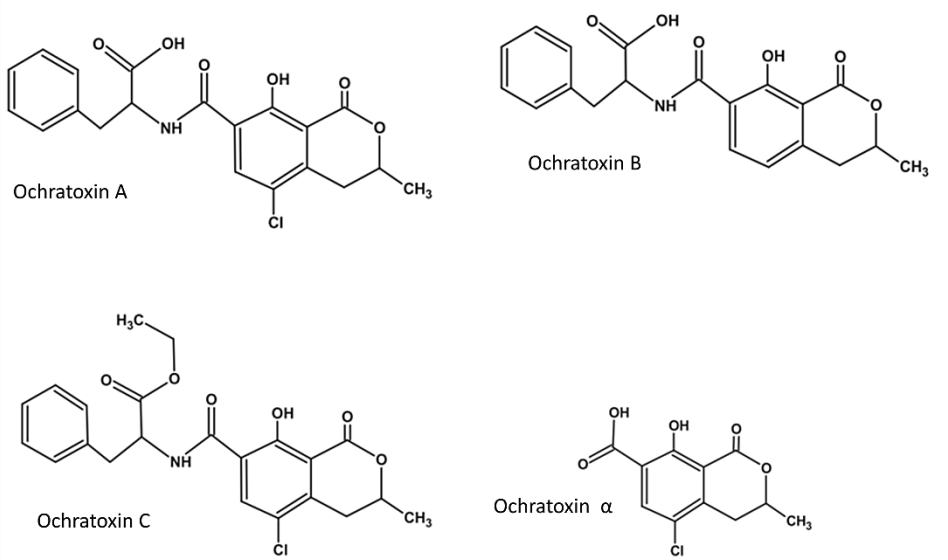


Figure 14. Chemical structure of major types of ochratoxins [123].

### 1.3.1 Established methods in mycotoxins detection

Thin-layer chromatography (TLC) has been widely used to detect and identify the presence of mycotoxins. Other methods with superior analytical performance are currently used for quantitative determination of mycotoxins. Most official methods are based on high-performance liquid chromatography (HPLC) coupled with ultraviolet (UV), fluorescence (FLD) or mass spectrometry (MS) detectors. For example, official methods for

detection of OTA include thin-layer chromatography fluorescence detection (TLC-FD) and high performance liquid chromatography - fluorescence detection (HPLC-FD).

These techniques provide with very low detection limits, but sometimes their cost, need of skilled personnel and limitations to perform *in situ* analysis can be overcome by alternative techniques. Routine screening of mycotoxins is commonly performed by ELISA, which can process a large number of samples in one assay. Nevertheless, they involve long, laborious procedures and cross-reactivity phenomena that, even though sometimes could be useful for the evaluation of the total toxicity, can give rise to false positive results for a single mycotoxin determination. Moreover, some matrix effects can arise, sometimes minimized by extract clean-up and/or dilution and addition of detergents [125].

### 1.3.2 Biosensors for ochratoxin A detection

The presence of OTA in food samples at very low concentration may induce toxic effects, therefore selective and sensitive detection of OTA is highly required in order to guarantee food safety and to minimize the potential risk to human and environmental health. In the last years, biosensors have emerged as reliable and promising alternative analysis tools to classical methods. Table 2 shows a summary of biosensors developed for the detection of Ochatoxin A reported in literature. Sensitive and accurate biosensors have been developed based on different transduction methods and most of them using aptamers and antibodies as bioreceptors.

Table 2. Reported detection methods for ochratoxin A.

| Transducer | Bioreceptor | Assay type | Detection limit (ng $mL^{-1}$) | Reference |
|---|---|---|---|---|
| Surface Plasmon Resonance | Antibody | Indirect | 0.060 | [126] |
| | Antibody | Indirect | 0.042 | [127] |
| Fluorescence | Antibody | Indirect | 0.012 | [128] |
| | Aptamer | Indirect | 2 | [129] |
| Quartz Crystal Microbalance | Antibody | Direct | 16.1 | [130] |
| Amperometry | Antibody | Indirect | 0.7 | [131] |
| Differential Pulse Voltammetry | Antibody | Indirect | 0.3 | [131] |
| | Aptamer | Indirect | 0.07 | [132] |
| | Aptamer | Indirect | 1.6 | [133] |
| | Aptamer | Indirect | 0.0001 | [134] |
| Electrochemical Impedance Spectroscopy | Antibody | Direct | 1 | [135] |
| | Antibody | Direct | 0.5 | [136] |
| | Aptamer | Direct | 0.048-0.16 | [137] |
| | Aptamer | Direct | 0.00025 | [138] |
| | Aptamer | Direct | 0.1 | [139] |

Different optical transduction methods have been used for OTA detection (Table 2). SPR sensors using signal amplification were developed by Urusov *et al* [126] and Yuan *et al* [127]. Urusov *et al* [126] achieved an improved limit of detection by an order of magnitude (down to 0.06 ng $mL^{-1}$) using additional binding step of specific antibodies to gold–anti-species antibody conjugates. Yuan *et al* [127] also improved the limit of detection

dramatically using gold nanoparticles (0.042 ng $mL^{-1}$). Finally, a sensitive fluorescence-based immunosensor was developed by Prieto-Simón *et al* [128], showing a LOD of 0.012 ng $mL^{-1}$ in the assay solution enabled by the affinity of the anti-OTA antibody.

The simplicity of gravimetric techniques, such as quartz crystal microbalance, has also been used to develop immunosensors for the detection of OTA. Tsai and Hsieh [130] used piezoelectric immunosensor based on a competitive format obtaining a LOD of 16.1 ng $mL^{-1}$.

The high sensitivity of electrochemical techniques has also been used to develop immunosensors for OTA detection. Immunosensors based on voltammetric detection methods require electroactive labels, while impedimetric-based sensors show the advantage of being label-free. Prieto-Simon *et al* [131] compared two indirect competitive ELISA strategies and electrochemical immunosensors based on different enzyme-labelled secondary antibodies. The obtained LOD was 0.7 and 0.3 ng $mL^{-1}$ for HRP- and alkaline phosphatase (ALP)-labelled immunosensors, respectively.

Direct, label-free detection of OTA using EIS based on immunosensors composed of OTA sensitive antibodies immobilized on various substrates have also been developed. Specific antibodies were adhered onto a gold surface using carbodiimide chemistry and a LOD of 0.5 ng $mL^{-1}$ was obtained [136]. A chitosan–polyaniline hybrid conducting biopolymer film on an ITO electrode was also used for this objective (LOD=1 ng $mL^{-1}$) [135].

Despite the fact that immunosensors are rather popular, the disadvantage of these methods consists in the necessity of using stable antibodies. Biosensors based on antibodies are difficult to regenerate. Aptamers could therefore be a good alternative instead of antibodies. A fluorescence aptasensor based on displacement of a fluorescently labeled oligo from the aptamer by the target was detected by fluorescence

polarization (LOD = 2 ng $mL^{-1}$) [129]. Bonel *et al* [132] reported the fabrication of an electrochemical competitive biosensor for OTA based on DNA biotinylated aptamers with a detection limit of 0.07 ng $mL^{-1}$. Wu *et al* [134] developed a one-step electrochemical aptasensor using the thiol- and methylene blue- (MB-) dual-labeled aptamer modified gold electrode for the determination of ochratoxin A (LOD 0.1 pg $mL^{-1}$). Finally, a limit of detection of 1.6 ng $mL^{-1}$ was obtained for the detection of OTA using a novel sensing strategy for electrochemical aptamer-based sensors [133].

A few aptamer-based impedimetric sensors have also been published. Castillo *et al* [137] reported a high sensitive impedimetric biosensor based on DNA aptamers (LOD = 0.048-0.16 ng $mL^{-1}$ equivalent to 0.12-0.40 nM). Hayat *et al* [138] and Prabhakar *et al* [139] reported the development of OTA impedimetric aptasensors exploring different aptamer immobilizations, obtaining LOD of 0.25 ng $L^{-1}$ and 0.1 ng $mL^{-1}$, respectively.

Several biosensors examples have been described in the literature for the detection of OTA. However, there is still a challenge to develop alternative assays for OTA analysis and for simultaneous detection of different mycotoxins. Electrochemical biosensor arrays are the emerging analytical approaches in which innovation can be expected. The detection of multiple analytes simultaneously makes these systems interesting in the analysis of samples with multi-toxin profiles. Nevertheless, often different toxins require different extraction protocols, making complicated the harmonization of protocols for the integration of several biosensors in a same platform. As a consequence, compromised experimental conditions are sometimes required. These complexities explain the scarce number of arrays for toxins, but once optimized, arrays will certainly contribute to the multi-toxin analysis field.

## 1.4 Outlook and objectives of the thesis

Biosensors have brought new and promising approaches for the development of rapid methods for the detection of bacteria and toxins. Biosensors are devices that are easy to use without training, yield results in nearly real-time with sensitivity and selectivity comparable to the traditional methods. Detecting several targets in the same biological sample is possible if different surface regions are functionalized with different bioreceptors. Multiplexing is desirable because it reduces both cost and sample volume per data point. It is possible to detect various analytes using a single readout circuit because electrical signals are readily steered. Regardless of readout mechanism, multiplexed detection is complicated by cross-reactivities which severely limits the possible degree of multiplexing and is especially troublesome in real-world situations. Thus, efforts to develop multiplexed biosensors will surely continue.

This thesis, entitled "*Development of a multi-electrode impedimetric biosensor: detection of pathogenic bacteria and mycotoxins*", aims the development of a multi-electrode platform with applications on different biosensing fields: (i) detection of pathogenic bacteria and (ii) detection of the mycotoxin OTA. For most label-free biosensors, including impedance biosensors, the principal limitation on multiplexing arises from the affinity step. Therefore, a great part of the research work described here deals with the characterization, optimization and evaluation of different functionalization strategies for biosensing. These surface functionalization strategies developed here are applied for the final development of the multi-electrode platform biosensor. The specific objectives of each chapter are described hereafter:

In **Chapter 2**, we take advantage of the outstanding properties of ITO material for the development of an ITO-based immunosensor for detecting pathogenic *E. coli* O157:H7 bacteria. The sensor build-up consisted on a simple, efficient and direct covalent binding of anti-*E. coli* O157 antibodies onto the ITO substrates. The functionalization methodology was fully characterized by multiple techniques, showing the specific binding of *E. coli* O157:H7 to the antibody-functionalized surface. The detection capacity of the ITO-based immunosensor was finally tested by EIS and a novel highly sensitive and selective sensor was obtained. This work was developed in collaboration with the GRF-Functional Coatings Group (University of Minho, Braga, Portugal) and Dr. Eduard Torrents and Prof. Antonio Juárez (IBEC, Barcelona, Spain).

In **Chapter 3**, we developed a gold-based electrochemical immunosensor for the detection of pathogenic *E. coli* O157:H7 bacteria. Gold is bio-compatible, can be easy obtained and it is easy to pattern using photolithography. In order to enhance the sensor performance, the functionalization protocol was optimized and antibodies were immobilized onto gold electrodes following two different strategies. Both functionalization strategies were evaluated and characterized by several techniques and the strategy showing better antibody immobilization and response was selected for the development of a highly sensitive label-free immunosensor. The immunosensor showed a very low limit of detection and low interference with other pathogenic bacteria, such as *Salmonella typhimurium*. This work was partially developed in collaboration with Prof. Maria Pilar Marco and Dr. Núria Pascual from the Institute for Advanced Chemistry of Catalonia (IQAC), CSIC (Barcelona, Spain).

In **Chapter 4**, we applied the functionalization strategies developed in the previous chapter 3 to develop a miniaturized multi-electrodes array for

the detection of pathogenic bacteria. The multi-electrodes were fabricated in gold and consisted of multiple equally independent gold electrodes. This allowed high-throughput and independent experiments, in parallel and under the same experimental conditions. Multi-electrodes were fabricated by standard photolithography techniques and characterized by several surface analysis and electrochemical techniques, confirming the quality of the fabrication process. We demonstrated the biosensing capabilities of the multi-electrode platform for the detection of pathogenic bacteria using different bioreceptors, including antibodies and AMPs. This work was partially developed in collaboration with Prof. Fernando Alberício and Dr. Hortensia Rodríguez from the Institute for Research in Biomedicine, IRB (Barcelona, Spain) and Prof. José Antonio Plaza from the National Centre for Microelectronics CNM-CSIC (Cerdanyola del Vallès, Spain).

In **Chapter 5**, we applied the multi-electrodes platform for the development of an aptasensor for the detection of mycotoxins. We focused on the specific case of ochratoxin A, one of the most abundant food-contaminating mycotoxins. Two strategies for aptamer immobilization were presented, both based on the hybridization onto the biosensor surface through partially complementary oligonucleotides. Cyclic voltammetry and EIS techniques were used to characterize all the functionalization steps. The developed multi-sensor was capable to detect OTA concentrations and the promising results obtained prove the successful application of the multi-electrodes strategy for the detection of mycotoxins and the advantages of using multi-electrode platform. This work was developed in collaboration with Prof. Jean Louis Marty and Dr. Cheng Yang at the IMAGES laboratory (Université de Perpignan, Perpignan, France).

## 1.5 References

[1] J. Kirsch, C. Siltanen, Q. Zhou, A. Revzin, A. Simonian, Biosensor technology: recent advances in threat agent detection and medicine, Chem. Soc. Rev. (2013) 8733–8768.

[2] J. Castillo, S. Gáspar, S. Leth, M. Niculescu, A. Mortari, I. Bontidean, et al., Biosensors for life quality design, development and applications, Sens. Actuators B 102 (2004) 179–194.

[3] J.M. Walker, A. Rasooly, K.E. Herold, Biosensors and Biodetection, Humana Press, Totowa, NJ, 2009.

[4] M. Nayak, A. Kotian, S. Marathe, D. Chakravortty, Detection of microorganisms using biosensors - a smarter way towards detection techniques, Biosens. Bioelectron. 25 (2009) 661–7.

[5] A. Rasooly, K.E. Herold, eds., Biosensors and Biodetection Methods and protocols, Volume 503, Springer Protocols, 2009.

[6] B.D. Mallotra, A.P.F. Turner, Advances in Biosensors perspectives in biosensors, Elsevier Science B.V., 2003.

[7] V. Velusamy, K. Arshak, O. Korostynska, K. Oliwa, C. Adley, An overview of foodborne pathogen detection: In the perspective of biosensors, Biotechnol. Adv. 28 (2010) 232–254.

[8] D. Grieshaber, Electrochemical Biosensors - Sensor Principles and Architectures, Sensors. 8 (2008) 1400–1458.

[9] H. Sharma, R. Mutharasan, Review of biosensors for foodborne pathogens and toxins, Sens. Actuators B 183 (2013) 535–549.

[10] M. Zourob, S. Elwary, A. Turner, Principles of bacterial detection: biosensors, recognition receptors and microsystems, Springer, 2008.

[11] T. Vo-Dinh, Micro and nanoscale biosensors and materials: biosensors and biochips, Springer, 2008.

[12] S.B. Shinde, C.B. Fernandes, V.B. Patravale, Recent trends in in-vitro nanodiagnostics for detection of pathogens., J. Control. Release. 159 (2012) 164–80.

[13] T. Vo-Dinh, B. Cullum, Biosensors and biochips: advances in biological and medical diagnostics, Fresenius. J. Anal. Chem. 366 (2008) 540–51.

[14] X. Zhang, H. Ju, Electrochemical sensors, biosensors and their biomedical applications, Elsevier, 2008.

[15] V. Perumal, U. Hashim, Advances in biosensors: Principle, architecture and applications, J. Appl. Biomed. 12 (2014) 1–15.

[16] J.C. Vidal, L. Bonel, A. Ezquerra, S. Hernández, J.R. Bertolín, C. Cubel, et al., Electrochemical affinity biosensors for detection of mycotoxins: A review., Biosens. Bioelectron. 49 (2013) 146–58.

[17] O. Lazcka, F.J. Del Campo, F.X. Muñoz, Pathogen detection: a perspective of traditional methods and biosensors., Biosens. Bioelectron. 22 (2007) 1205–17.

[18] N.S. Lipman, L.R. Jackson, L.J. Trudel, F. Weis-Garcia, Monoclonal versus polyclonal antibodies: distinguishing characteristics, applications, and information resources, ILAR J. 46 (2005) 258–68.

[19] R.H. Hall, Biosensor technologies for detecting microbiological foodborne hazards., Microbes Infect. 4 (2002) 425–32.

[20] K.V. Ragavan, N.K. Rastogi, M.S. Thakur, Sensors and biosensors for analysis of bisphenol-A, Trends Anal. Chem. 52 (2013) 248–260.

[21] C. Moina, G. Ybarra, Fundamentals and Applications of Immunosensors, Advances in Immunoassay Technology, N.H.L. Chiu (Ed.), 2012.

[22] P.D. Skottrup, M. Nicolaisen, A.F. Justesen, Towards on-site pathogen detection using antibody-based sensors, Biosens. Bioelectron. 24 (2008) 339–48.

[23] B. Byrne, E. Stack, N. Gilmartin, R. O'Kennedy, Antibody-based sensors: principles, problems and potential for detection of pathogens and associated toxins, Sensors 9 (2009) 4407–45.

[24] E.P. Medyantseva, E. V Khaldeeva, G.K. Budnikov, Immunosensors in biology and medicine : analytical capabilities, problems, and prospects, J. Anal. Chem. 56 (2001) 886–900.

[25] D. Marazuela, M.C. Moreno-Bondi, Fiber-optic biosensors -an overview, Anal. Bioanal. Chem. 372 (2002) 664–82.

[26] R.H. Yolken, Enzyme-linked immunosorbent assay (ELISA): a practical tool for rapid diagnosis of viruses and other infectious agents, Yale J. Biol. Med. 53 (1980) 85–92.

[27] L.C. Clark LC, Electrode systems for continuous monitoring in cardiovascular surgery, Ann NY Acad Sci. (1962) 29–45.

[28] S.V. Dzyadevych, V.N. Arkhypova, a. P. Soldatkin, a. V. El'skaya, C. Martelet, N. Jaffrezic-Renault, Amperometric enzyme biosensors: Past, present and future, Irbm. 29 (2008) 171–180.

[29] H. Ohnuki, R. Honjo, H. Endo, T. Imakubo, M. Izumi, Amperometric cholesterol biosensors based on hybrid organic–inorganic Langmuir–Blodgett films, Thin Solid Films. 518 (2009) 596–599.

[30] A. Amine, H. Mohammadi, I. Bourais, G. Palleschi, Enzyme inhibition-based biosensors for food safety and environmental monitoring, Biosens. Bioelectron. 21 (2006) 1405–23.

[31] C. Malitesta, M.R. Guascito, Heavy metal determination by biosensors based on enzyme immobilised by electropolymerisation, Biosens. Bioelectron. 20 (2005) 1643–7.

[32] E. Zapp, D. Brondani, I.C. Vieira, C.W. Scheeren, J. Dupont, A.M.J. Barbosa, et al., Biomonitoring of methomyl pesticide by laccase inhibition on sensor containing platinum nanoparticles in ionic liquid phase supported in montmorillonite, Sens. Actuators B 155 (2011) 331–339.

[33] C. Lui, N.C. Cady, C. a. Batt, Nucleic acid-based detection of bacterial pathogens using integrated microfluidic platform systems, Sensors 9 (2009) 3713–3744.

[34] A. Chua, C.Y. Yean, M. Ravichandran, B. Lim, P. Lalitha, A rapid DNA biosensor for the molecular diagnosis of infectious disease., Biosens. Bioelectron. 26 (2011) 3825–3831.

[35] J. Bang, L.R. Beuchat, H. Song, M.B. Gu, H.-I. Chang, H.S. Kim, et al., Development of a random genomic DNA microarray for the detection and identification of Listeria monocytogenes in milk, Int. J. Food Microbiol. 161 (2013) 134–41.

[36] V. Trevino, F. Falciani, H.A. Barrera-saldaña, DNA microarrays: a powerful genomic tool for biomedical and clinical Research, Mol Med. 13 (2007) 527–541.

[37] X.-H. Yang, W.-J. Kong, M.-H. Yang, M. Zhao, Z. Ouyang, Application of aptamer identification technology in rapid analysis of mycotoxins, Chinese J. Anal. Chem. 41 (2013) 297–306.

[38] X. Luo, J.J. Davis, Electrical biosensors and the label free detection of protein disease biomarkers, Chem. Soc. Rev. 42 (2013) 5944–62.

[39] B. Van Dorst, J. Mehta, K. Bekaert, E. Rouah-Martin, W. De Coen, P. Dubruel, et al., Recent advances in recognition elements of food and environmental biosensors: a review, Biosens. Bioelectron. 26 (2010) 1178–94.

[40] S. Song, L. Wang, J. Li, J. Zhao, C. Fan, Aptamer-based biosensors, Trends Anal. Chem. 27 (2008).

[41] Z. Zhang, W. Yang, J. Wang, C. Yang, F. Yang, X. Yang, A sensitive impedimetric thrombin aptasensor based on polyamidoamine dendrimer, Talanta 78 (2009) 1240–1245.

[42] H. Yang, J. Ji, Y. Liu, J. Kong, B. Liu, An aptamer-based biosensor for sensitive thrombin detection, Electrochem. Commun. 11 (2009) 38–40.

[43] A. Wochner, M. Menger, D. Orgel, B. Cech, M. Rimmele, V.A. Erdmann, et al., A DNA aptamer with high affinity and specificity for therapeutic anthracyclines, Anal. Biochem. 373 (2008) 34–42.

[44] J. Zhao, L. Zhang, C. Chen, J. Jiang, R. Yu, A novel sensing platform using aptamer and RNA polymerase-based amplification for detection of cancer cells, Anal. Chim. Acta. 745 (2012) 106–11.

[45] Y.J. Lee, S.R. Han, J.-S. Maeng, Y.-J. Cho, S.-W. Lee, In vitro selection of Escherichia coli O157:H7-specific RNA aptamer, Biochem. Biophys. Res. Commun. 417 (2012) 414–20.

[46] J.R. Uzarski, C.M. Mello, Detection and Classification of Related Lipopolysaccharides via a Small Array of Immobilized Antimicrobial Peptides, Anal. Chem. 84 (2012) 7359–66.

[47] N. V Kulagina, M.E. Lassman, F.S. Ligler, C.R. Taitt, Antimicrobial peptides for detection of bacteria in biosensor assays, Anal. Chem. 77 (2005) 6504–8.

[48] M.S. Mannoor, S. Zhang, A.J. Link, M.C. McAlpine, Electrical detection of pathogenic bacteria via immobilized antimicrobial peptides, Proc. Natl. Acad. Sci. U. S. A. 107 (2010) 19207–12.

[49] S. Arcidiacono, P. Pivarnik, C.M. Mello, A. Senecal, Cy5 labeled antimicrobial peptides for enhanced detection of Escherichia coli O157:H7., Biosens. Bioelectron. 23 (2008) 1721–7.

[50] Y. Rosenfeld, Y. Shai, Lipopolysaccharide (Endotoxin)-host defense antibacterial peptides interactions: role in bacterial resistance and prevention of sepsis, Biochim. Biophys. Acta. 1758 (2006) 1513–22.

[51] N. V Kulagina, K.M. Shaffer, G.P. Anderson, F.S. Ligler, C.R. Taitt, Antimicrobial peptide-based array for Escherichia coli and Salmonella screening., Anal. Chim. Acta. 575 (2006) 9–15.

[52] N. V. Kulagina, G.P. Anderson, L.S. Frances, K.M. Shaffer, C.R. Taitt, Antimicrobial Peptides: New Recognition Molecules for Detecting Botulinum Toxins, Sensors 7 (2007) 2808–2824.

[53] A.W. Wark, J. Lee, S. Kim, S.N. Faisal, H.J. Lee, Bioaffinity detection of pathogens on surfaces, J. Ind. Eng. Chem. 16 (2010) 169–177.

[54] F. Long, A. Zhu, C. Gu, Recent Progress in Optical Biosensors for Environmental Applications, 2013.

[55] F. Long, A. Zhu, H. Shi, Recent advances in optical biosensors for environmental monitoring and early warning., Sensors 13 (2013) 13928–48.

[56] M.A. Cooper, Optical biosensors in drug discovery, Nat. Rev. Drug Discov. 1 (2002) 515–28.

[57] Y. Fang, Label-Free Cell-Based Assays with Optical Biosensors in Drug Discovery, Assay Drug Dev. Technol. 4 (2006) 583–595.

[58] B.-K. Oh, Y.-K. Kim, K.W. Park, W.H. Lee, J.-W. Choi, Surface plasmon resonance immunosensor for the detection of Salmonella typhimurium., Biosens. Bioelectron. 19 (2004) 1497–504.

[59] Nobelprize.org, The Fluorescence Microscope, Http://www.nobelprize.org/educational/physics/microscopes/fluorescence/. (2013).

[60] J.W. Lichtman, J. Conchello, Fluorescence microscopy, Nat. Methods. 2 (2005).

[61] A.J. Tudos, R.B.M. Schasfoort, Introduction to Surface Plasmon Resonance, 1968.

[62] R. Konradi, M. Textor, E. Reimhult, Using complementary acoustic and optical techniques for quantitative monitoring of biomolecular adsorption at interfaces, Biosensors 2 (2012) 341–376.

[63] J. Vörös, J.J. Ramsden, G. Csúcs, I. Szendrö, S.M. De Paul, M. Textor, et al., Optical grating coupler biosensors, Biomaterials 23 (2002) 3699–3710.

[64] N. Adányi, M. Varadi, N. Kim, I. Szendro, Development of new immunosensors for determination of contaminants in food, Curr. Appl. Phys. 6 (2006) 279–286.

[65] L. Diéguez, N. Darwish, M. Mir, E. Martínez, M. Moreno, J. Samitier, Effect of the refractive ndIex of buffer solutions in evanescent optical biosensors, Sens. Lett. 7 (2009) 851–855.

[66] W.K. Hartmann, N. Saptharishi, X.Y. Yang, G. Mitra, G. Soman, Characterization and analysis of thermal denaturation of antibodies by size exclusion high-performance liquid chromatography with quadruple detection, Anal. Biochem. 325 (2004) 227–239.

[67] L. Diéguez, D. Caballero, J. Calderer, M. Moreno, E. Martínez, J. Samitier, Optical gratings coated with thin Si3N4 layer for efficient immunosensing by optical waveguide lightmode spectroscopy, Biosensors 2 (2012) 114–126.

[68] N. Adányi, E. Németh, A. Halász, I. Szendro, M. Váradi, Application of electrochemical optical waveguide lightmode spectroscopy for studying the effect of different stress factors on lactic acid bacteria, Anal. Chim. Acta. 573-574 (2006) 41–7.

[69] I. Szendro, K. Erdelyi, M. Fabian, Z. Puskas, N. Adanyi, K. Somogyi, Combination of the optical waveguide lightmode spectroscopy method with electrochemical measurements, Thin Solid Films. 516 (2008) 8165–8169.

[70] J.S. Daniels, N. Pourmand, Label-Free impedance biosensors: opportunities and challenges., Electroanalysis 19 (2007) 1239–1257.

[71] F. Lisdat, D. Schäfer, The use of electrochemical impedance spectroscopy for biosensing., Anal. Bioanal. Chem. 391 (2008) 1555–67.

[72] Y. Wang, Z. Ye, Y. Ying, New trends in impedimetric biosensors for the detection of foodborne pathogenic bacteria, Sensors 12 (2012) 3449–71.

[73] X. Guo, A. Kulkarni, A. Doepke, H.B. Halsall, S. Iyer, W.R. Heineman, Carbohydrate-based label-free detection of Escherichia coli ORN 178 using electrochemical impedance spectroscopy, Anal. Chem. 84 (2012) 241–6.

[74] H. Chen, C. Heng, P. Puiu, X. Zhou, a Lee, T. Lim, et al., Detection of immobilized on self-assembled monolayer (SAM) of alkanethiolate using electrochemical impedance spectroscopy, Anal. Chim. Acta. 554 (2005) 52–59.

[75] V. Escamilla-Gómez, S. Campuzano, M. Pedrero, J.M. Pingarrón, Gold screen-printed-based impedimetric immunobiosensors for direct and sensitive Escherichia coli quantisation, Biosens. Bioelectron. 24 (2009) 3365–71.

[76] P. Leonard, Advances in biosensors for detection of pathogens in food and water, Enzyme Microb. Technol. 32 (2003) 3–13.

[77] R. Maalouf, C. Fournier-Wirth, J. Coste, H. Chebib, Y. Saïkali, O. Vittori, et al., Label-free detection of bacteria by electrochemical impedance spectroscopy: comparison to surface plasmon resonance, Anal. Chem. 79 (2007) 4879–86.

[78] H.T. Ng, A. Fang, L. Huang, S.F.Y. Li, Protein microarrays on ITO surfaces by a direct covalent attachment scheme, Langmuir 18 (2002) 6324–6329.

[79] L. Yang, Y. Li, G.F. Erf, Interdigitated Array microelectrode-based electrochemical impedance immunosensor for detection of Escherichia coli O157:H7, Anal. Chem. 76 (2004) 1107–13.

[80] P. D'Orazio, Biosensors in clinical chemistry, Clin. Chim. Acta. 334 (2003) 41–69.

[81] S.K. Parida, S. Dash, S. Patel, B.K. Mishra, Adsorption of organic molecules on silica surface., Adv. Colloid Interface Sci. 121 (2006) 77–110.

[82] A.A. Karyakin, G. V. Presnova, M.Y. Rubtsova, A.M. Egorov, Oriented immobilization of antibodies onto the gold Surfaces via their native thiol groups, Anal. Chem. 72 (2000) 3805–3811.

[83] I.S. Park, N. Kim, Thiolated Salmonella antibody immobilization onto the gold surface of piezoelectric quartz crystal, Biosens. Bioelectron. 13 (1998) 1091–7.

[84] F. Heitz, N. Van Mau, Protein structural changes induced by their uptake at interfaces, Biochim. Biophys. Acta. 1597 (2002) 1–11.

[85] H. Zhou, K.A. Dill, Stabilization of proteins in confined spaces, Biochemistry 40 (2001) 1–5.

[86] S. Cosnier, Biosensors based on electropolymerized films: new trends, Anal. Bioanal. Chem. 377 (2003) 507–20.

[87] J.C. Love, L. A. Estroff, J.K. Kriebel, R.G. Nuzzo, G.M. Whitesides, Self-assembled monolayers of thiolates on metals as a form of nanotechnology., Chem. Rev. 105 (2005) 1103–69.

[88] G.T. Hermanson, Bioconjugate Techniques, second edi, Academic Press, 2008.

[89] World Health Organization, Food safety and foodborne illness, Fact Sheet N° 237. (2007) Available at http://www.who.int/mediacentre/factsh.

[90] N. Camps, A. Domínguez, M. Company, M. Pérez, J. Pardos, T. Llobet, et al., A foodborne outbreak of Salmonella infection due to overproduction of egg-containing foods for a festival, Epidemiol. Infect. 133 (2005) 817.

[91] E. Alocilja, Market analysis of biosensors for food safety, Biosens. Bioelectron. 18 (2003) 841–846.

[92] M. Abadias, J. Usall, M. Anguera, C. Solsona, I. Viñas, Microbiological quality of fresh, minimally-processed fruit and vegetables, and sprouts from retail establishments, Int. J. Food Microbiol. 123 (2008) 121–9.

[93] World Health Organization, EHEC outbreak: Increase in cases in Germany, EHEC Outbreak Increase Cases Ger. World Heal. Organ. (2011) Available at http://www.who.int/csr/don/2011_06_02.

[94] C. Frank, M. Faber, M. Askar, H. Bernard, A. Fruth, A. Gilsdorf, et al., Large and ongoing outbreak of haemolytic uraemic syndrome, Euro Surveill. 16 (2011) 7–9.

[95] T. Tims, D. V. Lim, Confirmation of viable E. coli O157:H7 by enrichment and PCR after rapid biosensor detection, J. Microbiol. Methods. 55 (2003) 141–147.

[96] D. Li, Y. Feng, L. Zhou, Z. Ye, J. Wang, Y. Ying, et al., Label-free capacitive immunosensor based on quartz crystal Au electrode for rapid and sensitive detection of Escherichia coli O157:H7, Anal. Chim. Acta. 687 (2011) 89–96.

[97] O. Tokarskyy, D.L. Marshall, Immunosensors for rapid detection of Escherichia coli O157:H7 - perspectives for use in the meat processing industry, Food Microbiol. 25 (2008) 1–12.

[98] L. Yang, R. Bashir, Electrical/electrochemical impedance for rapid detection of foodborne pathogenic bacteria, Biotechnol. Adv. 26 (2008) 135–50.

[99] B. Ge, J. Meng, Advanced technologies for pathogen and toxin detection in foods: current applications and future directions, J. Assoc. Lab. Autom. 14 (2009) 235–241.

[100] K. Abu-Rabeah, A. Ashkenazi, D. Atias, L. Amir, R.S. Marks, Highly sensitive amperometric immunosensor for the detection of Escherichia coli, Biosens. Bioelectron. 24 (2009) 3461–6.

[101] A. Wolter, R. Niessner, M. Seidel, Detection of Escherichia coli O157:H7, Salmonella typhimurium, and Legionella pneumophila in water using a flow-through chemiluminescence microarray readout system, Anal. Chem. 80 (2008) 5854–63.

[102] S.-H. Chen, V.C.H. Wu, Y.-C. Chuang, C.-S. Lin, Using oligonucleotide-functionalized Au nanoparticles to rapidly detect foodborne pathogens on a piezoelectric biosensor., J. Microbiol. Methods. 73 (2008) 7–17.

[103] H. Tang, W. Zhang, P. Geng, Q. Wang, L. Jin, Z. Wu, et al., A new amperometric method for rapid detection of Escherichia coli density using a self-assembled monolayer-based bienzyme biosensor, Anal. Chim. Acta. 562 (2006) 190–196.

[104] A. Taylor, Q. Yu, S. Chen, J. Homola, S. Jiang, Comparison of E. coli O157:H7 preparation methods used for detection with surface plasmon resonance sensor, Sens. Actuators B 107 (2005) 202–208.

[105] A.D. Taylor, J. Ladd, Q. Yu, S. Chen, J. Homola, S. Jiang, Quantitative and simultaneous detection of four foodborne bacterial pathogens with a multi-channel SPR sensor, Biosens. Bioelectron. 22 (2006) 752–8.

[106] B.-K. Oh, W. Lee, B.S. Chun, Y.M. Bae, W.H. Lee, J.-W. Choi, The fabrication of protein chip based on surface plasmon resonance for detection of pathogens, Biosens. Bioelectron. 20 (2005) 1847–50.

[107] J. Waswa, J. Irudayaraj, C. Debroy, Direct detection of E. Coli O157:H7 in selected food systems by a surface plasmon resonance biosensor, LWT - Food Sci. Technol. 40 (2007) 187–192.

[108] J. Choi, B. Oh, Optical Detection of pathogens using protein chip, (2008) 348–362.

[109] Y. Su, X.L. , Li, A self-assembled monolayer-based piezoelectric immunosensor for rapid detection of Escherichia coli O157:H7, Biosens. Bioelectron. 19 (2004) 563–574.

[110] Z.-Q. Shen, J.-F. Wang, Z.-G. Qiu, M. Jin, X.-W. Wang, Z.-L. Chen, et al., QCM immunosensor detection of Escherichia coli O157:H7 based on beacon immunomagnetic nanoparticles and catalytic growth of colloidal gold, Biosens. Bioelectron. 26 (2011) 3376–81.

[111] D. Ivnitski, I. Abdel-hamid, P. Atanasov, E. Wilkins, Biosensors for detection of pathogenic bacteria, Science (80-. ). 14 (1999) 599–624.

[112] Z. Muhammad-Tahir, E.C. Alocilja, Fabrication of a disposable biosensor for Escherichia coli O157:H7 detection, IEEE Sens. J. 3 (2003) 345–351.

[113] C. Ruan, H. Wang, Y. Li, A bienzyme electrochemical biosensor coupled with immunomagnatic separation for rapid detection of Escherichia coli O157:H7 in food samples, Trans. ASABE. 45 (2002) 249–255.

[114] A.G. Gehring, D.L. Patterson, S.I. Tu, Use of a light-addressable potentiometric sensor for the detection of Escherichia coli O157:H7, Anal. Biochem. 258 (1998) 293–8.

[115] C. Ercole, M. Del Gallo, L. Mosiello, S. Baccella, a. Lepidi, Escherichia coli detection in vegetable food by a potentiometric biosensor, Sens. Actuators B 91 (2003) 163–168.

[116] C. Ruan, L. Yang, Y. Li, Immunobiosensor Chips for Detection of Escherichia coli O157:H7 Using Electrochemical Impedance Spectroscopy, Anal. Chem. 74 (2002) 4814–4820.

[117] P. Geng, X. Zhang, W. Meng, Q. Wang, W. Zhang, L. Jin, et al., Self-assembled monolayers-based immunosensor for detection of Escherichia coli using electrochemical impedance spectroscopy, Electrochim. Acta. 53 (2008) 4663–4668.

[118] A. Bogomolova, E. Komarova, K. Reber, T. Gerasimov, O. Yavuz, S. Bhatt, et al., Challenges of electrochemical impedance spectroscopy in protein biosensing, Anal. Chem. 81 (2009) 3944–9.

[119] D. Zhang, S. Chen, L. Qin, R. Li, P. Wang, Y. Li, The novel immunobiosensors for detection of Escherichia coli O157:H7 using electrochemical impedance spectroscopy., Proc. IEEE Eng. Med. Biol. 7 (2005) 7111–3.

[120] N.W. Turner, S. Subrahmanyam, S. a Piletsky, Analytical methods for determination of mycotoxins: a review., Anal. Chim. Acta. 632 (2009) 168–80.

[121] Food safety watch, the science of food safety, Ochratoxins, http://www.foodsafetywatch.org/factsheets/ochratoxins/ (2013).

[122] A. el Khoury, A. Atoui, Ochratoxin A: general overview and actual molecular status, Toxins. 2 (2010) 461–93.

[123] S.C. Duarte, C.M. Lino, A. Pena, Ochratoxin A in feed of food-producing animals: An undesirable mycotoxin with health and performance effects, Vet. Microbiol. 154 (2011) 1–13.

[124] S.S. Moises, M. Schäferling, Toxin immunosensors and sensor arrays for food quality control, Bioanal. Rev. 1 (2009) 73–104.

[125] M. Campàs, D. Garibo, B. Prieto-Simón, Novel nanobiotechnological concepts in electrochemical biosensors for the analysis of toxins, Analyst. 137 (2012) 1055–67.

[126] A.E. Urusov, S.N. Kostenko, P.G. Sveshnikov, A. V Zherdev, B.B. Dzantiev, Ochratoxin A immunoassay with surface plasmon resonance registration: Lowering limit of detection by the use of colloidal gold immunoconjugates, Sens. Actuators B 156 (2011) 343–349.

[127] J. Yuan, D. Deng, D.R. Lauren, M.-I. Aguilar, Y. Wu, Surface plasmon resonance biosensor for the detection of ochratoxin A in cereals and beverages, Anal. Chim. Acta. 656 (2009) 63–71.

[128] B. Prieto-Simón, I. Karube, H. Saiki, Sensitive detection of ochratoxin A in wine and cereals using fluorescence-based immunosensing, Food Chem. 135 (2012) 1323–9.

[129] J. A. Cruz-Aguado, G. Penner, Fluorescence polarization based displacement assay for the determination of small molecules with aptamers, Anal. Chem. 80 (2008) 8853–5.

[130] C.-K. Tsai, W.-C. , Hsieh, QCM-based immunosensor for the detection of ochratoxin A, Anal. Lett. 40 (2007) 1979–1991.

[131] B. Prieto-Simón, M. Campàs, J.-L. Marty, T. Noguer, Novel highly-performing immunosensor-based strategy for ochratoxin A detection in wine samples, Biosens. Bioelectron. 23 (2008) 995–1002.

[132] L. Bonel, J.C. Vidal, P. Duato, J.R. Castillo, An electrochemical competitive biosensor for ochratoxin A based on a DNA biotinylated aptamer, Biosens. Bioelectron. 26 (2011) 3254–9.

[133] B. Prieto-Simón, J. Samitier, “Signal Off” Aptasensor Based on Enzyme Inhibition Induced by Conformational Switch, Anal. Chem. (2014).

[134] J. Wu, H. Chu, Z. Mei, Y. Deng, F. Xue, L. Zheng, et al., Ultrasensitive one-step rapid detection of ochratoxin A by the folding-based electrochemical aptasensor, Anal. Chim. Acta. 753 (2012) 27–31.

[135] R. Khan, M. Dhayal, Chitosan/polyaniline hybrid conducting biopolymer base impedimetric immunosensor to detect Ochratoxin-A, Biosens. Bioelectron. 24 (2009) 1700–5.

[136] A. Radi, X. Mu, V. Lates, J. Marty, Label-free impedimetric immunosensor for sensitive detection of ochratoxin A, Biosens. Bioelectron. 24 (2009) 1888–1892.

[137] G. Castillo, I. Lamberti, L. Mosiello, T. Hianik, Impedimetric DNA aptasensor for sensitive detection of Ochratoxin A in food, Electroanalysis. 24 (2012) 512–520.

[138] A. Hayat, A. Sassolas, J.-L. Marty, A.-E. Radi, Highly sensitive ochratoxin A impedimetric aptasensor based on the immobilization of azido-aptamer onto electrografted binary film via click chemistry, Talanta 103 (2013) 14–9.

[139] N. Prabhakar, Z. Matharu, B.D. Malhotra, Polyaniline Langmuir-Blodgett film based aptasensor for ochratoxin A detection, Biosens. Bioelectron. 26 (2011) 4006–11.

# **Chapter 2.** ITO-based immunosensor for the detection of pathogenic bacteria

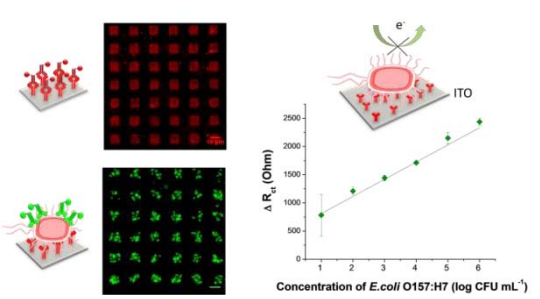


In this chapter, we take advantage of the outstanding properties of ITO material for the development of a novel highly sensitive and selective ITO-based immunosensor for the detection of pathogenic *E. coli* O157:H7 bacteria. The sensor build-up consisted on a simple, efficient and direct covalent binding of anti-*E. coli* O157 antibodies onto the ITO substrates. The functionalization methodology was fully characterized by multiple techniques, showing the specific binding of *E. coli* O157:H7 to the antibody-functionalized surface. The detection capacity of the ITO-based immunosensor was finally tested by EIS and very low concentrations of bacteria were detected (1 CFU $mL^{-1}$) in a large linear working range (10-$10^6$ CFU $mL^{-1}$). No significant adsorption of non-specific bacteria *Salmonella typhimurium* and *E. coli* k12 was observed. Our results reveal the applicability of ITO for the development of highly sensitive and specific label-free impedimetric immunosensors.

## Chapter index

## 2.1 Introduction

Indium tin oxide is a well-known transparent semiconducting oxide thin film, typically 90% of indium (III) oxide ($In_2O_3$) and 10% of tin (IV) oxide ($SnO_2$) by weight. ITO thin films have been produced by almost all physical and chemical methods, including reactive evaporation [1], reactive DC and RF sputtering [2], sol-gel process[3] and chemical vapor deposition [4]. Sputtering is the most versatile technique used for deposition of ITO thin films, offering high quality, purity and homogeneity in the overall sheet properties [5].

ITO has been widely applied in various optoelectronic devices, infrared reflectors, and display devices due to its high optical transmittance in the visible and near infrared regions, and high reflectance in the infrared region [6]. It has also been extensively used as transparent electrodes for spectroelectrochemical studies because of its low electrical resistivity and its wide electrochemical window [7–10]. The reversible change in the conductivity of ITO upon exposure to reducing gases and its high sensitivity towards toxic gases, such as nitric oxide, have also suggested the potential use of this material in sensors [11].

Besides its applicability in the above-mentioned areas, recent studies show that ITO could also be used as an ideal electrode for electrochemistry of biomolecules. The functional groups such as carboxylic acids, thiols and amines are reported to be responsible for achieving effective and stable immobilization. This suggests the feasibility of utilizing ITO as a novel substrate for performing direct one-step immobilization of small or even macro-biomolecules. Efficient immobilization of proteins, cells, oligonucleotide primers onto ITO optimized surfaces could be applied in

several fields such as the biosensor technologies, chip-based techniques for genomics and proteomics. The unique electrical and optical properties of ITO may potentially provide more efficient ways for signal transductions compared to traditional methods used in these fields. Figure 15 shows some examples of immobilization strategies applied in ITO-based biosensors.

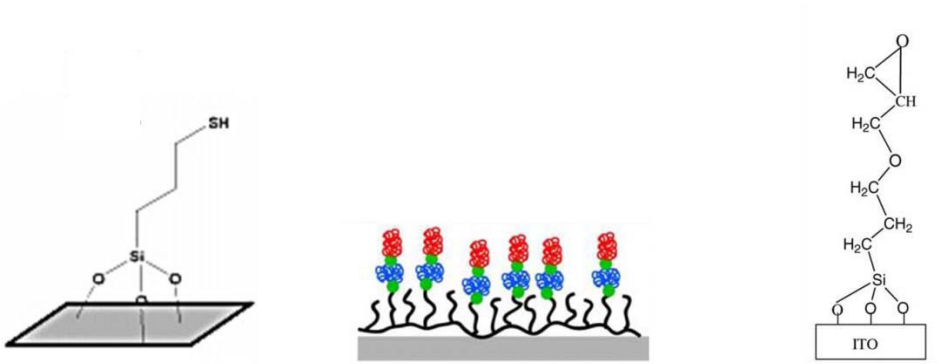


(a) Moore *et al* (b) Grieshaber *et al* (c) Yang *et al*

Figure 15. Immobilization strategies for the development of ITO-based biosensors described on literature. (a) DNA biosensor based on silanization functionalization; (b) enzyme biosensor using biotin-streptavidin strategy; (c) immunosensor using epoxysilanes.

Grieshaber *et al* [12] described a biotin-avidin strategy using biotin-poly(L-lysine)-g-poly(ethylene glycol) (biotin-PLL-g-PEG) for the immobilization of enzymes (Figure 15 (b)). Other described functionalization strategies of ITO is silanization using trifunctional silanes (Figure 15 (a)) [13], including epoxysilanes (Figure 15 (c)) [14]. Epoxysilane molecules adhere firmly on the ITO surface, being densely packed with virtually normal molecular orientation with their epoxy groups serving as surface groups. This arrangement allows the epoxysilane monolayer to serve as a template for chemical anchoring of the antibody layer [14]. In addition, the organic SAMs could render the surface hydrophobic for the later modification and form

very thin film insulating layers that prevent leak currents, unspecific adsorption, and the surface decomposition in aqueous electrolyte which is critically important especially for electrochemical biosensors.

Examples of ITO-based biosensors include DNA biosensors (Moore *et al* [13]), enzymes biosensors for early cancer diagnostics (Grieshaber *et al* [12]) or immunosensors for pathogenic detection (Yang *et al* [14]). In the last case, some immunosensors based on ITO surfaces for the detection of *E. coli* have been described [15–17] and they are shown in Figure 16.

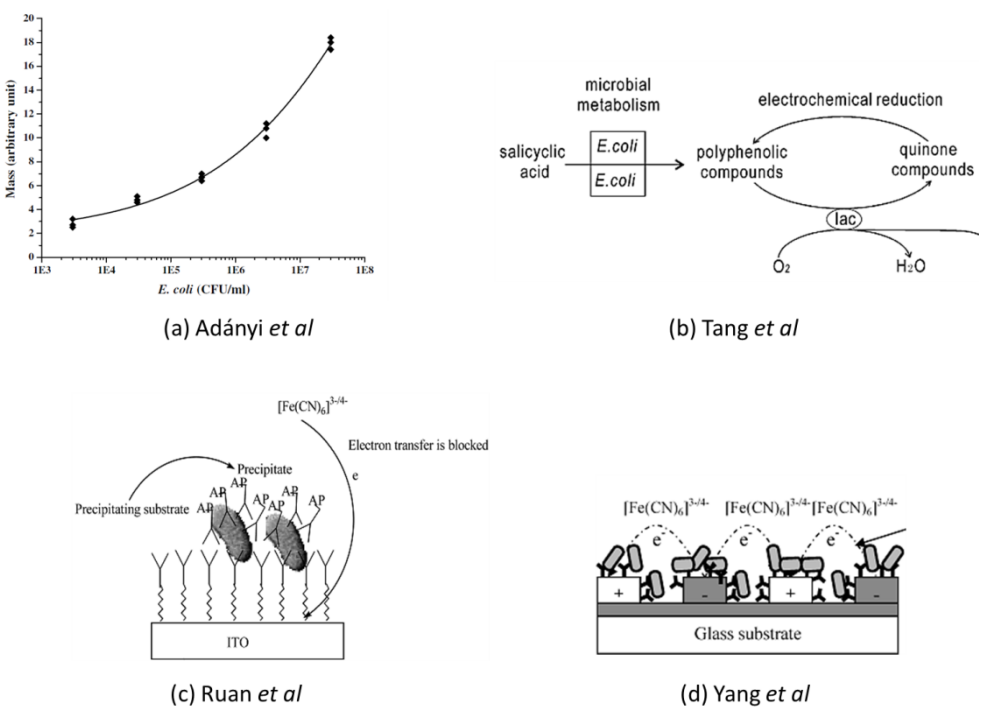


Figure 16. Examples of immunosensors based on ITO for the detection of *E. coli*. (a) OWLS immunosensor; (b) amperometric culture-based method; (c) label dependent impedimetric immunosensor; (d) label-free EIS immunosensor using an interdigitated array microelectrode.

Adányi *et al* [15] (Figure 16 (a)) developed a new label-free immunosensor using OWLS, obtaining a LOD of $3\times10^4$ CFU $mL^{-1}$ over a linear response between $3\times10^4$ and $3\times10^7$ CFU $mL^{-1}$. An amperometric culture-based method was developed by Tang *et al* [16] (Figure 16 (b)) for rapid detection of viable *E. coli* in water. This technique could shorten detection time down to 2 h with a detection limit of $4.5\times10^6$ CFU $mL^{-1}$. Ruan *et al* [17] (Figure 16 (c)) developed a label dependent immunosensor based on EIS, in which alkaline phosphatase-labelled secondary antibodies were used to amplify the signal by catalyzing the formation of an insoluble precipitate. They reported a linear response between $6\times10^4$ and $6\times10^7$ CFU $mL^{-1}$, with a limit of detection of $6\times10^3$ CFU $mL^{-1}$. Finally, Yang *et al* [18] described a label-free EIS immunosensor using an interdigitated array microelectrode, reporting a LOD of $1\times10^6$ CFU $mL^{-1}$.

Nonetheless, and as mentioned earlier, the high virulence and the extremely low infectious dose of *E. coli* O157:H7 required to origin infection diseases (less than 10 cells) [19, 20] foment the development of a more sensitive and specific immunosensor. In this chapter, an ITO-based immunosensor is proposed for the detection of very low concentration of pathogenic bacteria *E. coli* O157:H7. We use a direct and robust silanization method to efficiently functionalize the ITO electrodes. EIS is used for the label-free detection and monitorization of antibody-antigen coupling. The label-free characteristics of the impedimetric sensor avoid additional and unnecessary functionalization steps that complicate the system. This allows the development of more efficient, reliable and cheaper devices.

## 2.2 Experimental procedures

### 2.2.1 Chemicals and reagents

Phosphate-buffered saline (PBS), 3,3',5,5'-tetramethylbenzidine (TMB), 3-Glycidoxypropyldimethoxymethylsilane, 2-(2-aminoethoxy)ethanol (AEE), albumin from bovine serum (BSA), ammonium hydroxide (30%), and polyoxyethylenesorbitan monolaurate (Tween 20) were purchased from Sigma Aldrich (St.Louis, Mo, USA). Sodium hydrogen carbonate, hydrogen peroxide, acetone and absolute ethanol were supplied by Panreac (Barcelona, Spain). Potassium hexacyanoferrate(III) ($K_3Fe(CN)_6$) and potassium hexacyanoferrate(II) ($K_4Fe(CN)_6$) were from Fluka (Buchs, Switzerland).

Mouse monoclonal anti-*E. coli* O157 antibodies (primary capture antibody) and rabbit polyclonal anti-*Salmonella* horseradish peroxidase (HRP) conjugate were supplied from Abcam (Cambridge, UK). Polyclonal anti-*E. coli* HRP conjugate and polyclonal anti-*E. coli* FITC (fluorescein isothiocyanate) conjugate were purchased from Thermo Fisher Scientific (Rockford, IL, USA). Goat anti-rabbit IgG (Alexa Fluor 546) and Alexa Fluor 594 FluoroNanogold Fab' fragment of goat anti-mouse IgG were obtained from Invitrogen (Eugene, OR, USA).

A 10 mM PBS solution was used for all the experiments, coating buffer was prepared with 50 mM carbonate/bicarbonate at pH 9.6, and PBS-T buffer solution was PBS with 0.05% Tween 20. All the solutions were prepared with Milli-Q water (Millipore, USA).

### 2.2.2 Bacteria and culture plating methods

Bacteria samples were obtained in collaboration with the laboratories of Prof. Antonio Juárez and Dr. Eduard Torrents (IBEC, Barcelona, Spain). *Escherichia coli* O157:H7 Δ*stx*, *Escherichia coli* K12 and *Salmonella* enterica serovar *typhimurium* (*S. typhimurium*) wild-type SV5015 were routinely grown in Luria–Bertani (LB) medium at 37ºC. For cell quantification, overnight cultures were pelleted by centrifugation at 5000 × *g* for 5 min, and cells were re-suspended in 10 ml of PBS. The concentration of viable cells (CFU $mL^{-1}$) was obtained by plating a range of aliquots on LB agar plates (Figure 17). Standard samples of heat killed *E.coli* O157:H7 (KP-50-95-90) and *Salmonella typhimurium* (KP-50-74-01) were obtained from KPL (Gaithersburg, MD, USA).

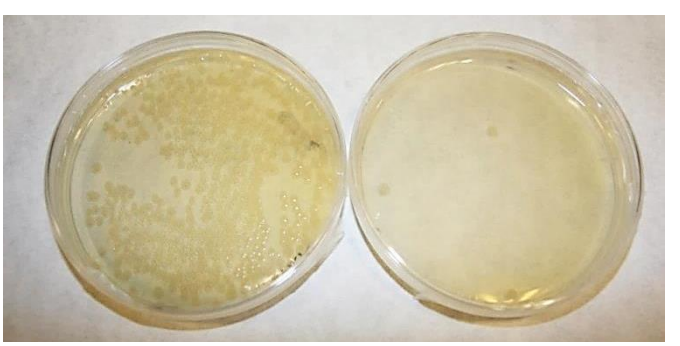

Figure 17. Examples of LB agar plates with different concentrations of viable *E. coli* O157:H7 bacteria.

### 2.2.3 ITO deposition and characterization

ITO electrodes were fabricated in collaboration with the GRF-Functional Coatings Group at the University of Minho (Braga, Portugal). The

ITO thin films were deposited on a 10×10 $mm^2$ glass (NTB, Switzerland) and on a 76 mm × 26 mm × 0.95 mm conventional glass microscope slide (Normax) by means of the DC Magnetron Sputtering system [21] from a 75 mm oxide sputtering target, $In_2O_3$:$SnO_2$=90:10wt.% (acquired from Goodfellow) without intentional heating.

Before film deposition, the sputtering chamber was pumped down to $3.5\times10^{-5}$ mbar using a combinatory system of a rotary pump (Alcatel ANNECY Ty-2033, PS – 33 $m^3\ h^{-1}$) and a diffusion pump (Edwards Vapor Pump EO4, PS – 600 L $s^{-1}$), which work together to maintain a high vacuum. Prior to each deposition, the ITO ceramic target was pre-sputtered for 5 min. Table 3 shows a summary of the deposition parameters used. An image of the fabricated ITO substrate is shown in Figure 18.

Table 3. Parameters used for sputtering ITO deposition.

| **Parameter** | **Value** |
|---|---|
| Base pressure (mbar) | $3.5x10^{-5}$ |
| Working pressure (mbar) | $2.7x10^{-3}$ |
| Deposition time (min) | 14:50 |
| Oxygen flow (sccm) | 0.8 |
| Argon flow (sccm) | 7.5 |
| Target current (mA) | 500 |
| Target/substrate distance (mm) | 80 |
| Deposition temperature (ºC) | RT* |

* *Room temperature*

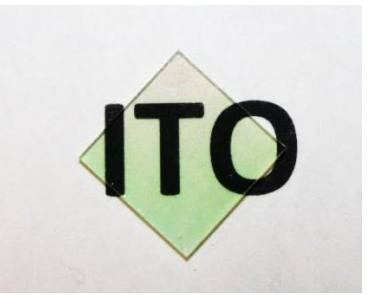


Figure 18. Image of the fabricated ITO substrate. Note its transparent optical properties.

The surface morphology and roughness of the produced thin films were analyzed using a commercial Dimensional 3100 Atomic Force Microscope (Veeco Instruments, USA). The Atomic Force Microscopy (AFM) measurements were performed in air using a silicon tip (MikroMasch, Estonia, NSC15/AIBS with spring constant of 40 N $m^{-1}$, resonance frequency of 325 kHz and a nominal tip radius of 10 nm) in tapping mode, at RT. AFM images were analysed with the WSxM software (Nanotec Electrónica SL) [22].

The optical transmittance spectra were recorded in a Shimadzu UV-310 PC Scanning Spectrophotometer. The resistivity of ITO thin films was measured by van der Pauw method, while the refractive index was analyzed by ellipsometry.

### 2.2.4 Surface cleaning and functionalization procedures

A schematic diagram for the immunosensor build-up is shown in Figure 19. ITO electrodes were functionalized with anti- *E. coli* O157 antibodies adhered onto an epoxide monolayer through an epoxy-amine reaction [17, 23]. The ITO substrates were first rinsed with acetone, absolute ethanol, and Milli-Q water (Millipore, USA). Afterwards, they were immersed

for 1 h in a solution of $H_2O_2$ (30%)/$NH_4OH$ (30%)/$H_2O$ (1:1:5 by volume), washed extensively with Milli-Q water, and dried under a stream of nitrogen (1). Afterwards, ITO substrates were immersed in a 3-Glycidoxypropyldimethoxymethylsilane ethanolic solution (1%) for 20 min. Subsequently, the samples were dried and placed in an oven at 110 ºC for 1 h. They were then thoroughly washed with ethanol and dried (2).

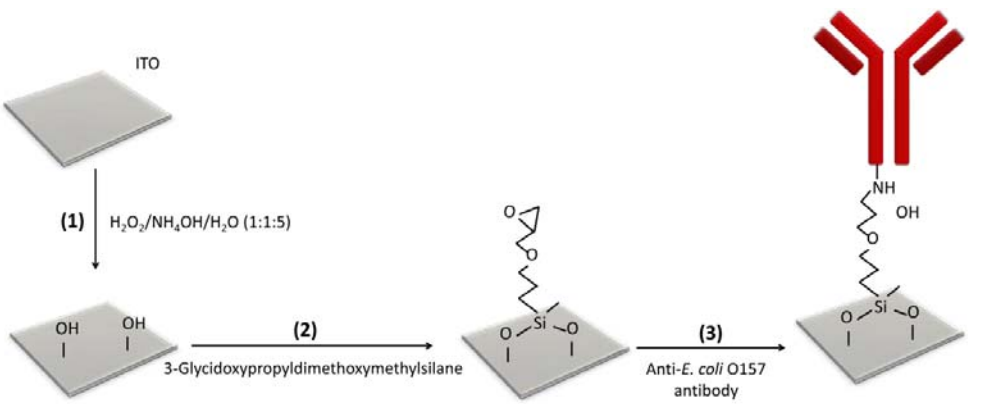


Figure 19. Schematic diagram showing the immunosensor fabrication: (1) hydroxylation, (2) SAM formation and (3) antibody binding.

The substrates were incubated with anti-*E. coli* O157 antibodies (15 µg $mL^{-1}$ solution in PBS) for 1h at RT (3). Finally, the substrates were washed with PBS and immersed in a 100 mM AEE in sodium bicarbonate buffer (pH 8) for 30 min to block the non-reacting chemical groups. Finally, it was washed and stored in a PBS solution at 4ºC prior to use.

### 2.2.5 OWLS experiments

A commercial OWLS instrument from MicroVacuum Ltd. (Budapest, Hungary) was used for real-time monitoring of the antibody-antigen

interaction using commercial ITO-coated sensor chips (OW 2400c Sensor Chip, MicroVacuum, Hungary). For electrochemical-OWLS (Ec-OWLS) experiments, a CH Instruments potentiostat (Austin, USA) was used.

The different solutions were injected with a peristaltic pump (Ismatec, Switzerland) at a flow of 56 µL $min^{-1}$. A solution of anti-*E. coli* O157 antibodies (15 µg $mL^{-1}$ in PBS) was injected and passed over the surface of the epoxysilane-functionalized ITO chips. After blocking the surface with a solution of AEE (10 mM), various concentrations of *E. coli* O157:H7 were incubated for 45 min and the response of the system was monitored. Electrochemical measurements were performed in 5 mM $Fe(CN)_6^{3-/4-}$ PBS solution (potential: 0.25 mV; amplitude: 10mV; frequency: 100 KHz – 0.1Hz).

### 2.2.6 Patterning of anti-*E. coli* O157 antibodies for bacteria detection

An anti-*E. coli* O157 antibody array was patterned on ITO surfaces using microcontact printing technique [24]. Firstly, a poly(dimethylsiloxane) (PDMS, Sylgard 184, Dow Corning) stamp with a regular array of square posts of 10 $\mu m^2$ and a pitch of 10 µm was replicated from a silicon master (Centre Nacional de Microelectrònica – CNM, Spain) as described elsewhere [25]. The stamp was incubated for 15 min with an anti-*E. coli* O157 solution (15 µg $mL^{-1}$ in PBS) and dried under a nitrogen flow. Afterwards, the PDMS stamp was placed in contact with the epoxysilane-modified ITO substrate for 2 min (see section 2.4). Non-patterned regions were blocked with 100 mM of AEE solution for 30 min. A secondary antibody labeled with Alexa Fluor 594 was used to confirm the patterned antibody (FluoroNanogold Fab' fragment of goat anti-mouse IgG).

The anti-*E. coli*-patterned substrate was incubated for 45 min with 400 µL of *E. coli* O157:H7 in PBS ($10^8$ CFU $mL^{-1}$). A sandwich structure was obtained by incubation with a secondary anti-*E. coli* polyclonal antibody labeled with a FITC fluorescent dye (0.1 mg $mL^{-1}$) for 1 h. To confirm the selectivity of the system, the same protocol was followed using non-specific bacterium (*S. typhimurium*). In this case, the sandwiched structure was obtained using a second rabbit anti-*Salmonella* antibody (1 µg $mL^{-1}$) and a secondary antibody labeled with a red fluorescent dye (5 µg $mL^{-1}$).

An Eclipse E1000 upright microscope (Nikon, Japan) equipped with a charge-coupled-device (CCD) camera was used for sample characterization. The fluorescence images were acquired using a 40× Nikon air objective and a FITC or G2A filter, and analyzed using ImageJ as image processing software.

### 2.2.7 Electrochemical measurements

EIS experiments were performed on a VMP2 multipotentiostat (Princeton Applied Research, France), using a three-electrode electrochemical cell (Figure 20) with an ITO working electrode (iii), a platinum counter electrode (iv) and an Ag/AgCl reference electrode (v), placed into a Faraday cage.

Measurements were performed in 5 mM $Fe(CN)_6^{3-/4-}$ PBS solution at RT, over a frequency range from 100 kHz to 1 Hz. The perturbation amplitude used was 10 mV and the potential was kept constant at 0.25 V. The data acquisition and analysis were accomplished using EC-Lab software (Bio-Logic SAS, France).

ITO electrodes functionalized with anti-*E. coli* O157 antibodies were exposed to different concentrations of *E. coli* O157:H7 for 45 min and the

impedance was measured after washing the surface with PBS. The same protocol was used to verify the specificity of the system with *Salmonella enterica* serovar *typhimurium* and *E.coli* K12.

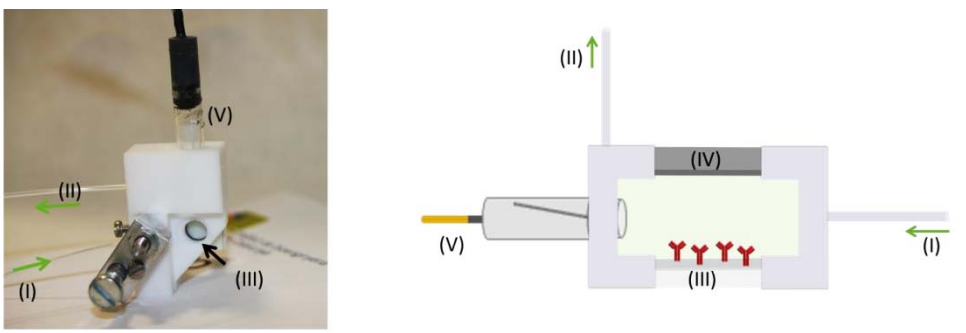


**Legend:**

(I) Inlet (II) Outlet (III) Working electrode (ITO)
(IV) Counter electrode (V) Reference electrode

Figure 20. *(Left)* Image of the electrochemical cell used for the detection of bacteria. *(Right)* Schematic diagram highlighting the different elements of the electrochemical cell.

Real complex samples were also monitored. For that purpose, blood plasma samples were obtained from the Hospital de Vall d'Hebron (Barcelona, Spain). A 100-fold plasma dilution (plasma 1%) was spiked with several concentrations of *E. coli* O157:H7, ranging from 10 to $10^6$ CFU $mL^{-1}$, and it was injected in the immunosensor. Samples without bacteria were used as negative controls.

### 2.2.8 ELISA protocol

Microtiter 96-well plates (Maxisorp, Nunc, Denmark) were coated overnight at 4ºC with an anti-*E. coli* O157 solution (15 µg $mL^{-1}$ in 0.05 M

carbonate buffer, pH 9.6). A blocking step was carried out using 2% BSA in PBS buffer. Afterwards, *E. coli* O157:H7 solutions at different concentrations (from $1\times10^4$ to $1\times10^5$ CFU $mL^{-1}$) were incubated to allow the immunological reaction. HRP-labeled polyclonal anti-*E. coli* solution (0.1 µg $mL^{-1}$) was then added. Each step was carried out for 1 h at RT. Finally, TMB solution was incubated for 15 min and the absorbance was read at 620 nm using a Benchmark Plus microplate spectrophotometer (Bio-Rad Laboratories Inc, USA). Between each step, the wells were thoroughly rinsed with PBS-T buffer and assays were performed in triplicate.

## 2.3 Results and discussion

In this section, we first describe the fabrication of the ITO-based electrodes followed by an accurate characterization of their morphology and physical properties. We next fully characterize and optimize the functionalization strategy needed for the development of the immunosensor. We finally study the performance of the sensor by means of different techniques and analyze its sensing capabilities by EIS.

### 2.3.1 Characterization of the ITO-surface fabrication and its functionalization

ITO thin films were deposited by means of DC Magnetron using the optimized conditions described in section 2.2.3. This process produces films of higher purity with better-controlled compositions, greater adhesive strength and homogeneity. The produced ITO substrates of 500 nm in thickness presented an optical transmittance above 80% in the visible region,

a refractive index of about 1.93 and low sheet resistance (about 45 Ω/square). The morphology of the deposited ITO was first characterized by means of AFM (Figure 21(a)).

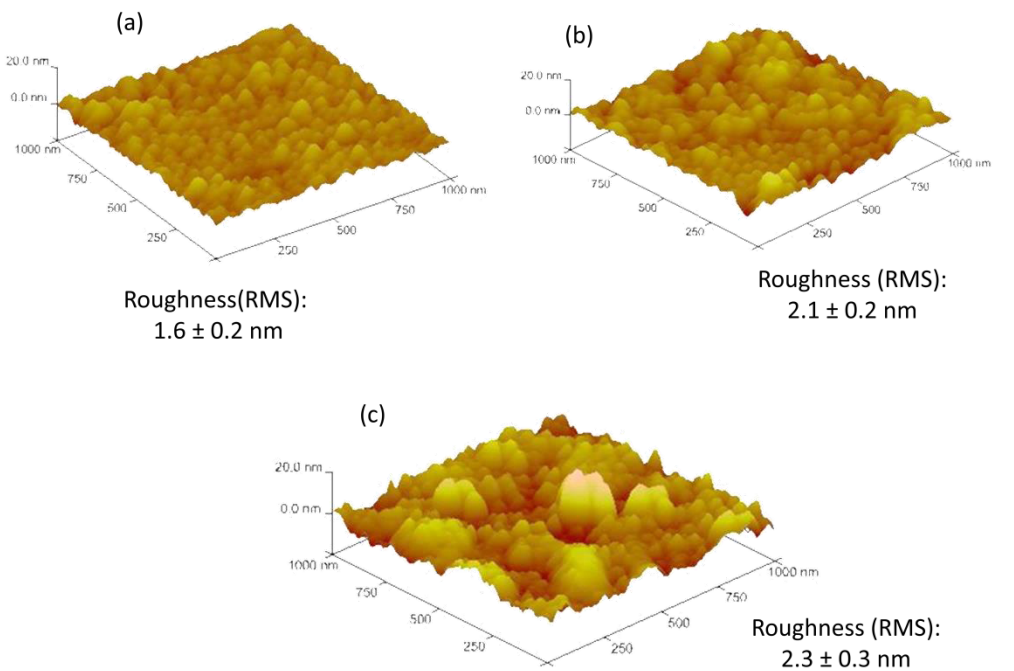


Figure 21. Topographic AFM images of (a) the bare ITO electrode, (b) the epoxysilane monolayer deposited on the ITO electrode, and (c) the immobilized antibody layer attached on the epoxysilane monolayer. Data is shown as mean ± s.d.

The bare ITO surface showed a uniform surface with an RMS roughness value of 1.6 ± 0.2 nm, favourable for the coverage of a functional layer and the binding of biomolecules [16]. The surface morphology of the ITO surface revealed grainy structures on the surface as described in previous works [26].

After functionalizing the electrodes with epoxysilane (Figure 21(b)) and subsequently with anti-*E. coli* O157 (Figure 21(c)), a roughness value of 2.1 ± 0.2 nm and 2.3 ± 0.3 nm was obtained, respectively. This increase in

roughness suggests the covalent attachment of the epoxysilane on the ITO surface and the antibodies immobilization on the epoxysilane monolayer. Comparing the morphology of the substrate before and after antibody attachment, we can observe that the latter shows bigger globular-looking structures, in agreement with the expected protein nature morphology of the antibodies.

We next studied the antibody surface coverage and surface functionalization by OWLS (Figure 22). OWLS presents several advantages compared to other characterization techniques regarding the quantification of molecules present on the sensor surface. In addition, it can be combined with electrochemistry measurements providing a better insight into the functionalization procedure [27].

First, cyclic voltammetry was used to characterize the epoxysilane attachment to the ITO surface (Figure 22 (a)). For this purpose, the response of the bare ITO electrode was measured in $Fe(CN)_6^{3-/4-}$ (blue line). A reversible cyclic voltammogram was obtained with the oxidation and reduction peaks of this redox couple clearly visible. After epoxysilane modification, a decrease in the current was detected (orange line) thereby confirming epoxysilane attachment to the ITO surface. The formation of the monolayer on the ITO electrode resulted in an insulating surface and thus blocked the faradic currents arising to the electrode surface. However, taking into account that the electrode current is not completely reduced (almost 50%) when compared with gold surfaces (see chapter 3, section 2.2.1), this could indicate that the silanization does not form a highly compacted layer and thus enables the access of the electroactive species to the electrode surfaces.

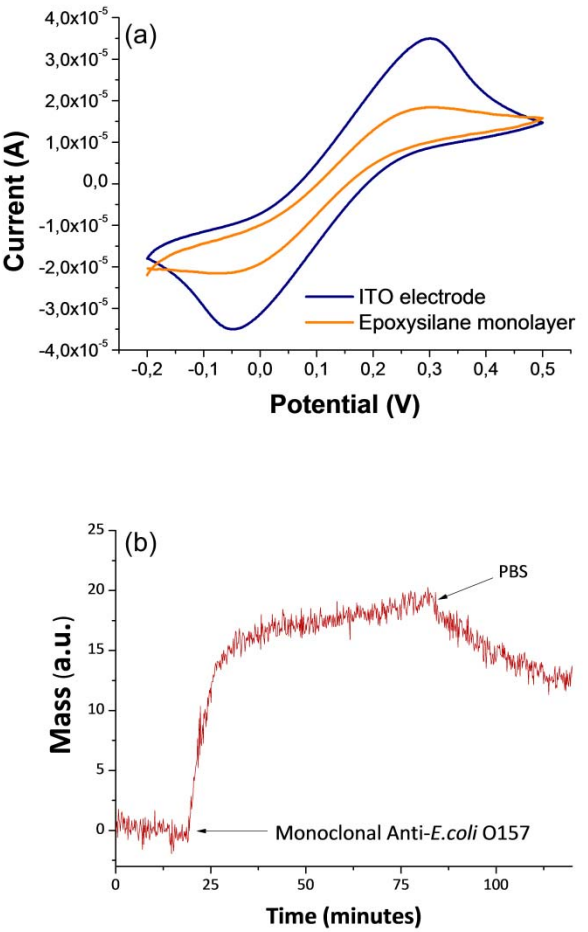


Figure 22. Characterization of the ITO electrode functionalization. (a) Cyclic voltammogram of the ITO electrode before (in blue) and after (in orange) modification with epoxysilane. (b) OWLS plot showing the anti-*E. coli* O157 antibody mass immobilization onto the epoxysilane-modified ITO chip.

We next measured the mass increase upon injection of the antibody solution (Figure 22 (b)). A small decrease in the signal was observed when PBS buffer was added, most probably due to the removal of loosely bound molecules. The variation of mass obtained for the anti-*E. coli* O157 antibody adsorbed onto the epoxysilane-modified surface was 12 ng $cm^{-2}$ (0.08 pmol $cm^{-2}$).

Altogether, these results show that the epoxysilane monolayer was successfully adhered onto the ITO electrodes as well as the antibodies. We will evaluate in the next section the recognition properties of the anti- *E. coli* O157 antibodies, critical step for the development of an immunosensor.

### 2.3.2 Evaluation of the surface functionalization and antibody detection capabilities

The specificity of the surface functionalization was first evaluated by fluorescence microscopy using an antibody array created by microcontact printing. An anti-*E. coli* O157 antibodies array was printed onto the epoxysilane monolayer using a PDMS stamp with an array of 10 × 10 $\mu m^2$ square posts (see section 2.2.6), which served as reactive sites for subsequent binding of the bacteria. The remaining free spots on the substrate were blocked with AEE. The fluorescent signal of the antibody pattern can be seen in Figure 23 (a), where a fluorescent secondary antibody specific to the capture antibodies was used (anti-mouse IgG labeled with a red fluorescent dye). Results indicate that the pattern of antibodies was successfully linked to the epoxysilane monolayer.

A secondary anti-*E. coli* antibody tagged with a green FITC fluorescent label was used to visualize the specific binding of bacteria to the primary antibody pattern (Figure 23 (b)). As expected, *E. coli* O157:H7 specifically bound to the patterned anti-*E. coli* O157 antibody surface, thus confirming the detection capacity of the antibodies and the complete functionalization protocol (including blocking steps). By considering the mean number of bacterial cells per spot (n = 100) and we estimated approximately 9±2

bacteria cells per square spots (100 $\mu m^2$), confirming a homogeneous and uniform distribution of captured bacterial cells around the ITO surface.

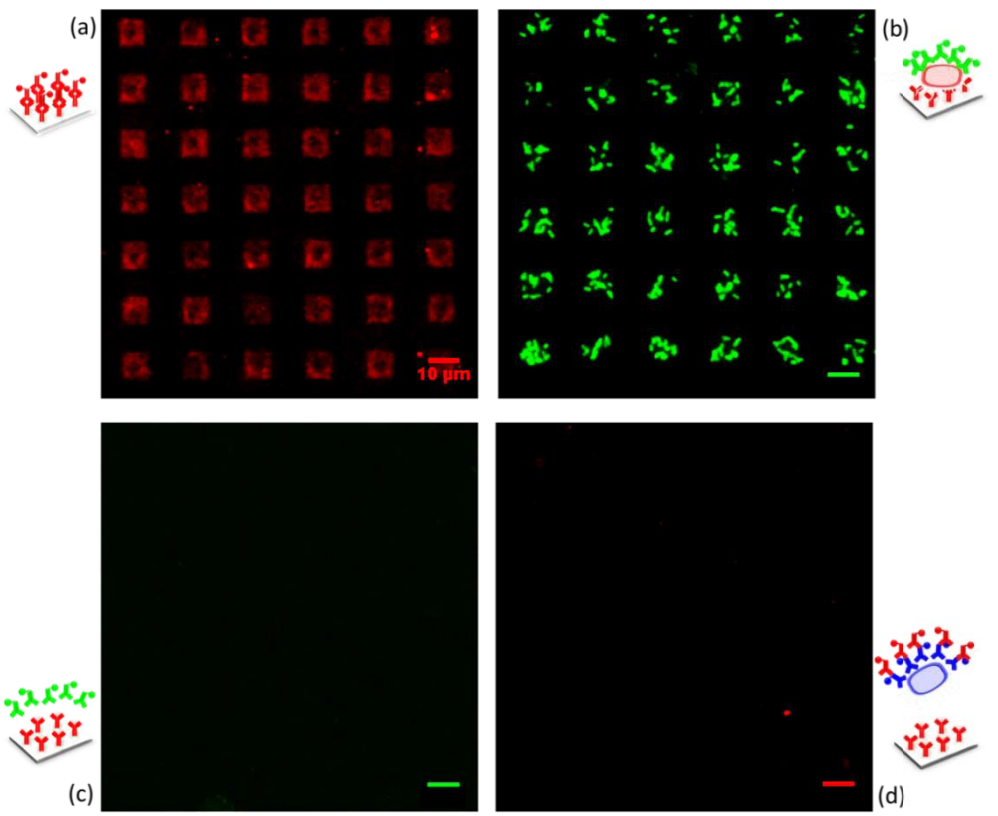


Figure 23. Fluorescence microscopy images of (a) an anti-*E. coli* O157 antibody pattern deposited on an epoxysilane monolayer with (b) *E. coli* O157:H7, (c) without bacteria and (d) using non-specific pathogenic bacteria *S. typhimurium*. Specific secondary fluorescent labelled antibodies were used (Scale bar: 10 µm).

We next performed two control experiments: the first one without any bacteria (Figure 23 (c)) and the second one using a non-specific bacteria *S. typhimurium* (Figure 23 (d)). On the latter, anti-*Salmonella* and Texas Red fluorescent labelled detection antibody were used to visualize *S. typhimurium*. No fluorescence signal was observed when no bacteria were added and almost non-specific adsorption of *Salmonella* was observed. The

binding of *S. typhimurium* on the antibody pattern was also estimated and compared to *E. coli* O157:H7. Considering the same number of antibody spots (100), a ratio of 1:500 *S. typhimurium / E. coli* O157:H7 cells was obtained, thereby confirming the efficiency and selectivity of the functionalization procedure. We next evaluate the detection capability of the immunosensor, in terms of sensitivity and its dynamic range.

### 2.3.3 Detection of *E. coli* O157:H7 by OWLS

OWLS was used to detect *E. coli* O157:H7 bacteria using the optimized functionalization strategy. The relationship between the bacteria concentration and mass variation (*Δm*) was plotted in a logarithmic scale as can be seen in Figure 24.

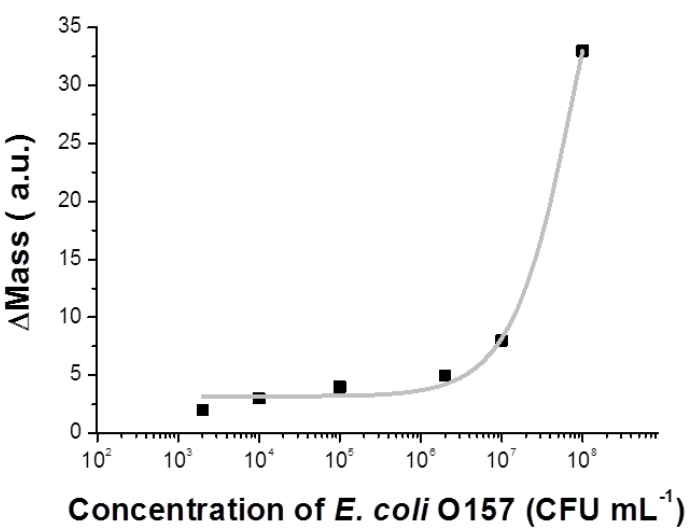


Figure 24. OWLS plot showing the variation of mass *vs E. coli* O157:H7 concentrations. Experimental data is shown as black squares and the line represents the fitting.

A significant mass variation was only achieved for bacteria concentrations higher than $1\times10^4$ CFU $mL^{-1}$, when compared with the blank or the control value (*S. typhimurium*, $\Delta m$ = 2 a.u.). Similar results were obtained by Adányi *et al* [15], in which the label-free and direct OWLS immunosensor was only able to detect $3\times10^4$ CFU $mL^{-1}$. Considering this high limit of detection and the extremely low infectious dose of *E. coli* O157:H7 required to origin infection [19, 20], further immunosensor development should be made to increase the sensitivity of the detection. For this purpose, immunodetection of *E. coli* O157:H7 bacteria were also evaluated in parallel with EIS using an external potentiostat. In this case, high differences in impedance spectrum were observed for bacteria concentrations lower than $10^4$ CFU $mL^{-1}$. This suggests that EIS is a more sensitive and adequate technique for being applied for the detection of bacteria, as it has been also described in literature [28].

### 2.3.4 Detection of *E. coli* O157:H7 by EIS

An impedimetric immunosensor was developed using a typical three-electrode electrochemical cell (see Methods on section 2.3.4.). Immunodetection of *E. coli* O157:H7 using EIS was based on the measurement of the faradaic impedance in the presence of the redox couple $[Fe(CN)_6]^{3-/4-}$. The electron transfer resistance of the redox probe reflects the number of bacteria cells attached on the surface in a concentration-dependent manner. Impedance spectra (Nyquist plot) were recorded for increasing concentrations of *E. coli* O157:H7, ranging from 0-$10^7$ CFU $mL^{-1}$, using ITO electrodes covered with specific detection antibodies (Figure 25 (a)).

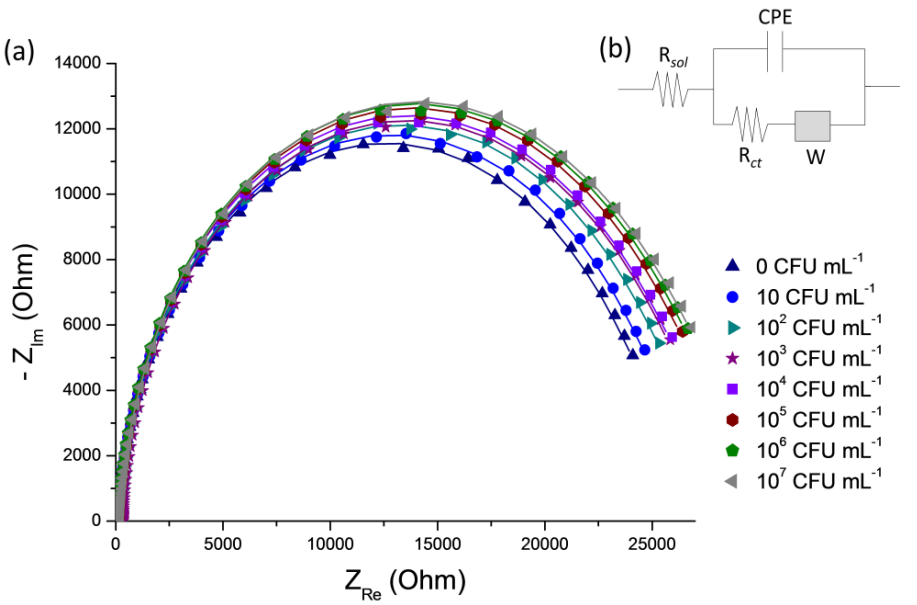


Figure 25. (a) Nyquist plot of impedance spectra for different *E.coli* O157:H7 concentrations in presence of $Fe(CN)_6^{3-/4-}$ as a redox probe. (Perturbation amplitude: 10 mV; potential: 0.25 V; frequency: 100 kHz to 1 Hz). The solid lines represent the data fitting obtained using the equivalent circuit model shown in (b).

In order to assess the physical origin of the observed impedance variation, we modelled the sensor response using an equivalent electrical circuit. The changes in the electrochemical properties of the redox probe were modelled fitting the experimental data using a Randles equivalent circuit model as shown in Figure 25 (b). In this equivalent circuit, $R_{ct}$ is the charge transfer resistance, *CPE* the constant phase element, *W* the Warburg impedance, and $R_{sol}$ the resistance of the solution (see section 1.1.2.2). As mentioned earlier, the Warburg impedance results from the diffusion of ions from the bulk electrolyte to the electrode. The $R_{sol}$ arises from the finite conductance of the ions in bulk solution. The *CPE* reflects inhomogeneities and defects of the layer and it is often modeled instead of a pure capacitance. Defects in the deposition of the insulating layer (pin-holes) and the presence of ions and water molecules within the protein structure are believed to be

the major reasons for the observed non-ideal dielectric behavior. The *CPE* is defined as $1/(Aj\omega)^{\alpha}$, where *A* is the equivalent of a capacitance, $\omega$ is the frequency (rad $s^{-1}$) and 0.5 <$\alpha$ <1 [29].

The electron-transfer kinetics and diffusion characteristics can be extracted from the impedance spectrum (see Figure 25 (a)), where the intercept of the semicircle with $Z_{re}$ axis at high frequencies is equal to $R_{sol}$ and the semicircle diameter equals $R_{ct}$. The data shows a clear increase in the semi-circles curves upon addition of the different bacteria concentrations. The quality of the fitting was evaluated by an acceptable error value ($\chi^2$ < 0.01) and the results are shown in Table 4.

Table 4. Fitting data for the observed impedance variation using a Randles equivalent circuit.

| [*E. coli* O157:H7] (CFU $mL^{-1}$) | $R_{sol}$ (Ω) | CPE (nF $s^{(\alpha-1)}$) | α | $R_{ct}$ (Ω) | W (Ω $s^{-1/2}$) |
|---|---|---|---|---|---|
| 0 | 109.3±0.2 | 1269.0±0.3 | 0.96±0.50 | 24342±8 | 2246±6 |
| 10 | 119.5±0.2 | 1242.0±0.3 | 0.96±0.50 | 24864±8 | 2424±7 |
| $10^2$ | 179.9±0.2 | 1229.0±0.3 | 0.96±0.50 | 25507±8 | 2520±7 |
| $10^3$ | 337.2±0.2 | 1212.0±0.3 | 0.96±0.50 | 25750±8 | 2714±7 |
| $10^4$ | 103.3±0.2 | 1204.0±0.3 | 0.96±0.50 | 26063±8 | 2741±7 |
| $10^5$ | 138.9±0.2 | 1198.0±0.3 | 0.96±0.50 | 26567±8 | 2799±7 |
| $10^6$ | 105.5±0.2 | 1189.0±0.3 | 0.96±0.50 | 26826±8 | 2874±7 |
| $10^7$ | 188.5±0.2 | 1178.6±0.3 | 0.96±0.50 | 26978±8 | 2874±7 |

As shown in Table 4, a slight variation of $R_{sol}$ and an increase in the *W* values can be seen for all the concentrations. Since the bacterial cells are attached to the surface, this impairs the diffusion of redox species to the electrode, thereby increasing the Warburg impedance. Ideally, these

parameters represent bulk properties of the electrolyte solution and diffusion features of the redox probe in solution, thus are not affected by modifications that occur on the surface of the electrode.

The parameters $R_{ct}$ and *CPE* are determined by the insulating and dielectric characteristics at the interface of the electrode and electrolyte solution, and consequently are affected by the changes on electrode surfaces. Considering the impedance characteristics of the cell membranes, as reported by Pethig *et al* [30] that natural cell membranes (thickness 5–10 nm) show a membrane capacitance of 0.5–1.3 μF $cm^{-2}$ and a membrane resistance of $10^2$–$10^5$ Ω $cm^{-2}$, the binding of *E. coli* to the electrode surface should affect the impedance response of the system.

Experimental data revealed a decrease in the *CPE* when the concentration of *E. coli* O157:H7 increased (see Table 4). A linear relationship was observed between 10 and $10^4$ CFU $mL^{-1}$ (*CPE*=-0.0132 log ([*E. coli* O157:H7])-0.0075, $R^2$ = 0.999). The $\alpha$ values were close to 1 for all the concentrations tested. This observation indicates that the CPE behaved as a typical double layer capacitance, $C_{dl}$ (see section 1.1.2.2). The $C_{dl}$ has been reported to be correlated with the number of bacteria attached to the electrode surface which is defined by $C_{dl} = \frac{\varepsilon\varepsilon_0 A}{d}$, where ε is the dielectric constant of the electrolyte and $\varepsilon_0$ is the permittivity of the free space, whereas *A* is the electrode area and *d* is the thickness of the double layer [29]. Considering that the area and electrolyte composition were constant, the $C_{dl}$ would be dependent mainly on the thickness of the double layer. The attachment of the bacterial cells onto the modified electrode blocked the surface and consequently $C_{dl}$ decreased.

The $R_{ct}$ was highly sensitive to changes produced by the binding of *E. coli* O157:H7 to the antibody-modified ITO surface and therefore it was

chosen as the ideal parameter to quantify the sensor performance. The $R_{ct}$ increased upon the addition of consecutive concentrations of *E. coli* O157:H7 (see Table 4). A linear relationship between the variation of electron-transfer resistance, $\Delta R_{ct}$, and the logarithmic concentration of *E. coli* O157:H7, ranging from 10-$10^6$ CFU $mL^{-1}$, is shown in Figure 26. This increase might be related to the number of bacterial cells captured on the electrode surface, delaying the interfacial electron-transfer kinetics and increasing the electron transfer resistance [17].

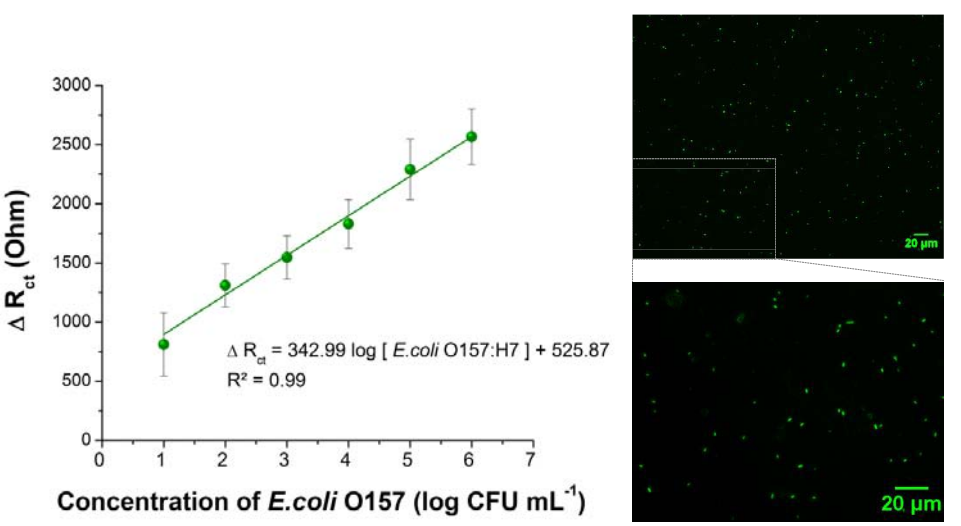


Figure 26. *(Left)* Variation of the charge transfer resistance ($\Delta R_{ct}$) versus *E. coli* O157:H7 concentrations (log CFU $mL^{-1}$) for the ITO-based impedimetric immunosensor. Data is shown as mean ± s.d. *(Right)* Fluorescent images of the ITO antibody-modified electrode after impedance measurements showing the adhered bacteria (in green).

A very low LOD (1 CFU $mL^{-1}$) was obtained in 1 h (including incubation) by the developed label-free immunosensor. The LOD was calculated using the equation $y_b + 3 \times Std_b$ [31], where $y_b$ is the value for the blank ($R_{ct}$ of the PBS solution without bacteria) and $Std_b$ is the standard deviation. To the best of

our knowledge, this LOD is much lower than those previously reported for other impedimetric immunosensors based on ITO electrodes [17, 18, 32] and highlights the performance of our developed immunosensor (see table 1). This low LOD might be attributed with the surface functionalization protocol, together with the binding efficiency of the immobilized anti-*E. coli* O157 antibody to the bacteria.

According to Solomun *et al* [33], the use of difunctional alkoxysilanes, instead of the widely used trifunctional silanes, to silanize substrates and immobilize biomolecules is more favorable. Their results showed that the trifunctional silanes produce branched and cyclic siloxanes moieties, while the difunctional silane creates mainly short straight siloxane chains. Following our approach, we achieved a 30% increase in binding efficiency using difunctional silane when compared to previous studies that used trifunctional silanes [17]. This binding efficiency was calculated on the basis of the average number of *E. coli* O157:H7 cells observed by fluorescence microscopy (9 bacterial cells/100 $\mu m^2$, section 2.3.2) when 400 µL of *E. coli* O157:H7 ($10^8$ CFU $mL^{-1}$) was added to the substrate. Many factors such as the immobilization and affinity of the antibodies, affinity of the antibodies and the nature between of the immune-reaction the antigens and the cell surface may lead to the increase of the binding efficiency of the antibody-modified surface, as claimed by Yang *et al* [14].

Additionally, our approach shows a large linear detection range from 10-$10^6$ CFU $mL^{-1}$ ($\Delta R_{ct}$ = 343 log ([*E. coli* O157:H7]) + 526, R = 0.99) (see Figure 26). This large range could allow measurements using real samples with unknown concentration by simply measuring series of dilutions without the need for sample pre-treatment or concentration steps. Figure 26 also shows fluorescence microscopy images of the electrode after the impedance

measurements. The images demonstrate that the bacteria were successfully adhered on the antibody-modified ITO surface.

We finally tested the developed immunosensor for the detection of heat-killed *E. coli* O157:H7 samples. Bacterial inactivation methods can cause cell disruption that could be involved in antigen release which results in an increased detectability. Increasing concentrations of heat-killed *E. coli* O157:H7 bacteria were added on the system and a linear relationship between the difference of electron-transfer resistance and the logarithmic of *E. coli* O157:H7 concentration was obtained in the range $3\times10$ -$3\times10^5$ CFU $mL^{-1}$ ($\Delta R_{ct}$ = 318 log [*E. coli* O157:H7] + 307, $R^2$ = 0.93). Almost the same limit of detection (2 CFU $mL^{-1}$) and sensitivity were obtained for heat-killed *E. coli* O157:H7 bacteria compared with viable bacteria. This is critically important in order to truly rely in the detection capabilities and efficiency of the developed sensor.

### 2.3.5 Reproducibility, stability and specificity of the impedrimetric immunosensor

Important parameters for the development of a highly performance immunosensor are reproducibility, stability and specificity. We first studied the reproducibility by preparing several immunosensors and we then compared their $R_{ct}^{Ab+bacteria}/R_{ct}^{Ab}$ ratios. A relative standard deviation (RSD) of 3% was obtained (n=3), indicating a good reproducibility.

Immunosensor stability was first addressed by storing the sample at 4ºC in PBS for 48 h. No significant reduction in the detection capacity of the sensor was observed when compared to freshly prepared sensors. However,

sensitivity of the device decreased by 30% when stored for 2 weeks, indicating a degradation of the biorecognition layer.

Finally, the sensor specificity was studied using non-specific *S. typhimurium* bacteria. Figure 27 shows the ratio of $R_{ct}$ variation for the bacteria at a range of concentrations. Results show that the immunosensor was not sensitive to *S. typhimurium,* thus proving the efficiency of the system. In addition, non-pathogenic bacteria *E. coli* K12 were also used to test the specificity. Even at high concentrations ($10^6$ CFU $mL^{-1}$) the signal was lower than 20%, thereby demonstrating the specificity of the system to different *E. coli* strains.

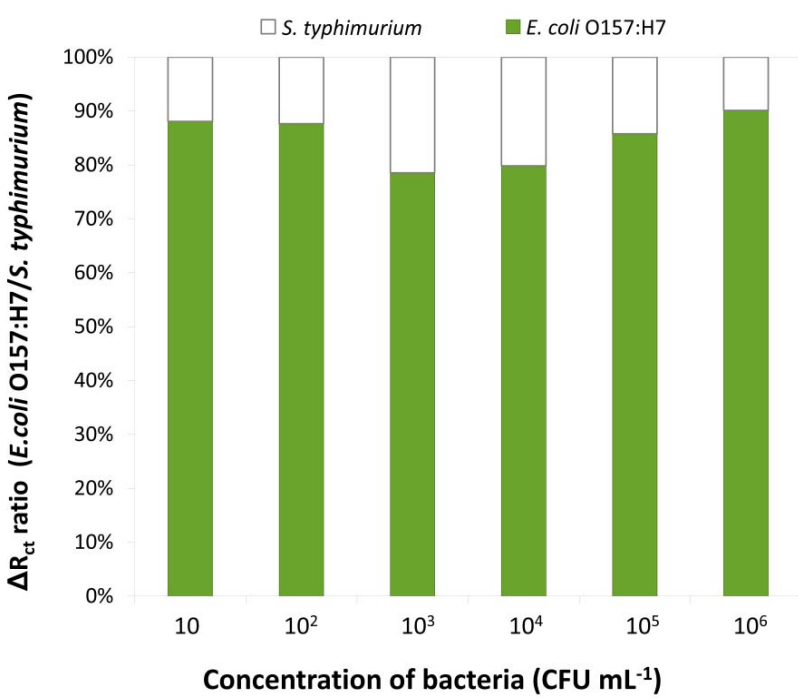


Figure 27. Study of the immunosensor specificity using the ratio between $\Delta R_{ct}$ of *E. coli* O157:H7 and *Salmonella typhimurium*.

In summary, the developed immunosensor demonstrated the following properties: (i) highly sensitive; (ii) showed good reproducibility; (iii) presented high stability; (iv) it was high specific. We then compared these results with those obtained using other techniques commonly used for bacteria detection.

### 2.3.6 Comparison with standard detection methodologies: ELISA test

ELISA is a conventional immunological method applied for pathogen detection [34]. We used this technique in order to study the immunoreaction response between the anti-*E. coli* O157 antibody and the *E. coli* O157:H7 and compare it with the characteristics demonstrated by our ITO-based EIS immunosensor (see section 2.3.5).

We used the same anti-*E. coli* O157 antibody as a capture antibody, while the detection antibody was linked to an enzyme (HPR). Figure 28 shows the obtained linear relationship response between the absorbance and the concentration of *E. coli* O157:H7 (Absorbance = $5\times10^{-7}$ [*E. coli* O157:H7] + 0.081, R = 0.999).

Results indicate that the anti-*E. coli* O157 antibody and the *E. coli* O157:H7 immunoreact over a linear range between $4\times10^{4}$ and $7.5\times10^{5}$ CFU $mL^{-1}$ (Figure 28), with a LOD of $1x10^{4}$ CFU $mL^{-1}$. The data shows that, when compared to the EIS ITO-based immunosensor, both the linear range and the LOD show a weaker response.

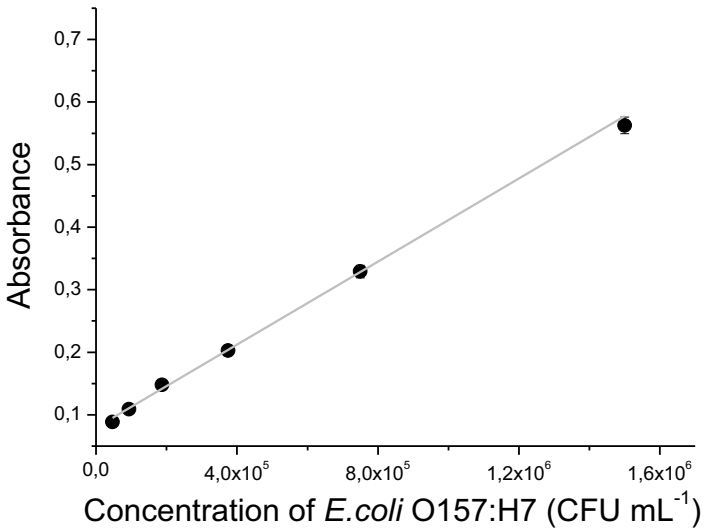


Figure 28. ELISA test of the reactivity of anti-*E.coli* O157 antibodies to *E.coli* O157:H7. The graphic shows the absorbance as function of bacteria concentration.

Altogether, this confirms that the combination of biosensor strategy on ITO substrates with EIS is appropriate for the development of sensitive pathogen impedimetric immunosensors and provides an interesting potential alternative to commercially available ones. For this purpose, we will finally test our device using a complex (real) sample and study sensor performance.

### 2.3.7 Measurements in real samples

According to researchers from Departament of Microbiology headed by Dr. Guillem Prats at the Hospital Vall d'Hebron (Barcelona, Spain) and the report "*Annual Report Communicable Diseases in Epidemiologic Europe"* at the *"European Center for Disease Prevention and Control*" (ECDC, 2007) [35], three main pathogenic species are of great clinical relevance: *Escherichia coli*, *Aureginosa Pseudomonas* and *Staphylococcus aureus* (Figure 29). They cause

nosocomial diseases in which, in some cases, antimicrobial resistance is very pronounced, endangering the patient because of late diagnosis and inadequate treatment.

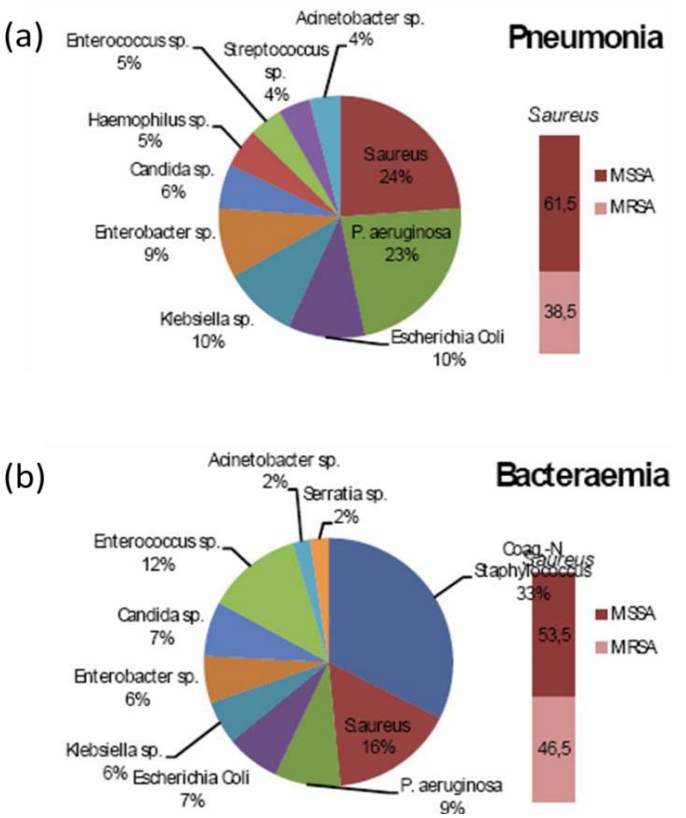


Figure 29. The graphs show the main microorganisms causing (a) pneumonia and (b) bacteraemia in hospitals. The bars show the alarming percentage of cases in which the microorganisms are resistant to treatment with the usual antibiotic (MRSA: Metaciclin-Resistant Staphylococcus aureus; MSSA: Metaciclin-Sensitive Staphylococcus aureus) [*Source*: internal report].

The concentration of microorganisms may differ widely depending on the disease, the idiosyncrasies of the patient and the type of sample that is analyzed to identify the organism. Thus, cerebrospinal fluid can have between 1 to 1000 CFU $mL^{-1}$; urine can have between $10^3$ to $10^6$ CFU $mL^{-1}$ and

in the case of septicemia a level of only 1-10 CFU $mL^{-1}$ indicates a severe state of the patient. If the diagnosis is not made promptly and properly treated, the patient may progress rapidly to a septic shock leading to death in 50% of cases. This highlights the critical importance of developing novel and alternative detecting methods, which includes new protocols, technologies and/or materials.

We used complex samples such plasma samples of human blood with *E. coli* O157:H7 and evaluated the response of the ITO-based immunosensor. In this case, plasma was diluted with PBS to minimize the matrix effect. The variation of $R_{ct}$ between the PBS and plasma (10 % and 1%) was compared. An increase of 41% and 9% was obtained for plasma 10% and plasma 1%, respectively. Considering these results we used plasma 1% for the experiments due to the smaller background signal.

Since plasma contains dissolved proteins and this complex media could affect the sensor response, the influence of successive injections of plasma 1% on the immunosensor surface was studied. For this purpose, normalized $R_{ct}$ $((R_{ct} - R_{ct}^{Plasma})/R_{ct}^{Plasma})$ was calculated for successive injection of plasma 1%. A mean of 0.059 ± 0.014 (n=7) was obtained and it was subtracted from the data obtained in plasma samples spiked with *E. coli* O157:H7. Figure 30 shows the plot of the normalized $R_{ct}$, without plasma inaccuracy, as a function of the logarithmic *E. coli* O157:H7 concentration in plasma 1%.

The $R_{ct}$ increased with the concentration of bacteria in plasma 1%. A linear relationship between 10 to $10^6$ CFU $mL^{-1}$ was achieved (Normalized $R_{ct}$ = 0.038 log [*E. coli* O157:H7] -0.024, $R^2$ = 0.97). Comparing these results with the ones obtained in PBS (Normalized $R_{ct}$ = 0.0147 log [*E. coli* O157:H7] - 0.0128, $R^2$ = 0.97), a 35% increase in the slope of the calibration curves was

obtained. This increase may be due to the unspecific affinity of substances in the biological samples and the sample complexity. In addition, almost no signal was observed for the lower concentrations (10 CFU $mL^{-1}$), the maximum limit expected to determine for the diagnosis of septicemia.

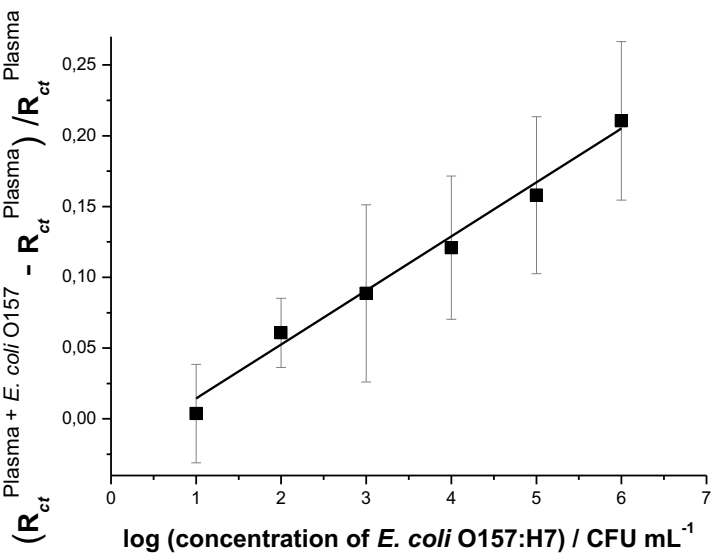


Figure 30. Normalized signal of $R_{ct}$ versus *E.coli* O157:H7 concentrations in plasma 1% (log CFU $mL^{-1}$) for the ITO-based impedimetric immunosensor. Data is shown as mean ± s.d..

We conclude that the improvement of the sensor sensitivity together with a fast response time is a hallmark for the development of efficient and reliable commercial immunosensors when applied in real complex samples. This still remains a challenge and will become a field of prolific research in the upcoming years.

## 2.4 Conclusions and perspectives

In this chapter, a label-free immunosensor for the detection of very low concentrations of pathogenic *E. coli* O157:H7 bacteria on ITO electrodes was described. The sensor properties and detection capabilities were studied and characterized by means of multiple techniques, including AFM, fluorescence microscopy and OWLS techniques. Results showed the efficiency and high selectivity of the developed sensing platform.

The functionalization protocol was optimized and applied for the detection of *E. coli* O157:H7 bacteria by means of electrochemical impedance spectroscopy. A limit of detection of 1 CFU $mL^{-1}$ was obtained, over a wide linear dynamic range. It was also demonstrated that the immunosensor was equally sensitive to heat-killed bacteria compared to whole bacteria or viable bacteria.

To our knowledge, this is the first impedimetric immunosensor based on ITO with such a low limit of detection. This opens the door to the development of new sensing devices based on ITO. In particular, this work could have important applications for the detection of low concentrations of pathogenic bacteria, and potentially, becoming an alternative to more standard and conventional detection methods. However, detection of very low concentrations of *E. coli* O157:H7 in complex samples such as blood plasma remains still a challenge. In this case, additional pre-concentration steps or adding a finely filtration step prior detection could optimized the sensor response.

## 2.5 References

[1] M. Yamaguchi, A. Ide-Ektessabi, H. Nomura, N. Yasui, Characteristics of indium tin oxide thin films prepared using electron beam evaporation, Thin Solid Films. 447-448 (2004) 115–118.

[2] N. Danson, I. Safi, G.W. Hall, R.P. Howson, Techniques for the sputtering of optimum indium-tin oxide films on to room-temperature substrates, Surf. Coatings Technol. 99 (1998) 147–160.

[3] M.J.U. Alam, D.C. Cameron, Optical and electrical properties of transparent conductive ITO thin films deposited by sol- gel process, Thin Solid Films. 377-378 (2000) 455–459.

[4] K. Maki, N. Komiya, A. Suzuki, Fabrication of thin films of ITO by aerosol CVD, Thin Solid Films. 445 (2003) 224–228.

[5] C. H. L. Hartnagel, A. L. Dawar, A. K. Jain, C. Jagadish, Semiconducting transparent thin films, Institute of Physical Publishing: Bristol, 1995.

[6] H. Kim, a. Piqué, J.S. Horwitz, H. Mattoussi, H. Murata, Z.H. Kafafi, et al., Indium tin oxide thin films for organic light-emitting devices, Appl. Phys. Lett. 74 (1999) 3444.

[7] A. Malinauskas, R. Holze, A UV-vis spectroelectrochemical study of redox reactions of solution species at a polyaniline electrode in the conducting and the reduced state, J. Electroanal. Chem. 461 (1999) 184–193.

[8] S. Vico, V. Carlier, C. Buess-Herman, Spectroelectrochemical study of the influence of anions on the behaviour of poly(N-vinylcarbazole) films, J. Electroanal. Chem. 475 (1999) 1–8.

[9] S.E. Ross, C.J. Seliskar, W.R. Heineman, Spectroelectrochemical sensing based on multimode selectivity simultaneously achievable in a single device. 9. Incorporation of planar waveguide technology., Anal. Chem. 72 (2000) 5549–55.

[10] D.R. Dunphy, S.B. Mendes, S.S. Saavedra, N.R. Armstrong, The electroactive integrated optical waveguide: ultrasensitive spectroelectrochemistry of submonolayer adsorbates., Anal. Chem. 69 (1997) 3086–94.

[11] H. Yumoto, T. Inoue, S.J. Li, T. Sako, K. Nishiyama, Application of ITO films to photocatalysis, Thin Solid Films. 345 (1999) 38–41.

[12] D. Grieshaber, E. Reimhult, J. Voros, Enzymatic biosensors towards a multiplexed electronic detection system for early cancer diagnostics, 2nd IEEE Int. Conf. Nano/Micro Eng. Mol. Syst. (2007) 402–405.

[13] E.J. Moore, M. Curtin, J. Ionita, A.R. Maguire, G. Ceccone, P. Galvin, Selective release of DNA from the surface of indium-tin oxide thin electrode films using thiol-disulfide exchange chemistry, Anal. Chem. 79 (2007) 2050–7.

[14] L. Yang, Y. Li, AFM and impedance spectroscopy characterization of the immobilization of antibodies on indium-tin oxide electrode through self-assembled monolayer of epoxysilane and their capture of Escherichia coli O157:H7, Biosens. Bioelectron. 20 (2005) 1407–16.

[15] N. Adányi, M. Varadi, N. Kim, I. Szendro, Development of new immunosensors for determination of contaminants in food, Curr. Appl. Phys. 6 (2006) 279–286.

[16] H. Tang, W. Zhang, P. Geng, Q. Wang, L. Jin, Z. Wu, et al., A new amperometric method for rapid detection of Escherichia coli density using a self-assembled monolayer-based bienzyme biosensor, Anal. Chim. Acta. 562 (2006) 190–196.

[17] C. Ruan, L. Yang, Y. Li, Immunobiosensor chips for detection of Escherichia coli O157:H7 using electrochemical impedance spectroscopy, Anal. Chem. 74 (2002) 4814–4820.

[18] L. Yang, Y. Li, G.F. Erf, Interdigitated Array microelectrode-based electrochemical impedance immunosensor for detection of Escherichia coli O157:H7, Anal. Chem. 76 (2004) 1107–13.

[19] O. Tokarskyy, D.L. Marshall, Immunosensors for rapid detection of Escherichia coli O157:H7 - perspectives for use in the meat processing industry, Food Microbiol. 25 (2008) 1–12.

[20] B. Ge, J. Meng, Advanced Technologies for Pathogen and Toxin Detection in foods: current applications and future directions, J. Assoc. Lab. Autom. 14 (2009) 235–241.

[21] J.O. Carneiro, V. Teixeira, a. Portinha, a. Magalhães, P. Coutinho, C.J. Tavares, et al., Iron-doped photocatalytic TiO2 sputtered coatings on plastics for self-cleaning applications, Mater. Sci. Eng. B. 138 (2007) 144–150.

[22] I. Horcas, R. Fernández, J.M. Gómez-Rodríguez, J. Colchero, J. Gómez-Herrero, a M. Baro, WSXM: a software for scanning probe microscopy and a tool for nanotechnology, Rev. Sci. Instrum. 78 (2007) 013705.

[23] G.T. Hermanson, Bioconjugate Techniques, second edi, Academic Press, 2008.

[24] D. Caballero, J. Samitier, J. Bausells, A. Errachid, Direct patterning of anti-human serum albumin antibodies on aldehyde-terminated silicon nitride surfaces for HSA protein detection, Small. 5 (2009) 1531–4.

[25] D. Caballero, M. Pla-Roca, F. Bessueille, C.A. Mills, J. Samitier, A. Errachid, Atomic Force Microscopy characterization of a microcontact printed, self-assembled thiol monolayer for use in biosensors, Anal. Lett. 39 (2006) 1721–1734.

[26] S. Azevedo, L. Diéguez, P. Carvalho, J.O. Carneiro, V. Teixeira, E. Martínez, et al., Deposition of ITO thin films onto PMMA substrates for waveguide based biosensing devices, J. Nano Res. 17 (2012) 75–83.

[27] J.P. Bearinger, J. Vörös, J. a Hubbell, M. Textor, Electrochemical optical waveguide lightmode spectroscopy (EC-OWLS): a pilot study using evanescent-field optical sensing under voltage control to monitor polycationic polymer adsorption onto indium tin oxide (ITO)-coated waveguide chips., Biotechnol. Bioeng. 82 (2003) 465–73.

[28] R. Maalouf, C. Fournier-Wirth, J. Coste, H. Chebib, Y. Saïkali, O. Vittori, et al., Label-free detection of bacteria by electrochemical impedance spectroscopy: comparison to surface plasmon resonance, Anal. Chem. 79 (2007) 4879–86.

[29] J.S. Daniels, N. Pourmand, Label-free impedance biosensors: opportunities and challenges, Electroanalysis. 19 (2007) 1239–1257.

[30] R. Pethig, Dielectric properties of biological materials: biophysical and medical applications, IEEE Trans. Electr. Insul. EI-19 (1984) 453–474.

[31] J. Miller, J. Miller, Statistic and Chemometrics for analytical chemistry, Fifth edit, Pearson Prentice Hall, 2005.

[32] D. Zhang, S. Chen, L. Qin, R. Li, P. Wang, Y. Li, The novel immunobiosensors for detection of Escherichia coli O157:H7 using electrochemical impedance spectroscopy, Proc. IEEE Eng. Med. Biol. 7 (2005) 7111–3.

[33] T. Solomun, R. Mix, H. Sturm, Immobilization of silanized DNA on glass: influence of the silane tether on the DNA hybridization, ACS Appl. Mater. Interfaces. 2 (2010) 2171–4.

[34] O. Lazcka, F.J. Del Campo, F.X. Muñoz, Pathogen detection: a perspective of traditional methods and biosensors, Biosens. Bioelectron. 22 (2007) 1205–17.

[35] European centre for disease prevention and control, Annual epidemiological report on communicable diseases in Europe 2010, Stockholm: ECDC, 2010.

# **Chapter 3.** Gold-based immunosensor for the detection of pathogenic bacteria

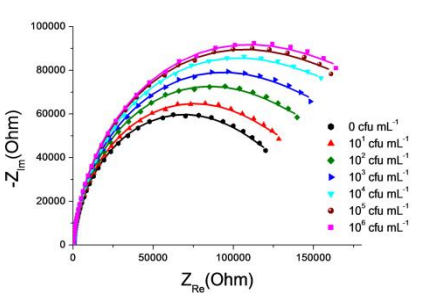



In this chapter, we develop a gold-based electrochemical immunosensor for the detection of pathogenic *E. coli* O157:H7 bacteria. EIS is applied to detect bacteria using a label-free, immunoassay-based detection method. In order to enhance the sensor performance the functionalization protocol was optimized. Anti-*E. coli* antibodies were immobilized onto gold electrodes following two different strategies: (i) linking biotinylated anti-*E. coli* to Neutravidin on a mixed-SAM and (ii) via chemical bond formation between antibody amino groups and a carboxylic acid containing SAM. Both functionalization strategies were evaluated by SPR to monitor the antibody immobilization. The strategy with the better response was selected for the development of a highly sensitive label-free immunosensor. The immunosensor showed a very low limit of detection (2 CFU $mL^{-1}$), a large linear range ($3\times10\text{-}3\times10^4$ CFU $mL^{-1}$) and low interference with other pathogenic bacteria, such as *Salmonella typhimurium*.

## Chapter index

## 3.1 Introduction

The chemistry of the biosensor surface on which the biological receptors are immobilized is an important factor that affects the detection sensitivity and specificity. Various types of chemistries have been tested as platforms for biosensors. We have seen in Chapter 2 that silane-based compounds can be successfully used to functionalize ITO electrodes with antibodies. This strategy provided significant and promising results in terms of sensor performance. However, other strategies and materials are widely available.

Self-assembled monolayers (SAM) have been investigated extensively since 1983, focusing on assemblies formed by the adsorption of organosulfur compounds from solution or vapour phase onto metal substrates of gold and silver [1–3]. Later, in the 1990s, the study of SAMs evolved into efforts to broaden the types of substrates and molecules used to form them [4]. The most extensively studied class of SAMs is derived from the adsorption of n-alkanethiols on gold, silver, copper, palladium, platinum and mercury. The formation of these well-defined organic surfaces with useful and highly alterable chemical functionalities is possible by the high affinity of sulphur for noble and coinage metals. SAMs provide huge advantages for biosensor development as they are easy to prepare and functionalize in an ordinary chemistry laboratory, they can form on surfaces of any size, and allow linking molecular-level structures to macroscopic interfacial phenomena [5].

Gold became the standard substrate for SAM formation for various reasons: it is easy to obtain, it is easy to pattern using photolithography, and it is bio-compatible [6]. Besides the different types of SAMs, alkanethiolate SAMs are widely used mainly on gold surfaces due to their many advantages:

they are resistant to non-specific adsorption and form a well-ordered and dense monolayer structure that can be easily prepared by mild incubation for a sufficient time period [7, 8].

SAMs are often the basis for the subsequent immobilization of the recognition elements described previously (antibodies, nucleic acids, aptamers, peptides, etc.). The possibilities are endless, since the functional groups provided by the SAM layer termination can be tailored to suit any particular requirements. As discussed in Chapter 2, the detection of low concentration of bacteria is a field of prolific research because of the low doses that are required to origin diseases [9].

Several impedimetric immunosensors based on gold surfaces for *E. coli* detection have been developed and different functionalization strategies applied. Figure 31 shows some examples of SAMs used for the immobilization of antibodies. Maalouf *et al* [8] used biotinylated anti-*E. coli* linked to a mixed SAM (biotinylated thiol and a spacer alcohol thiol) on a gold electrode, through a strong biotin-neutravidin interaction (Figure 31 (a)). A LOD of 10 CFU $mL^{-1}$ was obtained for the detecion of *E. coli*. This strategy is based on the natural strong binding of avidin for the small molecule biotin. The glycoprotein avidin contains four identical subunits (tetramer) and each of these subunits contains one binding site for biotin. The dissociation constant of this complex is $1.3\times10^{-15}$ M, which makes it one of the strongest non-covalent affinities known [6]. The bond formation is rapid and extremely stable. This strategy has been widely applied in different biosensor fields since functional biotin groups can be added to proteins, nucleic acids, and other molecules through well-known reactions [10–12].

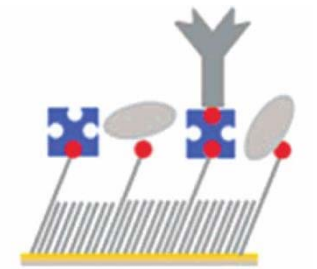

(a) Maalouf *et al*

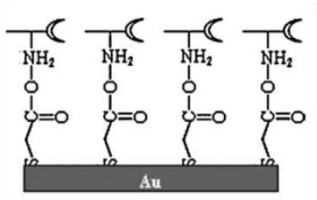


(b) Geng *et al*

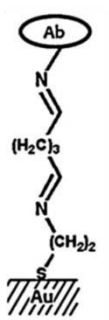


(c) Joung *et al*

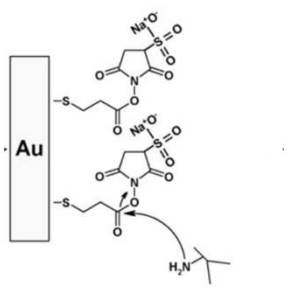


(d) Escamille-Gomez *et al*

Figure 31. Examples of impedimetric immunosensors based on gold surfaces for the detection of *E.coli* O157:H7. (a) Biotin-neutravidin affinity interaction; (b) carboxylic and amine groups interaction by exploiting EDC/NHS chemistry; (c) glutaraldehyde activation; (d) covalent attachment by dithiobis[sulfosuccinimidylpropionate].

Geng *et al* [13] developed an impedimetric immunosensor for the detection of *E. coli* by immobilizing anti-*E. coli* antibodies onto a SAM-modified gold substrate (Figure 31 (b)). The immobilization of antibodies was carried out through a stable acyl amino ester intermediate generated by 1-ethyl-3-(3-dimethylaminopropyl) carbodiimide (EDC) and N-hydroxysuccinimide (NHS). This commonly used strategy consists in cross-binding between carboxylic and amine groups (-$NH_2$) exploiting EDC/NHS chemistry. Co-addition of EDC and NHS can facilitate the formation of a

suitable intermediate to condense antibodies on the SAM [14] and enhance the sensitivity of the developed immunosensor (LOD of $1\times10^3$ CFU $mL^{-1}$).

Joung *et al* [15] showed the immobilization of antibodies onto a mercaptoethylamine monolayer through modification with glutaraldehyde (Figure 31 (c)). They compared an immunosensor based on modified SAM with another functionalized using a biocompatible and hydrophilic layer of hyaluronic acid (HA). The latter showed a limit of detection of 7 CFU $mL^{-1}$. Another immunosensor based on SAMs on gold surfaces can be found in Escamille-Gomez *et al* [16]. This immunosensor was based on the covalent immobilization of anti-*E. coli* using the homobifunctional cross-linker 3,3'-dithiobis[sulfosuccinimidylpropionate] (DTSSP) (Figure 31 (d)). They reported a lower LOD (3.3 CFU $mL^{-1}$) within a linear range from 5 to $1.0\times10^8$ CFU $mL^{-1}$ using a thiolated antibody-based configuration.

Other electrochemical methods such as amperometry and potentiometry have also been widely used in gold surfaces. Different groups have reported amperometric detection of *E. coli* [17,18] achieving limits of detection of $1.6\times10^1$ to $6\times10^2$ CFU $mL^{-1}$. Limits of detection between $10^1$ to $7\times10^2$ CFU $mL^{-1}$ were also obtained using potentiometry [19,20]. The examples described above relate to the detection of *E. coli* by electrochemical methods, but other techniques have also been reported for *E. coli*. As an example, Su and Li [21] developed a quartz crystal microbalance immunosensor, capable to detect $10^3$ CFU $mL^{-1}$. Choi and Oh [22] used fluorescence microscopy for the detection of *E. coli* O157:H7 and reported a LOD of $10^2$ CFU $mL^{-1}$. These techniques provide larger LODs compared to the ones obtained by electrochemical techniques.

Others works have also reported the use of SPR for *E. coli* detection. The first SPR sensor for the detection of bacterial cells was published by

Fratamico in 1998 [19]. The specific biosensor detected $5\times10^9$ CFU $mL^{-1}$ viable *E. coli* O157:H7 by using a sandwich assay. In 1999, Fratamico *et al* [23] tried to improve the detection limits using an inhibition assay to detect *E. coli* O157:H7, obtaining detection limits between $10^6$ and $10^7$ CFU $mL^{-1}$. In 2002, Oh *et al* [24] used a SPR sensor for direct detection of *E. coli* O157:H7 with a detection limit of $10^4$ CFU $mL^{-1}$. In 2005, Meeusen *et al* [25] achieved a LOD of $87\times10^6$ CFU $mL^{-1}$ for direct detection of viable *E. coli* O157:H7. In the same year, Taylor *et al* [26] reported a comparison of immunosensors with amplification for the detection of *E. coli* O157:H7 prepared by several sample treatment methods. Detergent-lysed samples produced the lowest LOD at $10^4$ CFU $mL^{-1}$, while the LOD was $10^5$ CFU $mL^{-1}$ for heat-killed samples and $10^6$ CFU $mL^{-1}$ for untreated samples, respectively. Subramanian *et al* [27] used a SPR sensor for the detection of viable *E. coli* O157:H7 based on a sandwich assay. The sensing surface was functionalized with an amine-coupled antibody on an OEG-SAM. The LOD was $10^6$ CFU $mL^{-1}$ for direct detection [6]. Altogether, this demonstrates the limitations in the detection capabilities of the above-described methodologies for the detection of *E. coli* O157:H7. The large LOD and the low bacteria dose needed to produce infection require the development of new approaches.

In this chapter, we present the fabrication and characterization of a label-free impedimetric immunosensor based on gold surfaces for the detection of pathogenic bacteria *E. coli* O157:H7. We focus our attention on the optimization of the functionalization protocols. Anti-*E. coli* antibodies were immobilized onto gold surfaces functionalized with SAMs following two different strategies. First, through affinity interactions between a biotinylated anti-*E. coli* and Neutravidin on a mixed-SAM, and second, via chemical bond formation between antibody amino groups and a carboxylic acid containing

SAM. The antibody immobilization and its ability to selectively graft *E. coli* strands on the sensing surface were fully characterized by SPR and fluorescence microscopy techniques, while the detection capabilities of the sensor were evaluated by EIS.

## 3.2 Experimental procedures

### 3.2.1 Chemicals and reagents

N,N-diisopropylethylamine (DIEA), 16-mercaptohexadecanoic acid (MHDA), 2,3,4,5,6-pentafluorophenol (PFP), EDC, PBS, AEE, triethylene glycol mono-11-mercaptoundecyl ether (PEG3-thiol), SH-$C_{11}$-$(PEG)_6$-$OCH_2$-COOH, SH-$C_{11}$-$(PEG)_4$-OH, TMB, BSA and Tween 20, N- hydroxysuccinimide (NHS) were purchased from Sigma Aldrich (St. Louis, MO, USA). Sodium hydrogen carbonate, hydrogen peroxide ($H_2O_2$), sulphuric acid ($H_2SO_4$), acetone and absolute ethanol were purchased from Panreac (Barcelona, Spain), while potassium hexacyanoferrate(III) ($K_3Fe(CN)_6$) and potassium hexacyanoferrate(II) ($K_4Fe(CN)_6$) were obtained from Fluka (Buchs, Switzerland).

Biotinylated alkanethiol (BAT) was obtained using solid-phase methodology as described previously [28] and were kindly supplied by Prof. F. Albericio and Dr. E. Prats-Alfonso (IRB, Barcelona, Spain). Neutravidin was purchased from Cultek (Madrid, Spain).

Polyclonal anti-*E. coli* (PA1-7213), was obtained from ABR Affinity Bioreagents (Golden, CO, USA). Detection antibodies, polyclonal anti-*E. coli* horseradish peroxidise (HRP) conjugate (PA1-73030) and polyclonal anti-*E.coli* FITC conjugate (PA1-73029), were obtained from Thermo Fisher Scientific

(Rockford, IL, USA). Rabbit polyclonal anti-*Salmonella* HRP conjugate (ab69254) was obtained from Abcam and goat anti-rabbit IgG (Alexa Fluor 546) from Invitrogen (Eugene, OR, USA). Standard samples of heat killed *E. coli* O157:H7 (KP-50-95-90, conc. approx: $3x10^9$ CFU $mL^{-1}$) and *Salmonella typhimurium* (KP-50-74-01, conc. approx: $5x10^9$ CFU $mL^{-1}$) were obtained from KPL (Gaithersburg, MD, USA). Viable *Escherichia coli* O157:H7 Δ*stx*, and *Salmonella* enterica serovar *typhimurium* (*S. typhimurium*) wild-type SV5015 were obtained as described in chapter 2 (section 2.2.2).

Antibodies against *E. coli* (PA1-7213; Affinity Bioreagents) were biotinylated in collaboration with Prof. Maria Pilar Marco and Dr. Núria Pascual from the AMRg (IQAC, CSIC, Spain). Briefly, an aliquot of Biotin-hydroxysuccinimide ester (FLUKA) was mixed with the antibody (1/10 the weight of the antibody) in borate buffer (0.2 M boric acid-sodium borate; pH 8.7) for 2h and subsequently dialyzed in PBS (0.5 mM; 3 x 5 L) to remove unreacted biotin.

### 3.2.2 Gold cleaning procedures

For SPR measurements, gold SPR sensor chips (GWC technologies Inc., USA) were cleaned with Milli-Q water (Millipore, USA) and absolute ethanol. For fluorescence microscopy and AFM characterization, gold substrates were fabricated by deposition of a 50 nm gold layer and a 3 nm titanium adhesion promoting layer on float glass slides (NTB, Switzerland) and subsequently cut into pieces of 1x1 $cm^2$. The gold substrates were first rinsed and ultrasonically cleaned with acetone and subsequently with ethanol to remove possible contaminants. Afterwards, they were immersed into Piranha solution (3:7 v/v

$H_2O_2$:$H_2SO_4$) for 10 minutes, rinsed thoroughly with Milli-Q water, absolute ethanol and dried under a stream of nitrogen.

Gold disc working electrodes with 1.6 mm of diameter (Bioanalytical System Corp.) were used for electrochemical measurements. The gold working electrodes were manually polished in sequential order with 0.3 and 0.05 µm alumina (polishing kit BASi) and sonicated for 10 min in Milli-Q water and afterwards in ethanol. The electrodes were finally cleaned electrochemically by performing cyclic voltammograms in 0.1 M $H_2SO_4$ solution between 0 V and +1.6 V vs. Ag/AgCl at 200 mV $s^{-1}$.

### 3.2.3 Functionalization procedures

Two functionalization strategies were used to immobilize the antibodies onto the gold surface:

*(i) Strategy I: biotin-neutravidin functionalization*

Strategy I is based on the strong non-covalent interaction between a biotin derivative and neutravidin, which can bind up to four biotin molecules (see Figure 32). Mixed thiol SAMs were prepared by immersion of the gold surface in 0.1 mM biotinylated ethyleneglycolalkylmercaptane and tetraethyleneglycol-undecylmercaptane (PEG-thiol)) ethanolic solution (ratio of 1:9 (w/w) for 16–20 h to obtain a uniform SAM surface coverage (1). The mixed SAM allows easy control of the surface binding site density for neutravidin molecules as a function of BAT percentage in the solution used to prepare the surface [29]. Neutravidin ($10^{-7}$ M in PBS) was added for 1 h at RT to the mixed monolayer (2). Subsequently, the biotinylated antibody ($10^{-7}$ in

PBS) was allowed to react with the remaining binding positions of the Neutravidin for 1 h at RT (3).

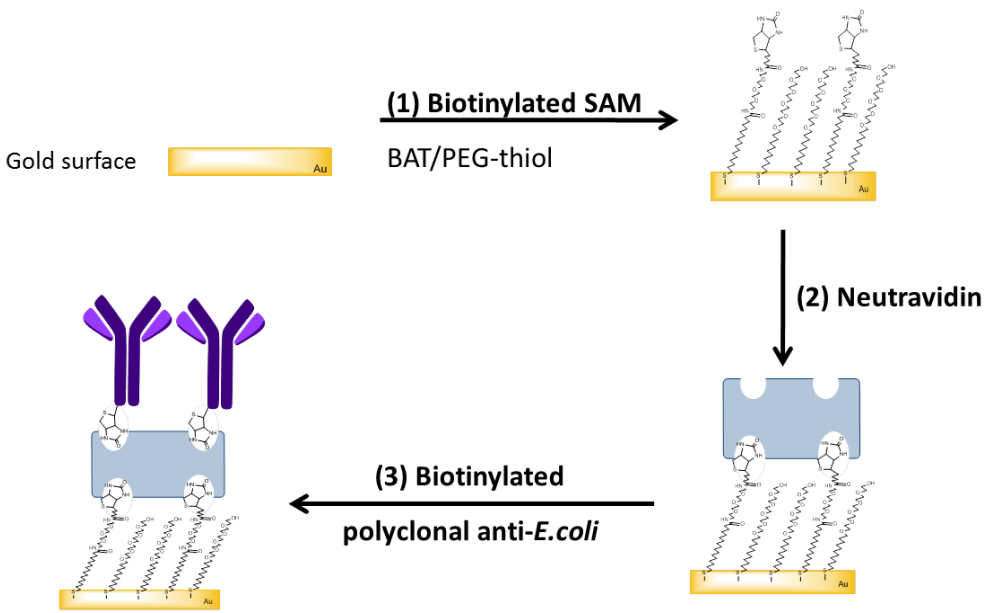


Figure 32. Schematic diagram of the functionalization strategy I for the fabrication of the gold-based immunosensor. *Steps:* (1) Biotinylated SAM, (2) neutravidin adhesion and (3) antibody binding by biotin groups.

*(ii) Strategy II: amide coupling functionalization*

Strategy II is shown in Figure 33 and it is based on anchoring the antibodies onto a reactive monolayer by means of the amide coupling technique. First, a MHDA SAM was formed on the cleaned gold surfaces using the strong gold-thiol interaction by immersion into a 2 mM ethanolic solution overnight at 4ºC (1). Subsequently, the carboxylic acid groups were activated using a mixture of EDC (0.2 M), PFP (0.2 M), and DIEA (0.2 M) in absolute ethanol during 30 min at RT (2). Then, the substrates were rinsed with

absolute ethanol and dried with $N_2$. Primary antibodies (15 µg $mL^{-1}$ or $10^{-7}$ M solution in PBS) were covalently immobilized by amide-bond formation during 2 h at RT (3). Carboxylic acid functionalities were activated by reaction with a mixture of EDC and PFP to form a pentafluorophenyl ester intermediate, which reacted with the alkyl amine groups of the antibodies to attach them covalently to the electrode surface by means of amide bonds [29, 30]. Afterwards, the sample was rinsed with PBS and the remaining active ester functionalities were blocked by immersing the substrate into a 10 mM of AEE solution (4) in sodium bicarbonate buffer (pH 8.3) during 30 min. Finally, the substrates were washed and stored in PBS solution at 4ºC prior to use.

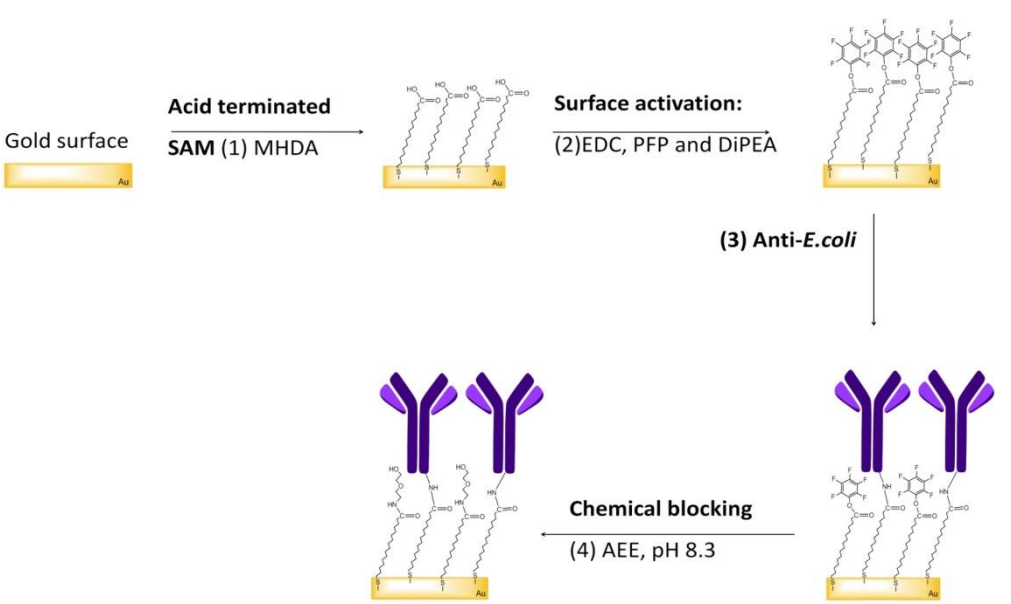


Figure 33. Schematic diagram of the functionalization strategy II for the fabrication of the gold-based immunosensor. *Steps:* (1) Self-assembled carboxylic acid, (2) surface activation, (3) antibody binding and (4) chemical blocking.

### 3.2.4 Surface Plasmon Resonance measurements

For strategy I, SPR experiments were conducted on a GWC Technologies SPR Imager II instrument (GWC Technologies, USA). Measurements were performed at a fixed angle of incidence collecting the changes on the reflected light intensity by imaging the SPR chip with a CCD camera. A mixed thiol monolayer was first formed on the SPR chips as described in section 3.2.3. Then, the chips were index-matched to the prism and fitted with a flow cell connected to a peristaltic pump from Ismatec (Glattbrugg, Switzerland). Neutravidin in PBS solution ($10^{-7}$ M) was added to the modified-gold chip and the biotinylated antibodies ($10^{-7}$ M in PBS) were then conjugated non-covalently to the neutravidin layer. Finally, standard PBS solutions of bacteria *E. coli* O157:H7 were added. The SPR response was recorded until a plateau in the signal was observed. The surface was washed with PBS buffer between each step, in order to get rid of unbound molecules.

For strategy II, SPR experiments were conducted on a SPR RT2005 instrument (RES-TEC GmbH, Max Planck Institute for Polymer Research, Germany). The activated carboxylic acid functionalized gold SPR chips (see section 3.2.3) were index-matched to the prism and fitted into a flow cell connected to a peristaltic pump (Ismatec, Switzerland). The variation of reflectivity was measured as a function of time at a fixed angle near from the SPR angle. Then, a solution of primary antibodies (15 µg $mL^{-1}$ in PBS) was injected and passed over the substrate until the SPR signal indicated complete surface coverage by reaching a plateau. Subsequently, unbound antibodies were removed by washing with PBS and the remaining active carboxylic groups were blocked with 10 mM AEE. Finally, standard solutions of bacteria *E. coli* O157:H7 or *Salmonella typhimurium* were injected ($10^7$ CFU

$mL^{-1}$). After each bacteria injection the sample was rinsed with PBS. In all the experiments, a flow of 56 µL $min^{-1}$ was used.

Finally, in strategy II, different types of SAMs were tested by SPR: mixed SAMs (1 mM) of SH-$C_{11}$-$(PEG)_6$-$OCH_2$-COOH and SH-$C_{11}$-$(PEG)_4$-OH at different ratios (3:7 and 1:10) and MUA (2mM). Additionally, the activation method based on NHS (0.1 M) and EDC (0.4 M) was also tested in order to have the most specific and sensitive method.

### 3.2.5 Fabrication of antibody microarray by microcontact printing

PDMS (Sylgard 184, Dow Corning) stamps with a regular array of cylindrical posts of 10 µm in diameter and a pitch of 10 µm were fabricated by pouring a 10:1 mixture of pre-polymer and curing agent onto a silicon master (Centre Nacional de Microelectrònica – CNM, Spain) and cured for 2 h at 70ºC. The PDMS stamp was released from the master and inked with a 2 mM MHDA ethanolic solution for 1 h. Then, the stamp was rinsed with absolute ethanol and dried under a nitrogen flow. Next, the PDMS stamp was placed in contact with the gold substrate for 2 min at RT to transfer the thiol pattern to the gold surface. Non-patterned regions were blocked with a 5 mM PEG3-thiol ethanolic solution for 2 h.

Primary antibodies were immobilized on the patterned thiol sample using strategy II, as described in section 3.2.3. A secondary antibody (Anti-Rabbit labeled with Alexa Fluor 546) was incubated during 1 h to demonstrate the effectiveness of the functionalization protocol. Bacteria detection was performed by means of a sandwiched assay by incubation first, *E. coli* O157:H7 bacteria ($10^7$ CFU $mL^{-1}$) onto the antibody pattern, and

second, a secondary FITC-conjugated anti-*E. coli* polyclonal antibody (0.1 mg $mL^{-1}$) for 1 h. To confirm the selectivity of the system, the same protocol was followed using non-specific bacteria (*Salmonella typhimurium*, $10^7$ CFU $mL^{-1}$). In this case, a second antibody specific to *Salmonella* (Rabbit Anti-*Salmonella*) was used and the fluorescent signal was obtained using a secondary antibody specific to the Rabbit Anti-*Salmonella* (Anti-Rabbit labeled with Alexa fluor 546). Between each step the substrates were thoroughly washed with PBS. The same procedure was applied for the detection of *Salmonella typhimurium*, using as primary antibodies the monoclonal anti-*Salmonella*.

### 3.2.6 Fluorescence and Atomic Force Microscopy characterization

#### *3.2.6.1 Fluorescence Microscopy:*

For fluorescence microscopy experiments, an Eclipse E1000 upright microscope (Nikon, Japan) equipped with a CCD camera was used. Fluorescence images were obtained using a 40 × Nikon air objective and a FITC or G2A filter. Captured images were analyzed with image processing software (ImageJ, NIH, USA).

#### *3.2.6.2 Atomic Force Microscopy:*

Samples were characterized by a commercial Dimension 3100 AFM (Veeco Instruments, USA). The AFM topographic measurements were performed in air using a silicon AFM tip (MikroMasch NSC15/AIBS with spring constant of 40 N $m^{-1}$, resonance frequency of 325 kHz and a nominal tip radius of 10 nm) in Tapping™ mode and at RT. AFM images were analysed with WSxM software (Nanotec Electrónica S.L.) [31].

### 3.2.7 Electrochemical measurements

Cyclic voltammetry (CV) and EIS experiments were performed on a VMP2 multipotentiostat (Princeton Applied Research), using a three-electrode electrochemical cell with a gold disk working electrode, a platinum wire counter electrode and an Ag/AgCl reference electrode, placed into a Faraday cage. Measurements were performed in PBS / 5 mM $K_3[Fe(CN)_6]$ solution at RT. Cyclic voltammetry was performed at 100 mV $s^{-1}$, over a potential range between -0.5 V and 0.8 V. During the EIS measurements the potential was kept at 0 V and the perturbation amplitude at 10 mV, over a frequency range from 100 kHz to 1 Hz. Data acquisition and analysis were accomplished using EC-Lab software (Bio-Logic SAS). The functionalized electrodes (section 3.2.3) were exposed to different *E. coli* O157:H7 and *Salmonella typhimurium* concentrations for 45 min and the immunoreactions were monitored in real time.

### 3.2.8 ELISA protocol

First, 96-well microtiter plates (Maxisorp, Nunc) were coated overnight at 4ºC with anti-*E. coli* solution (15 µg $mL^{-1}$ in 0.05 M of carbonate buffer, pH 9.6). A blocking step was then carried out using 2% BSA. Afterwards, the immunological reaction was performed using *E. coli* O157:H7 solutions at different concentrations (from $1x10^4$ to $1x10^5$ CFU $mL^{-1}$ in PBS). Then, HRP-labelled polyclonal anti-*E. coli* solutions (0.1-0.2 µg $mL^{-1}$ in PBS) was added. Each step was carried out for 1 h with shaking, at RT. Finally, TMB liquid substrate was incubated for 15 min and the microplate was protected from the light. Between each step, the wells were thoroughly rinsed with

PBS-T buffer containing 0.05% Tween 20. Absorbance was read at 620 nm using a Benchmark Plus microplate spectrophotometer (Bio-Rad Laboratories Inc., USA) and assays were performed in triplicate.

## 3.3 Results and discussion

The results described in this chapter are divided in two main parts, according to the type of surface functionalization strategy applied. Two different types of immobilization methods for gold surfaces were investigated in order to obtain the best sensor performance and non-specific adsorption resistance (see Figure 34 and section 3.2.3).

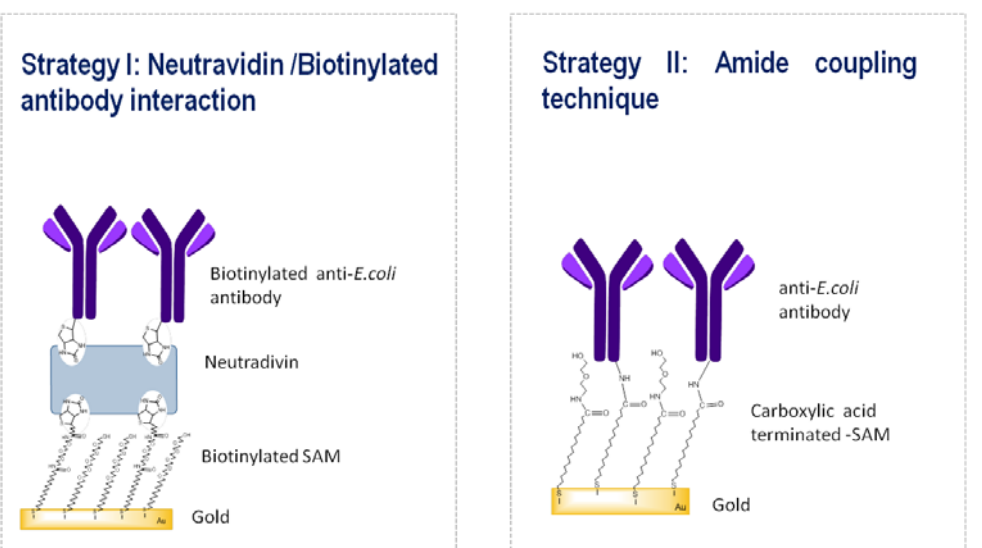


Figure 34. Gold surface functionalization strategies applied. *(Left)* Strategy I based on Neutravidin/Biotinylated antibody interaction. *(Right)* Strategy II based on amide coupling technique.

Briefly, anti-*E. coli* antibodies were immobilized onto gold by linking a biotinylated anti-*E. coli* to Neutravidin on a mixed-SAM (strategy I) or

alternatively, via chemical bond formation between the antibody amino groups and a carboxylic acid-terminated SAM (strategy II).

Evaluation, optimization and characterization of the surface functionalization were addressed by optical methods (SPR and fluorescence microscopy) and electrochemical methods (cyclic voltammetry and EIS). EIS was used for the detection of pathogenic bacteria *E. coli* O157:H7.

### 3.3.1 Strategy I: optimization and characterization of the surface antibody functionalization

The optimization and characterization of the surface antibody functionalization was first demonstrated by SPR. The SPR is a well suited technique for evaluating functionalization procedures, since it provides sensitive measurements of surface processes in real time (see section 1.1.2.1) [8]. First, a mixed self-assembled monolayer was formed on the gold surface through thiol groups as shown in section 3.2.3 and considering the best conditions as described in [32]. The binding of Neutravidin to the biotinylated SAM and the immobilization of biotin conjugated polyclonal antibody against *E. coli* is shown in Figure 35.

Exposing the functionalized surface to a $10^{-7}$ M neutravidin solution led to a rapid increase in the SPR signal. A decrease was observed after washing with PBS due to the removal of loosely bound molecules. The immobilization of the anti-*E. coli* through neutravidin/biotin chemistry was proved by the considerable change in SPR signal. The SPR intensity shift upon neutravidin binding to the SAM-modified surface was measured to be 2.9 a.u., while a variation of 2 a.u. was observed for the biotinylated antibody. A ratio of antibody bounded to the neutravidin of 69% was obtained,

corresponding to two binding sites. Neutravidin has four binding sites: two binding sites are probably used for the attachment on the SAM monolayer and the others are available for the attachment of the antibodies. This suggests that some binding sites remain free. BSA is often used in traditional immunoassays to block uncoated surface sites and to reduce non-specific adsorptions [8]. Here, a 5 mg $mL^{-1}$ PBS solution of BSA was used for passivating non-coated regions.

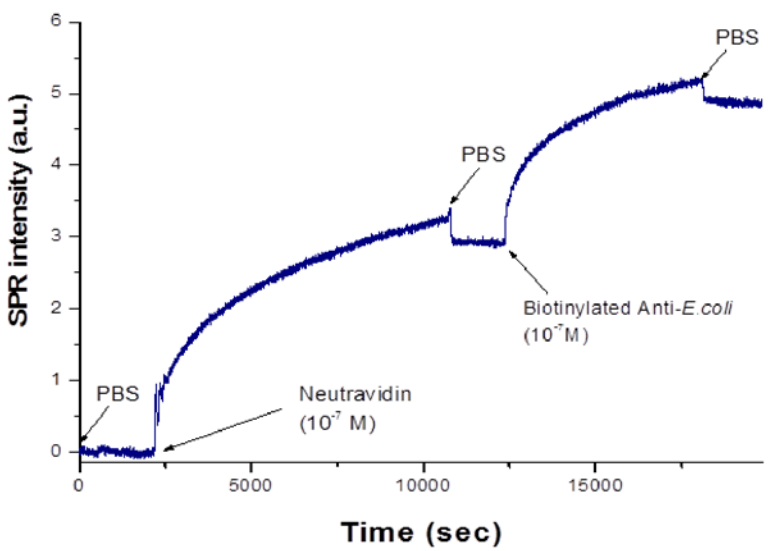


Figure 35. SPR time-dependent sensogram obtained using strategy I functionalization (biotin-neutravidin system).

The obtained results confirm the successful immobilization of antibody on the functionalized gold surface using strategy I. However, upon the addition of different concentrations of *E. coli* O157:H7, no significant change in the SPR signal was observed. Direct detection of *E. coli* by SPR has been attempted but there are multiple problems associated with direct detection methods, mostly due to lack of sensitivity [23, 29]. The effective penetration depth of the evanescent field in SPR is typically 200–300 nm. This

indicates that only refractive index changes occurring within this short distance from the surface will cause a change in the SPR signal [33]. The large size of bacterial cells (typically 1-5 µm in diameter) suggests that only a small fraction of the cell that is in close contact with the sensor surface will contribute to refractive index changes [7]. The same problem with SPR applies not only to bacteria but to other large biomolecules such as some viruses and fungi [34].

A more sensitive technique – EIS – was used for the direct detection of these pathogenic bacteria. Again, a gold electrode was functionalized with the optimized strategy described before (see section 3.2.3 and 3.3.1). We first characterized the sample by cyclic voltammetry to probe the physical properties of the SAM. This technique is commonly employed for probing the blocking/barrier properties of insulating films such as SAMs by measuring changes in cyclic voltammograms [35, 36]. The quality of the SAM formed onto the gold electrode surface, as well as the antibody immobilization, was investigated in the presence of the redox probe. Figure 36 shows a typical cyclic voltammogram recorded for the different functionalization steps.

Results show that the electric current through the electrode is effectively reduced in the presence of the monolayers, confirming that compact monolayers were formed. The binding of antibody reduces slightly the penetration of the redox probe and decreases the current response (Figure 3, inset). This proves the successful attachment of the antibodies onto the neutravidin-modified gold surface as it was previously demonstrated by SPR. Then, EIS was used for the immunodetection of *E. coli* O157:H7 as it is described in the next section.

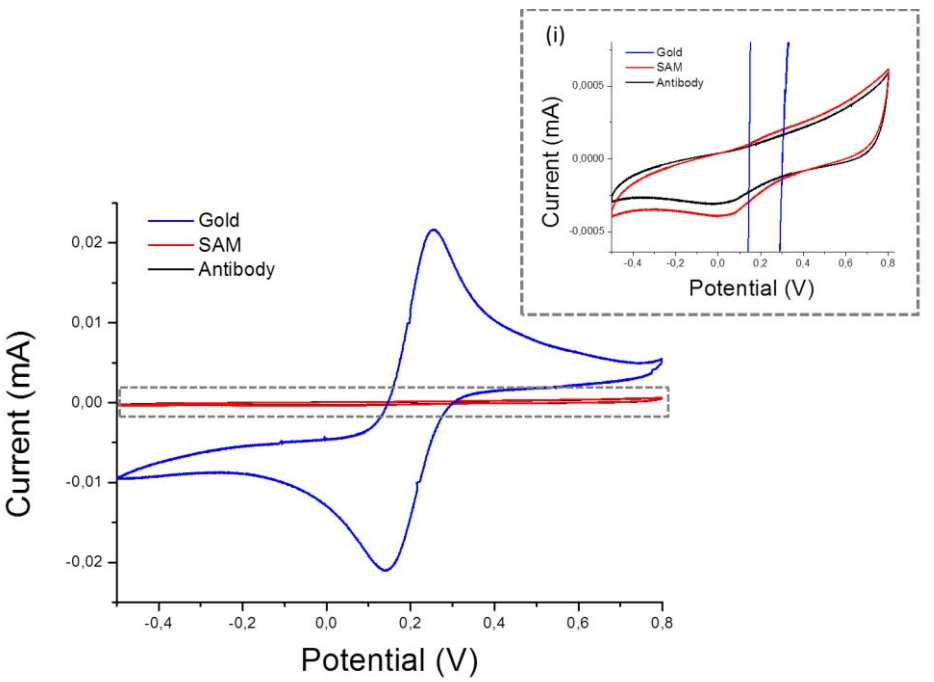


Figure 36. Cyclic voltammogram for a gold bare electrode (in blue) before and after its functionalization using strategy I (in red, SAM and in black, antibody). *(i)* Inset, a zoomed image of the highlighted region showing the CV curves for the SAM and antibodies immobilization.

### 3.3.2 Strategy I: detection of *E. coli* O157:H7 bacteria by EIS

Figure 37 shows the Nyquist plots of impedance spectra recorded for increasing concentrations of *E. coli* O157:H7 bacteria, ranging from 0 - $10^4$ CFU $mL^{-1}$. A significant impedance difference upon the increase of bacteria concentrations was observed for the first added concentration. At *E. coli* O157:H7 concentrations higher than $3\times10^2$ CFU $mL^{-1}$ the difference diminished, suggesting the saturation of the system.

To understand the physical origin of the observed response, the data was simulated and fitted by the Randles equivalent circuit model (see

Figure 38 (a)) with an acceptable error value ($\chi^2$ = 0.04). In this equivalent circuit, $R_{ct}$ is the charge transfer resistance, *CPE* the constant phase element, *W* the Warburg impedance and $R_{sol}$ the resistance of the solution.

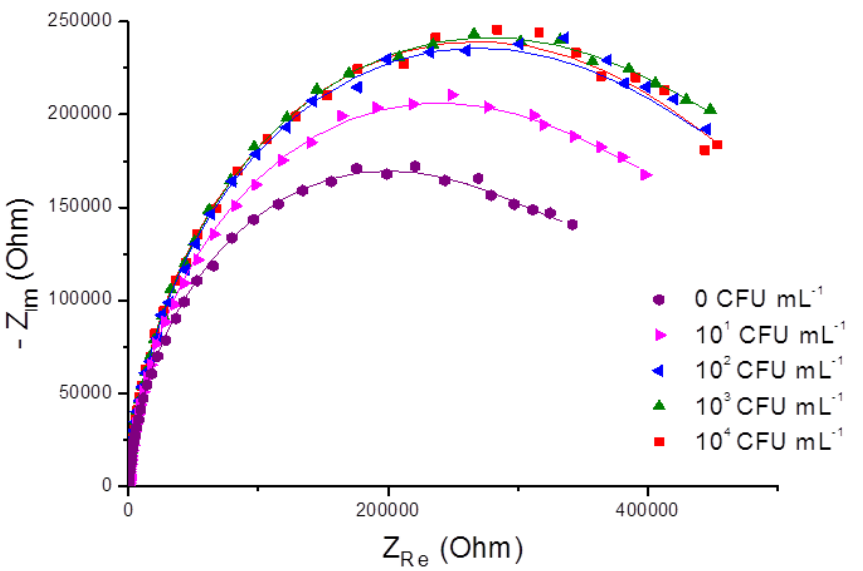


Figure 37. Impedance Nyquist plot for different *E. coli* O157:H7 concentrations (10-$10^4$ CFU $mL^{-1}$) in presence of ferrocyanide as a redox probe.

As mentioned earlier, $R_{sol}$ and *W* impedance represent bulk properties of the electrolyte solution and diffusion features of the redox probe in solution. These parameters are usually not affected by physicochemical transformations occurring at the electrode surface and consequently not modified by the antibody-bacteria binding. On the other hand, other parameters such as $R_{ct}$ and the capacitance of the double layer $C_{dl}$ depend on the dielectric and insulating features at the interface electrode and electrolyte solution [37]. To fit better the impedance spectrum, a constant

phase element *CPE* was introduced into the circuit as a capacitance. The constant phase element reflects inhomogeneities and defect areas of the layer [38] (see sections 1.1.2.2 and 2.3.4).

$R_{ct}$ is very sensitive to electrode modifications produced by the binding of *E. coli* bacteria to the antibodies biorecognition layer. This process would retard the interfacial electron transfer kinetics and increase the electron transfer resistance. Therefore, the number of captured bacteria on the electrode surface could be reflected by the electron transfer resistance of the redox probe in a concentration dependent manner, even for low concentration of analyte [39].

Figure 38 (b) shows the result of the $\Delta R_{ct}$ ($R_{ct}^{\text{Antibody+bacteria}}$- $R_{ct}^{\text{Antibody}}$) as a function of the logarithmic *E. coli* O157:H7 concentration. The system detects very low concentration of *E. coli* O157:H7 (10 CFU $mL^{-1}$), but it is saturated for higher concentrations. This limits the sensitivity and the overall performance of the immunosensor. In addition, the reproducibility of the sensor was evaluated to be unsatisfactory, suggesting the influence of the used functionalization strategy in the obtained results.

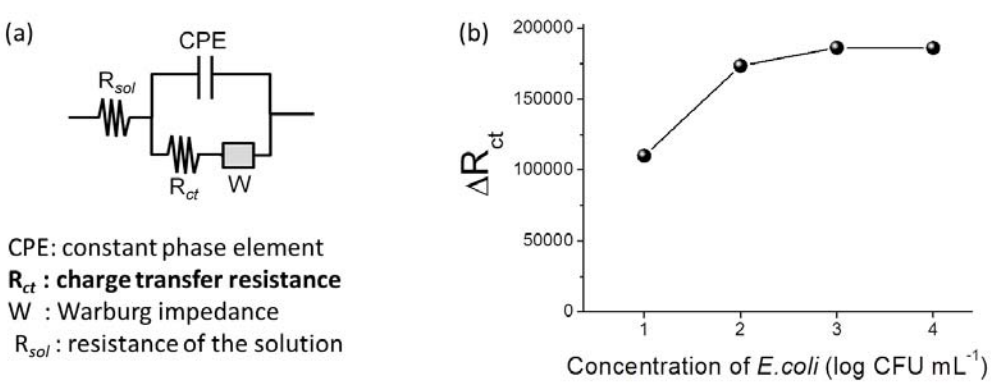


Figure 38. Simulation and analysis of the sensor response. (a) Randles equivalent circuit model used to fit the data. (b) Relationship between $\Delta R_{ct}$ and *E. coli* O157:H7 concentration.

Biotin-avidin system is an effective method to immobilize bio-recognition elements on the surface of solid supports. However, this strategy has some disadvantages besides the limitations shown for biosensing applications. The high cost of the reagents involved and the need for a suitable linker molecule, such as BAT, limits the applicability of this strategy [40]. Additionally, biotinylation of the antibody also occurs unspecifically on all amino groups and may result in reduced recognition capability [41].

Altogether, the obtained results encouraged us to evaluate the functionalization strategy based on amide coupling technique (strategy II) for the detection of pathogenic bacteria.

### 3.3.3 Strategy II: optimization and characterization of the surface antibody functionalization

Figure 39 (a) shows a SPR sensogram showing the change in reflectivity intensity (R) versus time during the immobilization of the polyclonal anti-*E. coli* antibodies onto an activated SAM, according to the strategy II (see section 3.2.3).

The SPR signal increased upon injection of the antibody solution and stabilized after 2 h, suggesting an optimal surface coverage. This time was used as a reference for the subsequent functionalization experiments. The reflectivity shift, defined as the difference between the SPR signal before the anti-*E. coli* injection and after the washing step, was 13.7% proving the efficient covalent binding of the antibody. A small decrease in the signal was observed when PBS buffer was added most probably due to the removal of loosely bound molecules. The change in resonance angle can be converted into surface mass using a factor of 120 m◦ per 100 ng $cm^{-2}$ [42]. Considering

the shift in angle of minimum reflectivity (Δθ), before and after antibody incubation (Figure 39 (b)), the estimated antibody density was 476 ± 16 ng $cm^{-2}$.

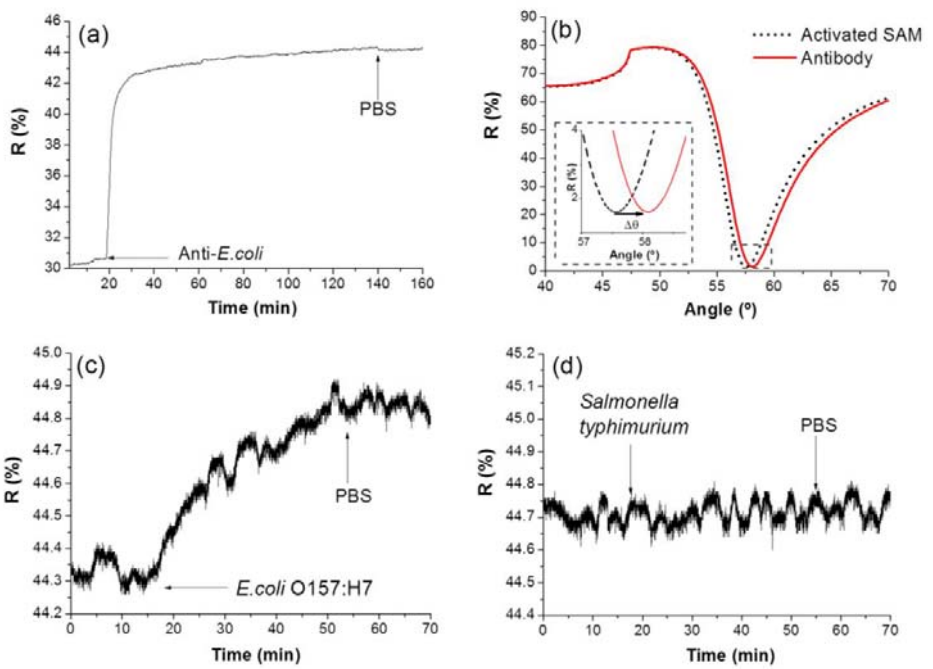


Figure 39. (a) SPR time-dependent sensogram and (b) surface plasmon spectra for the immobilization of 15 μg $mL^{-1}$ anti-*E. coli* antibody onto the actived SAM. SPR time-dependent sensogram after the addition of (c) *E. coli* O157:H7 and (d) *Salmonella typhimurium* ($10^7$ CFU $mL^{-1}$) to the immunosensor.

Upon injection of *E. coli* O157:H7 solution to the system, the bacteria started to bind on the sensor surface functionalized with anti-*E. coli* antibodies (Figure 39(c)). The signal reached a maximum value after about 45 min, time which was selected for all the following incubation experiments. Significant increase in SPR response could only be observed for concentrations higher than $10^7$ CFU $mL^{-1}$. This high detection limit is in agreement with results found by other groups using SPR label-free and direct

detection systems [8, 26]. As expected, no SPR response was obtained upon addition of non-specific bacteria *Salmonella typhimurium* (Figure 39(d)).

In order to improve the detection limit using the same system, different SAM composition and activation methods were tested. Table 5 shows the variation of reflectivity (%) for antibody immobilization and *E. coli* O157:H7 detection using the different types of SAMs, including mixed SAM at different ratios, and/or activation methods. So far, we have employed single-component SAMs (MHDA, defined as SAM 3). We also tested 11-mercaptoundecanoic acid (MUA, defined as SAM 4), which are n-alkanethiols with high-quality packing [43]. Mixtures of organothiols having different terminal groups have also been tested in this work. The mixed SAMs were composed of a mixture of a carboxylic acid functionalized derivative (SH-$C_{11}$-$(PEG)_6$-$OCH_2$-COOH) and an alcohol functionalized derivative (SH-$C_{11}$-$(PEG)_4$-OH) at different ratios (SAM 1: [3:7] and SAM 2 [1:10]) (see Table 5). The mixture of these two molecules allowed the creation of a range of surfaces of varying hydrophilicity, providing carboxylic groups that are in a disordered state and that are exposed at the surface, hence being optimally located for reaction [44].

As it can be seen in Table 5, almost no SPR response for antibody immobilization was observed in mixed SAMs (SAM 1 and 2), being the higher SPR response obtained for the activation method with PFP/EDC/DIEA. A significant difference between the activation methods was also observed for MHDA (SAM 3). An increase of 10-fold of SPR response was obtained for PFP/EDC/DIEA compared to NHS/EDC. It is well known that fluorophenylesters are effective intermediates for amide bond formations while less prone to hydrolysis than N- hydroxysuccinimide esters [45].

Table 5. SPR response (variation of reflectivity, %) of the antibody immobilization ($10^{-7}$ M) and bacterial binding ($10^{7}$ CFU $mL^{-1}$) using different SAMs and/or activation strategies.

| SAM | Activation method | Antibody immobilization ΔR (%) | *E. coli* O157:H7 detection ΔR (%) |
|---|---|---|---|
| **SAM 1**<br>SH-$C_{11}$-$(PEG)_6$-$OCH_2$-COOH :<br>SH-$C_{11}$-$(PEG)_4$-OH [3 : 7] | (NHS/EDC) | 0.1 | 0 |
| **SAM 2**<br>SH-$C_{11}$-$(PEG)_6$-$OCH_2$-COOH :<br>SH-$C_{11}$-$(PEG)_4$-OH [1 : 10] | (NHS/EDC)<br>(PFP/EDC/DIEA) | 0.4<br>1.0 | 0<br>0 |
| **SAM 3**<br>MHDA | (NHS/EDC)<br>(PFP/EDC/DIEA) | 1.3<br>13.7 | 0.2<br>0.5 |
| **SAM 4**<br>MUA | (PFP/EDC/DIEA) | 14.7 | 1.1 |

As expected, the SPR signal of antibody immobilization was lower for the mixed SAMs (SAM 1 and 2) compared with 100% SAM (SAM 3 and 4), due to the lower amount of terminated carboxylic acid that reacts with the amine groups of the antibody. However, no response to the pathogenic bacteria was observed. Despite the fact the best SPR response for antibody immobilization and *E. coli* O157:H7 detection was obtained for SAM 4, non-specific adsorption of *Salmonella typhimurium* was observed. These results confirm the effectiveness of the functionalization protocol used in SAM 3 with PFP/EDC/DIEA as activation method (see Figure 39) and consequently, it was used for all the following experiments.

The bacteria detection capabilities of the system were further studied by immunofluorescence. Microcontact printing technique was first used to pattern a microarray of anti-*E. coli* antibodies onto the COOH-terminated

gold surface. Non-patterned regions were blocked with a PEG3-thiol ethanolic solution.

Figure 40(a) shows an AFM image of the gold surface before patterning. As it can be observed a very smooth and homogeneous surface was obtained with a RMS roughness of 0.56 nm. After the micropatterning of the SAM, a perfect array of circular features of 10 µm of diameter was obtained (Figure 40 (b)).

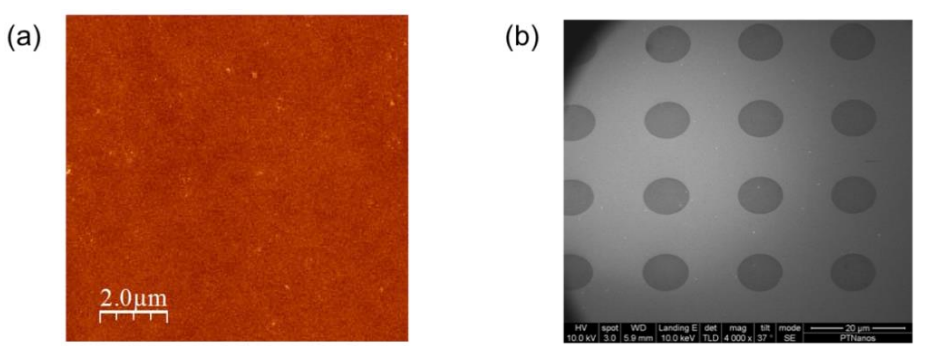


Figure 40. (a) Topography AFM image of the gold surface before patterning. (b) Scanning electron microscope (SEM) image of a COOH-terminated thiol microarray created by microcontact printing.

The patterned sample was then activated using the above-described optimized protocols (see section 3.2.6 and 3.3.3) and incubated with a solution of anti-*E. coli* antibodies ($10^{-7}$ M). Figure 41 (a) shows an immunofluorescence image of the sample which was incubated with a secondary anti-Rabbit antibody. As it can be observed, the secondary antibody specifically recognized the anti-*E. coli* array, demonstrating an optimal immobilization of the primary capture antibodies onto the activated SAM.

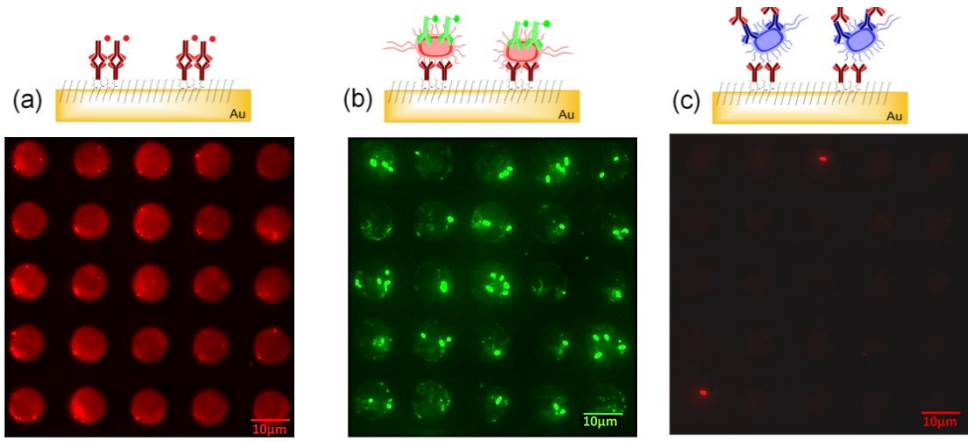


Figure 41. Fluorescence microscopy images of a microcontact printed array of (a) primary polyclonal anti-*E. coli* antibodies, (b) after incubation with *E. coli* O157:H7 and (c) control experiment using non-specific *Salmonella typhimurium* bacteria ($10^7$ CFU $mL^{-1}$) .

Bacteria detection was performed by means of a sandwiched assay by incubating *E. coli* O157:H7 bacteria onto the antibody pattern followed by a secondary FITC-conjugated anti-*E. coli* polyclonal antibody (see Figure 41 (b)). *E. coli* O157:H7 bacteria specifically bound onto the antibody microarray and no bacteria was detected outside it. This proves the effective inhibition of non-specific adsorption for proteins or bacteria.

The quality of the antibody pattern was further studied by AFM (see Figure 42). The samples showed a regular and smooth surface for each spot. The bacteria were again localized exclusively onto the anti-*E. coli* regions as previously shown in the fluorescence images. Cross section analysis provided height differences between the antibody and the bacteria with respect the PEG3-thiol regions of about 5 nm and 300 nm, respectively (Figure 42 (b) and Figure 42 (c)).

We also measured the dimensions of the bacteria and typical values of around 1 µm x 2 µm were obtained. The smaller value obtained for the antibody layer (5 nm) compared to its theoretical height (10-15 nm) is

probably due to the fact that the AFM images were captured in air using dried samples.

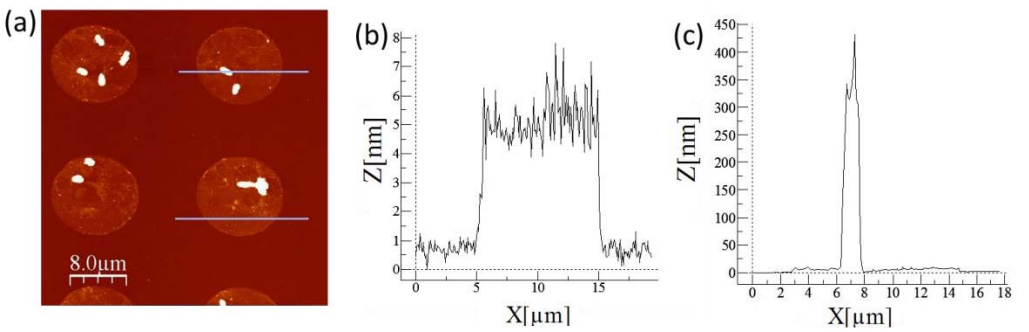


Figure 42. (a) Topography AFM image of an anti-E. *coli* antibody micropattern showing several immobilized *E. coli* O157:H7. (b) Profile plot of the antibody pattern and (c) *E. coli* O157:H7 over one antibody spot.

Finally, the selectivity of the system was examined using different non-specific pathogenic bacteria such as *Salmonella typhimurium*. As it can be observed in Figure 41(c), no fluorescence signal arises due to the weak interaction with the anti-*E. coli* capture antibody. We quantified the amount of *S. typhimurium* bacteria binding to the anti-*E. coli* microarray compared to *E. coli* O157:H7. Considering the same amount of analyzed antibody spots (100 spots) a ratio of *S. typhimurium / E. coli* O157:H7 of 1:18 was obtained. Less than 6% of non-specific adsorption was found confirming the specificity of the antibody and functionalization protocol.

Surface functionalization was also studied for the detection of other pathogenic bacteria such as *S. typhimurium* bacteria, using in this case specific antibodies to these bacteria (monoclonal anti-*Salmonella*). Figure 43 shows fluorescence microscopy images of an array of primary monoclonal

anti-*Salmonella* antibodies after incubation with *S. typhimurium* depending on the type of bacteria: (a) heat-killed and (b) viable bacteria.

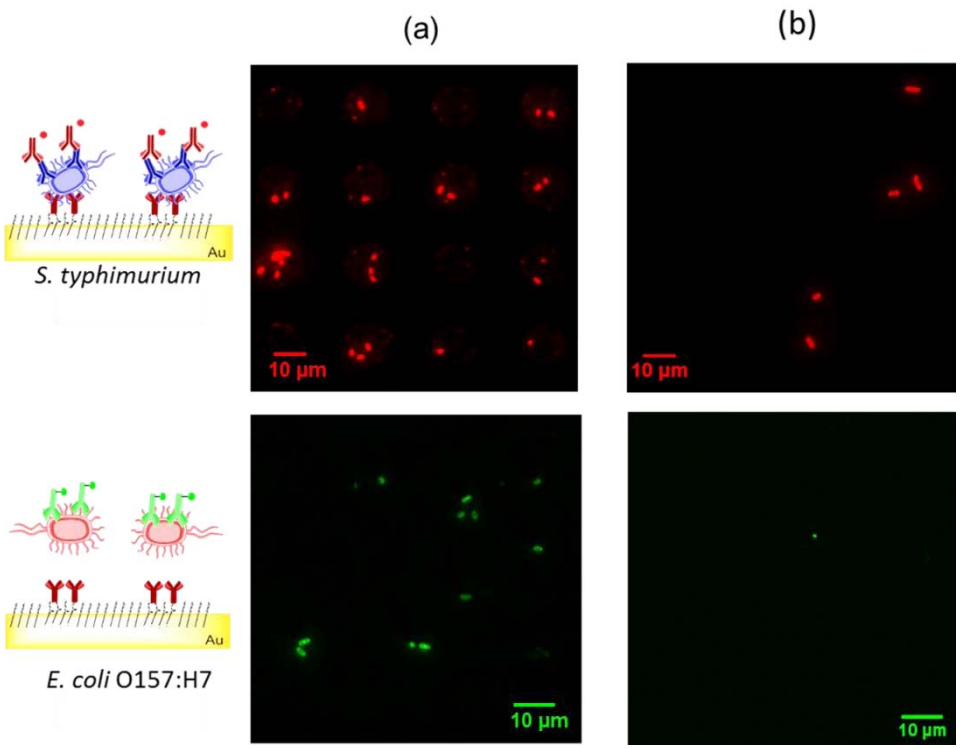


Figure 43. Fluorescence microscopy images of a microcontact printed array of primary monoclonal anti-*Salmonella* antibodies after incubation with *S. typhimurium* and non-specific bacteria *E. coli* O157:H7 ($10^8$ CFU $mL^{-1}$). (a) Heat-killed bacteria and (b) viable bacteria.

A significant increase in captured bacteria can be seen in Figure 43, comparing heat-killed with viable *S. typhimurium*. Monoclonal anti-*salmonella* antibodies are specific to *Salmonella* including *S. Typhimurium* but do not cross-react with *S. Typhi* or other Enterobacteriaceae including *E. coli* (various serotypes). No fluorescent signal was observed for non-specific *E. coli* O157:H7 using viable bacteria. However, very low *S. typhimurium* bacteria were found in the microarray, suggesting the low affinity of the

antibody to this type of bacteria. Additionally, Figure 43 also shows the non-specific adsorption of *E. coli* O157:H7 for heat-killed bacteria.

Altogether, these results show the limitations of the selected antibody in terms of sensitivity and specificity. We have demonstrated that it is not adequate for the detection of *S. typhimurium* due to the low affinity to the bacteria or as a consequence of non-specific adsorption, in particular for sample composed of pathogenic *E. coli* O157:H7 bacteria.

Finally, it is worth to mention that, besides the appropriateness of a functionalization strategy in terms of simplicity or selectivity, the specificity and sensitivity of the biorecognition elements (*e.g.* antibodies) are fundamental parameters for the development of biosensors or multi-analyte devices.

### 3.3.4 Strategy II: detection of E. coli O157:H7 bacteria by EIS

Detection of pathogenic bacteria *E. coli* O157:H7 was performed using the optimized functionalization strategy II by EIS. Figure 44 (a) shows the Nyquist plots of impedance spectra recorded for increasing concentrations of *E. coli* O157:H7 bacteria, ranging from 0 - $10^6$ CFU $mL^{-1}$.

A significant impedance difference upon the increase of bacteria concentrations can be observed. At *E. coli* O157:H7 concentrations higher than $3\times10^5$ CFU $mL^{-1}$ the difference diminished, suggesting the saturation of the system. To understand the physical origin of the observed response, the data was fitted and simulated using a Randles equivalent circuit model (see section 3.3.2 and Figure 44 (b)) by an acceptable error value ($\chi^2 = 0.035$).

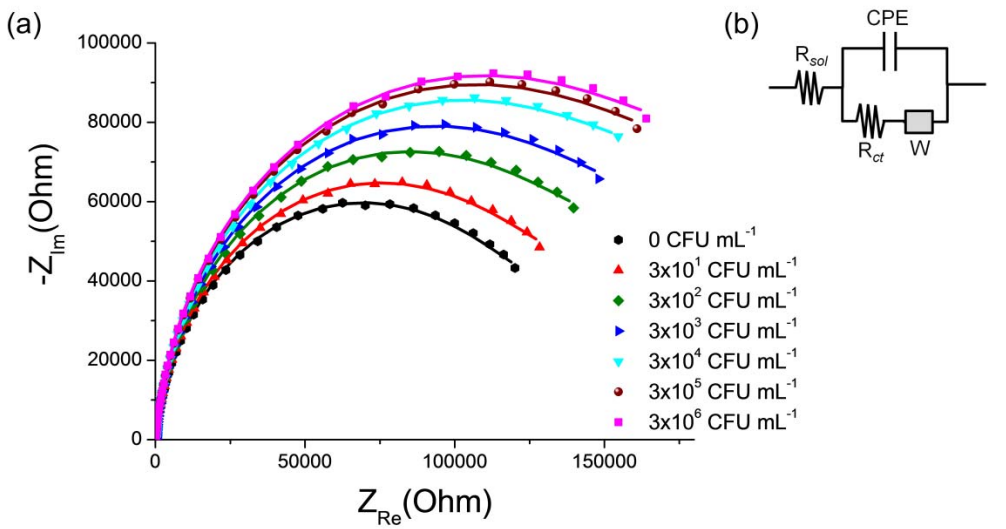


Figure 44. (a) Impedance Nyquist plot for different *E. coli* O157:H7 concentrations in presence of ferrocyanide as a redox probe (range 0-$10^6$ CFU mL$^{-1}$). The solid lines represent the fitting data obtained using the equivalent circuit model detailed in (b).

As mentioned earlier, $R_{ct}$ is very sensitive to electrode modifications produced by the binding of *E.coli* bacteria to the antibodies biorecognition layer. The result of the $\Delta R_{ct}$ ($R_{ct}^{Ab+bacteria}$ - $R_{ct}^{Ab}$) as a function of *E. coli* O157:H7 concentration is shown in Figure 45. A linear relationship was found in the range from 10-$10^4$ CFU mL$^{-1}$ ($\Delta R_{ct}$ = 15441 log ([*E.coli* O157:H7]) - 12176 ; R = 0.998).

The LOD of the immunosensor was 2 CFU mL$^{-1}$, being calculated using the equation $y_b$+3*$Std_b$ [46], where $y_b$ is the value for the blank (charge transfer resistance of the PBS solution without bacteria) and $Std_b$ is the standard deviation. To our best knowledge, this limit of detection is much lower than those reported previously [8, 13, 15, 16]. This low LOD might be due to the effectiveness and high selectivity of the functionalization protocol, as demonstrated in our results, together with the selectivity and affinity between the antibodies and the bacteria.

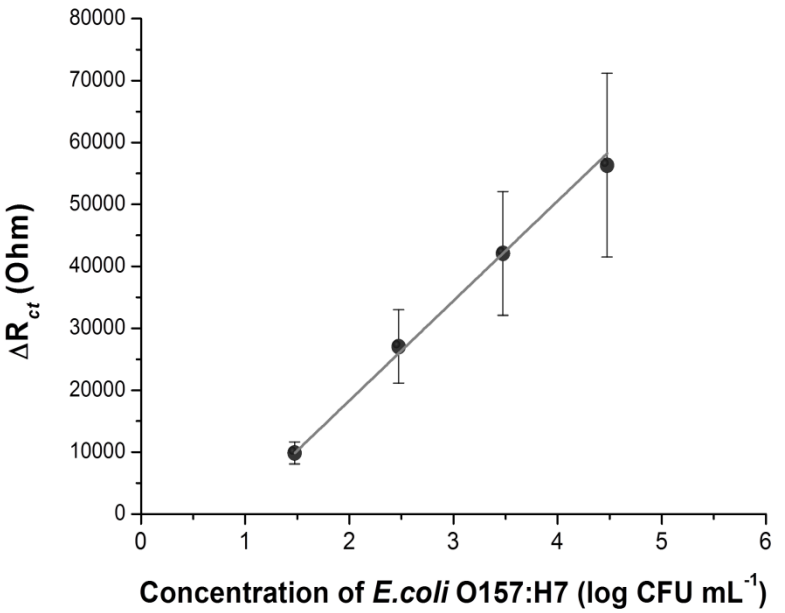


Figure 45. Relationship between $\Delta R_{ct}$ and *E.coli* O157:H7 concentrations with its corresponding linear fitting.

Sensor selectivity was quantitatively addressed by exposing the immunosensor to the non-specific bacteria strain Salmonella typhimurium. The ΔRct ratio values of *E. coli* O157:H7/*Salmonella typhimurium* bacterial cells for different bacteria concentration are shown in Figure 46; less than 20% of non-specific adsorption was observed, showing the specificity of the developed immunosensor.

Finally, the reproducibility and stability of the immmunosensor were also evaluated. First, the reproducibility was studied by constructing different immunosensors under the same optimized conditions. Comparing $R_{ct}^{Ab+bacteria}/R_{ct}^{Ab}$ value for the different immunosensors, a RSD value of 2% was obtained (n=3), indicating good reproducibility. The stability of the immunosensor was first addressed by storing it at 4ºC in PBS for 72 h. Then,

no significant reduction in its detection capabilities was observed when performing EIS measurements compared to fresh samples.

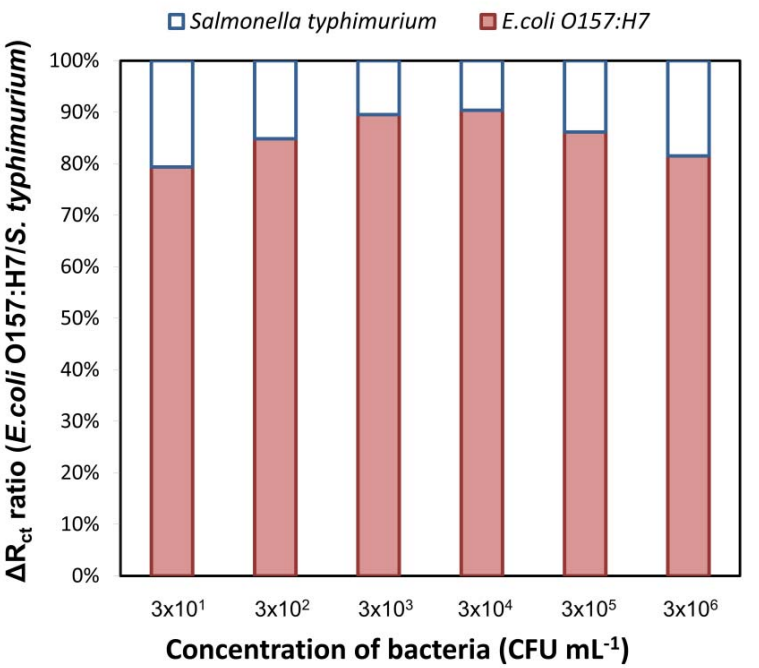


Figure 46. $\Delta R_{ct}$ ratio between *E.coli* O157:H7 and *Salmonella* for different concentrations.

It is worth noting that due to the high performance demonstrated by our sensor in terms of sensitivity, specificity and selectivity, this work could have important applications for the detection of low concentrations of pathogenic bacteria being potentially a promising alternative to more standard and conventional detection methods, such as ELISA (see next section).

### 3.3.5 Comparison with ELISA technique

The immunoreaction between the anti-*E. coli* antibody and the bacteria was compared with ELISA. Two polyclonal anti-*E. coli* antibodies were used in a sandwich assay as capture and detection antibodies. The anti-*E. coli* antibody employed to functionalize the gold surfaces was used as capture antibody, while detection antibody was linked to an enzyme (HPR).

Figure 47 shows the linear relationship between the absorbance and the concentration of *E. coli* O157:H7 (Absorbance = $5.74 \times 10^{-6}$ [*E. coli* O157:H7] + 0.110, R = 0.9986).

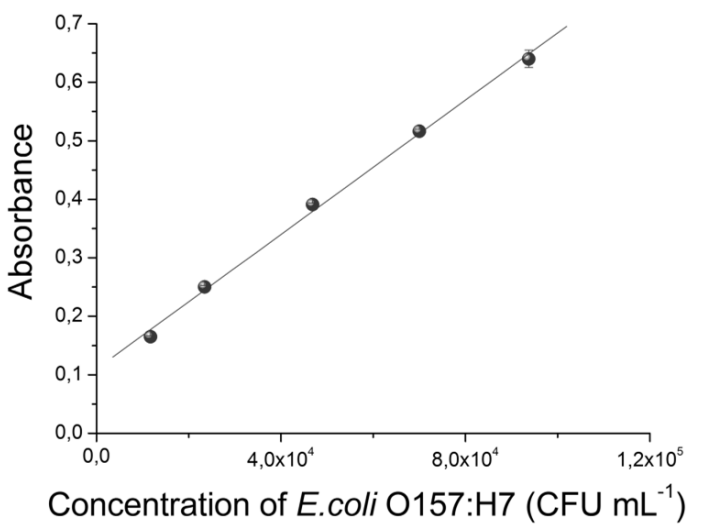


Figure 47. Test of the reactivity of anti-*E.coli* antibodies to *E.coli* O157:H7

These results indicate that the immunoreaction between the anti-*E. coli* antibody and the bacteria occurs over a linear range between $1 \times 10^4$ and $9 \times 10^4$ CFU $mL^{-1}$ with a LOD of $6 \times 10^3$ CFU $mL^{-1}$ [46]. The lower LOD of our

developed device confirms that the combination of biosensor strategy with EIS is appropriate for the development of highly sensitive pathogen sensors and offers an alternative to the existing ELISA assays, incorporating the simplicity and advantages of biosensors.

## 3.4 Conclusion and perspectives

In this chapter, we have fabricated and characterized a label-free EIS-based immunosensor for the detection of *E. coli* O157:H7 using two different strategies. The efficiency of the sensing platform was first demonstrated by SPR technique allowing the optimization and characterization of the surface antibody functionalization. Although the successful immobilization of the antibodies with both strategies was demonstrated, the lack of reproducibility and the low linear detection range obtained for strategy I, made it not appropriate for the development of a reliable immunosensor for the detection of *E. coli* O157:H7. For this reason, the functionalization protocol described in strategy II was selected for the detection and quantification of *E. coli* O157:H7 bacteria by EIS.

A limit of detection as low as 2 CFU $mL^{-1}$ was obtained, being the lowest LOD reported using gold surfaces and, very importantly, in agreement with the results obtained on ITO surfaces. Additionally, this approach shows a large linear detection range, which could be used to perform measurements on real samples with unknown concentration by simply measuring a dilution series without the need for sample pre-treatment or concentration steps.

Finally, the specificity of the system was demonstrated by EIS and fluorescence microscopy. This makes our approach very attractive for the development of multi-analyte devices. Multi-electrodes platform has strong

potential application for being applied in parallel sensing of different analytes under the same experimental conditions.

## 3.5 References

[1] J.C. Love, L.A. Estroff, J.K. Kriebel, R.G. Nuzzo, G.M. Whitesides, Self-assembled monolayers of thiolates on metals as a form of nanotechnology, Chem. Rev. 105 (2005) 1103–69.

[2] C.D. Bain, J. Evall, G.M. Whitesides, Formation of monolayers by the coadsorption of thiols on gold : variation in the head group , tail group , and solvente, J. Am. Chem. Soc. 111 (1989) 7155–7164.

[3] R.G. Nuzzo, D.L. Allara, Adsorption of bifunctional organic disulfides on gold surfaces, J. Am. Chem. Soc. 105 (1983) 4481–4483.

[4] M. Mrksich, G.M. Whitesides, Patterning self-assembled monolayers using microcontact printing: A new technology for biosensors?, Trends Biotechnol. 13 (1995) 228–235.

[5] S.K. Arya, P.R. Solanki, M. Datta, B.D. Malhotra, Recent advances in self-assembled monolayers based biomolecular electronic devices., Biosens. Bioelectron. 24 (2009) 2810–7.

[6] M. Zourob, S. Elwary, A. Turner, Principles of bacterial detection: biosensors, recognition receptors and microsystems, Springer, 2008.

[7] M.J. Linman, K. Sugerman, Q. Cheng, Detection of low levels of Escherichia coli in fresh spinach by surface plasmon resonance spectroscopy with a TMB-based enzymatic signal enhancement method, Sens. Actuators B 145 (2010) 613–619.

[8] R. Maalouf, C. Fournier-Wirth, J. Coste, H. Chebib, Y. Saïkali, O. Vittori, et al., Label-free detection of bacteria by electrochemical impedance spectroscopy: comparison to surface plasmon resonance, Anal. Chem. 79 (2007) 4879–86.

[9] O. Tokarskyy, D.L. Marshall, Immunosensors for rapid detection of Escherichia coli O157:H7 - perspectives for use in the meat processing industry, Food Microbiol. 25 (2008) 1–12.

[10] L.S. Jung, K.E. Nelson, C.T. Campbell, P.S. Stayton, S.S. Yee, V. Pe, et al., Surface plasmon resonance measurement of binding and dissociation of wild-type and mutant streptavidin on mixed biotin-containing alkylthiolate monolayers, Sens. Actuators 54 (1999) 137–144.

[11] Z.-Q. Shen, J.-F. Wang, Z.-G. Qiu, M. Jin, X.-W. Wang, Z.-L. Chen, et al., QCM immunosensor detection of Escherichia coli O157:H7 based on beacon immunomagnetic nanoparticles and catalytic growth of colloidal gold, Biosens. Bioelectron. 26 (2011) 3376–81.

[12] Y.S. Kim, H.S. Jung, T. Matsuura, H.Y. Lee, T. Kawai, M.B. Gu, Electrochemical detection of 17beta-estradiol using DNA aptamer immobilized gold electrode chip, Biosens. Bioelectron. 22 (2007) 2525–31.

[13] P. Geng, X. Zhang, W. Meng, Q. Wang, W. Zhang, L. Jin, et al., Self-assembled monolayers-based immunosensor for detection of Escherichia coli using electrochemical impedance spectroscopy, Electrochim. Acta. 53 (2008) 4663–4668.

[14] J. Lahiri, L. Isaacs, J. Tien, G.M. Whitesides, A Strategy for the generation of surfaces presenting ligands for studies of binding based on an active ester as a common reactive intermediate : a surface plasmon resonance study, Anal. Chem. 71 (1999) 777–790.

[15] C.-K. Joung, H.-N. Kim, H.-C. Im, H.-Y. Kim, M.-H. Oh, Y.-R. Kim, Ultra-sensitive detection of pathogenic microorganism using surface-engineered impedimetric immunosensor, Sens. Actuators B 161 (2012) 824–831.

[16] V. Escamilla-Gómez, S. Campuzano, M. Pedrero, J.M. Pingarrón, Gold screen-printed-based impedimetric immunobiosensors for direct and sensitive Escherichia coli quantisation, Biosens. Bioelectron. 24 (2009) 3365–71.

[17] Z. Muhammad-Tahir, E.C. Alocilja, Fabrication of a disposable biosensor for Escherichia coli O157:H7 detection, IEEE Sens. J. 3 (2003) 345–351.

[18] D. Ivnitski, I. Abdel-hamid, P. Atanasov, E. Wilkins, Biosensors for detection of pathogenic bacteria, Biosens. Bioelectron. 14 (1999) 599–624.

[19] P.M. Fratamico, T.P. Strobaugh, M.B. Medina, A.G. Gehring, Detection of Escherichia coli O157 : H7 using a surface plasmon resonance biosensor, Biotechnology. 12 (1998) 571–576.

[20] Ercole, C., DelGallo, M., Mosiello, L., Baccella, S., Lepidi, A., Escherichia coli detection in vegetable food by a potentiometric biosensor, Sens. Actuators B 91 (2003) 163–168.

[21] Y. Su, X.L. , Li, A self-assembled monolayer-based piezoelectric immunosensor for rapid detection of Escherichia coli O157:H7, Biosens. Bioelectron. 19 (2004) 563–574.

[22] B.K. Choi, J.W., Oh, Optical Detection of Pathogens using Protein Chip, Adv. Environ. Monit. 19 (2008) 348–362.

[23] P.M. Fratamico, T.P. Strobaugh, M.B. Medina, A.G. Gehring, A surface plasmon resonance biosensor for real-time immunologic detection of Escherichia Coli O157:H7, New Techniques in the Analysis of Foods. Kluwer Academic, New York,, 1999.

[24] B.-K. Oh, W. Lee, W.H. Lee, J.-W. Choi, Nano-scale probe fabrication using self-assembly technique and applications to detection of Escherichia coli O157:H7, Biotechnol. Bioprocess Eng. 8 (2003) 227–232.

[25] C. Meeusen, E. Alocilja, W. Osburn, Detection of E-coli O157: H7 using a miniaturized surface plasmon resonance biosensor, Trans. Asae. 48 (2005) 2409–2416.

[26] A. Taylor, Q. Yu, S. Chen, J. Homola, S. Jiang, Comparison of E. coli O157:H7 preparation methods used for detection with surface plasmon resonance sensor, Sens. Actuators B 107 (2005) 202–208.

[27] A. Subramanian, J. Irudayaraj, T. Ryan, A mixed self-assembled monolayer-based surface plasmon immunosensor for detection of E. coli O157:H7, Biosens. Bioelectron. 21 (2006) 998–1006.

[28] E. Prats-Alfonso, F. García-Martín, N. Bayo, L.J. Cruz, M. Pla-Roca, J. Samitier, et al., Facile solid-phase synthesis of biotinylated alkyl thiols, Tetrahedron. 62 (2006) 6876–6881.

[29] J. Vidic, M. Pla-Roca, J. Grosclaude, M.-A. Persuy, R. Monnerie, D. Caballero, et al., Gold surface functionalization and patterning for specific immobilization of olfactory receptors carried by nanosomes, Anal. Chem. 79 (2007) 3280–90.

[30] R.S. Kane, S. Takayama, E. Ostuni, D.E. Ingber, G.M. Whitesides, Patterning proteins and cells using soft lithography, Biomaterials 20 (1999) 2363–76.

[31] I. Horcas, R. Fernández, J.M. Gómez-Rodríguez, J. Colchero, J. Gómez-Herrero, a M. Baro, WSXM: a software for scanning probe microscopy and a tool for nanotechnology., Rev. Sci. Instrum. 78 (2007) 013705.

[32] K.E. Nelson, L. Gamble, L.S. Jung, M.S. Boeckl, E. Naeemi, S.L. Golledge, et al., Surface characterization of mixed self-assembled monolayers designed for streptavidin immobilization, Society (2001) 2807–2816.

[33] P. Leonard, S. Hearty, J. Quinn, R. O'Kennedy, A generic approach for the detection of whole Listeria monocytogenes cells in contaminated samples using surface plasmon resonance, Biosens. Bioelectron. 19 (2004) 1331–5.

[34] B. Byrne, E. Stack, N. Gilmartin, R. O'Kennedy, Antibody-based sensors: principles, problems and potential for detection of pathogens and associated toxins., Sensors 9 (2009) 4407–45.

[35] R. Maalouf, W.M. Hassen, C. Fournier-Wirth, J. Coste, N. Jaffrezic-Renault, Comparison of two innovatives approaches for bacterial detection: paramagnetic nanoparticles and self-assembled multilayer processes, Microchim. Acta. 163 (2008) 157–161.

[36] Y. Hou, S. Helali, A. Zhang, N. Jaffrezic-Renault, C. Martelet, J. Minic, et al., Immobilization of rhodopsin on a self-assembled multilayer and its specific detection by electrochemical impedance spectroscopy, Biosens. Bioelectron. 21 (2006) 1393–402.

[37] L. Yang, R. Bashir, Electrical/electrochemical impedance for rapid detection of foodborne pathogenic bacteria, Biotechnol. Adv. 26 (2008) 135–50.

[38] J.S. Daniels, N. Pourmand, Label-Free impedance biosensors: opportunities and challenges, Electroanalysis 19 (2007) 1239–1257.

[39] C. Ruan, L. Yang, Y. Li, Immunobiosensor chips for detection of Escherichia coli O157:H7 using electrochemical impedance spectroscopy, Anal. Chem. 74 (2002) 4814–4820.

[40] Y. Wang, Z. Ye, Y. Ying, New trends in impedimetric biosensors for the detection of foodborne pathogenic bacteria, Sensors 12 (2012) 3449–71.

[41] M. Barreiros dos Santos, C. Sporer, N. Sanvicens, N. Pascual, A. Errachid, E. Martinez, et al., Detection of pathogenic Bacteria by Electrochemical Impedance Spectroscopy: Influence of the immobilization strategies on the sensor performance, Procedia Chem. 1 (2009) 1291–1294.

[42] A. Rachkov, S. Patskovsky, A. Soldatkin, M. Meunier, Surface plasmon resonance detection of oligonucleotide sequences of the rpoB genes of Mycobacterium tuberculosis, Talanta 85 (2011) 2094–9.

[43] F.S. Damos, R.C.S. Luz, L.T. Kubota, Determination of thickness, dielectric constant of thiol films, and kinetics of adsorption using surface plasmon resonance, Langmuir 21 (2005) 602–9.

[44] A.J. Guiomar, J.T. Guthrie, S.D. Evans, Use of mixed self-assembled monolayers in a study of the effect of the microenvironment on immobilized glucose oxidase, Langmuir 15 (1999) 1198–1207.

[45] G.T. Hermanson, Bioconjugate Techniques, second edi, Academic Press, 2008.

[46] J. Miller, J. Miller, Statistic and Chemometrics for analytical chemistry, Fifth edit, Pearson Prentice Hall, 2005.

# **Chapter 4.** Detection of pathogenic bacteria by means of multi-electrode platform

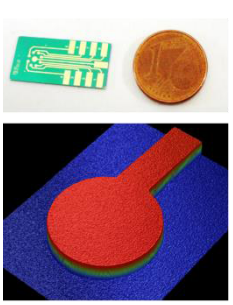

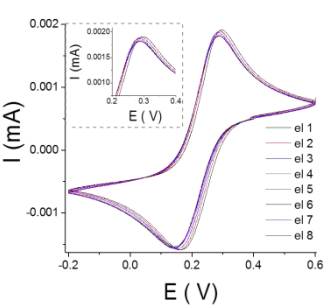


In this chapter, we used all the knowledge acquired in the previous chapter 3 in order to develop a miniaturized multi-electrodes array for the detection of pathogenic bacteria. The multi-electrodes were fabricated in gold and consisted of multiple equally independent gold electrodes. This allowed high-throughput and independent experiments, in parallel and under the same experimental conditions. Multi-electrodes were fabricated by standard photolithography techniques and characterized by several surface analysis and electrochemical techniques, confirming the quality of the fabrication process. The biosensing capabilities of the multi-electrode platform were demonstrated through the detection of pathogenic bacteria using antibodies or AMPs, and encouraging results were obtained.

## Chapter index

## 4.1 Introduction

Standard electrochemical sensors are based on single working electrodes and, as a consequence, lack of high-throughput characteristics. This limits the number of samples that can be analyzed and can also lead to false positives. These limitations led to the development of multi-electrode platforms (also called arrays of multiple working electrodes). These systems bring several advantages to the electrochemical detection, such as parallel and multiple identical experiments or the possibility to perform repetitive experiments with the corresponding increase in reproducibility.

Examples of arrays of working electrodes have been widely described in the area of genosensing, aiming the substitution of fluorescent DNA chips by electrochemical detection, for easier on-site or point-of-care use [1, 2]. In the past 5 years, arrays for electrochemical DNA/oligonucleotide detection have been widely reported. They differ from the method used for the electrochemical detection, the geometry and in specific characteristics of the arrays (Figure 48). The number of individually addressed working electrodes vary from 3 (Figure 48 (a)) [3] to 48 (Figure 48 (b)) [4] and their size from mm (Figure 48 (c)) [5, 6] to µm-scale (Figure 48 (d)), resulting in microarrays [4, 7, 8]. They also differ in their integrated components. In some cases, they show individual 3-electrode units with external reference/counter electrodes (Figure 48 (e)) [9] whereas in other cases multiple working electrodes with integrated shared counter and reference electrodes are described (Figure 48 (c)) [3, 5, 6]. Finally, in some other cases, microfluidics modules are included in the sensing device (Figure 48 (a)) [3, 10].

A variety of electrochemical methods have been used for the detection of different electrochemical labels (HRP or ALP conjugates,

methylene blue, ferrocene and electroactive nanoparticles), such as amperometry [4, 9], CV [9], voltammetry [3] or differential pulse voltammetry [6]. The array approach is gaining popularity combined with other electrochemical methods, such as EIS.

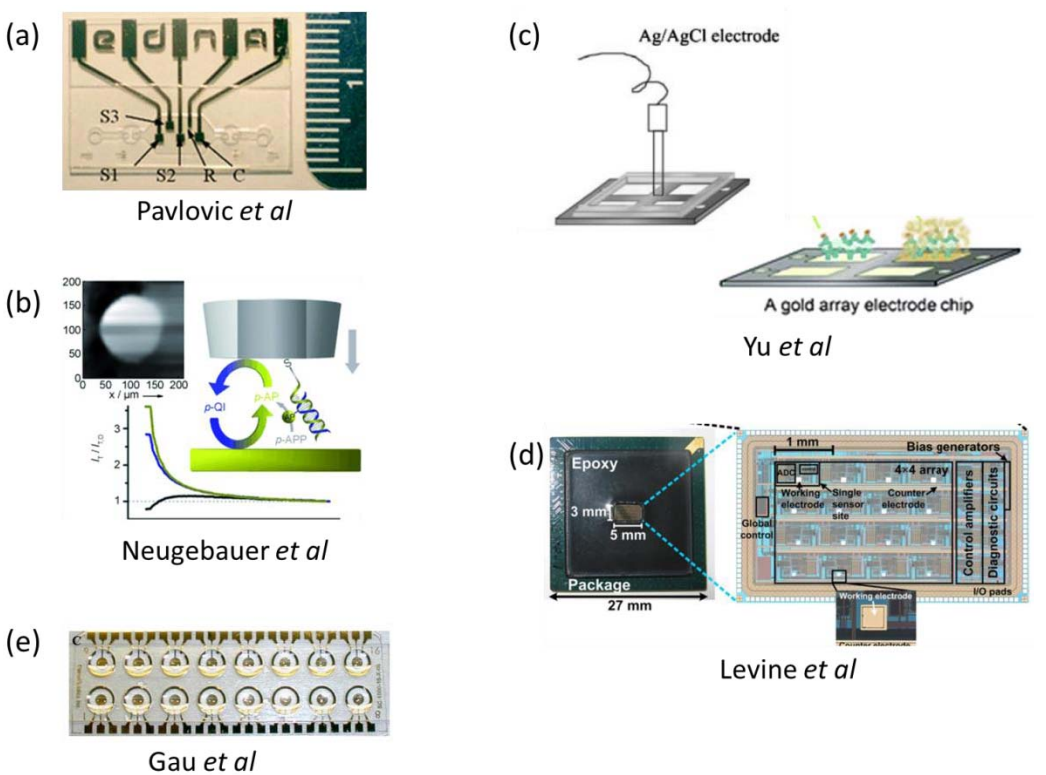


Figure 48. Examples of electrochemical arrays with (a) 3 and (b) 48 working electrodes, ranging from (c) mm to (d) µm scale. Different types of configurations are also shown: (e) arrayed individual 3-electrode units or (c) multi-working electrode with shared reference and counter electrodes.

EIS can be used for immunosensing (see Chapter 2 and 3), aptamer-based protein biosensing as well as for genosensing [11, 12]. EIS is widely used for electrochemical measurements of molecular interactions and compared to other electrochemical methods, such as CV or DPV, it is less

destructive to the measured biological interactions. Electrochemically inert species can be measured by EIS in the presence of a redox agent, such as iron ferrocyanide(s), which undergoes oxidation and reduction at the surface of the electrode, thus making possible label-free detection [13].

EIS was used in the 4-electrode multispecific array setup for immunosensing by enzyme-induced precipitation [5] and on an 8-electrode microarray chip for label-free oligonucleotide mismatch detection (with all microelectrodes undergoing similar modification) [7]. The sensitive EIS technique together with the multiplexing capability of microarrays neglected the possibility of false positives providing high performance characteristics to the device. Altogether, this demonstrates that the combination of multi-electrode arrays with EIS is a powerful strategy for the development of high performance and high-throughput electrochemical biosensors.

In this chapter, we present a multi-electrode device for the impedimetric detection of pathogenic bacteria *E. coli* O175:H7. Our main objectives in the design of the multi-electrode array are: (i) multispecificity, (ii) cost-efficiency and (iii) experimental convenience and speed.

The electrochemical device is based on multi-electrodes with four (ME 4), six (ME 6) or eight (ME 8) individual working electrodes. The multi-electrodes were fabricated in gold surfaces since it is a material with very well defined properties and considering the good results obtained in chapter 3, including the optimized functionalization strategy. Gold is bio-compatible, easy to obtain and defined structures can be easily fabricated by means of photolithography. Photolithography is a standard microfabrication method used to transfer by UV exposure a design (*e.g.* an array of structures) from a photomask onto a photoresist spin-coated on a substrate. The structured photoresist can be used then to protect or open desired areas on the

substrate material during the wet etching step for subsequent patterning. The photolithography process is divided into the following procedural steps: substrate cleaning and preparation, photoresist application (spin-coating), UV light exposure, developing (such as etching or lift-off) and photoresist removal.

The multi-electrodes platforms were characterized by means of several techniques in order to evaluate its manufacturing quality and operational performance. Then, the multi-electrodes were applied for the detection of pathogenic bacteria using antibodies as biorecognition elements. The antibody immobilization on the individual gold electrodes was performed following the optimized protocols described in chapter 3. Finally, a proof-of-concept of its detection capabilities was evaluated by EIS using pathogenic bacteria *E. coli* O175:H7 as detection target.

Additionally, the detection capabilities of the multi-electrode were also evaluated using an increasingly popular bio-recognition element: antimicrobial peptides. AMP is a part of the host's innate immune system in many organisms and serves as the first line of defense against microbial invasion. Highly stable to adverse conditions, AMPs bind semi-selectively to microbial cell surfaces and exert their antimicrobial activity through membrane disruption [14]. The ease of synthesis and intrinsic stability of AMPs render them particularly interesting candidates for use as molecular recognition elements in biosensing platforms since they are much more stable than typical globular proteins. The replacement of current antibody-based affinity probes with more stable and durable AMPs in biological sensors may thus help to increase the shelf life of current diagnostic platforms [15].

## 4.2 Experimental procedures

### 4.2.1 Chemicals and reagents

DIEA, 6-mercaptohexanoic acid (MHA), 6-mercapto-1-hexanol 97% (MCH), MHDA, PFP, EDC, PBS and AEE were purchased from Sigma Aldrich. Sodium hydrogen carbonate, hydrogen peroxide, sulphuric acid, acetone and ethanol absolute were purchased from Panreac, while potassium hexacyanoferrate(III) and potassium hexacyanoferrate(II) from Fluka.

Gold etch solution potassium iodine (type TFA, Transene Company Inc.), AZ5214E photoresist, AZ726 MIF developer and AZ100 remover (MicroChemicals GmbH) were used for microfabrication.

All the capture and detection antibodies, as well the bacteria samples used in this chapter, were already described in chapters 2 and 3 (sections 2.2.1 and 3.2.1). Magainin I (GIGKFLHSAGKFGKAFVGEIMKS), a class of AMP, was synthesized with an additional cysteine residue at the C terminus in collaboration with the group of Prof. Fernando Albericio and Dr. Hortensia Rodríguez (IRB, Barcelona, Spain).

### 4.2.2 Multi-electrodes fabrication procedure

Gold substrates consisting of a 200 nm gold layer and a 50 nm titanium adhesion layer on silicon oxide slides (NTB, Switzerland) were used as substrates to fabricate the multi-electrodes by photolithography. Photolithography was performed using a spin coater (WS-650MZ-23NPP/LITE, Laurell Technologies Corporation) and a mask aligner (MJB4, SUSS MicroTec;

350 W Hg lamp). Figure 49 shows a scheme of the complete fabrication process.

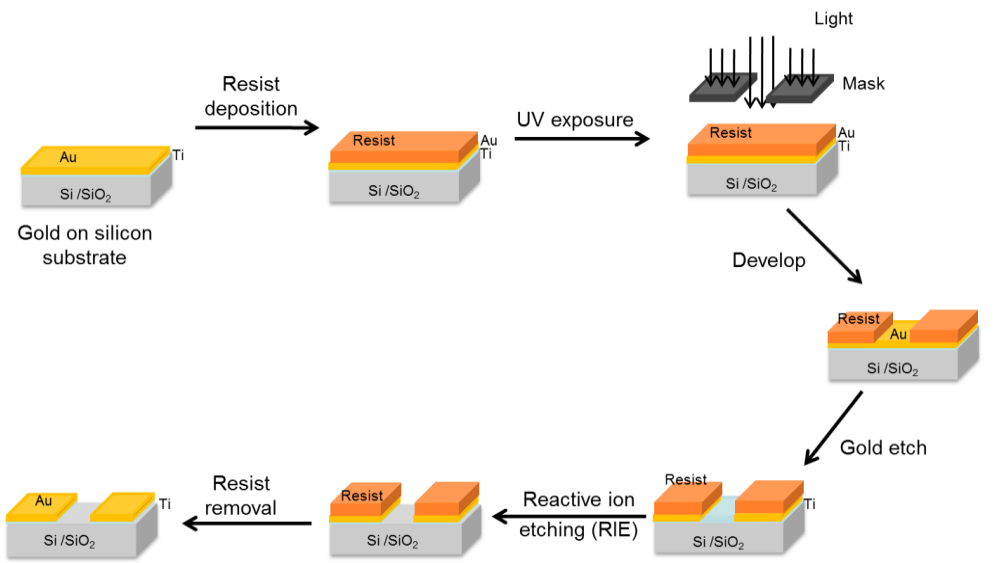


Figure 49. Scheme of the multi-electrodes fabrication procedure.

Briefly, a layer of AZ5214 E photoresist was deposited onto the gold wafer by spin-coating for 20 s at 2000 rpm (revolutions per minute). The photoresist was initially soft baked on a hotplate (Selecta, Spain) for 120 s at 95 ◦C and then exposed to UV light (wavelength = 365 nm) for 7.2 s with an exposure of 200.16 mJ $cm^{-2}$ using a positive mask. Resist development was achieved by immersion in AZ726 MIF developer for 30 s and gold etching was completed by immersion in TFA for 70 s. Titanium layer was eliminated by reactive ion etching (RIE) (Plasmalab 80, Oxford instruments, UK) using a mixture of gases ($CHF_3$ and $Cl^-$). Finally, the remaining photoresist was removed by immersion in AZ100 for 40 s and the substrate was rinsed with Milli-Q water and dried with nitrogen.

### 4.2.3 Passivation procedure

The non-active gold areas of the multi-electrodes were passivated to avoid unspecific adsorption. This passivation step was performed in collaboration with the group of Dr. José Antonio Plaza at CNM-CSIC (Cerdanyola del Vallès, Spain) also using photolithography processes. Briefly, a layer of $SiO_2/Si_3N_4$ mixture (4 µm of $SiO_2$ and 7 µm of $Si_3N_4$) was deposited onto the gold-silicon substrate. The photoresist was deposited and exposed to UV light creating an inverse multi-electrode structure after the development. Reactive ion etching (RIE) was applied in order to eliminate the $SiO_2/Si_3N_4$ layer over the gold active areas. Finally, the photoresist was removed and the multi-electrodes were ready to use.

The multi-electrodes platforms were fabricated on a 3´´ wafer, including the 4, 6 and 8 working electrodes designs. After the fabrication and passivation process, each single chip was cut in individual pieces of around 1 cm x 2 cm.

### 4.2.4 Multi-electrodes characterization

An optical and electrochemical characterization was performed to check the fabrication quality and operational performance of the fabricated multi-electrodes. An interferometer WYKO NT1100 (Veeco Instruments, USA), an optical microscopy Eclipse L150 (Nikon Instruments Inc., Netherlands) and a profilometer DEKTAK 6M (Veeco Instruments, USA) were used for optical characterization.

CV and EIS experiments were performed on a VMP2 multipotentiostat (Princeton Applied Research, France) with EC-Lab software (Bio-Logic SAS) or

by Autolab PGSTAT100 potentiostat/galvanostat with Nova 1.6 software (Eco Chemie, The Netherlands). For all the electrochemical experiments, a three-electrode electrochemical cell placed into a Faraday cage in the dark was used (Figure 50). The multi-electrode platform was used as working electrode, a platinum as counter electrode and an Ag/AgCl reference electrode. The multi-electrodes array was connected to the array holders with 4 contacting pins.

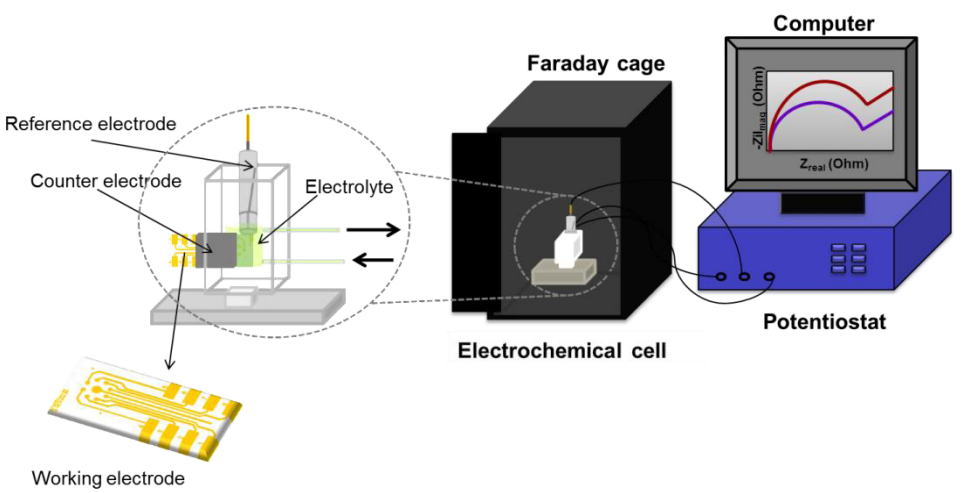


Figure 50. Scheme of the setup used for the electrochemical measurements using the multi-electrodes.

EIS measurements were accomplished in PBS (5 mM) $K_3[Fe(CN)_6]$ /$K_4[Fe(CN)_6]$ solution at RT over a frequency range from 100 kHz to 1 Hz, using a perturbation amplitude of 10 mV. During the measurements the potential was kept at 0.2 V. CV measurements were achieved at 100 mV $s^{-1}$, between -0.2 V and 0.6 V. Data analysis was accomplished using EC-Lab software (Bio-Logic SAS). A mixed SAM (1 mM) of mercaptodecanoic acid and mercaptohexanol (1:9) was used to characterize electrochemically the functionalization and regeneration steps of the multi-electrodes.

### 4.2.5 Gold cleaning procedure

The gold working electrodes were first rinsed and cleaned with acetone, and subsequently with ethanol and Milli-Q water to remove possible organic contaminants. Afterwards, they were immersed into Piranha solution (3:7 v/v $H_2O_2$:$H_2SO_4$) for 10 minutes, rinsed thoroughly with Milli-Q water and absolute ethanol, and dried under a stream of nitrogen. In some cases, the multi-electrodes were also cleaned electrochemically by performing cyclic voltammograms in 0.1 M and/or 0.5 M $H_2SO_4$ solution between -0.2 V and +1.6 V vs Ag/AgCl at 100 mV $s^{-1}$ (see section 4.3.1.2).

### 4.2.6 Antibody immobilization procedure

The antibody immobilization was performed according to the previous optimized procedure described in chapter 3 (section 3.2.3). Briefly, SAMs of MHDA were formed on the previously cleaned gold surfaces by immersion into a 2 mM ethanolic solution overnight. Carboxylic acid groups were then activated using a mixture of EDC (0.2 M), PFP (0.2 M), and DIEA (0.2 M) in absolute ethanol during 30 min. Subsequently, the substrates were washed and antibodies (15 μg $mL^{-1}$ solution in PBS) were incubated for 1 h depositing a very small drop (<1 μL) on each electrode. The electrodes were again washed and the remaining active ester functionalities were blocked by immersing the electrodes into a 10 mM AEE solution in sodium bicarbonate buffer (pH 8.3) during 30 min. Finally, the substrates were washed and stored under PBS solution at 4ºC.

### 4.2.7 Antimicrobial peptides immobilization procedure

The immobilization of the AMPs onto the working electrodes was performed by optimized condition according to Manoor *et al* [15]. Briefly, magainin I in PBS buffer (800 µg $mL^{-1}$) was incubated onto the cleaned gold multi-electrodes for 60 min under static conditions. The functionalized electrodes were then thoroughly washed with PBS to remove any unbound AMPs, rinsed with Milli-Q water and dried with $N_2$.

### 4.2.8 Electrochemical detection

Electrochemical detection of pathogenic bacteria was performed on a VMP2 multipotentiostat (Princeton Applied Research, France) and a CH Instruments potentiostat (Austin, USA) for the immunosensor and antimicrobial peptide-based multi-electrodes, respectively. EIS measurements were performed in PBS / 5 mM $K_3[Fe(CN)_6]$ / $K_4[Fe(CN)_6]$ solution at RT over a frequency range from 100 kHz to 1 Hz, using a perturbation amplitude of 10 mV. During the measurements the potential was kept at 0.2 V.

The samples of bacterial cells (*E. coli* O157:H7 and *S. typhimurium*) were incubated with the immobilized antibody or magainin I multi-electrode for 45 min in the dark, at RT. After incubation, the gold surfaces were washed with PBS buffer and impedance measurements were performed. Data analysis was accomplished using EC-Lab software (Bio-Logic SAS, France).

### 4.2.9 Immunofluorescence

Bacteria detection was performed by means of a sandwich assay by incubation of *E. coli* O157:H7 bacteria onto the antibody-modified multi-electrode and a secondary FITC-conjugated anti-*E. coli* polyclonal antibody (0.1 mg $mL^{-1}$) for 1 h. An Eclipse E1000 upright epifluorescence microscope (Nikon, Japan) equipped with a CCD camera was used for the immunofluorescence characterization. Fluorescence images were obtained using a 40X Nikon air objective and a FITC filter. Captured images were analyzed with image processing software (ImageJ, NIH, USA).

## 4.3 Results and discussion

As described above, a multi-electrode platform was developed in order to perform multiple and repetitive experiments in parallel under the same experimental conditions increasing the speed and the reproducibility of the measurements. By using this system, it is possible to perform single analyte-binding experiments using working electrodes modified with different bioreceptors. Alternatively, each working electrode can also be incubated with a different analyte by depositing very small drops on top of each electrode (< 1 µL).

Figure 51 shows the different designs of the multi-electrodes containing 4 (Figure 51 (a)), 6 (Figure 51 (b)) and 8 (Figure 51 (c)) working electrodes. The multi-electrodes were specifically designed to fit into a home-made teflon-based electrochemical cell, which can be filled with a small volume (200 µL) of the analyte solution or measuring buffer. The array of circular working electrodes were equally distributed having different

diameters (1000 µm, 800 µm and 600 µm) for the 4, 6 and 8 working electrodes, respectively.

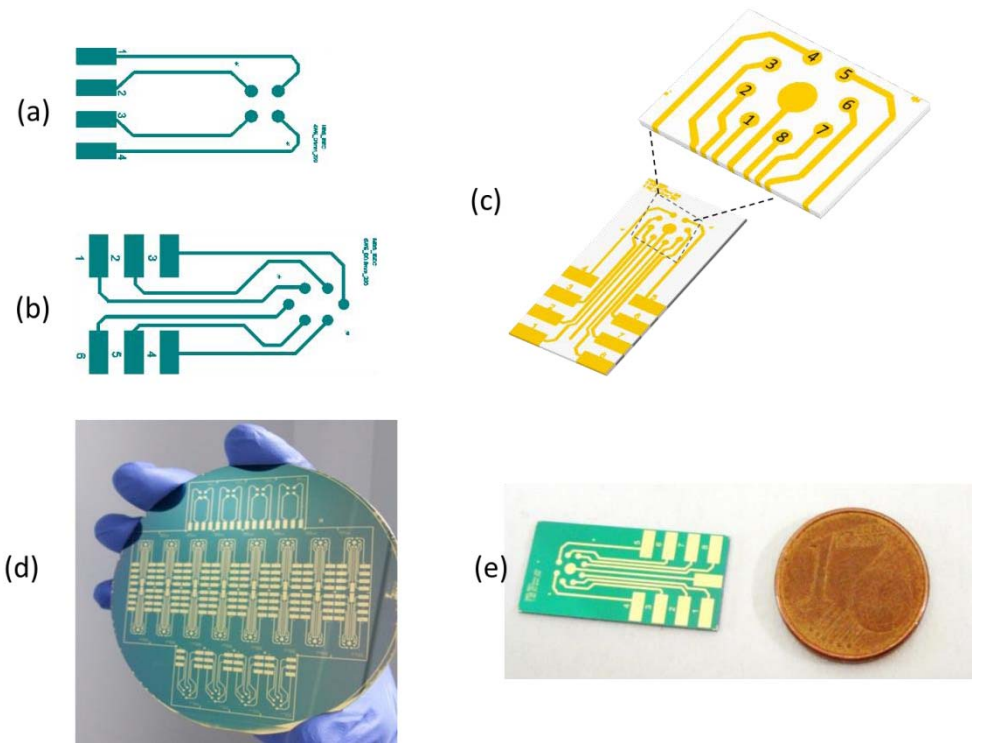


Figure 51. Schematic illustration of the different multi-electrodes designs containing (a) 4, (b) 6 and (c) 8 working electrodes. (d) Photography of the fabricated multi-electrodes wafer and (e) a zoomed image of a multi-electrode unit containing 8 working electrodes.

Figure 51 (d) shows a picture of the silicon wafer containing the fabricated multi-electrodes with different number of working electrodes. A zoomed image of a ME8 multi-electrode is shown in Figure 51 (e). Although the fabrication of the electrode array is cost-effective (estimated 25€ per multi-electrode), this cost can be reduced in mass production or by using

cheaper gold deposited materials such as the polymer-based technology as described elsewhere [16].

### 4.3.1 Multi-electrodes manufacture

In this section, we describe the optical and electrochemical characterization of the multi-electrodes to check the quality of the manufacturing process and their operational properties. After that, we present a proof-of-concept of its detection capabilities of *E. coli* O157:H7 pathogenic bacteria using first, commercially-available antibodies and second, antimicrobial peptides.

#### *4.3.1.1 Optical characterization*

Figure 52 (a) shows a 3D image of a single working electrode of a ME 8 multi-electrode measured by white light interferometry. The typical dimensions of the gold electrode can be seen in Figure 52 (b).

A perfect defined working electrode is observed and the measured diameter is in agreement with the theoretical value (diameter = 600 µm). The quality and reproducibility of the fabrication process was evaluated. We measured the mean diameters of the multi-electrodes ME 4, ME 6 and ME8 obtaining values of 996±3 µm (n=3), 799±3 µm (n=5) and 599±1 µm (n=7), respectively.

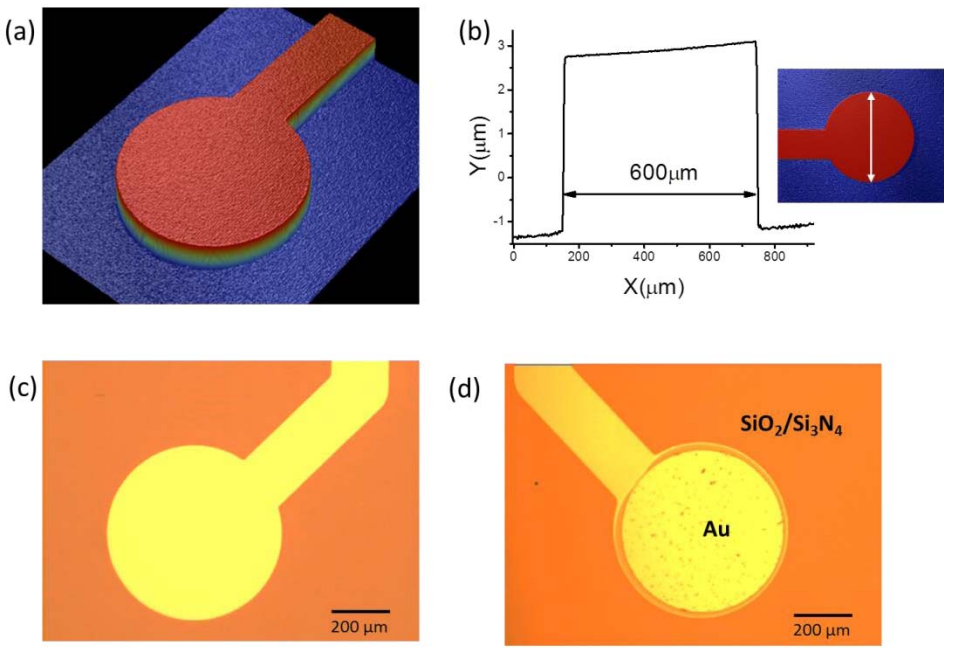


Figure 52. (a) Interferometer 3D image of a single working electrode and (b) subsequent cross-section plot. Optical microscopy images of a working electrode (c) before and (d) after the passivation process with $SiO_2/Si_3N_4$.

To minimize non-specific absorption, multi-electrodes were passivated. A thin layer of $SiO_2/Si_3N_4$ was deposited around the different working electrodes (see section 4.2.3). Comparing the optical microscopy images before (Figure 52 (c)) and after (Figure 52 (d)) the passivation process, it can be seen the successful passivation of the non-active areas of the multi-electrodes. The circular gold region on the electrode (named as Au in Figure 52 (d)) is the only part to be functionalized and used as the biorecognition area.

Altogether, the fabrication of the multi-electrodes was shown to be highly reproducible, including both the procedure as well as the passivation process.

#### *4.3.1.2 Electrochemical characterization*

Multi-electrodes were further characterized by electrochemical methods in order to evaluate its operational performance. A cyclic voltammogram for the 8 working electrodes using the same ME8 multi-electrode is shown in Figure 53.

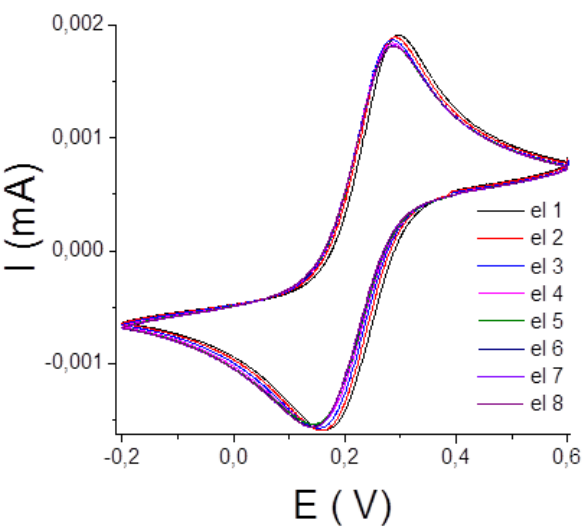


Figure 53. Typical cyclic voltammogram obtained for the 8 working electrodes of a ME 8 chip (*el:* electrode).

It was possible to verify the current peaks related to the $Fe(CN)_6^{3-/4-}$ maximum oxidation and reduction. The measured current for the oxidation peak for the 8 working electrodes was 1.59 ± 0.3 µA. The overall oxidation peak current showed a coefficient of variation of 2%, indicating very good precision and fabrication reproducibility of the electrodes.

We next evaluated the response of the sensor using EIS technique. Figure 54 shows the typical Nyquist plots of impedance spectra recorded for the 8 gold electrodes of one ME8 multi-electrode.

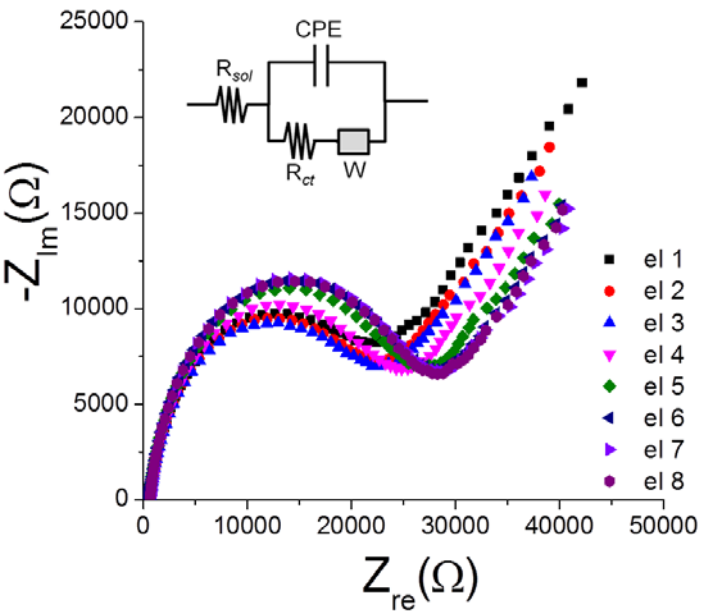


Figure 54. Typical Nyquist impedance spectrum obtained for the 8 working electrodes of a ME 8 chip (*el:* electrode). *Inset*: Randles equivalent circuit model used to simulate the impedance data.

The 8 electrodes showed a very similar response: a semicircular region followed by a straight line characteristic of diffusion phenomena. The data was simulated with the Randles equivalent circuit model (see inset), as described in previous chapters, with an acceptable error value ($\chi^2$ = 0.01). In the equivalent circuit, $R_{ct}$ is the charge transfer resistance, *CPE* the constant phase element, *W* the Warburg impedance and $R_{sol}$ the resistance of the solution. The average value of $R_{ct}$ was 23282 ± 2346 Ohm, showing a coefficient of variation of 10%, and consequently, indicating good electrochemical reproducibility between the electrodes from the same multi-electrode platform.

We further studied the reproducibility of different platforms. For this purpose, the $R_{ct}$ of several multi-electrodes was measured and compared by

measuring its coefficient of variation as shown in Table 6. The coefficient of variation represents the ratio of the standard deviation to the mean. Since gold surface cleanness is directly related to the efficiency of bioreceptor immobilization and the accuracy of further measurements, two electrochemical cleaning methods were also tested: sulphuric acid ($H_2SO_4$) with and without piranha solution (see section 4.2.5).

Table 6. Coefficient of variation in $R_{ct}$ for bare gold depending on the cleaning method.

| | **Cleaning method** | **Coefficient of variation ($R_{ct}$)** |
|---|---|---|
| **Gold** | $H_2SO_4$ | < 11% |
| | Piranha + $H_2SO_4$ | < 11% |

As it can be seen in Table 6, low values for the coefficients of variation were obtained in $R_{ct}$ for different multi-electrodes (n=3). Additionally, no significant differences between the cleaning methods were observed.

The reproducibility of the functionalized multi-electrodes was also studied. In this case, the multi-electrodes were cleaned with different methods and a SAM was formed overnight (see section 4.2.4). The results of the coefficient of variation obtained for $R_{ct}$ values are shown in Table 7.

Table 7. Coefficient of variation in $R_{ct}$ for multi-electrodes functionalized with a SAM depending on the cleaning method.

| | **Cleaning method** | **Coefficient of variation ($R_{ct}$)** |
|---|---|---|
| **SAM** | $H_2SO_4$ | <17% |
| | Piranha + $H_2SO_4$ | <16% |
| | Piranha | < 18% |

Comparing the different cleaning methods no significant differences were again appreciated. Similar results were obtained using bare gold multi-electrodes (see Table 6), but a higher coefficient of variation was obtained when the multi-electrodes were functionalized. This feature can be explained as a result of inhomogeneities during SAM formation on gold. These inhomogeneities can appear due to defects in the formation of the thiol monolayer [17], pinholes or collapsed-site defects. The latter could be the result of imperfect adsorption of the alkanethiol on the gold surface during the self-assembly step and/or subsequent loss of the thiol during rinsing, storage or use [17, 18].

We next studied the regeneration of the gold surface. This is a very important parameter in the development of biosensors because it allows the successive uses of the gold multi-electrodes and consequently reduces the cost of the platform. SAM desorption from the gold electrodes can be attained by chemical or physical methods [19]. Amongst the chemical methods are the piranha treatment [20] and an "exchange" method which consists on introducing the recovered substrate into another thiol solution. In this way the SAM can gradually (in minutes to hours) replace the thiols adsorbed onto the surface with the ones in solution [21, 22]. Photo-oxidation (UV irradiation) has been demonstrated to be an efficient physical method for SAM removal [23, 24]. Finally, electrochemical methods are also effective in regenerating surfaces. The application of a negative potential causes the reductive desorption of the thiols [25, 26].

We analyzed how the value of $R_{ct}$ was affected by using different regeneration methods: *(i)* piranha and sulphuric acid ($H_2SO_4$) and *(ii)* cyclic voltammetry (CV) applying potentials from -1 to 1 V. Figure 55 shows the

results of the regeneration study on gold multi-electrodes functionalized with a SAM using the above-mentioned methods.

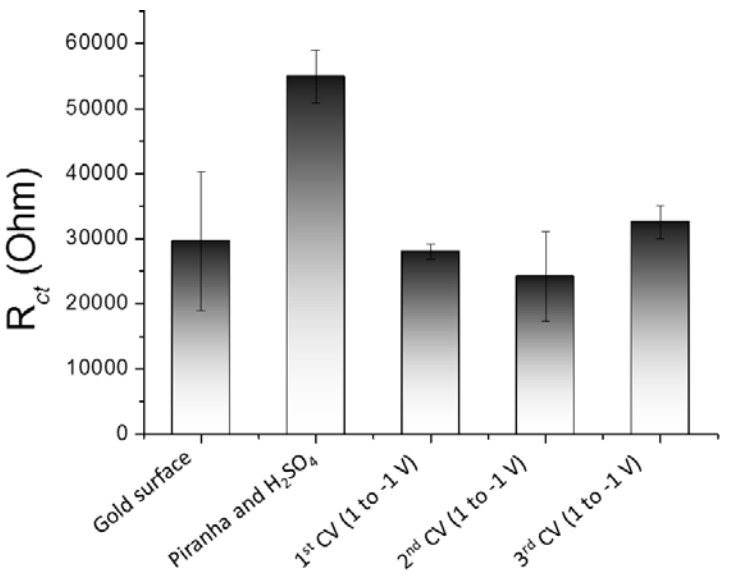


Figure 55. Regeneration study using different methods. Comparison of the $R_{ct}$ values measured after regeneration with those obtained using fresh gold electrodes.

The multi-electrode was not completely regenerated when piranha and sulphuric acid were used sequentially (one after the other); a signal increase >45% in $R_{ct}$ was observed. However, the value of $R_{ct}$ was recovered by CV varying the potential from -1 to 1 V, suggesting that the multi-electrode was completely regenerated. Using this approach, the multi-electrode could be regenerated up to three times in a quite rapid, simple and low cost way.

In conclusion, the multi-electrodes were successfully developed and fabricated by photolithographic processes, as well as characterized by optical and electrochemical methods. We demonstrated that the electrodes were responding precisely and equally after EIS and CV experiments confirming their optimal working performance. Additionally, reproducible working

electrodes were obtained and the multi-electrode could be regenerated for at least 3 times. In the next sections, results related with the detection of pathogenic bacteria using antibodies or peptides (AMPs) as a biorecognition layer will be discussed.

### 4.3.2 Antibody functionalized platform for the detection of pathogenic bacteria

We will use the experience acquired in the previous chapters using antibodies as a biorecognition layer and apply it to the multi-electrodes platform. We will first functionalize and characterize the multi-electrodes response and then, test its detection capabilities.

#### *4.3.2.1 Immobilization of antibodies onto a multi-electrode platform*

The multi-electrodes were functionalized with antibodies using the strategy II described in chapter 3 (section 2.2.3 (*ii*)). Briefly, anti-*E. coli* antibodies were immobilized onto gold by chemical bond formation between the antibody amino groups and a carboxylic acid from the SAM monolayer. An example of a ME8 multi-electrode is shown in this section in order to study its functionalization. Figure 56 shows an example of the sensor response using cyclic voltammograms before (in black) and after (zoomed region) the incubation of all the electrodes with the SAM.

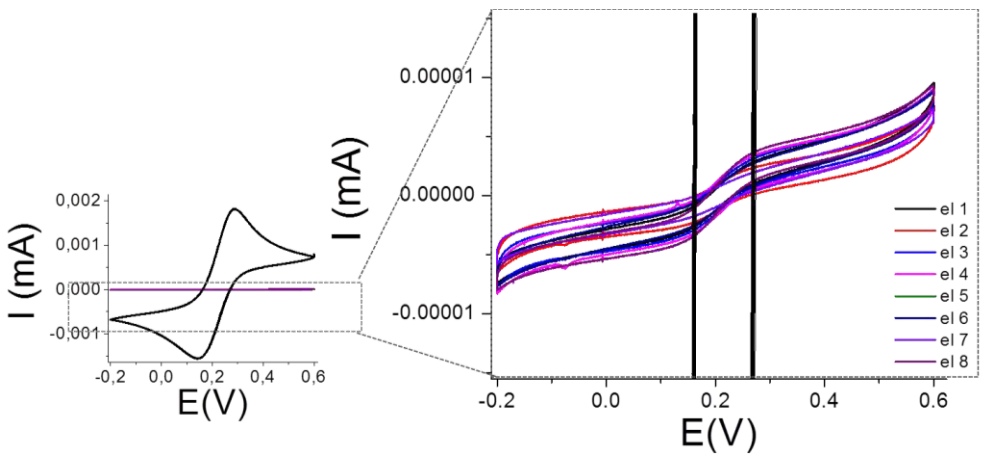


Figure 56. Typical cyclic voltammogram obtained for the 8 working electrode of a ME 8 chip, before (in black) and after SAM modification (*zoomed region)* for the different electrodes.

Results show how the electric current through the electrode is effectively reduced in the presence of the monolayer, confirming that compact monolayers were formed (Figure 56, *zoom*). Additionally, comparable current responses were obtained between the different electrodes.

Similarly, impedance changes were monitored in order to characterize the multi-electrodes functionalization. We recorded the impedance spectra for each step and electrode. Figure 57 shows the simulated values of the charge transfer resistance ($R_{ct}$) after SAM and antibody modification of the different electrodes. Note that all the working electrodes (WE) were modified with a MHDA SAM but different antibodies were immobilized in the array. Electrodes 2-4 and 6-8 were incubated with anti- *E. coli* and anti-*Salmonella*, respectively, whereas electrodes 1 and 5 were used as controls (without antibodies).

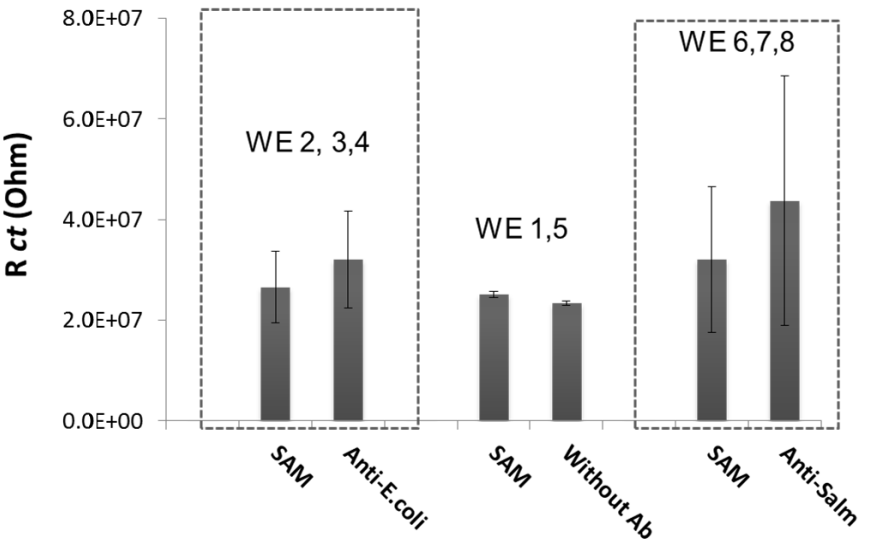


Figure 57. Charge transfer resistance ($R_{ct}$) values obtained for the 8 working electrodes. Anti-*E.coli* (2,3,4) and anti-*Salmonella* (6,7,8) antibodies were immobilized depending on the electrode number. Electrodes 1 and 5 were used as controls. Data is shown as mean ± s.d..

As it can be seen in Figure 57, small fluctuations in $R_{ct}$ values for the electrodes only functionalized with the SAM were observed. Similar results were obtained in section 4.3.1.2 and this variation could be related to inhomogeneities during SAM formation onto gold as previously described. Nonetheless, a very good SAM coverage was obtained: 99.91±0.02%. The surface coverage was calculated according to the following equation [17, 18, 27]:

$$Coverage = 1 - \frac{R_{ct}^{Au}}{R_{ct}^{SAM}} \times 100$$

where $R_{ct}$ corresponds to the charge transfer resistance of the gold (Au) substrate or the MHDA SAM. An increase in $R_{ct}$ after antibody immobilization was observed, both for anti-*E. coli* and anti-*Salmonella* (see Figure 57) . The

antibody attachment to the surface led to a change in the electron-transfer resistance, since the layer formed in each modification step was the barrier for the oxidation and reduction of the redox couple on the electrode surface.

A slight decrease in $R_{ct}$ was observed for the non-modified electrodes (WE 1 and 5). Charge transfer in the electrolyte could mainly explain this phenomenon. The redox probe of $[Fe(CN)_6]^{3-/4-}$ is negatively charged, and thus the redox probe was difficult to approach on the electrode surface due to the strong electrostatic repellency with carboxylic acid groups. The terminal carboxylic group of MHDA was then exposed to the solution of EDC/PFP/DIPEA and chemically blocked with AEE. The uncharged ester may have allowed the redox probe to approach the gold surface of the electrode through gaps in the MHDA monolayer, which resulted in a great decrease of the electron transfer resistance. Another possibility may be the possible desorption of the monolayer through several washing steps.

It is worth to mention that by this example it is possible to observe the importance of several controls in the same multi-electrode and under the same experimental conditions, understanding the complexity of the stepwise immunosensor fabrication. In this way, it is possible to guarantee that antibodies were correctly immobilized. In the next section, some examples of the detection of pathogenic bacteria *E. coli* O157:H7 by antibody-modified multi-electrodes will be described.

#### *4.3.2.2 Detection of E. coli O157:H7*

The detection of pathogenic bacteria *E. coli* O157:H7 was performed in a multi-electrode of 4 working electrodes (ME4) modified with anti-*E. coli*. Figure 58shows the normalized signal of $R_{ct}$ obtained from the fitting of the

impedance spectra. Impedance values differ significantly from each electrode. This highlights the need to normalize the $R_{ct}$ values to account for differences in antibody-modified electrode and analyze the relative changes in the $R_{ct}$.

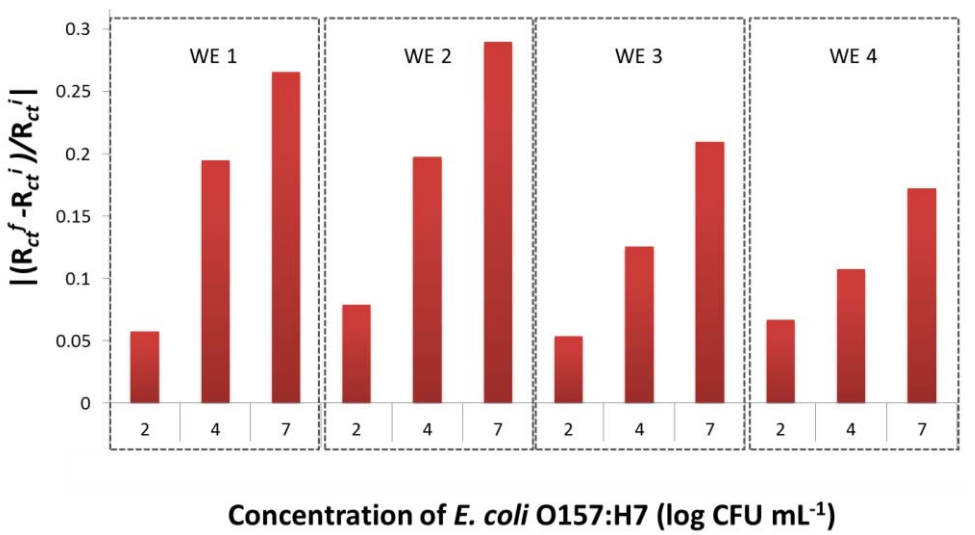


Figure 58. Normalized $R_{ct}$ obtained from the four different anti-*E. coli* modified-electrodes for the detection of pathogenic bacteria *E. coli* O157:H7.

It can be seen in Figure 58 an increase of the normalized $R_{ct}$ for each electrode for the different bacteria concentrations. $R_{ct}$ is very sensitive to electrode modifications produced by the binding of *E. coli* bacteria to the antibodies. Therefore, these results confirm the bacteria binding onto electrodes surfaces, which is also in agreement with the results obtained in previous chapters 2 and 3. Although some variations between the electrodes could be significant, a paired t-test showed that the results obtained between the several electrodes do not differ significantly at P=0.05.

In order to confirm the binding of the bacteria on the surface, a secondary antibody specific to *E. coli* O157: H7 was added to the multi-

electrode platform. Figure 59 (a) shows the fluorescent image of one electrode used after the impedance measurement demonstrating that the bacteria were successfully captured on the antibody-modified surface. A different pathogenic bacterium (*salmonella typhimurium*) was also added to a multi-electrode platform functionalized with anti-*E. coli* antibodies. In this case, and as expected, no fluorescence signal was observed with this type of bacterium (see Figure 59 (b)), confirming the specificity of the functionalized platform.

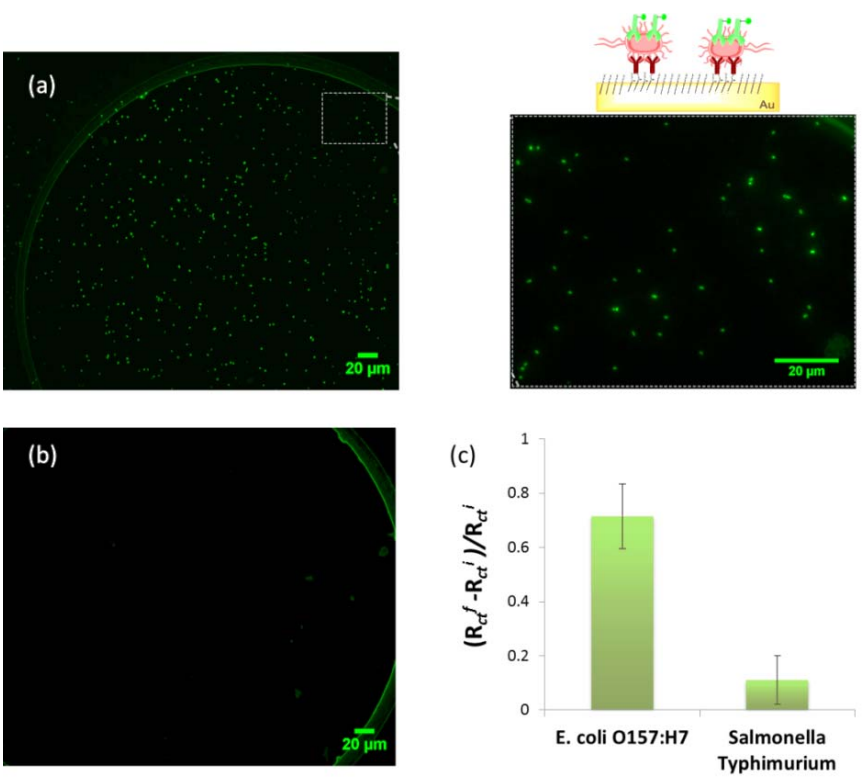


Figure 59. Fluorescence microscopy images of the multi-electrode functionalized with anti-*E. coli* used for the impedance measurements and incubated with a FITC-labeled secondary anti-*E. coli* antibody. Results show (a) the adhered *E. coli* O157:H7 bacteria (in green) and (b) no fluorescent signal for the control experiment using non-specific *Salmonella typhimurium* bacteria. (c) Normalized $R_{ct}$ signal obtained before and after addition of a second antibody (anti-*E. coli*) using *E. coli* O157:H7 and *Salmonella typhimurium*.

Additionally, the impedance signal was also recorded before and after incubation with the secondary antibody. The mean value of the normalized $R_{ct}$ signal obtained from the impedance spectra for the different bacteria is shown in Figure 59 (c). As it can be seen, we obtained a larger value of normalized $R_{ct}$ for *E. coli* O157:H7 bacteria ($10^7$ CFU $mL^{-1}$). On the other hand, non-specific *Salmonella typhimurium* ($10^7$ CFU $mL^{-1}$) led to a small increase in $R_{ct}$.

Elimination of the cross talk between electrodes is essential in multiplexed electrochemical immunoassays. Immunofluorescence was also used for the study of the cross-reactivity of pathogenic bacteria onto the immunosensor array. The cross-reactivity among the antibodies and non-specific antigen was studied by incubating individually the electrodes functionalized with different antibodies with a solution containing only *E. coli* O157:H7. Figure 60 shows the fluorescence images obtained for two different functionalized electrodes of the same multi-electrode: (a) anti-*E. coli* and (b) anti-*Salmonella*.

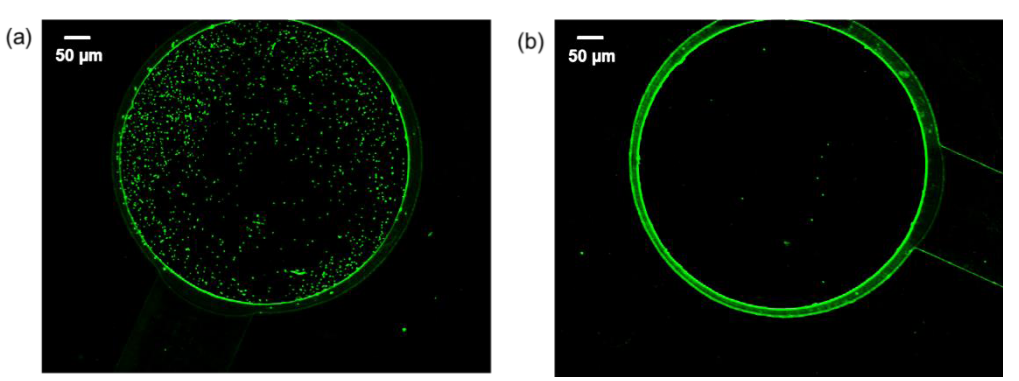


Figure 60. Fluorescence microscopy images obtained for two different functionalized electrodes: (a) anti-*E. coli* and (b) anti-*Salmonella,* using *E. coli* O157:H7.

Even though non-specific binding of a small number of *E. coli* O157:H7 was observed on the electrode modified with anti-*salmonella* (see Figure 60(b)), this reduced number can be considered to be within the ´noise´ of the system, in particular when compared with the large number of captured bacteria detected on the electrode functionalized with specific anti-*E. coli* antibodies. Therefore, we can conclude that the immunosensor array could eliminate properly the cross talk by using this system.

The examples described in this section provide a promising way for mass production of disposable immunosensor arrays for the specific detection of *E. coli* O157:H7. Although this initial study showed encouraging results, it still remains further work to be done. As an example, testing the performance of the multi-electrode using complex samples remains still a challenge. This is a bottleneck of most of the current immunosensors being developed in all the laboratories.

### 4.3.3 Antimicrobial peptides for the detection of pathogenic bacteria

Magainins, a class of antimicrobial peptide that can be found in the African clawed frog *Xenopus laevis* [28] are linear cationic peptides particularly attractive for microbial sensing applications because of their small molecular size and intrinsic stability. In particular, the positively charged magainin I (GIGKFLHSAGKFGKAFVGEIMKS) binds most selectively to the bacterial cell *E. coli* O157:H7 as a precursor to bactericidal activity [15]. For this reason, magainin I was used as molecular bioreceptor of our multi-electrode platform.

#### *4.3.3.1 Immobilization of magainin I onto a multi-electrode platform*

The specific and non-specific binding of AMPs and pathogenic bacteria strongly depends on the method used for peptide immobilization. According to Kulagina *et al* [14], direct attachment of magainin I to the substrate surface not only decreased non-specific cell binding but also resulted in improved detection limits for both *Salmonella* and *E. coli*.

A simple and direct technique for the immobilization of peptides on a gold surface could be by using native thiol groups present in cysteine residues. Cysteine residues can be synthetically introduced at a specific site of the peptide to form a properly oriented recognition layer [15]. Therefore, magainin I was synthesized with an additional cysteine residue at the C terminus, allowing for facile and site-specific covalent attachment to the gold electrodes. In Figure 61 (a) is presented a typical cyclic voltammogram for the immobilization of magainin I onto the gold electrodes of the multi-electrode platform.

The current peak of the redox process decreased gradually and the potential peak separation became larger. Both phenomena prove that the AMPs-modified layer blocked the electron transfer on the surface of the electrode. The coverage of the magainin I was calculated using EIS data fitted with the Randles equivalent circuit (see section 4.3.1.2) and according to the equation shown in section 4.3.2.1. The coverage was estimated considering 3 electrodes of the same multi-electrode platform. The obtained magainin I coverage was 97.1 ± 0.1%, demonstrating a practically complete surface coverage and the successful immobilization of the AMP. It is worth to mention the high reproducibility between the diverse working electrodes in

which a coefficient of variation of 1% was obtained. This variation was measured taking into account the values of $R_{ct}$ before and after peptide immobilization (see Figure 61 (b)).

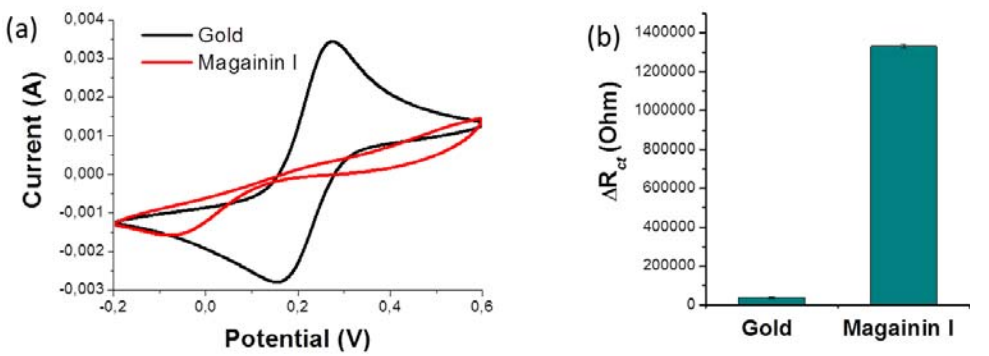


Figure 61. (a) Typical cyclic voltammogram curves for the gold multi-electrode platform before (in black) and after magainin I functionalization (in red). (b) Charge transfer resistance variation of gold before and after peptide immobilization.

Altogether, these results prove the successful functionalization and large coverage of the multi-electrodes with AMPs and their optimal reproducibility.

#### *4.3.3.2 Detection of E. coli O157:H7*

We next studied the detection capabilities of the multi-electrodes functionalized with AMPs. Figure 62 shows the Bode plot representation of the impedance measurements in presence of different concentrations of *E. coli* O157:H7 bacteria ($10^4$ to $10^7$ CFU $mL^{-1}$).

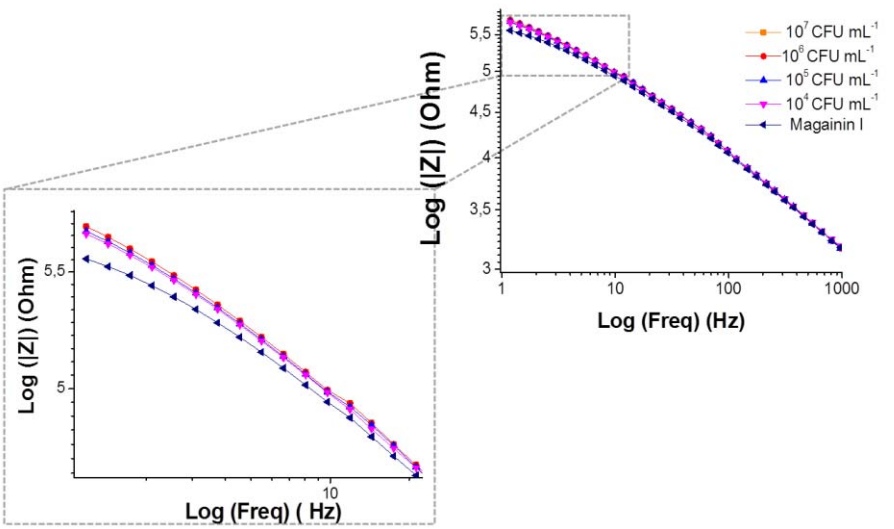


Figure 62. *(Top right)* Bode plot for the impedance measurement of an AMP-modified electrode, varying the concentration of *E. coli* O157:H7 from $10^4$ to $10^7$ CFUmL$^{-1}$. *(Bottom left)* Zoom of the Bode plot at lower frequencies.

The impedance responses over 1000 Hz were almost constant at different concentrations of bacteria and the most significant differences in the magnitude of the impedance were observed at lower frequencies (1-10 Hz). The inset from Figure 62 shows that at low frequencies, the different concentrations of bacterial cells have the effect of increasing the impedance (Z) in proportion to the number of cells present in the sample.

Figure 63 thus illustrates the normalized impedance, at a fixed frequency of 1 Hz, as a function of the *E. coli* O157:H7 concentration (log). The normalized impedance values are the mean of the impedance values in relation to the impedance of the immobilized peptide ($(Z_{bacteria} - Z_{Magainin\ I})/ Z_{Magainin\ I}$) , for different working electrodes of a multi-electrode platform.

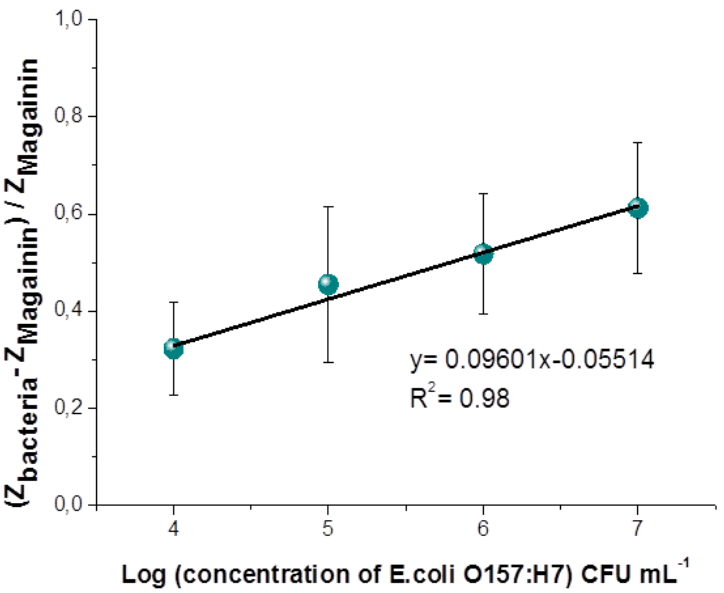


Figure 63. Normalized impedance values (($Z_{bacteria} - Z_{Magainin\ I}$)/ $Z_{Magainin\ I}$) as a function of bacteria concentration for different working electrode of a multi-electrode platform. Data is shown as mean ± s.d. (n=3).

The variation in the impedance is directly proportional to the number of bacterial cells bound to the immobilized AMPs and manifests a linear increase with respect to serially diluted bacterial concentrations. The detection limit of response of the AMP multi-electrode platform to *E. coli* O157:H7 was found to be $8\times10^3$ CFU $mL^{-1}$. This value was calculated using the value for the blank and 3 times the standard deviation as previously described in chapters 2 and 3 (see sections 2.3.4 and 3.3.4). This limit of detection is about the same range of other impedance-based biosensors using magainin I as bioreceptor [15] and compares favorably to AMP-based fluorescent assays [14].

The specificity of the magainin I to other pathogenic bacteria such as *Salmonella typhimurium* was also evaluated. The ratio of impedance for *E. coli* O157:H7 and *Salmonella typhimurium* ($10^7$ CFU $mL^{-1}$) was 98.5%. This

result shows that magainin I- biosensor was capable to detect both *E. coli* O157:H7 and *Salmonella typhimurium* and consequently the system is not specific. The same observation was reported by Kulagina *et al* [14, 29] and Mannoor *et al* [15]. Comparing the antibody-based impedance sensors, the limit of detection obtained with magainin I is higher, suggesting that in our case antibodies are more sensitive than peptides. Additionally, antibodies are more specific than magainin I.

Altogether, the obtained results show that AMPs have potential applicability for being used as biorecognition elements. They are simple to manipulate and to functionalize. However, they still present certain limitations in terms of sensitivity and specificity, especially when compared to the performance obtained using standard antibody-based sensors. This limits their integration on biosensing devices.

## 4.4 Conclusions and perspectives

In this chapter, a multi-electrode array was developed and successfully fabricated by photolithographic processes. The multi-electrode was fully characterized by optical and electrochemical methods demonstrating its excellent manufacturing quality and operational performance. Reproducible working electrodes were obtained and we showed that the multi-electrode could be regenerated for at least 3 times.

The detection capabilities of the multi-electrode were successfully evaluated. The multi-electrodes were functionalized with anti-*E. coli* antibodies and tested for the detection of pathogenic bacteria *E. coli* O157:H7. We showed that the several electrodes did not differ significantly; they all showed a similar electrochemical response. The biosensors were

specific, especially when using anti-*E. coli* as biorecognition layer. Magainin I peptides were also evaluated as an alternative to antibodies. Even though they showed interesting properties and promising results were obtained, some limitations regarding their specificity and sensitivity were observed.

The obtained results demonstrate the usefulness of the array approach for EIS sensing applications. Electrodes arrays can become a useful tool in pathogenic microorganism detection, allowing the use of different biorecognition elements (e.g. antibodies or AMPs) for the multiplexing analysis of pathogenic bacteria. This provides a substantial reduction of materials, time and allows the use of the same experimental conditions. This approach provides a promising way for mass production of disposable arrays for rapid detection of pathogenic bacteria, such as *E. coli* O157:H7, in an economical manner.

## 4.5 References

[1] P. Liepold, H. Wieder, H. Hillebrandt, a Friebel, G. Hartwich, DNA-arrays with electrical detection: a label-free low cost technology for routine use in life sciences and diagnostics, Bioelectrochemistry. 67 (2005) 143–50.

[2] R. Moeller, W. Fritzsche, Chip-based electrical detection of DNA, IEE Proc.-Nanobiotechnol. 152 (2005) 47–52.

[3] E. Pavlovic, R.Y. Lai, T.T. Wu, B.S. Ferguson, R. Sun, K.W. Plaxco, et al., Microfluidic device architecture for electrochemical patterning and detection of multiple DNA sequences, Langmuir. 24 (2008) 1102–7.

[4] S. Neugebauer, A. Zimdars, P. Liepold, M. Gebala, W. Schuhmann, G. Hartwich, Optimization of an electrochemical DNA assay by using a 48-

electrode array and redox amplification studies by means of scanning electrochemical microscopy, Chembiochem. 10 (2009) 1193–9.

[5] X. Yu, R. Lv, Z. Ma, Z. Liu, Y. Hao, Q. Li, et al., An impedance array biosensor for detection of multiple antibody-antigen interactions, Analyst. 131 (2006) 745–50.

[6] F. Farabullini, F. Lucarelli, I. Palchetti, G. Marrazza, M. Mascini, Disposable electrochemical genosensor for the simultaneous analysis of different bacterial food contaminants, Biosens. Bioelectron. 22 (2007) 1544–9.

[7] X. Li, J.S. Lee, H.-B. Kraatz, Electrochemical detection of single-nucleotide mismatches using an electrode microarray, Anal. Chem. 78 (2006) 6096–101.

[8] P.M. Levine, P. Gong, R. Levicky, K.L. Shepard, Real-time, multiplexed electrochemical DNA detection using an active complementary metal-oxide-semiconductor biosensor array with integrated sensor electronics, Biosens. Bioelectron. 24 (2009) 1995–2001.

[9] V. Gau, S.-C. Ma, H. Wang, J. Tsukuda, J. Kibler, D. a Haake, Electrochemical molecular analysis without nucleic acid amplification, Methods. 37 (2005) 73–83.

[10] S.-W. Yeung, T.M.-H. Lee, H. Cai, I.-M. Hsing, A DNA biochip for on-the-spot multiplexed pathogen identification, Nucleic Acids Res. 34 (2006) e118.

[11] A. Bogomolova, E. Komarova, K. Reber, T. Gerasimov, O. Yavuz, S. Bhatt, et al., Challenges of electrochemical impedance spectroscopy in protein biosensing, Anal. Chem. 81 (2009) 3944–9.

[12] H. Qi, L. Shangguan, C. Li, X. Li, Q. Gao, C. Zhang, Sensitive and antifouling impedimetric aptasensor for the determination of thrombin in undiluted serum sample, Biosens. Bioelectron. 39 (2013) 324–8.

[13] E. Komarova, K. Reber, M. Aldissi, A. Bogomolova, New multispecific array as a tool for electrochemical impedance spectroscopy-based biosensing, Biosens. Bioelectron. 25 (2010) 1389–94.

[14] N. V Kulagina, M.E. Lassman, F.S. Ligler, C.R. Taitt, Antimicrobial peptides for detection of bacteria in biosensor assays, Anal. Chem. 77 (2005) 6504–8.

[15] M.S. Mannoor, S. Zhang, A.J. Link, M.C. McAlpine, Electrical detection of pathogenic bacteria via immobilized antimicrobial peptides, Proc. Natl. Acad. Sci. U. S. A. 107 (2010) 19207–12.

[16] M. Kuphal, C. A. Mills, H. Korri-Youssoufi, J. Samitier, Polymer-based technology platform for robust electrochemical sensing using gold microelectrodes, Sens. Actuators B 161 (2011) 279–284.

[17] X. Lu, H. Yuan, G. Zuo, J. Yang, Study of the size and separation of pinholes in the self-assembled thiol-porphyrin monolayers on gold electrodes, Thin Solid Films. 516 (2008) 6476–6482.

[18] S. Campuzano, M. Pedrero, C. Montemayor, E. Fatás, J.M. Pingarrón, Characterization of alkanethiol-self-assembled monolayers-modified gold electrodes by electrochemical impedance spectroscopy, J. Electroanal. Chem. 586 (2006) 112–121.

[19] M. Zourob, S. Elwary, A. Turner, Principles of bacterial detection: biosensors, recognition receptors and microsystems, Springer, 2008.

[20] E.J. Calvo, C. Danilowicz, C.M. Lagier, J. Manrique, M. Otero, Characterization of self-assembled redox polymer and antibody molecules on thiolated gold electrodes, Biosens. Bioelectron. 19 (2004) 1219–28.

[21] J.B. Schlenoff, M. Li, H. Ly, Stability and self-Exchange in alkanethiol monolayers, J. Am. Chem. Soc. 117 (1995) 12528–12536.

[22] G. Yang, N.A. Amro, Z.B. Starkewolfe, G.-Y. Liu, Molecular-level approach to inhibit degradations of alkanethiol self-assembled monolayers in aqueous media, Langmuir 20 (2004) 3995–4003.

[23] N.J. Brewer, S. Janusz, K. Critchley, S.D. Evans, G.J. Leggett, Photooxidation of self-assembled monolayers by exposure to light of wavelength 254 nm: a static SIMS study, J. Phys. Chem. B. 109 (2005) 11247–56.

[24] J. Huang, Photooxidation of Thiols in Self-Assembled Monolayers on Gold, J. Am. Chem. Soc. 115 (1993) 3342–3343.

[25] T.W. Schneider, D.A. Buttry, Electrochemical quartz crystal microbalance studies of adsorption and desorption of self-assembled monolayers of alkyl thiols on gold, J. Am. Chem. Soc. 115 (1993) 12391–12397.

[26] W.R. Everett, I. Fritsch-faules, Factors that influence the stability of self-assembled organothiols on gold under electrochemical conditions, Anal. Chim. Acta. 307 (1995) 253–268.

[27] R.P. Janek, W.R. Fawcett, A. Ulman, Impedance spectroscopy of self-assembled monolayers on Au(111): sodium ferrocyanide charge transfer at modified electrodes, 7463 (1998) 3011–3018.

[28] V. Humblot, J.-F. Yala, P. Thebault, K. Boukerma, A. Héquet, J.-M. Berjeaud, et al., The antibacterial activity of Magainin I immobilized onto mixed thiols Self-Assembled Monolayers, Biomaterials 30 (2009) 3503–12.

[29] N. V Kulagina, K.M. Shaffer, G.P. Anderson, F.S. Ligler, C.R. Taitt, Antimicrobial peptide-based array for Escherichia coli and Salmonella screening, Anal. Chim. Acta. 575 (2006) 9–15.

# **Chapter 5.** Detection of ochratoxin A by means of a multi-electrode platform

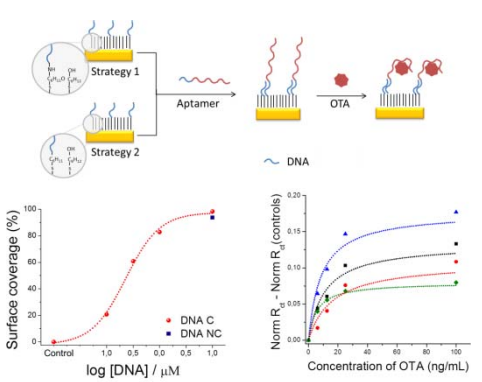


In this chapter, we applied the multi-electrodes platform described in chapter 4 for the development of an aptamer-based sensor for the detection of mycotoxins. We focused on the specific case of ochratoxin A (OTA), one of the most abundant food-contaminating mycotoxins. Two strategies for aptamer immobilization were presented, both based on the hybridization onto the biosensor surface through partially complementary oligonucleotides. Cyclic voltammetry and EIS tecnhiques were used to characterize all the functionalization steps. The multi-sensor was capable to detect OTA concentrations of 6.125 ng $mL^{-1}$ (15 nM) and the highest response was obtained for DNA concentration of 1 µM. Altogether, these promising results prove the successful application of the multi-electrodes strategy for the detection of mycotoxins and the advantages of using this kind of system. This work was developed in collaboration with Prof. Jean Louis Marty and Dr. Cheng Yang at the IMAGES laboratory (Université de Perpignan, France).

## Chapter index

## 5.1 Introduction

Ochratoxin A (OTA) is the most common naturally occurring mycotoxin and its detection is very important due to its toxicity and occurrence [1-4]. The standard analytical methods for the detection of OTA are based on TLC-FD and HPLC-FD [5, 6]. Since these methods need sophisticated equipment and trained personnel, other methods based on biosensor technology had emerged: ELISA [7], SPR [8] and electrochemical immunoassays [9]. These assays show low limits of detection but they all require a stable source of antibodies. Moreover, the production of antibodies involves laborious, expensive, and time-consuming procedures. Aptamers, short oligonucleotides (DNA/RNA), can bring some advantages compared with antibodies due to their inherent selectivity and affinity [10].

Aptamers for OTA detection were selected in 2008 by Cruz-Aguado *et al* [11, 12]. The identified aptamers exhibited a high level of binding specificity to OTA, which was revealed by a lack of affinity to structure analogues of OTA. OTA's aptamers have been widely used since then for the development of electrochemiluminescent- [13], colorimetric- [5] or electrochemical-based biosensors [10, 14–16]. The latter have been widely reported because of their simple instrumentation, easy operation, low cost, high sensitivity and rapid sensing time [15].

Figure 64 shows some examples of aptamer-based electrochemical biosensors for the detection of OTA. Kuang *et al* [15] developed an ultrasensitive and rapid electrochemical platform for the specific detection of OTA based on the change in redox current of MB (used as the electrochemical probe) after the binding of OTA to the aptamer (Figure 64 (a)). A sensitivity of 30 pg $mL^{-1}$ was reported over an effective sensing range from 0.1 to 20 ng $mL^{-}$

[1]. Similarly, Bonel *et al* [17] reported the fabrication of an electrochemical competitive biosensor for OTA based on DNA biotinylated aptamers with a detection limit of 0.07±0.01 ng $mL^{-1}$ (Figure 64(b)).

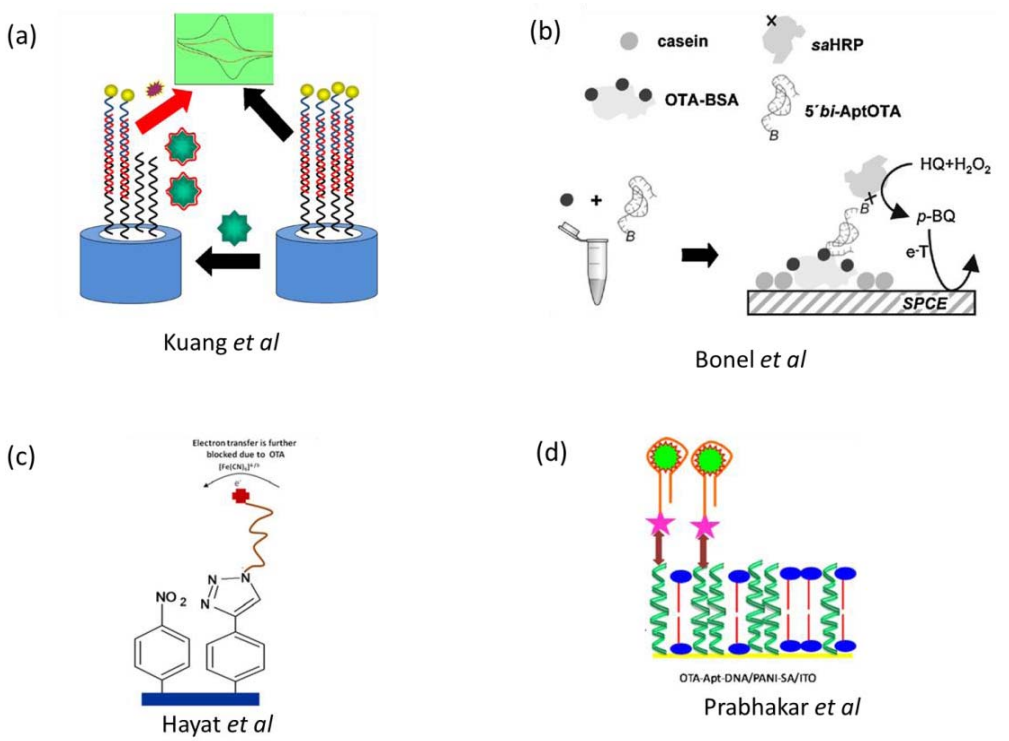


Figure 64. Examples of aptamer-based electrochemical biosensors for the detection of OTA, using (a) CV, (b) differential-pulse voltammetry and (c and d) EIS techniques.

The fabrication of sensitive electrochemical *impedimetric* aptasensors for the detection of ochratoxin A are shown in Figure 64(c) and (d). As described earlier, electrochemical impedance spectroscopy (EIS) is highly sensitive to surface modifications and allows the detection of affinity interactions on surfaces using the redox probe $[Fe(CN)6]^{3-/4-}$. This has been demonstrated in particular for the detection of proteins by DNA aptamers as receptors [18, 19]. Because DNA aptamers are negatively charged, the anionic redox probe will be repealed from the sensor surface causing an increase of

the charge transfer resistance ($R_{ct}$). Binding of proteins resulted in a decrease (lysozyme) [18] or increase (thrombin) [19] of the negative charge at the surface, causing decrease or increase of $R_{ct}$, respectively. This approach was used mostly for the detection of proteins, but Hayat *et al* [14] and Prabhakar *et al* [10] showed that this method could be also applied for the determination of small molecules like OTA [20].

The aptamer immobilization onto organized mixed layers of diazonium salts via *click* chemistry for the development of an OTA impedimetric aptasensor was explored by Hayat *et al* [14] (Figure 64(c)). A dynamic range from 1.25 ng $L^{-1}$ to 500 ng $L^{-1}$ with a detection limit of 0.25 ng $L^{-1}$ was reported. Figure 64(d) shows a Langmuir–Blodgett (polyaniline (PANI)–stearic acid (SA)) film deposited onto ITO coated glass plates that was used for the development of a highly sensitive and robust impedimetric aptasensor [10]. DNA Aptamer (Apt-DNA) specific to OTA was covalently immobilized onto mixed PANI–SA monolayer. The Apt-DNA/PANI–SA/ITO aptasensor showed a linear range of 0.1 - 10 ng $mL^{-1}$ and 1 -25 µg $mL^{-1}$ with detection limit of 0.1 ng $mL^{-1}$. Finally, Castillo *et al* [20] reported a high sensitive impedimetric biosensor based on DNA aptamers. Thiolated DNA aptamers specific to OTA were immobilized by chemisorption onto a gold electrode. Limits of detection between 0.12-0.40 nM were obtained, depending on the aptamer configuration.

Although some works have described the development of impedimetric sensors for the detection of OTA with low limits of detection, to our best knowledge it has not been reported OTA detection based on a multi-sensor array. As described in Chapter 4, the multi-sensor provides an array of several working electrodes with different specificities, which could include positive and negative controls in a single binding experiment. Additionally,

this system is very useful for the optimization of the experimental conditions, reducing the detection time and the reagents used.

In this chapter, we applied the multi-electrode platform for the detection of small molecules like OTA. This work was developed in collaboration with Prof. Jean Louis Marty and Dr. Cheng Yang from the *IMAGES* laboratory at the Université de Perpignan (Perpignan, France). The OTA aptamer immobilization is based on the hybridization through partially complementary oligonucleotides on the biosensor surface. The aptamers were hybridized to a short chain of nucleotides previously immobilized on the surface. This functionalization methodology has already been applied on biosensors, since the sensor can detect different targets (proteins, metal ions, DNA molecules…) by using different kinds of aptamers fixed onto the sensor surface [21].

For the fabrication of the aptamer-based impedimetric multi-sensor, two immobilization strategies were tested. The first strategy (*strategy I*) was based on the covalent attachment to chemically-modified surfaces, while the second strategy (*strategy II*) was based on the modification of DNA with a terminal thiol. Both strategies present some advantages and drawbacks. As an example, *strategy I* showed an increase of the specificity and a decrease of the interference signal of non-specific adsorption. However, it requires more complex chemical modifications that could introduce new interference factors. On the other hand, *strategy II* is simpler, does not require complex chemical surface modifications and can reach detections limits in the range of nanomolar concentrations but often presents a strong non-specific adsorption. Moreover, it is only applicable on gold surfaces [21].

We next describe all the material needed and methodology used for the functionalization of an ME-8 surface for both strategies (*I* and *II*). The

functionalized surfaces were fully characterized in order to select the most adequate one for being applied for the detection of OTA.

## 5.2 Experimental procedures

### 5.2.1 Chemicals and reagents

Potassium ferricyanide ($K_3[Fe(CN)_6]$), potassium ferrocyanide ($K_3[Fe(CN)_6]$), MHA, MCH, DIEA, PFP, EDC, tris(2-carboxyethyl)phosphine hydrochloride (TCEP), tris(hydroxymethyl)aminomethane ($(HOCH_2)_3CNH_2$) (Tris), sodium chloride (NaCl), sodium phosphate dibasic ($Na_2HPO_4$), potassium phosphate monobasic ($KH_2PO_4$), NHS, AEE, sodium hydrogen carbonate ($NaHCO_3$), magnesium chloride ($MgCl_2$) *and* hydrogen peroxide (33%) were supplied by Sigma-Aldrich. Sulphuric acid (95%) was purchased from BDH Prolabo GPR RECTAPUR.

OTA (from *Aspergillus ochraceous*), purchased from Sigma, was first dissolved in methanol and then diluted in PB buffer (10 mM PBS and 120 mM NaCl, pH 7.6). A 10 mM Tris-HCl buffer containing 120 mM NaCl (pH 8.2) was used as buffer for the electrochemical measurements. The binding buffer (BB) used consist in PB buffer containing 1 mM $MgCl_2$. The presence of divalent cations, $Ca^{2+}$ or $Mg^{2+}$, is essential for the specific recognition of OTA by aptamer as previously published by Castillo *et al* [20]. PB-TCEP solution, PB buffer and 10 mM TCEP, was used for the direct immobilization of DNA (strategy II). TCEP was used as a reducing agent to reduce disulfide bonds [22].

All the oligonucleotides sequences of DNA and aptamer used were purchased from Eurogentec (France) and they are shown in Table 8. The DNA oligonucleotides, C and C1 (complementary sequence for OTA aptamer) and NC (non-complementary sequence, negative control), were chemically functionalized by amine or thiol groups.

Table 8: Oligonucleotide sequences of DNA and aptamers used. The DNA was modified by 3´-Amine C7 (strategy I) or 5´-thiol C6 (strategy II).

| Name | Sequence from 5' to 3' | Modification |
|---|---|---|
| DNA C | TTT TTT TTT TCC GAT GCT CC | 5´- Amine C6 or 5´- thiol C6 |
| DNA C1 | CAC ACC CGA TC | 3´-Amine C7 |
| DNA NC | TTT TTT TTT | 5´- thiol C6 |
| OTA aptamer (OA) | GAT-CGG-GTG-TGG-GTG-GCG-TAA-AGG-GAG-CAT-CGG-ACA | (*) |

(*) This sequence was not modified.

### 5.2.2 Aptamer immobilization procedure

OTA aptamer exhibits a random coil structure in solution that switches to a rigid antiparallel G-quadruplex structure upon OTA binding according to previously circular dichroism spectroscopic studies [5, 20, 16]. The aptamer was immobilized through hybridization onto ssDNA-modified surface to keep the random coil structure. The OTA aptamer contains complementary oligonucleotides to the immobilized DNA and therefore it binds to the surface through DNA hybridization.

Two different strategies for DNA immobilization were tested and can be seen in Figure 65 and Figure 66. The multi-electrodes platforms were firstly cleaned with freshly prepared Piranha solution (7:3 v/v $H_2SO_4$:$H_2O_2$) for

10 min and subsequently rinsed thoroughly with Milli-Q water. Electrochemical cleaning by cyclic voltammetry performing successive cycles in 0.5 M and 0.1 M $H_2SO_4$ were applied to the gold electrodes in the potential range from +0.2 to +1.5 V with a scan rate of 100 mV/s. Finally, the electrodes were again thoroughly rinsed in Milli-Q water and dried.

#### *5.2.2.1 Strategy I: DNA immobilization by amide coupling technique*

Strategy I is based on anchoring amine-modified DNA oligonucleotides (DNA C or C1) onto a reactive surface monolayer by means of the amide coupling technique (Figure 65), as previously described in chapter 3 (section 3.2.3). Briefly, SAMs were formed on freshly cleaned gold surfaces by immersion into a SAM ethanolic solution (1 mM, 1:9 v/v MHA:MCH) overnight at 4ºC (1). The carboxylic acid groups were activated using a mixture of EDC (0.2 M), PFP (0.2 M), and DIEA (0.2 M) in absolute ethanol during 30 min at RT (2). The substrates were rinsed with absolute ethanol and dried. Then, 0.5 µL of DNA C in PB buffer was incubated during 2 h at 4ºC (different concentrations for each electrode, ranging from 0.1 to 100 µM) (3). Afterwards, the sample was rinsed with PB buffer and the remaining active ester functionalities were blocked by immersing the substrate for 30 min into a 10 mM AEE solution in sodium bicarbonate buffer (pH 8.3). Finally, the substrates were washed and OTA aptamer (0.1 or 1 µM in PB buffer) was incubated for 45-60 min (4). The same procedure was applied using a mixture of EDC (0.4 M) and NHS (0.1 M) to activate the surface and with DNA C1.

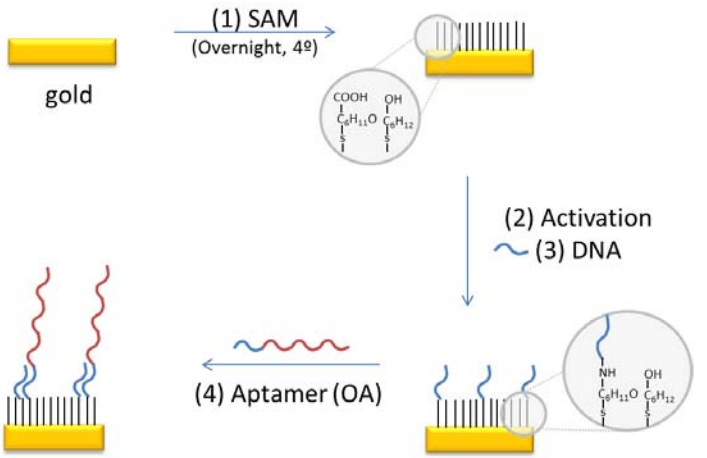


Figure 65. Schematic diagram of the functionalization *strategy I* for the DNA immobilization onto the multi-electrode platform. *Steps:* (1) SAM; (2) activation and (3) DNA immobilization; (4) Aptamer binding through the hybridization of the complementary sequence.

#### *5.2.2.2 Strategy II: DNA immobilization by chemisorption*

Thiolated DNA containing complementary oligonucleotides to the OA aptamer (DNA C) was immobilized on the gold electrode surface by chemisorption (Figure 66). DNA C was dissolved in PB-TCEP solution and 0.5 µL were deposited onto the multi-electrode (1). Each electrode was incubated with a different DNA concentration, ranging from 0 to 10 µM, and non-complementary DNA (10 µM). The solution was kept in a closed container to prevent solvent evaporation at 4ºC overnight. Then, the multi-electrodes were cleaned with PB solution and incubated in 1 mM MCH for 2 h at RT (2). This procedure removes physically-adsorbed DNA and blocks the uncovered electrodes surface, thus avoiding non-specific binding. Next, the OTA aptamer (1 µM in PB buffer) was incubated during 45-60 min (3). Finally, the multi-electrode was rinsed with PB solution and stored at 4ºC prior to use for OTA detection.

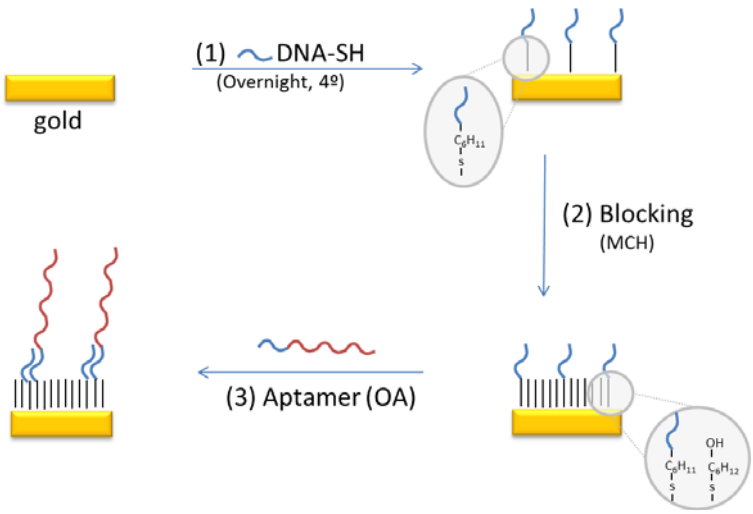


Figure 66. Schematic diagram of the functionalization *strategy II* for the DNA immobilization onto the multi-electrode platform. *Steps:* (1) DNA immobilization onto the gold electrode surface; (2) blocking with MCH; (3) aptamer binding through the hybridization of the complementary sequence.

### 5.2.3 Electrochemical measurements

Electrochemical measurements were performed using an Autolab PGSTAT100 potentiostat/galvanostat with Nova 1.6 software (Eco Chemie, Netherlands). The multi-electrode platform was mounted in a home-made electrochemical cell as shown in chapter 4 (section 4.2.4), with a platinum (1×1 $cm^2$) counter electrode and an Ag|AgCl|NaCl saturated reference electrode (BaSI, USA). A printed circuit board was used for individual and automatic measurements of the multi-electrodes.

The response of freshly prepared sensors was measured in the presence of 5 mM $[Fe(CN)_6]^{3-/4-}$ (redox probe) in tris-HCl buffer at RT. The surface functionalization was characterized by CV and EIS, whereas OTA detection was performed by EIS. CV was performed at 100 mV $s^{-1}$ over a

potential range between -0.5 V and +0.8 V. Impedance spectra were recorded using a constant potential (+0.2 V) and the perturbation amplitude at 10 mV, over a frequency range from 100 kHz to 1 Hz. Data analysis was accomplished using EC-Lab software (Bio-Logic SAS).

OTA was dissolved in binding buffer for EIS experiments. Different concentrations of the toxin (6-100 ng $mL^{-1}$) were incubated on the sensor surface for 30 min. After the addition of the desired OTA concentration, the response was measured in the presence of redox probe.

### 5.2.4 Surface Plasmon Resonance measurements

SPR experiments were conducted on a SPR RT2005 instrument (RES-TEC GmbH, Max Planck Institute for Polymer Research, Germany). The carboxylic acid functionalized gold SPR chips (1 mM, 1:9 v/v MHA:MCH) were index-matched to the prism and fitted into a flow cell connected to a peristaltic pump (Ismatec, Switzerland). The variation of reflectivity was measured as a function of time at a fixed angle near to the SPR angle.

The carboxylic acid groups were activated using a mixture of EDC (0.4 M) and NHS (0.1 M) in aqueous solution during 30 min at RT. The substrates were rinsed with water and the surface plasmon measured. Then, DNA C1 in PB buffer was incubated during 2 h at 4ºC (10 µM). Afterwards, the sample was rinsed with PB buffer and the remaining active ester functionalities were blocked by immersing the substrate for 30 min into a 10 mM AEE solution in sodium bicarbonate buffer (pH 8.3). Finally, the substrates were washed and OTA aptamer (0.1 and 1 µM in PB buffer) was incubated for 60 min. After each step, the surface was rinsed with PBS and a flow of 56 µL $min^{-1}$ was used.

## 5.3 Results and discussion

The OTA aptamer immobilization is based on the hybridization onto the biosensor surfaces through partially complementary oligonucleotides for both strategies. The two strategies used for the immobilization of short oligonucleotides chains (DNA C) are shown in Figure 67 (see Experimental Procedures for details). Briefly, *strategy I* uses a carboxylic acid SAM, subsequent activation and attachment of the amine-modified oligonucleotide by means of the amide coupling technique (Figure 67, *upper*). *Strategy II* uses a direct attachment of thiol-modified oligonucleotide DNA (DNA C) self-assembled through the gold-sulphur bond onto the gold electrode surfaces (Figure 67, *lower*).

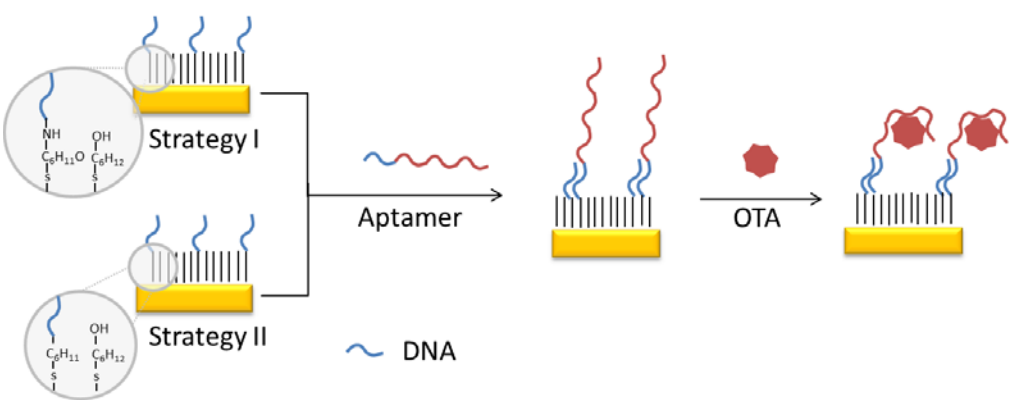


Figure 67. Strategies for aptamers´ immobilization used for OTA detection. *Strategy I* is based on the covalent attachment to chemically-modified surfaces. *Strategy II* is based on the self-assembling of a thiolated oligonucleotide.

On both strategies, the oligonucleotides were separated with MCH that blocked the electrodes surface which was not covered by the target DNA molecules. This prevented non-specific adsorption and thus a better binding of the OTA aptamer. A mixed SAM of mercaptodecanoic acid and

mercaptohexanol (1:9 v/v) was used in *strategy I*, while a two-step method was used in *strategy II*.

According to Herne *et al* [21], more precise control on the surface coverage is achieved by the two-step method. The main advantage of using this two-step process to form HS-DNA/MCH mixed monolayers is that non-specifically adsorbed DNA is largely removed from the surface. Thus, the majority of surface-bound probes is accessible for specific hybridization with complementary oligonucleotides and is able to discriminate between complementary and non-complementary oligonucleotides.

In the following sections, we describe the fabrication, characterization and optimization of the surface functionalization using both strategies on a ME-8 multi-electrode. Finally, the performance of the multi-sensor for the detection of OTA toxin is evaluated.

### 5.3.1 Strategy I: optimization and characterization of the surface functionalization

Multi-electrodes were used to optimize the functionalization strategy. After the formation of a carboxylic acid SAM (1:9 v/v MHA:MCH) and subsequent activation (mixture of PFP, EDC and DIEA, see Experimental Procedures), each electrode was incubated with a different concentration of DNA C ranging from 0.1 to 100 µM. Cyclic voltammetry was used to verify the changes on the electrode after each assembly step. Figure 68 shows a typical cyclic voltammogram for the different functionalization steps.

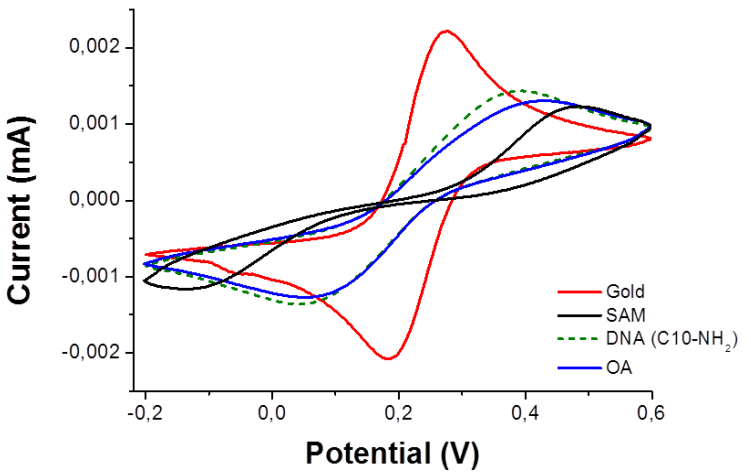


Figure 68. Typical cyclic voltammogram for all the functionalization steps for strategy I. CV curve of a gold electrode (in red) before and after its functionalization: SAM (in black), DNA C (dashed line in green, 1 µM) and OTA aptamer (OA 1 µM, in blue).

The redox probe $[Fe(CN)_6]^{3-/4-}$ reveals a reversible cyclic voltammogram for the gold electrode (red curve). After its coverage with a SAM of short-chain thiols (black curve) a decrease in the faradaic current was observed. This feature could be explained due to the high insulating surface and the high permeability of ions through the modified electrode.

Next, the SAM was activated and incubated with the DNA strains (dashed line). In this case, the current response was higher suggesting that the monolayer turned less insulating. Because DNA is a negatively charged molecule, it is expected that the anionic redox probe will repeal from the sensor surface causing a decrease in the faradaic current. This feature was though observed after aptamer addition (blue curve), but it was not observed with DNA. In order to understand this phenomenon, the charge transfer resistance ($R_{ct}$) difference obtained for all the functionalization steps and for different DNA C concentration was measured. Impedance spectra were

simulated with a previously described Randles equivalent circuit (see sections 2.3.4, 3.3.2 or 4.3.1.2).

Figure 69 shows the $R_{ct}$ values obtained on different electrodes of the multi-electrodes platform. The measurements were performed for the bare gold electrode (*left columns, in red*) and for all the functionalization steps (SAM, *in black*; DNA C, *in green;* aptamer, *in blue*). Note that three $R_{ct}$ values out of eight (ME 8) were discarded because they showed to malfunction. This is an added advantage of using this platform: incorrect working electrodes can be immediately identified and discarded. The $R_{ct}$ values are represented accordingly to DNA concentration, since each electrode was functionalized with a different one.

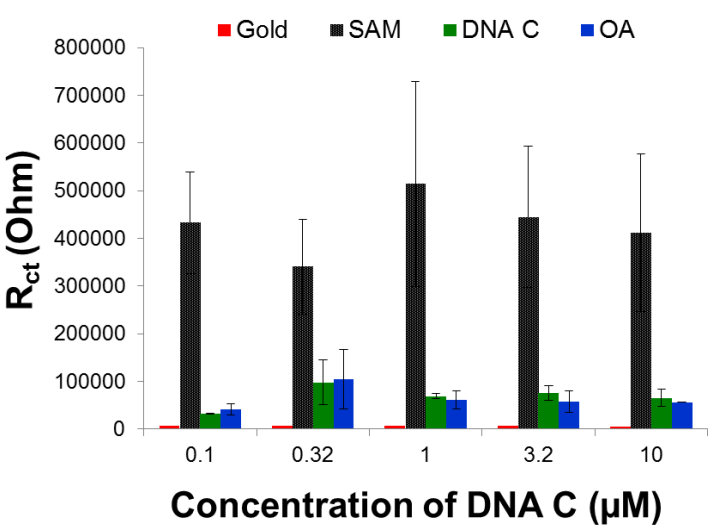


Figure 69. Values of $R_{ct}$ vs DNA concentration for the different electrodes of the multi-sensor: gold electrode (left columns, in red), SAM (in black), DNA C (in green) and OTA aptamer (1 µM OA, in blue). Data is shown as mean ± s.d. (n = 2).

A small $R_{ct}$ was obtained for the gold electrodes indicating a clean gold surface. This is in agreement with the results obtained in section 4.3.1.2. After the SAM formation, a large increase in $R_{ct}$ was observed for all the

electrodes (see Figure 69, *black*), indicating that the highly organized monolayer obstructed the interfacial electron transfer of the electrochemical probe. Similar results were obtained with CV (see Figure 68, *black*), proving the highly insulating surface after the SAM formation.

After the surface activation and its incubation with DNA C, a decrease in $R_{ct}$ was obtained. No significant difference between the $R_{ct}$ of the aptamer and the DNA was observed. Additionally, the decrease in the $R_{ct}$ upon the addition of DNA C could suggest desorption of SAM through the functionalization process. According to Mirsky *et al* [24], chemical activation in organic solution is destructive for the activated monolayer. However, they describe that desorption of SAM from the electrode is negligible when activated with NHS and carbodiimides in aqueous solution [25]. Therefore, activation with NHS and EDC in aqueous solution was next tested. Results of $R_{ct}$ values for the different functionalization steps are shown in Figure 70. In this case, a control experiment without DNA (control) was performed and a DNA with a different sequence complementary to OA (DNA C1) was used.

We obtained a similar electrode behavior compared to Figure 69: a decrease in $R_{ct}$ was observed after the surface activation and its incubation with DNA C1. No significant difference between the $R_{ct}$ of the aptamer and the DNA was observed. Finally, the control experiment without DNA also showed a decrease after DNA immobilization but a small variation after the addition of OTA aptamer. These results suggest that the aptamer did not bind onto the biosensor surface through the partially complementary oligonucleotide.

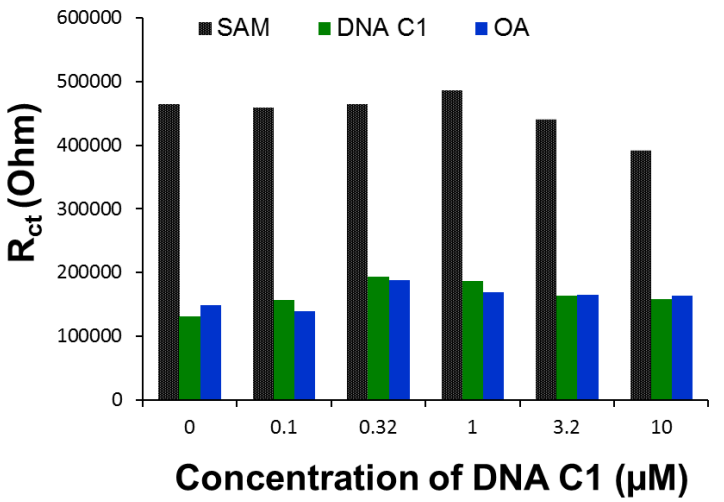


Figure 70. Values of $R_{ct}$ vs DNA concentration for the different electrodes of the multisensor using NHS and EDC activation in aqueous solution*:* SAM (in black), DNA C1 (in green) and OTA aptamer (OA, in blue).

This observation was also corroborated by SPR results: a variation of reflectivity of 0.1 % was obtained after adding the aptamer to the DNA-modified surface (Figure 71(a)). This feature could be related with almost no attachment of DNA to the activated surface. According to the obtained results, the variation of the reflectivity after the addition of DNA on the activated surface was about 0.2 % (Figure 71(b)).

As above-mentioned, the non-attachment of DNA to the activated surface is probably related with desorption of SAM from the surface as suggested by the EIS experiments. Mirsky *et al* [24] studied the stability of the capacitance of gold electrodes covered by mercaptohexadecanoic, mercaptoundecanoic, mercaptohexanoic and mercaptopropionic acids. Results showed the fast desorption of these compounds from the electrode surface with shorter alkyl chains. They demonstrated that, despite the generally accepted opinion on practically irreversible gold-thiol binding, short

chain ω-substituted alkylthiols spontaneously desorbed from the gold electrode at neutral pH.

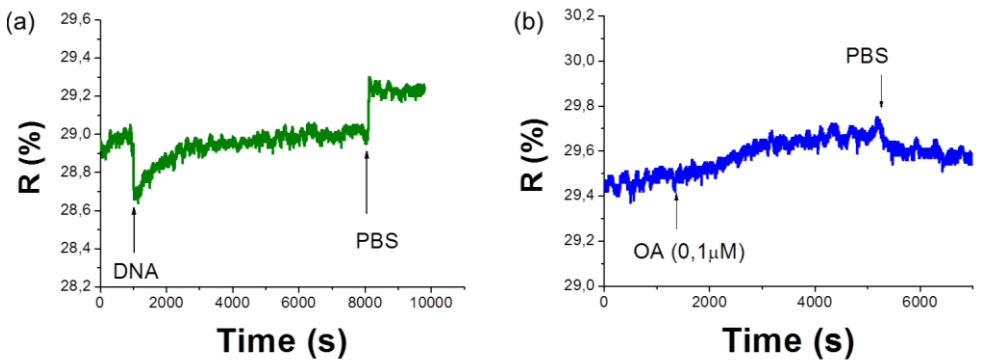


Figure 71. SPR time-dependent sensogram for the immobilization of (a) 10 μM DNA C1 onto the active SAM and (b) adding OTA aptamer (OA, 1 μM).

Altogether, the obtained results encouraged us to evaluate the functionalization strategy based on the direct attachment of thiol-modified oligonucleotide DNA on the gold surface due to the high affinity of the thiol group towards gold (*strategy II*).

### 5.3.2 Strategy II: optimization and characterization of the surface functionalization

Similar to section 5.3.1, multi-electrodes were used to optimize the functionalization strategy. A two-step method was used in *strategy II*. The first step was the functionalization of the gold electrodes by immersion in a DNA C solution. Then, the second step was the immersion of the DNA modified-electrodes into MCH solution. The changes on the electrode for each step were verified by cyclic voltammetry and EIS. Figure 72 shows a typical cyclic voltammogram for the different functionalization steps.

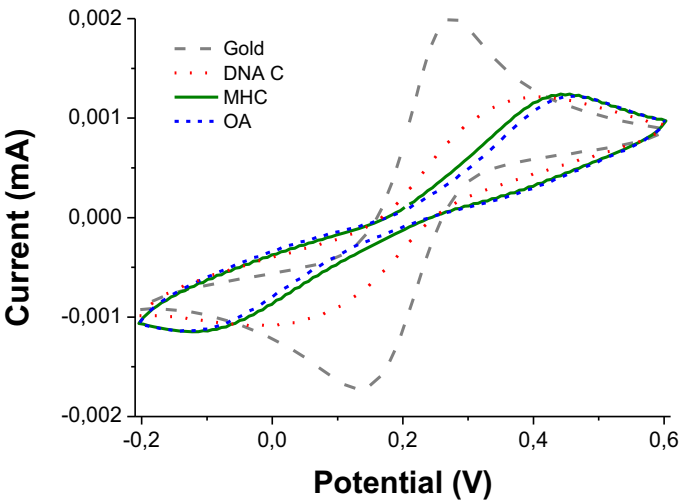


Figure 72. Typical cyclic voltammogram for all the functionalization steps for strategy II: bare gold electrode, DNA C (1 µM), MCH and OTA aptamer (OA, 1 µM).

As it can be seen in Figure 72, a decrease of intensity current is observed for DNA C, MHA and after hybridization of the aptamer. The current decrease for DNA and OTA aptamer is due to the repulsion between the negatively charged DNA and the redox pair in solution, while the current decrease for MHA suggest the blockage of the electrode surfaces which were not covered by the target DNA molecules.

Figure 73 (a) shows the $R_{ct}$ values obtained by EIS for the different concentrations of DNA oligonucleotides (one concentration per electrode), while Figure 73(b) shows the surface coverage of DNA onto the gold surface. The surface coverage was calculated as earlier described (see chapter 4, section 4.3.2.1.), where $R_{ct}$ corresponds to the charge transfer resistance of the gold substrate and the DNA SAM.

(a)

| | [DNA] µM | $R_{ct}$ Ohm |
|---|---|---|
| DNA C | 10 | 760000 |
| | 1 | 97470 |
| | 0.32 | 53255 |
| | 0.1 | 21900 |
| DNA NC | 10 | 259811 |
| No DNA | 0 | 13571 |

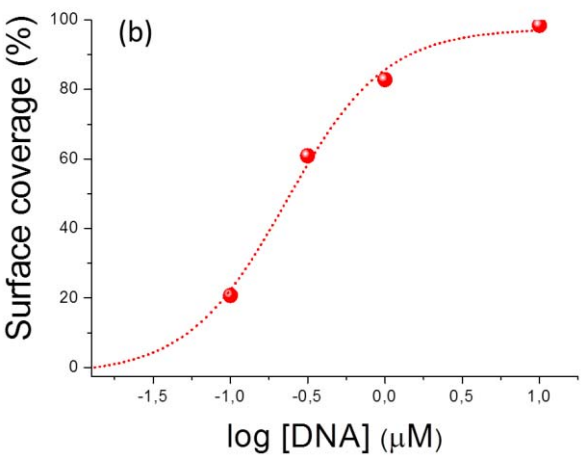


Figure 73. (a) Table with the $R_{ct}$ values obtained for the different DNA concentrations. (b) Surface coverage obtained for each electrode using different DNA concentrations. The dashed line corresponds to the sigmoidal fitting.

As it can be seen in Figure 73(a), the immobilization of increasing concentrations of DNA C induces an $R_{ct}$ increase. This feature is associated with the increase of DNA molecules on the surface and consequently the formation of a more negatively charged layer which acts as an electrostatic barrier between the electrode surface and the $[Fe(CN)_6]^{3-/4-}$ anions in the solution. This increase of DNA on the surface was also supported by the surface coverage plotted in Figure 73(b). The surface showed a near 100% coverage at 10 µM DNA C. As it can be observed, the surface coverage followed a sigmoidal behaviour for the different concentrations of DNA C. Note finally that the response to non-complementary DNA (DNA NC) oligonucleotides was also evaluated. We observed that at high concentrations, a similar surface coverage of about 100% was obtained demonstating the sucessful chemisorption of thiolated DNA oligonucleotides.

We next immersed the multi-electrode in MCH solution to prevent non-specific adsorption and after that the aptamer was added for the hybridization with the immobilized DNA C. Figure 74 shows the $R_{ct}$ values for the different DNA concentrations. Note that the red curve represents the above-mentioned $R_{ct}$ variation vs DNA immobilization onto the electrode array.

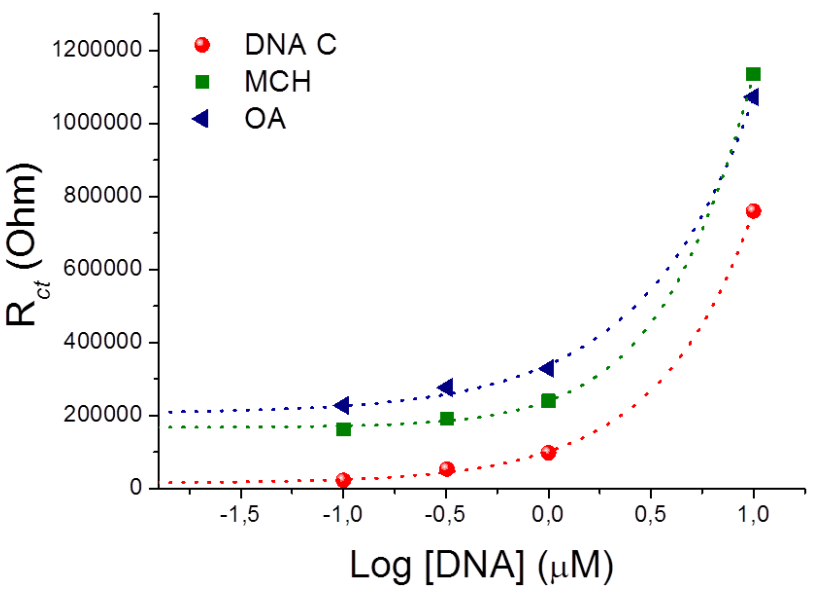


Figure 74. $R_{ct}$ values vs DNA concentration obtained for the different functionalization steps for strategy II using an electrode array: DNA C (in red), MCH (in green) and OTA aptamer (OA, in blue). The dashed lines correspond to the respective sigmoidal fitting.

An increase in $R_{ct}$ was observed after the addition of MCH, suggesting that MCH covered the non-modified gold surface. In this case, two main effects were observed: (i) an increase of negatively charged DNA and (ii) MCH blocked the surface, creating a high insulating surface and a high permeability of ions through the modified electrode.

We next added the OTA aptamer (OA). Because OA aptamer is negatively charged, the anionic redox probe was repealed from the sensor surface causing an increase of $R_{ct}$. The addition of OA caused an increase of the normalized $R_{ct}$ signal of 41%, 45% and 37% for the DNA concentrations of 0.1 µM, 0.32 µM and 1 µM, respectively. These values were calculated using the *normalized* $R_{ct}$ of OA and considering the $R_{ct}$ of MCH as the initial value, $(R_{ct}^{OA} - R_{ct}^{MCH})/R_{ct}^{MCH}$.

Note that at the highest DNA concentration (10 µM), no significant difference on the normalized $R_{ct}$ signal was observed (<5%). This suggests that no aptamer was bound on the modified surface. This could be related to steric hindrance due to the high compact layer of DNA (98% according to Figure 73(b)).

We finally studied the $R_{ct}$ variation for a *control* experiment without DNA. An increase of normalized $R_{ct}$ of 15% was obtained after the addition of the aptamer. This variation suggests that there is a slight non-specific adsoption of the aptamer onto the MCH-modified electrode. However, this variation could be related to posible changes in the impedance during the measurements. According to Bogomolova *et al* [26], non-specific impedance changes could occur, causing false-positive or false-negative results. In a similar work, the same authors used an electrode array for the detection of long DNA targets [27]. They found that measurement-related impedance increase can account for 10–20% of impedance increase on all electrodes. This value is in agreement with the obtained in our system. This corroborates the importance of incorporating negative controls within the same experiment for specificity studies that can be conveniently done using the developed multi-electrode platform.

### 5.3.3 Strategy II: detection of OTA

We next evaluated the detection capabilities of the multi-sensor by adding to the system different concentrations of OTA. Our results showed a decrease in $R_{ct}$ after the addition of OTA for all the DNA C concentrations and for two controls, one without DNA and the other using a non-specific DNA (DNA NC). Similar results were reported by Prabhakar *et al* [10]. When OTA molecules interact with the aptamer attached on the surface, the looping or folding of the aptamer around the OTA molecule, in the form of a quadruplex structure, occurs. This results in the formation of an aptamer–OTA complex that may result in improved electron transfer between the aptamer and the electrode surface [28].

Figure 75 shows the normalized $R_{ct}$ values vs DNA concentrations (individual functionalized electrodes) obtained for increasing OTA concentrations. The impedance values can differ significantly for the different electrodes and it could be difficult to distinguish between specific bindings from non-specific impedance increase. For this reason, we defined again normalized $R_{ct}$ as $NR_{ct} = (R_f - R_i)/R_i$, where $R_f$ is the final value of $R_{ct}$ (with OTA) and $R_i$ is the initial value of $R_{ct}$ (with aptamer). This allowed us to account for differences in probe densities and analyze the relative changes in $R_{ct}$. Additionally, the data was further normalized with the initial value (concentration of OTA = 0 ng $mL^{-1}$) to compare the results between the different concentrations of DNA C.

For all the DNA C concentrations, the $NR_{ct}$ reached a plateau (saturation) for concentrations larger than 25 ng $mL^{-1}$. The system was capable to detect OTA concentrations of 6.125 ng $mL^{-1}$ (15 nM). Our sensing device shows a LOD that enables the detection of OTA concentrations which

are below the limit set by the European Commission and it is comparable to those obtained using analytical methods based on TLC-FD (25 nM) [5].

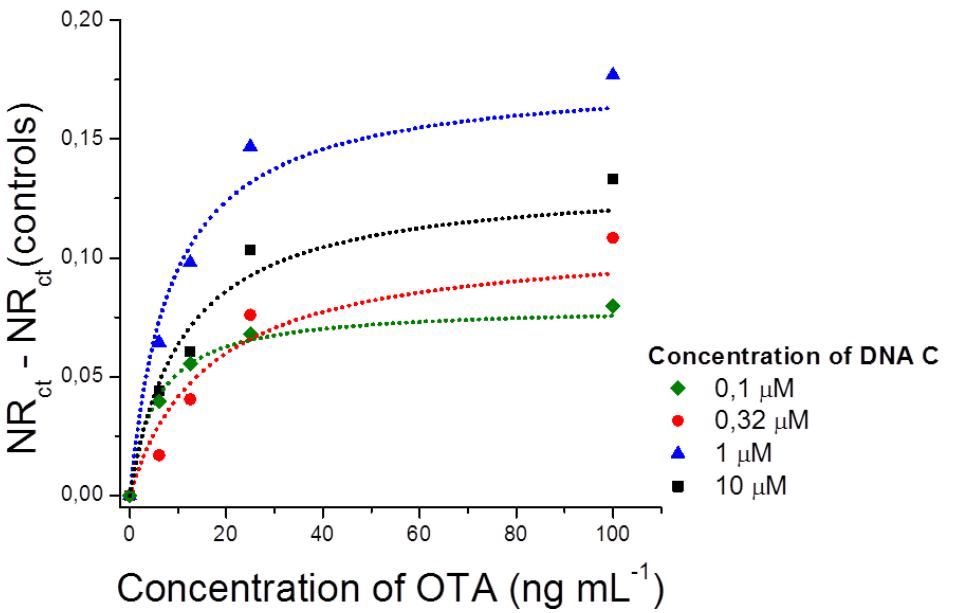


Figure 75. Plot of the normalized charge transfer resistance ($NR_{ct}$), substracting the values of the controls, as a function of increasing concentrations of OTA for different concentrations of immobilized DNA C on the electrodes. Dashed lines represent the Langmuir adsorption isotherm fitting.

All the curves showed a similar tendency for all the concentrations of DNA probe with the highest response obtained for 1 μM (see Figure 75). In order to characterize the binding properties of our developed sensor, we calculated the *association constant Ka* of the OA-OTA complex. The binding between aptamer OA and OTA can be described by a Langmuir adsorption isotherm [29, 30]. This equation relates the surface coverage (or adsorption of molecules) on a solid surface to concentration. In this case, we assumed that there was negligible intermolecular interaction between the adsorbed target DNA molecules and uniform binding sites, having equal binding energy,

on the surface [10]. The dis*sociation constant* $K_D$ values for the aptamer - OTA complex can be obtained using Langmuir equation [20]:

$$\text{Aptamer} + \text{Ochratoxin} \underset{K_D}{\overset{K_a}{\Leftrightarrow}} [\text{Aptamer} - \text{Ochratoxin}]\ \text{complex}$$

$$\frac{y}{y_{max}} = \frac{C_0}{K_D + C_0}$$

where $C_0$ is the concentration of OTA, $y$ the $NR_{ct}$ - $NR_{ct}$ *(controls*) and $y_{max}$ the maximum value of $NR_{ct}$ - $NR_{ct}$ *(controls)*. Considering that $K_D = 1/K_a$ and the second equation, the ratio between the slope and the $C_o/y$ at the origin gives the $K_a$ value, while the inverse of the slope gives $y_{max}$:

$$\frac{C_0}{y} = \frac{C_0}{y_{max}} + \frac{1}{y_{max}K_a}$$

Figure 76 shows the plot of $C_0/y$ versus $C_0$. We obtained a $K_a$ value of $1.05\text{x}10^{-1}$ mL $ng^{-1}$, which corresponds to a dissociation constant $K_D$ of 9.5 ng $mL^{-1}$ (23.5 nM). The obtained $K_a$ was much lower in comparison with the one obtained by Prabhakar *et al* [10], who reported an association constant of $2.99\times10^{1}$ mL $\mu g^{-1}$. Similarly, the obtained $K_D$ obtained was also much lower in comparison with that determined by fluorescence method for free aptamers [12]. However, lower dissociation constants were obtained by Castillo *et al* [20]. They reported $K_D$ from 17.3 nM to 1.2 nM, depending on the configuration of the aptamers.

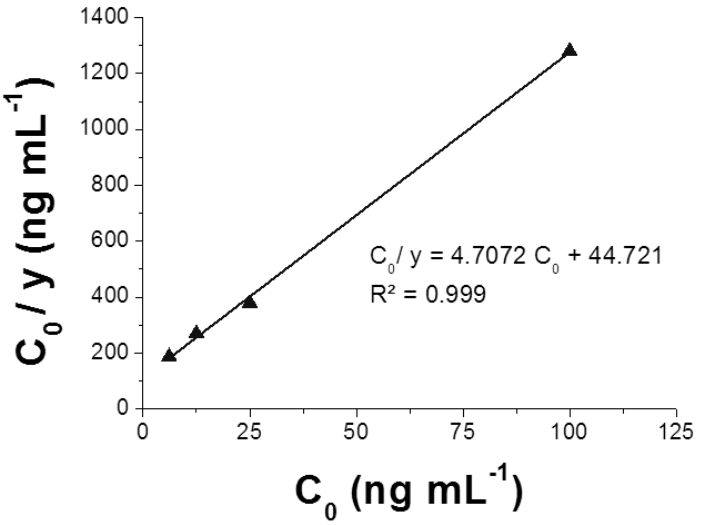


Figure 76. Linearized plot of the Langmuir isotherm data presented in Figure 75 for 1 µM DNA C.

The $K_D$ value is a measure of the affinity of the analyte to the receptor on the sensor surface. A lower dissociation constant corresponds to higher affinity, or higher stability of the analyte-receptor complex. The difference between our work and the work described by Castillo *et al* [20], could be related to the sequence of the aptamer immobilized or surface functionalization procedure used. The experimental results presented by Castillo *et al* indicated that the OTA aptamer, with a thiol modification at the 3' end for the attachment to the electrode surfaces, had a higher affinity constant and LOD compared to OTA aptamer with a thiol modification at the 5' end. Additionally, they used a thiolated DNA aptamer specific to OTA immobilized by chemisorption to a gold electrode surface, while in our case aptamers were immobilized through hybridization with partially complementary oligonucleotides.

Direct attachment of DNA on gold is the most simple and commonly used functionalization method. The 3' or 5' thiol-labeled aptamers self-

assemble through the gold-sulfur bond interaction and form ordered single-carrier membrane [21]. For example, Xiao *et al* [31] used this strategy to develop an aptasensor for the detection of thrombin. After its addition, current changes were detected as a result of the conformational change of aptamers upon specifically binding the targets.

The same strategy was applied on gold particles. Huang *et al* [32] immobilized thiol-labeled aptamer and MCH onto the surface of gold nanoparticles in suspension for the colorimetric detection of platelet-derived growth factors. The sensor was relatively simple, and the detection process could be observed by naked eyes and did not require complex and expensive chemical analysis or equipment. On the other hand, its sensitivity was only in the order of nM.

The aptamer hybridization with partially complementary oligonucleotides was also used on colorimetric aptasensors. Zhao *et al* [33] developed an aptamer sensor for adenosine detection using gold nanoparticles. The nanoparticles turned red due to electrostatic repulsion from much more negative charges on partially complementary double-stranded DNA. After the addition of target molecules –adenosine– in the reaction system, aptamers bound the adenosine and dissociated from nanoparticles. At this point, the nanoparticles fused together and changed to purple as the surface of gold nanoparticles reduced negative charges significantly. The advantage of this colorimetric sensors compared with the aptasensors developed by Huang *et al* [32] was that the generated optical signal was not dependent on the conformation change or multibinding sites of aptamers. Therefore, it is applicable for a diverse variety of sensors. However, due to the immobilization method involving annealing and hybridization, it is challenging to control all the experimental conditions. At

the same time, the partially complementary double-stranded chains (aptamers and short oligonucleotides) had the same electrical charges, and the electrostatic repulsion and steric hindrance would be much larger.

## 5.4 Conclusions and perspectives

In this chapter, we showed the sensing capabilities of the multi-electrode array by detecting different concentration of OTA mycotoxin. We characterized two different surface functionalization strategies for the immobilization of aptamers onto the multi-electrodes.

The results obtained with *strategy I* demonstrated that the DNA or OA aptamer did not adhere onto the gold surface, probably due to desorption of the SAM from the gold surface. On the other hand, *strategy II* showed a successful attachment of DNA on the gold surface as well as its hybridization with the aptamer. In this case, we observed that the DNA concentrations for which the addition of OTA aptamer increased the most ranged from 0.1 µM to 1 µM. The smallest OTA concentration that was detected by the aptamer multisensor for all the DNA concentrations was 6.125 ng $mL^{-1}$ (15 nM), and the highest response for OTA detection was obtained for the DNA C concentration of 1 µM.

We measured the binding properties of our aptasensor by measuring the association constant using a 1 µM DNA C concentration. We obtained a value of $1.05x10^{-1}$ mL $ng^{-1}$, which corresponded to a dissociaton constant $K_D$ of 9.5 ng $mL^{-1}$ (23.5 nM). Despite lower values of $K_D$ have been reported, the results are very promising taking into account the especial characteristics of our multi-electrode platform, i.e. high-throughput, mass-production, simple

and robust chemistry, and parallel measurements under the same conditions, among others.

Finally, we further demonstrated the advantages of using multi-electrodes as a biosensing platform: multiple negative controls can be performed and, as a consequence, the reliability of detection can be improved. This avoids measurement-related or incubation-related changes in the impedance spectra that can be distinguished from the specific changes.

Electrodes arrays could become a useful tool in system optimization, allowing rapid adjustment of different parameters, such as probe length and configuration, probe density or concentration, and binding buffer compositions. Finally, the multi-electrodes could also be a promising alternative for high-throughput, real-time, multiple target molecules' detection and rapid analysis of environmental and food contaminants in complex matrices.

## 5.5 References

[1] C. Yang, V. Lates, B. Prieto-Simón, J.-L. Marty, X. Yang, Rapid high-throughput analysis of ochratoxin A by the self-assembly of DNAzyme-aptamer conjugates in wine, Talanta. 116 (2013) 520–6.

[2] A. el Khoury, A. Atoui, Ochratoxin a: general overview and actual molecular status, Toxins 2 (2010) 461–93.

[3] R. Remiro, E. González-Peñas, E. Lizarraga, A. López de Cerain, Quantification of ochratoxin A and five analogs in Navarra red wines, Food Control. 27 (2012) 139–145.

[4] C. Yang, V. Lates, B. Prieto-Simón, J.-L. Marty, X. Yang, Aptamer-DNAzyme hairpins for biosensing of Ochratoxin A, Biosens. Bioelectron. 32 (2012) 208–12.

[5] C. Yang, Y. Wang, J.-L. Marty, X. Yang, Aptamer-based colorimetric biosensing of Ochratoxin A using unmodified gold nanoparticles indicator, Biosens. Bioelectron. 26 (2011) 2724–7.

[6] N.W. Turner, S. Subrahmanyam, S.A. Piletsky, Analytical methods for determination of mycotoxins: a review, Anal. Chim. Acta. 632 (2009) 168–80.

[7] F.-Y. Yu, T.-F. Chi, B.-H. Liu, C.-C. Su, Development of a sensitive enzyme-linked immunosorbent assay for the determination of ochratoxin A, J. Agric. Food Chem. 53 (2005) 6947–53.

[8] V. Hodnik, G. Anderluh, Toxin detection by surface plasmon resonance, Sensors 9 (2009) 1339–54.

[9] B. Prieto-Simón, M. Campàs, J.-L. Marty, T. Noguer, Novel highly-performing immunosensor-based strategy for ochratoxin A detection in wine samples, Biosens. Bioelectron. 23 (2008) 995–1002.

[10] N. Prabhakar, Z. Matharu, B.D. Malhotra, Polyaniline Langmuir-Blodgett film based aptasensor for ochratoxin A detection, Biosens. Bioelectron. 26 (2011) 4006–11.

[11] J.A. Cruz-aguado, G. Penner, Fluorescence polarization based displacement assay for the determination of small molecules with aptamers, Anal. Chem. 80 (2008) 8853–5.

[12] J.A. Cruz-Aguado, G. Penner, Determination of ochratoxin a with a DNA aptamer, J. Agric. Food Chem. 56 (2008) 10456–61.

[13] Z. Wang, N. Duan, X. Hun, S. Wu, Electrochemiluminescent aptamer biosensor for the determination of ochratoxin A at a gold-nanoparticles-modified gold electrode using N-(aminobutyl)-N-ethylisoluminol as a luminescent label, Anal. Bioanal. Chem. 398 (2010) 2125–32.

[14] A. Hayat, A. Sassolas, J.-L. Marty, A.-E. Radi, Highly sensitive ochratoxin A impedimetric aptasensor based on the immobilization of azido-aptamer onto electrografted binary film via click chemistry, Talanta. 103 (2013) 14–9.

[15] H. Kuang, W. Chen, D. Xu, L. Xu, Y. Zhu, L. Liu, et al., Fabricated aptamer-based electrochemical “signal-off” sensor of ochratoxin A, Biosens. Bioelectron. 26 (2010) 710–6.

[16] B. Prieto-Simón, J. Samitier, “Signal Off” Aptasensor Based on Enzyme Inhibition Induced by Conformational Switch, Anal. Chem. (2014).

[17] L. Bonel, J.C. Vidal, P. Duato, J.R. Castillo, An electrochemical competitive biosensor for ochratoxin A based on a DNA biotinylated aptamer, Biosens. Bioelectron. 26 (2011) 3254–9.

[18] M.C. Rodriguez, A.-N. Kawde, J. Wang, Aptamer biosensor for label-free impedance spectroscopy detection of proteins based on recognition-induced switching of the surface charge, Chem. Commun. (Camb). (2005) 4267–9.

[19] J.A. Lee, S. Hwang, J. Kwak, S. Il Park, S.S. Lee, K.-C. Lee, An electrochemical impedance biosensor with aptamer-modified pyrolyzed carbon electrode for label-free protein detection, Sens. Actuators B 129 (2008) 372–379.

[20] G. Castillo, I. Lamberti, L. Mosiello, T. Hianik, Impedimetric DNA aptasensor for sensitive detection of Ochratoxin A in food, Electroanalysis 24 (2012) 512–520.

[21] L. Zhou, M.-H. Wang, J.-P. Wang, Z.-Z. Ye, Application of biosensor surface immobilization methods for aptamer, Chinese J. Anal. Chem. 39 (2011) 432–438.

[22] A. Rasooly, K.E. Herold, Biosensors and Biodetection, Humana Press, 2009.

[23] M.J.T. Tonya M. Herne, Characterization of DNA probes immobilized on gold surfaces, J. Am. Chem. Soc. 119 (1997) 8916–8920.

[24] V.M. Mirsky, M. Riepl, O.S. Wolfbeis, Capacitive monitoring of protein immobilization and antigen-antibody reactions on monomolecular alkylthiol films on gold electrodes, Biosens. Bioelectron. 12 (1997) 977–89.

[25] X.L. Su, Y. Li, A self-assembled monolayer-based piezoelectric immunosensor for rapid detection of Escherichia coli O157:H7, Biosens. Bioelectron. 19 (2004) 563–574.

[26] A. Bogomolova, E. Komarova, K. Reber, T. Gerasimov, O. Yavuz, S. Bhatt, et al., Challenges of electrochemical impedance spectroscopy in protein biosensing, Anal. Chem. 81 (2009) 3944–9.

[27] E. Komarova, K. Reber, M. Aldissi, a Bogomolova, New multispecific array as a tool for electrochemical impedance spectroscopy-based biosensing, Biosens. Bioelectron. 25 (2010) 1389–94.

[28] Y. Peng, D. Zhang, Y. Li, H. Qi, Q. Gao, C. Zhang, Label-free and sensitive faradic impedance aptasensor for the determination of lysozyme based on target-induced aptamer displacement, Biosens. Bioelectron. 25 (2009) 94–9.

[29] D. Kambhampati, P.E. Nielsen, W. Knoll, Investigating the kinetics of DNA-DNA and PNA-DNA interactions using surface plasmon resonance-enhanced fluorescence spectroscopy, Biosens. Bioelectron. 16 (2001) 1109–18.

[30] B.T. Neumann, M. Johansson, D. Kambhampati, W. Knoll, Surface Plasmon Fluorescence Spectroscopy, Adv. Funct. Mater. 12 (2002) 575–586.

[31] Y. Xiao, A. Lubin, A.J. Heeger, K.W. Plaxco, Label-free electronic detection of thrombin in blood serum by using an aptamer-based sensor, Angew. Chemie. 44 (2005) 5456–9.

[32] C.-C. Huang, Y.-F. Huang, Z. Cao, W. Tan, H.-T. Chang, Aptamer-modified gold nanoparticles for colorimetric determination of platelet-derived growth factors and their receptors, Anal. Chem. 77 (2005) 5735–41.

[33] W. Zhao, W. Chiuman, M.A. Brook, Y. Li, Simple and rapid colorimetric biosensors based on DNA aptamer and noncrosslinking gold nanoparticle aggregation, Chembiochem. 8 (2007) 727–31.

# **Chapter 6.** General conclusions

In this thesis we developed a novel multi-electrode impedimetric biosensor platform for pathogenic bacteria and mycotoxins detection. The influence of the sensor (bio) interface in the development of a highly sensitive and selective biosensor was evaluated for detection of *E. coli* O157:H7. For this reason, different surface functionalization strategies and materials were tested, and all the steps were fully characterized. Finally, we developed and characterized the multi-electrode platforms and applied them for the detection of *E. coli* O157:H7 bacteria and mycotoxin OTA. In the following, we describe the general conclusions obtained for each of the chapters.

In **Chapter 2**, we described the fabrication of a label-free immunosensor for the detection of very low concentrations of pathogenic bacteria *E. coli* O157:H7 on ITO electrodes. We used a simple, direct and robust silanization method to efficiently functionalize the ITO electrodes. The sensor properties and detection capability were studied and characterized by means of AFM, fluorescence microscopy and OWLS. Results showed the high efficiency and specificity of the sensing platform developed. Finally, the detection capabilities of the developed immunosensor for the detection of *E. coli* O157:H7 were addressed by EIS and very low LOD over a wide linear dynamic range were obtained for viable and heat-killed bacteria (1-2 CFU $mL^{-1}$). To the best of our knowledge, this study is the first to report an impedimetric immunosensor based on ITO surfaces with such a low LOD. We conclude that our label-free immunosensor may have relevant applications for the detection of low concentrations of pathogenic bacteria and may provide a promising alternative to more standard and conventional detection materials and methodologies. However, detection of very low concentrations

of *E. coli* O157:H7 in complex samples, such as blood plasma, remains still a challenge.

In **Chapter 3**, we developed a gold-based electrochemical immunosensor for the detection of pathogenic *E. coli* O157:H7 bacteria testing different functionalization strategies. The efficiency of the sensing platform was first demonstrated by SPR allowing the optimization and characterization of the surface antibody functionalization. Fluorescence and AFM studies revealed the morphological features of the sensing platform, as well as demonstrated the selectivity of the antibody recognition capabilities. Finally, the recognition capabilities of the sensing platform were studied for *E. coli* O157:H7 bacteria by EIS. A limit of detection as low as 2 CFU $mL^{-1}$ were obtained, being the lowest LOD reported on gold surfaces and similar to the one obtained for ITO surface. The sensor showed high specificity and large linear detection range making our approach very attractive for application in the environmental, clinical and food industry fields.

In **Chapter 4**, we took advantage of the functionalization strategies studied in the previous chapter 3 to develop a miniaturized gold multi-electrode array. The multi-electrode was fabricated by photolithographic processes and fully characterized by optical and electrochemical methods to demonstrate its excellent manufacturing quality and operational performance; reproducible and re-usable working electrodes were obtained. Impedimetric measurements were performed for the detection of pathogenic bacteria. The multi-electrodes were functionalized with anti-*E. coli* antibodies and tested for the detection of pathogenic bacteria *E. coli* O157:H7. All the electrodes showed a uniform and specific response to *E. coli* O157:H7 bacteria. Magainin I peptides were also evaluated as an alternative to antibodies. Even though they showed interesting properties and promising

results were obtained, some limitations regarding their specificity and sensitivity were observed.

In **Chapter 5**, we applied the multi-electrodes platform for the development of an aptamer-based sensor for the detection of OTA. Two different surface functionalization strategies for the immobilization of aptamers were tested and characterized. We selected the strategy which showed an optimal attachment of DNA on the gold surface as well as its hybridization with the aptamer. In this case, we observed that the DNA concentrations for which the addition of OTA aptamer increased the most were within the range 0.1 µM - 1 µM. The smallest OTA concentration that was detected by the multi-aptasensor for all the DNA concentrations was 6.125 ng $mL^{-1}$ (15 nM), and the highest response for OTA detection was for DNA C concentration of 1 µM. An association constant value of $1.05x10^{-1}$ mL $ng^{-1}$ was obtained for this DNA C concentration, which corresponded to a dissociaton constant $K_D$ of 9.5 ng $mL^{-1}$ (23.5 nM). Although lower values of $K_D$ have been reported, the obtained values are very promising taking into account the especial characteristics of our multi-electrode platform, i.e. high-throughput and mass-production characteristics, simple and robust chemistry, and parallel measurements under the same working conditions, among others.

To conclude, in this work, we have demonstrated the advantages of using multi-electrodes as a biosensing platform: multiple negative controls can be performed and, as a consequence, the reliability of detection can be improved. The multi-electrodes could also be a promising alternative for high-throughput, real-time, multiple target molecules' detection and rapid analysis of environmental and food contaminants. Finally, it is worth mentioning that the developed work could have a positive impact for the development of

more reliable and efficient biosensors, and potentially, becoming an interesting alternative to those biosensors present in the market.

# Resumen en castellano

# **Capítulo 1.** Introducción general

## 1.1. Biosensores

Los biosensores son herramientas analíticas versátiles de gran importancia que pueden desempeñar un papel cada vez más determinante en la mejora de la calidad de vida [1]. Un biosensor está definido por la Unión Internacional de Química Pura y Aplicada (IUPAC) como "*un dispositivo que utiliza reacciones bioquímicas específicas mediadas por enzimas aisladas, inmunosistemas, tejidos, orgánulos, células, para la detección de compuestos químicos por lo general mediante señal eléctrica, térmica, u óptica*" [2, 3]. Un esquema de los componentes típicos de un biosensor se muestra en la Figura 1.

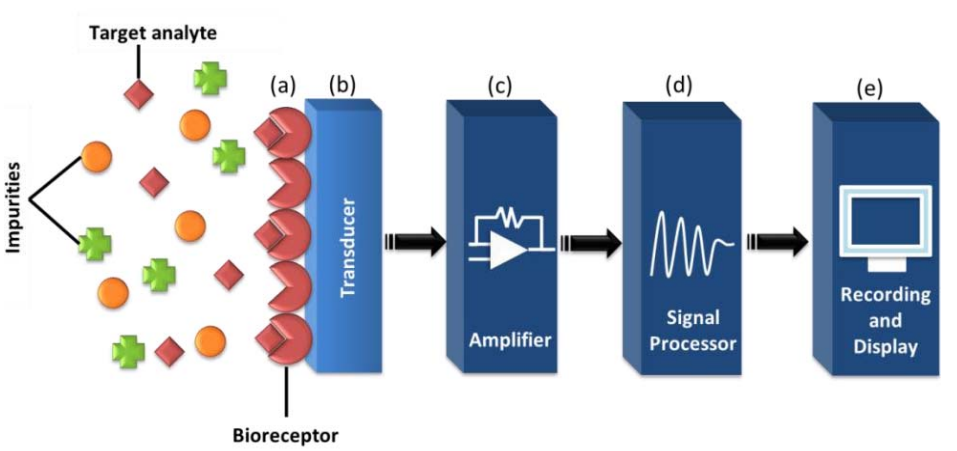


Figura 1. Esquema de los componentes típicos de un biosensor: (a) bioreceptor, (b) transductor, (c) amplificador, (d) procesamiento de señales y (e) grabación y exposición.

Un biosensor está formado por dos componentes principales: un elemento bioreceptor o capa de bioreconocimiento (a), y un transductor (b). La señal amplificada (c) se procesa por el procesador de señal (d) en el que más tarde puede ser almacenada, mostrada y analizada (e) [4–6].

El bioreceptor es generalmente un sistema biológico inmovilizado o un componente que es capaz de reconocer específicamente el analito de interés entre muchos otros elementos (impurezas) [11]. Los bioreceptores son la clave de la especificidad de los biosensores y, en general, se pueden clasificar en cuatro categorías principales: anticuerpo/antígeno, enzimas, ácidos nucléicos/ADN, y estructuras celulares/células. Los biosensores compuestos por anticuerpos (inmunosensores) son muy utilizados debido a que los anticuerpos son altamente específicos, versátiles, y se unen fuertemente de forma estable al antígeno [7]. Sin embargo, otros bioreceptores tales como aptámeros, péptidos, receptores biomiméticos y bacterio-fagos, se han usado también ampliamente durante los últimos años [5, 8, 9].

El transductor convierte las respuestas biológicas en una señal eléctrica medible y desempeña un papel importante en el proceso de detección de un biosensor. Aunque nuevos tipos de transductores se están constantemente desarrollando, los métodos de transducción óptica y electroquímica son los más populares y comunes [5, 10]. Otra forma de transducción que se ha utilizado ampliamente en los biosensores es la medición de pequeños cambios de masa. Los dos tipos de sensores de masa más comunes son la microbalanza de cristal de cuarzo (QCM) y la onda acústica de superficie (SAW) [11, 8, 5].

Los biosensores ópticos son probablemente los más populares en bioanálisis, debido a su selectividad y sensibilidad. Se han desarrollado para la detección rápida de contaminantes [12, 13], toxinas o fármacos [14, 15] e

incluso para bacterias patógenas [5, 15-17]. Recientemente, métodos basados en fluorescencia y resonancia de plasmones superficiales (SPR) han ganado popularidad debido a su alta sensibilidad [19].

Los biosensores basados en electroquímica utilizan un electrodo como elemento de transducción y representa una subclase importante de los sensores [20]. Estos biosensores se pueden clasificar en varias categorías, tales como amperométricos, potenciométricos e impedimétricos, en función de los parámetros medidos, como la corriente, el potencial y la impedancia, respectivamente [19]. La detección electroquímica tiene varias ventajas como el bajo coste, la capacidad para trabajar con muestras complejas y son de fácil miniaturización. Sin embargo, su sensibilidad y selectividad pueden presentar ciertas limitaciones [5]. La Espectroscopía de Impedancia Electroquímica (EIS) es una técnica ampliamente utilizada para el estudio de las interacciones de bioafinidad en las superficies y puede emplearse para investigar la detección de analitos no marcados o "*label-free*" a través de transducción impedimétrica. Los biosensores basados en impedancia tienen un gran potencial para la detección rápida de biomoléculas, *label-free*, de forma simple y con bajo coste [5, 21, 22].

Un paso clave en el desarrollo de los biosensores es la inmovilización del componente biológico en la superficie del transductor. Una amplia variedad de materiales y métodos de modificación de superficies se usan para el desarrollo de biosensores. Los materiales más comúnmente utilizados son el oro, silicio, óxido de silicio, nitruro de silicio, grafito y óxido de indio y estaño (ITO), entre otros [6].

El oro es un buen material para ser usado como electrodo en aplicaciones de biosensores debido a la posibilidad de formar fácilmente monocapas autoensambladas (SAM) de los elementos de bioreconocimiento.

El oro se ha convertido en el sustrato estándar para la formación de SAM porque es fácil de obtener, manipular y es biocompatible [18]. Por otro lado, el ITO se ha considerado como un material muy prometedor para la caracterización de sistemas biológicos. Su superficie es transparente (ideal para mediciones ópticas), conductora y estable en condiciones fisiológicas debido a sus propiedades polarizables.

El desarrollo de un biosensor requiere la funcionalización de la superficie para integrar los elementos de bioreconocimiento seleccionados. Este es uno de los pasos más importantes en el desarrollo de biosensores debido a que el rendimiento del biosensor (sensibilidad, rango dinámico, reproducibilidad y tiempo de respuesta) depende de que se mantengan las propiedades originales del bioreceptor después de su inmovilización. Las estrategias de inmovilización existentes incluyen la adsorción, el atrapamiento y encapsulación en polímeros o membranas, la silanización y la formación de SAM acoplando la biomolécula mediante "*cross-linking*" o a través de un enlace covalente [18, 23].

Las principales aplicaciones de los biosensores incluyen la medicina, el medio ambiente, la seguridad pública y la seguridad alimentaria [3,5]. La detección rápida de bacterias patógenas y micotoxinas presentes en los alimentos es de gran importancia para la reducción de enfermedades causadas por alimentos contaminados. Los biosensores pueden detectar patógenos en un tiempo mucho más corto con una sensibilidad y selectividad comparables a la de los métodos convencionales.

## 1.2. Detección de bacterias patógenas

La detección de bacterias patógenas es clave para la prevención e identificación de problemas relacionados con la salud y la seguridad. Las infecciones bacterianas siguen siendo la principal causa de muerte en las naciones en desarrollo, lo que representa aproximadamente el 40% de las muertes. Las infecciones más comunes transmitidas por los alimentos son las causadas por la bacteria *Escherichia coli* O157:H7 y la *Salmonella*.

La bacteria de la *Salmonella* es la que provoca la salmonelosis. Las personas infectadas desarrollan diarrea, fiebre y calambres abdominales entre 12 y 72 horas después de comer el alimento contaminado (dosis de infección 15-20 organismos). En casos raros, la infección puede extenderse al torrente sanguíneo y puede causar la muerte si no se trata [5]. Entre los más de 2000 serotipos que han sido identificados, la *Salmonella enteritidis* y la *Salmonella typhimurium* son los epidemiológicamente más importantes [16].

La *Escherichia coli* O157:H7 es una bacteria Gram negativa que se ha visto implicada en brotes de enfermedades debidas a la ingestión de carnes, agua y vegetales crudos. La ingestión de la bacteria causa diarrea aguda sanguinolenta y calambres abdominales dolorosos. En algunos casos, una complicación llamada síndrome urémico hemolítico (SUH) puede producir una hemorragia abundante e insuficiencia renal [16]. La detección y control de patógenos como *E. coli* O157: H7 son problemas muy difíciles de afrontar en cuanto a su alta virulencia y a la dosis infecciosa extremadamente baja requerida para causar la enfermedad (<10 organismos) [24–26].

Los métodos convencionales para la detección de bacterias patógenas incluyen los métodos de cultivo y el recuento de colonias, métodos basados en la inmunología tales como ensayos inmunoenzimáticos (ELISA) y la

reacción en cadena de la polimerasa (PCR). Aunque estos métodos son muy sensibles y selectivos, consumen mucho tiempo y requieren a menudo de un pre-tratamiento o purificación de la muestra inicial con el fin de detectar concentraciones bajas de patógenos. Las técnicas de detección basadas en biosensores son una alternativa interesante para la realización de mediciones simples, sensibles, rápidas, selectivas y fiables de las bacterias patógenas, siendo al mismo tiempo rentable y aplicable a la monitorización en tiempo real.

La detección de *E. coli* mediante biosensores puede realizarse mediante diferentes tipos de bioreceptores (anticuerpos, péptidos antimicrobianos, aptámeros y sondas de ADN) utilizando transductores ópticos y electroquímicos, entre otros. Los biosensores electroquímicos han sido objeto de especial atención en los últimos años debido a sus múltiples ventajas, como su rápida respuesta, su bajo coste, la posibilidad de producción en masa y la capacidad de miniaturización. Los sensores basados en EIS son particularmente atractivos porque permiten la detección"*label-free"* con una alta sensibilidad. Se han publicado límites de detección (LOD) tan bajos como 10 a $10^3$ Unidades Formadoras de Colonias (CFU) $mL^{-1}$ para *E. coli* mediante el uso de este tipo de inmunosensores impedimétricos [27, 28]. Sin embargo, aún se requieren límites inferiores para la detección de bacterias en alimentos o muestras clínicas, ya que las dosis infecciosas de *E. coli* O157: H7 son inferiores a 10 células [5, 24].

## 1.3. Detección de toxinas

De manera similar a las bacterias patógenas, la presencia de toxinas en alimentos y aguas es también una gran preocupación, ya que puede poner

en peligro la seguridad alimentaria y la protección de la salud pública. Las ocratoxinas son un pequeño grupo de metabolitos fúngicos tóxicos químicamente relacionados (micotoxinas). Son producidas por ciertos hongos de los géneros *Aspergillus* y *Penicillium* que crecen en una amplia gama de materias primas alimentarias. La ocratoxina más importante y más tóxica que se encuentra en los alimentos de forma natural es la ocratoxina A (OTA). Se ha encontrado OTA en una gran variedad de productos: cereales, legumbres, frutos secos, café, cerveza, vino y carne donde los animales fueron alimentados con pienso contaminado. Los límites varían según el producto, pero se extienden a partir de 2-10 microgramos/kg.

Los métodos establecidos para la detección de micotoxinas como la cromatografía líquida de alto rendimiento (HPLC) y la cromatografía en capa fina (TLC), proporcionan límites de detección muy bajos. Sin embargo, la necesidad de personal calificado, su alto coste y las limitaciones para llevar a cabo el análisis *in situ*, incentivan el uso de técnicas alternativas. En los últimos años, los biosensores han surgido como una prometedora herramienta de análisis fiable, alternativa a los métodos clásicos debido a su alta sensibilidad, selectividad, simplicidad, facilidad de uso, bajo coste y, en algunos casos, su capacidad de miniaturización, de integración en dispositivos automatizados y portabilidad. Biosensores sensibles y precisos se han desarrollado sobre la base de distintos métodos de transducción los cuales se basan en el uso de aptámeros y anticuerpos bioreceptores.

Varios ejemplos de biosensores para la detección de OTA han sido descritos en la literatura. Sin embargo, todavía existe un gran desafío para el desarrollo de ensayos alternativos para la detección de OTA y la detección simultánea de diferentes micotoxinas. La detección de múltiples analitos simultáneamente es altamente interesante para el análisis de muestras

compuestas de múltiples micotoxinas. Sin embargo, a menudo micotoxinas diferentes requieren diferentes protocolos de extracción, lo que complica la armonización de los protocolos para la integración de varios biosensores en una misma plataforma.

## 1.4. Perspectivas y objetivos de la tesis

Los biosensores han traído enfoques nuevos y prometedores para el desarrollo de métodos para la detección de bacterias y micotoxinas. Los biosensores son dispositivos fáciles de usar y sin necesidad de formación de personal especializado, los resultados de análisis se obtienen prácticamente en tiempo real con sensibilidad y selectividad comparable a los métodos tradicionales. La detección de varios analitos en la misma muestra biológica es posible si diferentes regiones de la superficie están funcionalizadas con diferentes bioreceptores. La detección multiplexada es deseable, ya que reduce tanto el coste como el volumen de la muestra.

Esta tesis, titulada "Desarrollo de un biosensor multi-electrodo impedimétrico: detección de bacterias patógenas y micotoxinas", tiene como objetivo el desarrollo de una plataforma de multi-electrodos para (i) la detección de bacterias patógenas y (ii) la detección de la micotoxina OTA. Una de las principales limitaciones en los biosensores multiplexados surge de la etapa de afinidad. Por lo tanto, una gran parte del trabajo de investigación que se describe aquí se refiere a la caracterización, optimización y evaluación de las diferentes estrategias de funcionalización de los biosensores desarrollados. Estas estrategias de funcionalización de superficies se aplicaran al final en la plataforma de multi-electrodos desarrollada.

# **Capítulo 2.** Immunosensor basado en ITO para la detección de bacterias patógenas

## 2.1. Introducción

El ITO es un óxido semiconductor transparente de capa fina que se ha aplicado ampliamente en varias áreas [29–34], como por ejemplo, en electroquímica, donde es usado como un electrodo ideal para la detección de biomoléculas. Las propiedades eléctricas y ópticas únicas del ITO pueden proporcionar métodos más eficientes para la transducción de la señal. Además, una inmovilización eficaz y estable de biomoléculas se puede lograr con grupos funcionales tales como ácidos carboxílicos, tioles y aminas.

En la literatura han sido descritas varias estrategias de inmovilización para el desarrollo de biosensores basados en ITO. Ejemplos de ello son: un biosensor de ADN [35] usando una funcionalización basada en silanos, un biosensor enzimático [36] utilizando la estrategia de biotina-estreptavidina y un inmunosensor para la detección de *E. coli* [37] usando epoxisilanos. En este último caso, varios trabajos sobre biosensores basados en ITO han sido desarrollados [38–41]. No obstante, la alta virulencia y la dosis infecciosa extremadamente baja de *E. coli* O157:H7 requerida para las enfermedades infecciosas (menos de 10 células), fomentan el desarrollo de un inmunosensor más sensible y específico.

En este capítulo se describe el desarrollo de un inmunosensor basado en ITO para la detección de muy bajas concentraciones de bacterias

patógenas *E. coli* O157:H7. Un método directo y robusto de silanización para la funcionalización eficiente de los electrodos de ITO es usado. EIS se utiliza para la detección *"label-free"* y para la monitorización del acoplamiento antígeno-anticuerpo.

## 2.2. Metodología

Un esquema del procedimiento de fabricación del inmunosensor basado en la reacción de epoxi-amina se muestra en la Figura 2. En primer lugar, se hidroxiló la superficie de ITO (1). Posteriormente, una monocapa acabada en un grupo funcional epoxi se formó mediante silanización con un epoxisilano (2). Por último, los anticuerpos anti-*E. coli* O157 con grupos alquilo amina se adhirieron covalentemente a los grupos epoxi por medio de enlaces de amina (3).

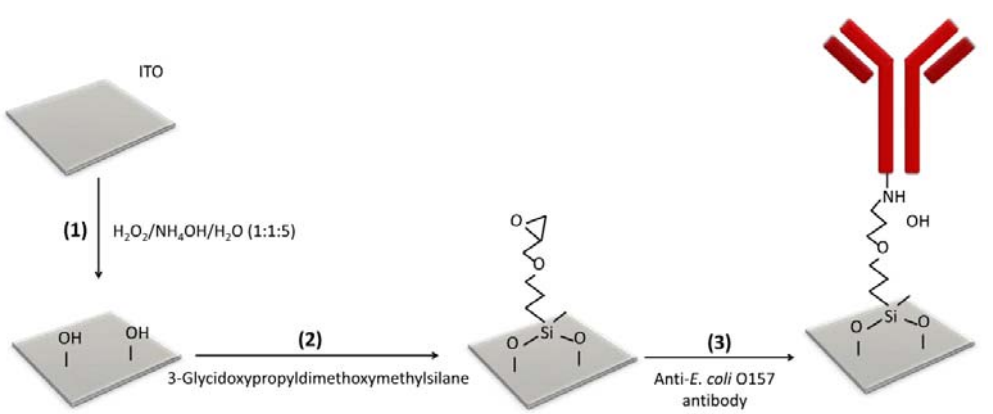


Figura 2. Diagrama esquemático de la fabricación del inmunosensor: hidroxilación (1), formación de SAM (2) y unión del anticuerpo (3).

La metodología de funcionalización se caracterizó mediante múltiples técnicas: microscopia de fuerza atómica (AFM), voltametría cíclica,

espectroscopía mediante una guía de ondas ópticas (OWLS) e inmunofluorescencia de muestras con un patrón de anticuerpos para la detección de bacterias. La capacidad de detección del inmunosensor se demostró mediante EIS.

Los electrodos de ITO fueron fabricados en colaboración con el "Grupo Coatings GRF-Funcional" del Departamento de Física de la Universidad de Minho (Braga, Portugal), mientras las muestras de bacterias se obtuvieron en colaboración con el grupo del Prof. Antonio Juárez y del Dr. Eduard Torrents (IBEC, Barcelona, España).

## 2.3. Resultados y discusión

El protocolo de funcionalización se caracterizó primero mediante AFM. El aumento de la rugosidad de la muestra sugirió la unión covalente del epoxisilano en la superficie de ITO y la inmovilización de anticuerpos sobre la monocapa de epoxisilano. El paso de inmovilización del epoxisilano sobre la superficie de ITO se caracterizó también por voltametría cíclica. Los datos obtenidos mostraron que el epoxisilano se adhirió aunque se obtuvo una monocapa aislante incompleta. La cobertura de anticuerpo en la superficie se cuantificó mediante OWLS. Se obtuvo una variación de masa de 12 ng $cm^{-2}$ (0,08 pmol $cm^{-2}$) de anticuerpo anti-*E. coli* O157 adsorbido en la superficie funcionalizada con epoxisilano.

La especificidad de la funcionalización en la superficie con anticuerpo se evaluó por medio de la técnica de impresión por micro-contacto. Los resultados indicaron que los anticuerpos anti-*E. coli* se adhirieron con éxito a la monocapa de epoxisilano y que la bacteria *E. coli* O157:H7 se unió específicamente a la superficie modificada con el anticuerpo, confirmando la

capacidad de detección del protocolo de funcionalización (incluyendo los pasos de bloqueo). La especificidad del sistema se estudió usando otra bacteria no específica (*S. typhimurium)* en el patrón de anticuerpos y se comparó con la obtenida de *E. coli* O157:H7. Se obtuvo una relación de 1:500 de *S. typhimurium* / *E. coli* O157:H7 confirmando de este modo la eficacia y la selectividad del procedimiento de funcionalización.

La detección de *E. coli* O157:H7 mediante un inmunosensor electroquímico se basó en la medición de la impedancia faradaica. Los cambios observados en la impedancia se modelaron ajustando los datos experimentales con un modelo de circuito equivalente *Randles*. La resistencia de transferencia de electrones ($R_{ct}$) fue muy sensible a los cambios producidos por la unión de *E. coli* O157:H7 a la superficie de ITO modificada con el anticuerpo y, por lo tanto, fue elegida como el parámetro ideal para la cuantificación del rendimiento del sensor.

La $R_{ct}$ aumentó tras la adición de concentraciones consecutivas de *E. coli* O157:H7. Se obtuvo una relación lineal entre la variación de la resistencia de transferencia de electrones, $\Delta R_{ct}$, y la concentración logarítmica de *E. coli* O157:H7 (Figura 3). Este aumento puede estar relacionado con el número las células bacterianas capturadas en la superficie del electrodo, retrasando la cinética de transferencia de electrones y causando una mayor resistencia a la transferencia de electrones [40].

Se obtuvo un límite de detección (LOD) muy bajo (1 CFU $mL^{-1}$) en 1 h (incluyendo la incubación bacteriana) para el inmunosensor *"label-free"* desarrollado. Además, nuestro enfoque muestra un amplio rango lineal de detección de 10-$10^6$ CFU $mL^{-1}$. La capacidad de detección de nuestro inmunosensor impedimétrico mostró un LOD más bajo comparado con otros tipos de biosensores (ELISA y OWLS).

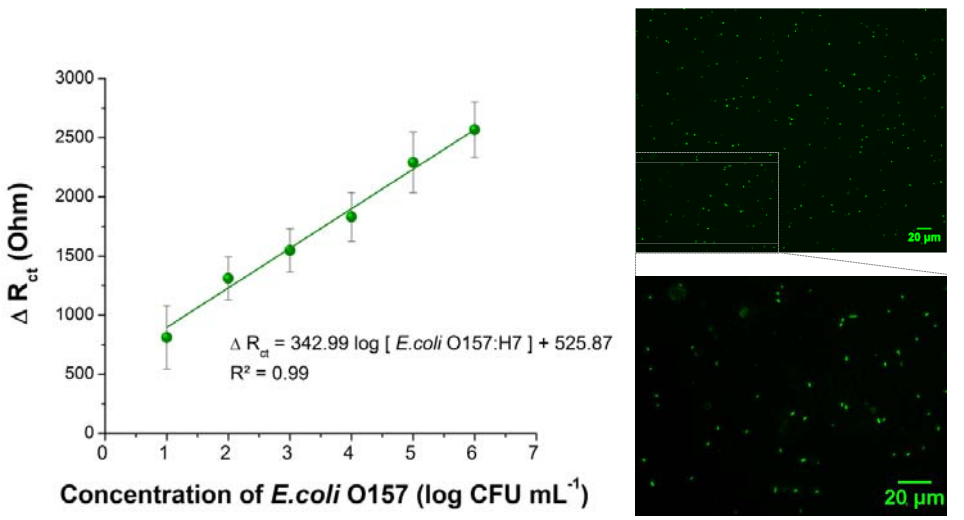


Figura 3 (Izquierda) Variación de la resistencia de transferencia de carga (ΔRct) en función de la concentración de *E. coli* O157:H7 (log CFU $mL^{-1}$) para el inmunosensor impedimétrico a base de ITO. Los datos se muestran como media ± s.d. (Derecha) imágenes de fluorescencia de un electrodo de ITO funcionalizado con anticuerpo después de las mediciones de impedancia mostrando las bacterias adheridas (en verde).

La figura 3 también muestra imágenes de fluorescencia del electrodo de ITO después de la medición de la impedancia demuestrando que las bacterias se unen con éxito sobre la superficie de ITO funcionalizada con el anticuerpo. El inmunosensor desarrollado también mostró una buena reproducibilidad, una excelente estabilidad y una alta especificidad. Finalmente, el sensor se utilizó también con éxito para la detección de bacterias en muestras reales.

## 2.4. Conclusiones

En este capítulo hemos descrito el desarrollo de un inmunosensor basado en electrodos de ITO para la detección de concentraciones muy bajas

de bacterias patógenas *E. coli* O157:H7. Hemos utilizado un método silanización simple, directo y robusto para funcionalizar de manera eficiente los electrodos de ITO. Se demostró una alta eficiencia, sensibilidad y especificidad de la plataforma de detección. Hasta donde sabemos, este es el primer inmunosensor impedimétrico basado en ITO con un límite de detección tan bajo. Sin embargo, la detección de concentraciones muy bajas de *E. coli* O157:H7 en muestras complejas, tales como el plasma sanguíneo, sigue siendo un reto. En este caso, pasos adicionales de pre-concentración o la adición de una etapa de filtración antes de la detección, podrían optimizar la respuesta del sensor en muestras complejas.

# **Capítulo 3.** Immunosensor basado en oro para la detección de bacterias patógenas

## 3.1. Introducción

La química de la superficie del biosensor donde se inmoviliza los receptores biológicos es un factor importante que afecta a la sensibilidad de detección y a su especificidad. Hemos visto en el capítulo 2 que los compuestos a base de silano pueden utilizarse con éxito para funcionalizar electrodos de ITO con anticuerpos. Esta estrategia proporciona resultados prometedores en términos de rendimiento del sensor. Sin embargo, otras estrategias y materiales están disponibles, como la utilización de SAM en superficies de oro.

Las SAMs proporcionan enormes ventajas para el desarrollo de biosensores debido a que son fáciles de preparar y funcionalizar en un laboratorio de química estándar. Se pueden formar en superficies de cualquier tamaño, y permiten que se unan estructuras a nivel molecular. El oro se ha convertido en un sustrato estándar para la formación de SAMs por varias razones: es fácil de obtener, fácil de estructurar utilizando fotolitografía, y es biocompatible [42]. Entre los distintos tipos de SAMs, las de alcanotiol son ampliamente utilizadas principalmente en superficies de oro debido a sus muchas propiedades: son resistentes a la adsorción no específica y forman una estructura de monocapa densa y bien ordenada.

Además, se pueden preparar fácilmente por incubación durante un período suficiente de tiempo [43, 44].

Como ya comentamos en el capítulo 2, la detección de bajas concentraciones de bacterias es de gran importancia, debido a las bajas dosis que se requieren para las enfermedades de origen. Se han desarrollado inmunosensores impedimétricos basados en superficies de oro aplicando distintas estrategias de funcionalización para la detección de *E. coli* [44, 27, 45, 46]. Sin embargo, estos sensores mostraron ciertas limitaciones en las capacidades de detección y altos LOD debido a las metodologías de funcionalización usadas. La baja dosis de bacterias necesaria para producir la infección requiere el desarrollo de nuevos sistemas y metodologías de detección.

En este capítulo, se presenta la fabricación y caracterización de un inmunosensor impedimétrico basado en superficies de oro para la detección de bacterias patógenas *E. coli* O157:H7. Nos centramos principalmente en la optimización, caracterización y evaluación de diferentes protocolos de funcionalización mediante técnicas de SPR y microscopía de fluorescencia, mientras que las capacidades de detección del sensor se evaluaron por EIS.

## 3.2. Metodología

Dos metodologías distintas de inmovilización de SAMs sobre superficies de oro fueron investigadas con el fin de obtener el mejor rendimiento del sensor y resistencia a la adsorción no específica (véase Figura 4). Los anticuerpos anti-*E. coli* fueron inmovilizados en oro mediante el acoplamiento de un anticuerpo anti-*E. coli* biotinilado con neutravidina depositada previamente sobre una SAM mixta (estrategia I).

Alternativamente, el anticuerpo se adhirió a través de la formación de un enlace químico entre los grupos amino de los anticuerpos y los grupos carboxilo de la SAM (estrategia II).

La evaluación, optimización y caracterización de la funcionalización de la superficie fueron estudiados mediante métodos ópticos (SPR y microscopía de fluorescencia) y métodos electroquímicos (voltametría cíclica - VC - y EIS). EIS se utilizó para la detección de bacterias patógenas de *E. coli* O157:H7.

Este trabajo fue desarrollado en colaboración con Prof. Maria Pilar Marco and Dr. Núria Pascual del Instituto de Química Avanzada de Cataluña (IQAC), CSIC (Barcelona, España).

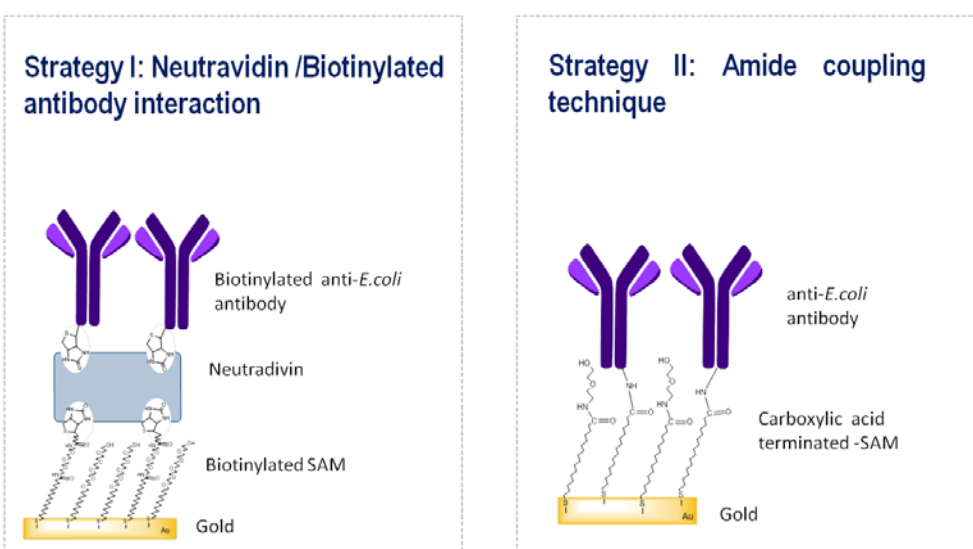


Figura 4. Principales estrategias de funcionalización aplicadas en superficie de oro. (Izquierda) Estrategia I basada en la interacción de anticuerpos neutravidina / biotina. (Derecha) Estrategia II basado en la técnica de acoplamiento de amida.

## 3.3. Resultados y discusión

En la estrategia I, los resultados obtenidos con SPR y VC confirman la inmovilización exitosa del anticuerpo a la superficie modificada. Sin embargo, tras la adición de diferentes concentraciones de *E. coli* O157:H7 no se observó ningún cambio significativo en la señal de SPR. Utilizando una técnica más sensible como EIS, se detectó una concentración muy baja de *E. coli* O157:H7 (10 CFU $mL^{-1}$), pero se saturó a concentraciones más altas limitando la sensibilidad y el rendimiento global del inmunosensor. Además, la reproducibilidad del sensor resultó ser insatisfactoria. Los resultados obtenidos nos animaron a evaluar la estrategia de funcionalización basada en la técnica de acoplamiento de la amida (estrategia II) para la detección de bacterias patógenas.

La optimización y caracterización de la funcionalización de la superficie con anticuerpos se estudió primero mediante SPR. Los resultados confirmaron la efectividad y selectividad del protocolo utilizado. La capacidad de detección del sistema fue después estudiada mediante inmunofluorescencia. Utilizamos la técnica de impresión por micro-contacto para crear un patrón de anticuerpos sobre la superficie de oro (Figura 5). La muestra se incubó con un anticuerpo secundario que reconoce específicamente el anticuerpo anti-*E. coli* (Figura 5 (a)), lo que demuestra una inmovilización óptima de los anticuerpos de captura primaria a la SAM activada.

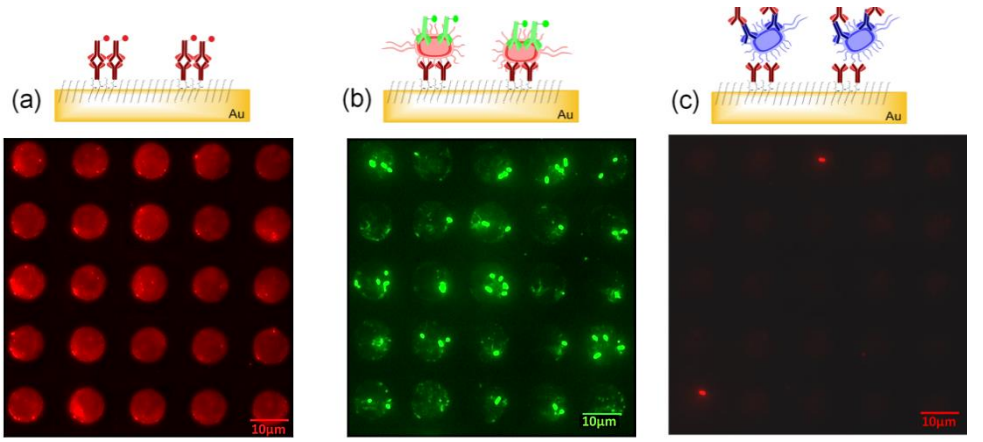


Figura 5. Imágenes de microscopía de fluorescencia de un patrón impreso por micro-contacto de (a) anticuerpos primarios anti-*E. coli*, (b) después de la incubación con *E. coli* O157:H7 y (c) control con bacterias no específicas (*Salmonella typhimurium)*.

La detección de bacterias se llevó a cabo del modo siguiente: se incubaron las bacterias sobre el patrón de anticuerpos y luego se utilizaron anticuerpos secundarios específicos para la detección. La Figura 5 (b) muestra que las bacterias *E. coli* O157:H7 se unieron específicamente al patrón de anticuerpos. Fuera de las zonas estampadas no se detectó bacteria alguna, lo que demuestra la inhibición de la adsorción no específica de proteínas o bacterias. La Figura 5 (c) no muestra señal alguna de fluorescencia sugiriendo que no se ha adherido *Salmonella typhimurium,* debido a la débil interacción con el anticuerpo de captura anti-*E. coli*. Se ha cuantificado una relación de *Salmonella typhimurium* / *E. coli* O157:H7 de 1:18 demostrando la eficacia y la alta selectividad del protocolo de funcionalización.

Finalmente, el rendimiento del sensor para la detección de bacterias patógenas de *E. coli* O157:H7 se realizó mediante EIS utilizando la estrategia de funcionalización descrita anteriormente. Los resultados muestran un incremento significativo de la impedancia a medida que se aumenta la concentración de bacterias; se obtuvo un LOD de 2 CFU $mL^{-1}$. El alto

rendimiento demostrado por nuestro sensor en términos de sensibilidad, especificidad y selectividad, podría tener importantes aplicaciones para la detección de bajas concentraciones de bacterias patógenas, siendo una alternativa prometedora a los métodos de detección estándares y convencionales, tales como ELISA.

## 3.4. Conclusiones

En este capítulo, hemos fabricado y caracterizado un inmunosensor *"label-free"* basado en EIS para la detección de *E. coli* O157:H7 utilizando dos estrategias de funcionalización distintas. Se ha seleccionado la Estrategia II, que ha aportado la mayor reproducibilidad y mayor rango de detección lineal para el desarrollo de un inmunosensor fiable para la detección de *E. coli* O157:H7. Se obtuvo un límite de detección tan bajo como 2 CFU $mL^{-1}$, que es el límite de detección más bajo reportado en la literatura sobre superficies de oro y está de acuerdo con los resultados obtenidos en el capítulo 2. Finalmente, se ha demostrado que el immunosensor era altamente específico y reproducible.

# **Capítulo 4.** Detección de bacterias patógenas mediante una plataforma de multi-electrodos

## 4.1. Introducción

Los sensores electroquímicos estándar se basan en electrodos de trabajo individuales. Esto limita el número de muestras que se pueden analizar y también puede dar lugar a falsos positivos. Esta limitación fomentó el desarrollo de plataformas de múltiples electrodos (también llamados plataformas de multi-electrodos). Estos sistemas tienen varias ventajas para la detección electroquímica, tal como la posibilidad de realizar medidas en paralelo y múltiples experimentos idénticos. Ejemplos de sensores con multi-electrodos han sido ampliamente descritos en el área de los genosensores [47–52], con el objetivo de sustituir los chips de ADN con detección basada en fluorescencia por los basados en detección electroquímica.

EIS se ha utilizado por otros grupos de investigación en una plataforma de multi-electrodos (o "*microarray"*) multiespecíficos para la immuno-detección por precipitación inducida por enzimas [48]. De igual modo, un microchip con 8 electrodos se utilizó para la detección *"label-free"* de un base desemparejada de un oligonucleótido (con todos los microelectrodos sometidos a una modificación similar) [51]. La sensibilidad de la técnica EIS junto con la capacidad de múltiples análisis de los *microarrays* descarta la posibilidad de falsos positivos, proporcionando al

dispositivo características de alto rendimiento. En definitiva, esto demuestra que la combinación de plataformas con múltiples electrodos con EIS es una poderosa estrategia para el desarrollo de biosensores electroquímicos de alto rendimiento.

En este capítulo se presenta un dispositivo impedimétrico de múltiples electrodos para la detección de bacterias patógenas *E. coli* O157:H7. El dispositivo está formado por múltiples electrodos (multi-electrodos) de oro idénticos. Los multi-electrodos fueron fabricados mediante técnicas estándar de fotolitografía y se caracterizaron mediante varias técnicas de caracterización de superficie y técnicas electroquímicas. Finalmente, las capacidades de detección de bacterias patógenas de la plataforma de multi-electrodos se estudiaron utilizando diferentes bioreceptores, incluyendo anticuerpos y péptidos antimicrobianos (AMP).

## 4.2. Metodología

El dispositivo electroquímico se basa en múltiples electrodos con cuatro (ME 4), seis (ME 6) u ocho (ME 8) electrodos de trabajo individuales (Figura 6 (a)-(c)). Los multi-electrodos fueron fabricados utilizando métodos fotolitográficos y se pasivaron las áreas de los electrodos de oro no activas para evitar la adsorción inespecífica. Este trabajo fue realizado en colaboración con el grupo del Dr. José Antonio Plaza del CNM-CSIC (Cerdanyola del Vallès, España).

La Figura 6 (d) muestra una imagen de la oblea de silicio que contiene los multi-electrodos fabricados con distintos número de electrodos de trabajo. Una imagen ampliada de una de estas unidades formada por 8 electrodos de trabajo (ME 8) se muestra en la Figura 6 (e). La calidad de

fabricación y de funcionamiento de los multi-electrodos se comprobó mediante caracterización óptica (interferometría, perfilometría y microscopía óptica) y electroquímica (VC y EIS)

La inmovilización de anticuerpos se realizó de acuerdo con el procedimiento anteriormente optimizado (véase capítulo 3). La inmovilización de las AMP sobre los electrodos de trabajo se llevó a cabo usando el protocolo descrito en Manoor *et al* [16]. Este trabajo fue desarrollado en colaboración con el Instituto de Investigación Biomédica IRB (Barcelona, España).

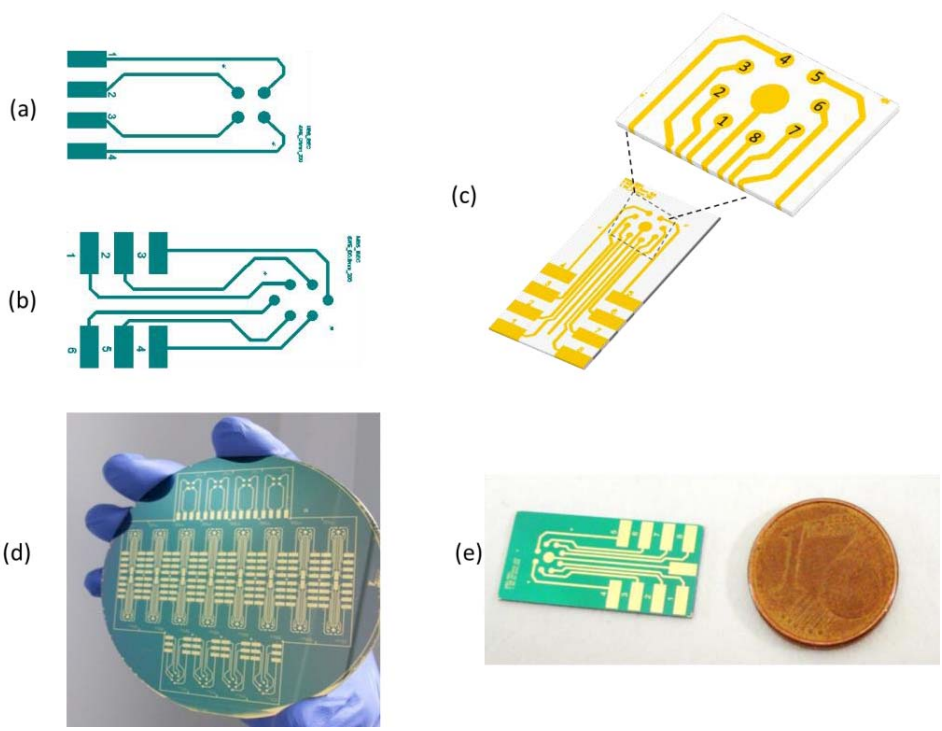


Figura 6. Ilustración esquemática de los diferentes diseños de múltiples electrodos que contienen 4 (a), 6 (b) y 8 (c) electrodos de trabajo. (d) Fotografía de la oblea fabricada con múltiples electrodos y (e) una imagen ampliada de una unidad de múltiples electrodos que contiene 8 electrodos de trabajo.

## 4.3. Resultados y discusión

Como se describió anteriormente, una plataforma de múltiples electrodos se desarrolló con el objetivo de realizar múltiples experimentos en paralelo usando las mismas condiciones experimentales, aumentando la velocidad y la reproducibilidad de las medidas. Mediante el uso de este sistema, es posible llevar a cabo experimentos de detección e identificación de un analito determinado usando electrodos de trabajo modificados con diferentes bioreceptores. Alternativamente, cada electrodo de trabajo puede también incubarse con un analito diferente mediante el depósito de volúmenes muy pequeños en la parte superior del electrodo (<1 μl).

Como se comentó anteriormente, los multi-electrodos fueron fabricados mediante procesos fotolitográficos y caracterizados mediante métodos ópticos y electroquímicos. Los multi-electrodos mostraron una respuesta precisa y uniforme mediante medidas de EIS y VC, confirmando un rendimiento óptimo. Además, se obtuvieron electrodos de trabajo reproducibles y con la posibilidad de ser regenerados y reutilizados hasta 3 veces.

A continuación, presentamos una prueba de concepto de sus capacidades de detección de bacterias patógenas *E. coli* O157:H7 utilizando como bioreceptores primero (i) anticuerpos y segundo (ii) péptidos antimicrobianos.

(i) Anticuerpos anti-*E.coli*

La detección de bacterias patógenas de *E. coli* O157:H7 se realizó usando un multi-electrodo de 4 electrodos (ME 4) modificado con anti-*E. coli*. En la Figura 7 se muestra la señal normalizada de $R_{ct}$ obtenida a partir del análisis de los espectros de impedancia.

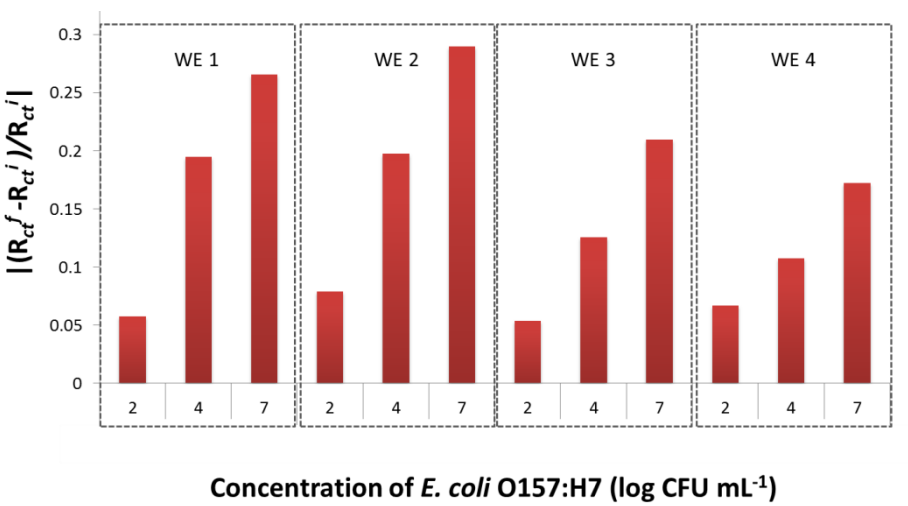


Figura 7. Variación de $R_{ct}$ normalizada obtenida a partir de un multi-electrodo ME 4 modificado con anti-*E. coli* para la detección de bacterias patógenas de E. coli O157:H7.

En la Figura 7 se observa un aumento de la $R_{ct}$ normalizada en cada electrodo para las diferentes concentraciones de bacterias. Estos resultados confirman que las bacterias se adhirieron en la superficie de los electrodos, lo que está de acuerdo con los resultados obtenidos en los capítulos 2 y 3.

Se observaron algunas fluctuaciones de la señal entre los distintos electrodos. De todos modos, un análisis estadístico (Student t-test) demostró que los resultados obtenidos entre los varios electrodos no diferían significativamente (P=0,05).

Con el fin de confirmar la unión de las bacterias en la superficie, un anticuerpo secundario específico para *E. coli* O157:H7 se añadió a los multi-electrodos. La Figura 8 (a) muestra una imagen de fluorescencia de un electrodo después de la medición de la señal de impedancia. La imagen demuestra que las bacterias fueron capturadas con éxito sobre la superficie.

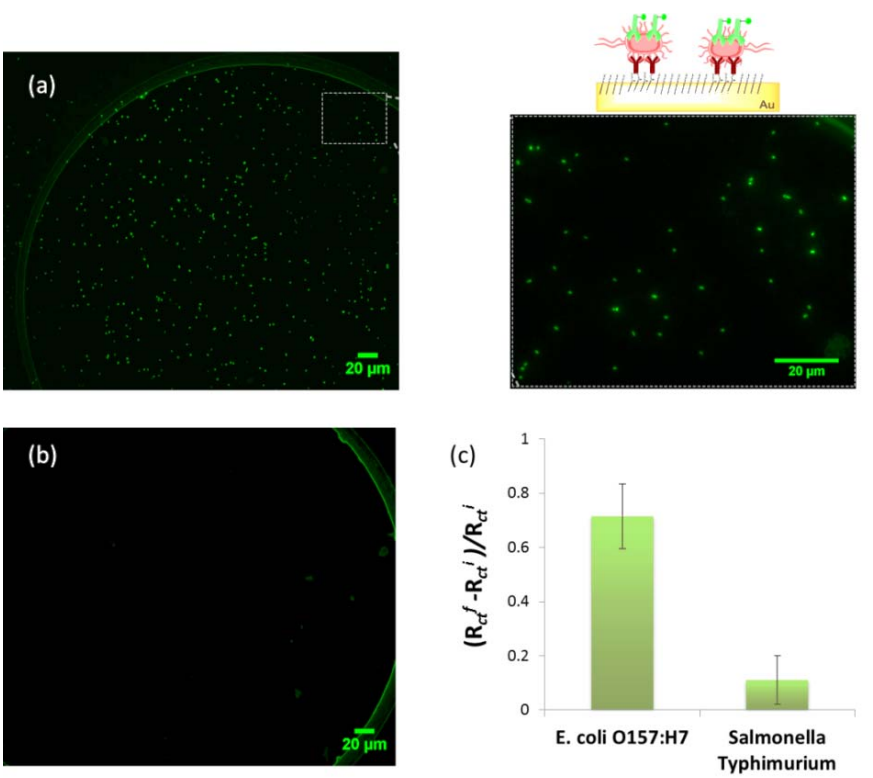


Figura 8. Imágenes de microscopía de fluorescencia de uno de los multi-electrodos funcionalizado con anti-*E. coli*. El multi-electrodo fue utilizado para las mediciones de impedancia y se incubó con un anti-*E. coli* secundario marcado con FITC. En (a) se muestra la bacteria *E. coli* O157: H7 (en verde) adherida en la superficie del electrodo. En (b) se muestra un control usando bacterias no específicas de *Salmonella typhimurium*; no se observa señal de fluorescencia. (c) Señal normalizada $R_{ct}$ obtenida antes y después de la adición de un segundo anticuerpo (anti-*E. coli*) utilizando diferentes bacterias.

También se registró la señal de impedancia antes y después de la incubación con el anticuerpo secundario. El valor medio de la señal de $R_{ct}$ normalizada obtenido a partir de los espectros de impedancia para las diferentes bacterias se muestra en la Figura 8 (c). Como se puede observar, se obtuvo un valor mayor de $R_{ct}$ normalizado para *E. coli* O157:H7 ($10^7$ CFU $ml^{-1}$). Por otro lado, para la bacteria no específica *Salmonella typhimurium* se obtuvo un incremento muy pequeño en $R_{ct}$.

Los ejemplos descritos en esta sección muestran una metodología prometedora para la detección específica de *E. coli* O157: H7 usando inmunosensores basados en multi-electrodos. Aunque este estudio inicial mostró resultados alentadores, aún queda trabajo por hacer como, por ejemplo, probar el rendimiento del multi-electrodo usando muestras complejas.

(ii) Péptidos antimicrobianos: Magainina I

La detección de bacterias patógenas de *E. coli* O157:H7 también se realizó en un ME 4 modificado con AMP como la Magainina I. La cobertura de Magainina I obtenida fue del 97,1 ± 0,1%, lo que demuestra una cobertura prácticamente completa de la superficie de los electrodos de oro. Los resultados demuestran la buena funcionalización y gran cobertura de los multi-electrodos con AMP y una reproducibilidad óptima. Los resultados obtenidos muestran que los AMP son fáciles de manipular y funcionalizar. Sin embargo, todavía presentan serias limitaciones en términos de sensibilidad y especificidad, especialmente en comparación con el rendimiento obtenido utilizando sensores basados en anticuerpos. Por lo tanto, esto limita su integración en dispositivos biosensores.

## 4.4. Conclusiones

En este capítulo, se desarrolló un multi-electrodo para la detección de de *E. coli* O157:H7. El multi-electrodo fue totalmente caracterizado mediante métodos ópticos y electroquímicos demostrando una excelente calidad de fabricación y rendimiento operativo. Se obtuvieron electrodos de trabajo reproducibles con una respuesta uniforme. Finalmente, se comprobó que los multi-electrodos podían ser regenerados hasta 3 veces.

Las capacidades de detección de los multi-electrodos se evaluaron con éxito. Los multi-electrodos fueron funcionalizados con anti-*E. coli* y posteriormente usados para la detección de bacterias patógenas *E. coli* O157:H7. Se demostró que los distintos electrodos no diferían en su respuesta de manera significativa. Se observó igualmente su especificidad, especialmente cuando se utilizó anti-*E. coli* como capa de bioreconocimiento. Se evaluó igualmente Magainina I como una alternativa a los anticuerpos. A pesar de que se observó propiedades interesantes y se obtuvieron resultados prometedores, se observaron también algunas limitaciones con respecto a su especificidad y sensibilidad.

# **Capítulo 5.** Detección de ocratoxina A mediante una plataforma de multi-electrodos

## 5.1. Introducción

La detección de la toxina OTA es muy importante debido a su toxicidad. Los métodos analíticos estándares precisan de equipos sofisticados y personal cualificado. De este modo, durante los últimos años han surgido otros métodos para su detección basados en la tecnología de biosensores, como ELISA [53], SPR [54] e immunoensayos electroquímicos [55]. Estos ensayos muestran límites de detección bajos pero todos ellos requieren una fuente estable de anticuerpos. Por otra parte, la producción de anticuerpos implica un trabajo laborioso, costoso, y requiere mucho tiempo en procedimientos. Los aptámeros, oligonucleótidos cortos (ADN/ARN), pueden proporcionar ciertas ventajas en comparación con los anticuerpos, debido a su selectividad inherente y afinidad [56].

Aptámeros para la detección de OTA fueron usados por Cruz-Aguado *et al* [57, 58]. Los aptámeros identificados mostraron un alto nivel de especificidad de unión a la OTA y se han utilizado ampliamente desde entonces para el desarrollo de biosensores como por ejemplo, biosensores electroquímicos [56, 59–61]. Estos han sido ampliamente descritos debido a su sencilla instrumentación, bajo coste, fácil operación, alta sensibilidad y un tiempo de detección reducido.

Aunque algunos trabajos han descrito el desarrollo de sensores impedimétricos para la detección de OTA con bajos límites de detección, no se ha reportado la detección de OTA basada en una plataforma multi-sensor. Tal y como se describe en el capítulo 4, el multi-sensor está compuesto por una serie de electrodos de trabajo con diferentes afinidades. Esto implica la posibilidad de incluir controles positivos y negativos en un solo experimento de detección. Además, este sistema es muy útil para la optimización de las condiciones experimentales, reduciendo el tiempo de detección y los reactivos utilizados.

En este capítulo, hemos aplicado la plataforma de multi-electrodos para la detección de OTA. Para la fabricación del multi-sensor impedimétrico a base de aptámero se ensayaron dos estrategias de inmovilización. La primera estrategia (estrategia I) se basa en la unión covalente a superficies modificadas químicamente, mientras que la segunda estrategia (estrategia II) se basa en la modificación de ADN con un tiol terminal. Las superficies funcionalizadas fueron completamente caracterizadas con el fin de seleccionar la estrategia más adecuada para ser aplicada a la detección de OTA.

## 5.2. Metodología

Para la inmovilización del aptámero de OTA (OA) se han utilizado dos estrategias que se basan en la hibridación en la superficie del biosensor a través de oligonucleótidos parcialmente complementarios. Las dos estrategias utilizadas para la inmovilización de las cadenas de oligonucleótidos cortos (ADN C) se muestran en la Figura 9.

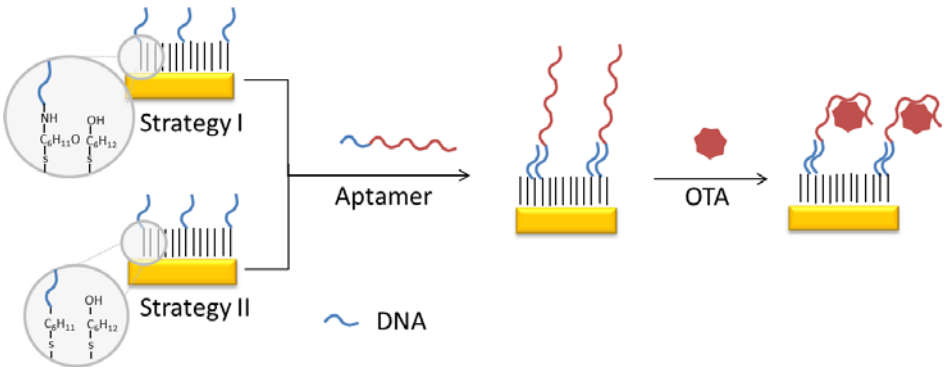


Figura 9. Estrategias para la inmovilización del aptámero utilizado para la detección de OTA. La estrategia I se basa en la unión covalente a superficies modificadas químicamente. La estrategia II se basa en el auto-ensamblaje de un oligonucleótido tiolado.

La estrategia I utiliza una monocapa auto-ensamblada con grupos carboxílico para su posterior activación y unión del oligonucleótido modificado con amina por medio de la técnica de acoplamiento de amida (Figura 9, *parte superior*). La estrategia II utiliza una unión directa de un oligonucleótido modificado con tiol (ADN C) auto-ensamblado a través de la unión de oro-azufre en las superficies de los electrodos de oro (Figura 9, *inferior*). Las técnicas de voltametría cíclica y EIS se utilizaron para caracterizar todas las etapas de funcionalización en la plataforma del multi-electrodo, mientras que la detección de OTA se realizó mediante EIS. Este trabajo ha sido desarrollado en colaboración con el laboratorio IMAGES (Université de Perpignan, Perpiñan, Francia).

## 5.3. Resultados y discusión

Los resultados obtenidos para la estrategia I con VC y EIS demostraron que el aptámero no se adhirió sobre la superficie de oro, probablemente debido a la desorción de la SAM. En cambio, la estrategia II mostró una unión

exitosa del ADN a la superficie de oro. La Figura 10 muestra la cobertura de la superficie de oro con ADN utilizando diferentes concentraciones en el mismo multi-electrodo.

La inmovilización de concentraciones crecientes de ADN C en cada uno de los distintos electrodos causó un incremento en los valores de $R_{ct}$ medidos mediante EIS (Figura 10 (a)) (una concentración por electrodo). Esto es debido a que la formación de una capa cargada más negativamente actúa como una barrera electrostática entre la superficie del electrodo y los aniones de $[Fe(CN)_6]^{3-/4-}$ de la solución. El aumento de ADN en la superficie también fue demostrado mediante el estudio de la cobertura de la superficie (Figura 10 (b)). La cobertura de la superficie siguió un comportamiento sigmoidal para las diferentes concentraciones de ADN C, siendo del 100% para 10 mM de ADN C y ADN (NC).

(a)

| | [DNA] µM | $R_{ct}$ Ohm |
|---|---|---|
| DNA C | 10 | 760000 |
| | 1 | 97470 |
| | 0.32 | 53255 |
| | 0.1 | 21900 |
| DNA NC | 10 | 259811 |
| No DNA | 0 | 13571 |

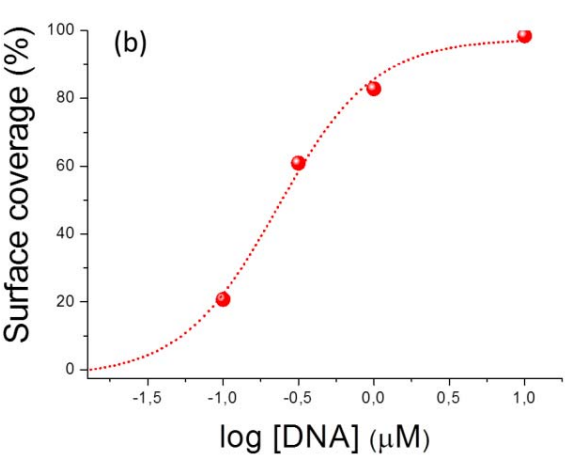


Figura 10. (a) Tabla con los valores de Rct obtenidos para las diferentes concentraciones de ADN. (b) Porcentaje de cobertura de la superficie obtenido para cada electrodo en función de las diferentes concentraciones de ADN. La línea punteada corresponde al ajuste sigmoidal.

Posteriormente, se demostró que el mercaptohexanol (MCH) cubría la superficie de oro no modificada y que la adición de OA provocó un aumento de la señal del 41%, 45% y 37% para las concentraciones de ADN de 0,1 µM, 0,32 µM y 1 µM, respectivamente. En cambio, en un control sin ADN prácticamente no se observó variación alguna después de añadir el aptámero. Esto corrobora la importancia de incorporar controles negativos en el mismo experimento para estudios de especificidad que puede hacerse fácilmente utilizando la plataforma de multi-electrodos desarrollada.

La formación del complejo aptámero-OTA puede resultar en la mejora de la transferencia de electrones entre el aptámero y la superficie del electrodo [62]. La Figura 11 muestra los valores normalizados de $R_{ct}$ *vs.* concentración de OTA obtenido para las diferentes concentraciones de ADN (electrodos funcionalizados individualmente). En este caso, se observó que la concentración de OTA más pequeña detectada mediante el multi-sensor fue de 6,125 ng $mL^{-1}$ (15 nM) para todas las concentraciones de ADN, y la respuesta más alta para la detección de OTA fue para la concentración de ADN C de 1 mM.

Todas las curvas muestran una tendencia similar para todas las concentraciones de ADN siendo la respuesta obtenida más alta para 1 µM. Con el fin de caracterizar las propiedades de unión de nuestro sensor, se calculó la constante de asociación Ka del complejo OA-OTA. Se obtuvo un valor de $1{,}05 \times 10^{-1}$ ng $mL^{-1}$, lo que corresponde a una constante disociación $K_D$ de 9,5 ng $mL^{-1}$ (23,527 nM). Aunque se han reportado valores más bajos de $K_D$, los valores obtenidos son muy prometedores teniendo en cuenta las inusuales características de nuestra plataforma multi-electrodo, como por ejemplo, múltiple analice, producción en masa, química simple y robusta, y la

posibilidad de realizar mediciones múltiples en paralelo usando las mismas condiciones experimentales, entre otras.

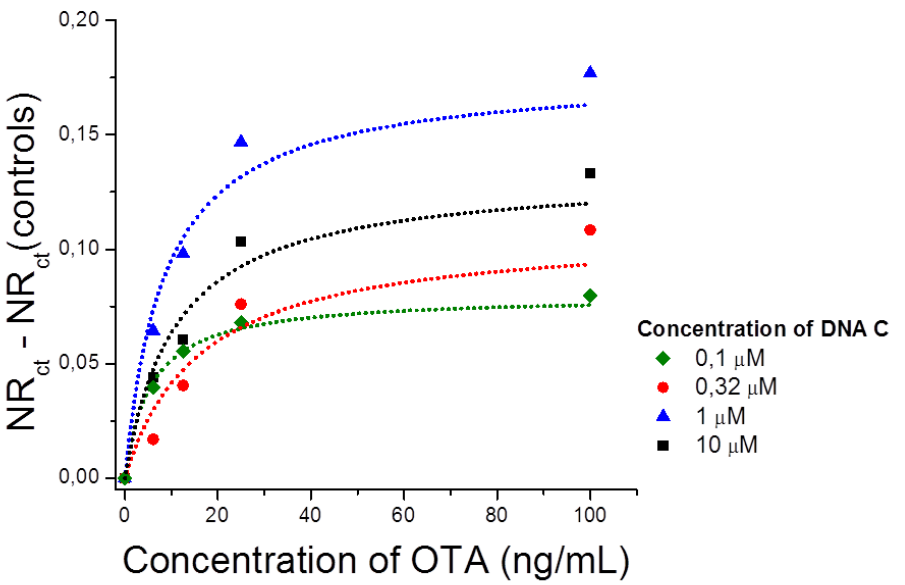


Figura 11. Variación de la resistencia de transferencia de carga Rct normalizada (NRct), restando los valores de los controles, en función de la concentración de OTA para distintas concentraciones de ADN C inmovilizado en los electrodos. Las líneas discontinuas representan el ajuste de los datos mediante la adsorción isoterma de Langmuir.

## 5.4. Conclusiones

En este capítulo se aplicó la plataforma multi-electrodos para el desarrollo de un sensor basado en aptámero para la detección de micotoxinas. Nos centramos en el caso concreto de la ocratoxina A (OTA), una de las micotoxinas más abundantes que contaminan los alimentos. El multi-sensor desarrollado fue capaz de detectar distintas concentraciones de OTA. Los resultados prometedores obtenidos demuestran la aplicabilidad de los

multi-electrodos para la detección de micotoxinas y las ventajas de la utilización de esta plataforma.

## Referencias

[1] J. Castillo, S. Gáspar, S. Leth, M. Niculescu, A. Mortari, I. Bontidean, et al., Biosensors for life quality design, development and applications, Sensors Actuators B. 102 (2004) 179–194.

[2] M. Nayak, A. Kotian, S. Marathe, D. Chakravortty, Detection of microorganisms using biosensors - a smarter way towards detection techniques, Biosens. Bioelectron. 25 (2009) 661–7.

[3] A. Rasooly, K.E. Herold, eds., Biosensors and Biodetection Methods and protocols, Volume 503, Springer Protocols, 2009.

[4] B.D. Mallotra, A.P.F. Turner, Advances in Biosensors perspectives in biosensors, Elsevier Science B.V., 2003.

[5] V. Velusamy, K. Arshak, O. Korostynska, K. Oliwa, C. Adley, An overview of foodborne pathogen detection: In the perspective of biosensors, Biotechnol. Adv. 28 (2010) 232–254.

[6] D. Grieshaber, Electrochemical Biosensors - Sensor Principles and Architectures, Sensors 8 (2008) 1400–1458.

[7] R.H. Hall, Biosensor technologies for detecting microbiological foodborne hazards, Microbes Infect. 4 (2002) 425–32.

[8] S.B. Shinde, C.B. Fernandes, V.B. Patravale, Recent trends in in-vitro nanodiagnostics for detection of pathogens, J. Control. Release. 159 (2012) 164–80.

[9] T. Vo-Dinh, B. Cullum, Biosensors and biochips: advances in biological and medical diagnostics, Fresenius. J. Anal. Chem. 366 (2008) 540–51.

[10] A.W. Wark, J. Lee, S. Kim, S.N. Faisal, H.J. Lee, Bioaffinity detection of pathogens on surfaces, J. Ind. Eng. Chem. 16 (2010) 169–177.

[11] P. Leonard, Advances in biosensors for detection of pathogens in food and water, Enzyme Microb. Technol. 32 (2003) 3–13.

[12] F. Long, A. Zhu, C. Gu, H. Shi, Recent progress in optical biosensors for environmental applications, Intech, 2013.

[13] F. Long, A. Zhu, H. Shi, Recent advances in optical biosensors for environmental monitoring and early warning, Sensors 13 (2013) 13928–48.

[14] M.A. Cooper, Optical biosensors in drug discovery, Nat. Rev. Drug Discov. 1 (2002) 515–28.

[15] Y. Fang, Label-Free Cell-Based Assays with Optical Biosensors in Drug Discovery, Assay Drug Dev. Technol. 4 (2006) 583–595.

[16] H. Sharma, R. Mutharasan, Review of biosensors for foodborne pathogens and toxins, Sens. Actuators B 183 (2013) 535–549.

[17] B.-K. Oh, Y.-K. Kim, K.W. Park, W.H. Lee, J.-W. Choi, Surface plasmon resonance immunosensor for the detection of Salmonella typhimurium, Biosens. Bioelectron. 19 (2004) 1497–504.

[18] M. Zourob, S. Elwary, A. Turner, Principles of bacterial detection: biosensors, recognition receptors and microsystems, Springer, 2008.

[19] O. Lazcka, F.J. Del Campo, F.X. Muñoz, Pathogen detection: a perspective of traditional methods and biosensors, Biosens. Bioelectron. 22 (2007) 1205–17.

[20] V. Perumal, U. Hashim, Advances in biosensors: Principle, architecture and applications, J. Appl. Biomed. 12 (2014) 1–15.

[21] J.S. Daniels, N. Pourmand, Label-Free impedance biosensors: opportunities and challenges, Electroanalysis 19 (2007) 1239–1257.

[22] F. Lisdat, D. Schäfer, The use of electrochemical impedance spectroscopy for biosensing, Anal. Bioanal. Chem. 391 (2008) 1555–67.

[23] P. D'Orazio, Biosensors in clinical chemistry, Clin. Chim. Acta. 334 (2003) 41–69.

[24] O. Tokarskyy, D.L. Marshall, Immunosensors for rapid detection of Escherichia coli O157:H7 - perspectives for use in the meat processing industry, Food Microbiol. 25 (2008) 1–12.

[25] L. Yang, R. Bashir, Electrical/electrochemical impedance for rapid detection of foodborne pathogenic bacteria, Biotechnol. Adv. 26 (2008) 135–50.

[26] B. Ge, J. Meng, Advanced technologies for pathogen and toxin detection in foods: current applications and future directions, J. Assoc. Lab. Autom. 14 (2009) 235–241.

[27] P. Geng, X. Zhang, W. Meng, Q. Wang, W. Zhang, L. Jin, et al., Self-assembled monolayers-based immunosensor for detection of Escherichia coli using electrochemical impedance spectroscopy, Electrochim. Acta. 53 (2008) 4663–4668.

[28] M.S. Mannoor, S. Zhang, A.J. Link, M.C. McAlpine, Electrical detection of pathogenic bacteria via immobilized antimicrobial peptides, Proc. Natl. Acad. Sci. U. S. A. 107 (2010) 19207–12.

[29] H. Kim, A. Piqué, J.S. Horwitz, H. Mattoussi, H. Murata, Z.H. Kafafi, et al., Indium tin oxide thin films for organic light-emitting devices, Appl. Phys. Lett. 74 (1999) 3444.

[30] A. Malinauskas, R. Holze, A UV-vis spectroelectrochemical study of redox reactions of solution species at a polyaniline electrode in the conducting and the reduced state, J. Electroanal. Chem. 461 (1999) 184–193.

[31] S. Vico, V. Carlier, C. Buess-Herman, Spectroelectrochemical study of the influence of anions on the behaviour of poly(N-vinylcarbazole) films, J. Electroanal. Chem. 475 (1999) 1–8.

[32] S.E. Ross, C.J. Seliskar, W.R. Heineman, Spectroelectrochemical sensing based on multimode selectivity simultaneously achievable in a single device. 9. Incorporation of planar waveguide technology, Anal. Chem. 72 (2000) 5549–55.

[33] D.R. Dunphy, S.B. Mendes, S.S. Saavedra, N.R. Armstrong, The electroactive integrated optical waveguide: ultrasensitive spectroelectrochemistry of submonolayer adsorbates, Anal. Chem. 69 (1997) 3086–94.

[34] H. Yumoto, T. Inoue, S.J. Li, T. Sako, K. Nishiyama, Application of ITO films to photocatalysis, Thin Solid Films 345 (1999) 38–41.

[35] E.J. Moore, M. Curtin, J. Ionita, A.R. Maguire, G. Ceccone, P. Galvin, Selective release of DNA from the surface of indium-tin oxide thin electrode films using thiol-disulfide exchange chemistry, Anal. Chem. 79 (2007) 2050–7.

[36] D. Grieshaber, E. Reimhult, J. Voros, Enzymatic biosensors towards a multiplexed electronic detection system for early cancer diagnostics, 2nd IEEE Int. Conf. Nano/Micro Eng. Mol. Syst. (2007) 402–405.

[37] L. Yang, Y. Li, AFM and impedance spectroscopy characterization of the immobilization of antibodies on indium-tin oxide electrode through self-assembled monolayer of epoxysilane and their capture of Escherichia coli O157:H7, Biosens. Bioelectron. 20 (2005) 1407–16.

[38] N. Adányi, M. Varadi, N. Kim, I. Szendro, Development of new immunosensors for determination of contaminants in food, Curr. Appl. Phys. 6 (2006) 279–286.

[39] H. Tang, W. Zhang, P. Geng, Q. Wang, L. Jin, Z. Wu, et al., A new amperometric method for rapid detection of Escherichia coli density using a self-assembled monolayer-based bienzyme biosensor, Anal. Chim. Acta. 562 (2006) 190–196.

[40] C. Ruan, L. Yang, Y. Li, Immunobiosensor chips for detection of Escherichia coli O157:H7 using electrochemical impedance spectroscopy, Anal. Chem. 74 (2002) 4814–4820.

[41] L. Yang, Y. Li, G.F. Erf, Interdigitated Array microelectrode-based electrochemical impedance immunosensor for detection of Escherichia coli O157:H7, Anal. Chem. 76 (2004) 1107–13.

[42] S.K. Arya, P.R. Solanki, M. Datta, B.D. Malhotra, Recent advances in self-assembled monolayers based biomolecular electronic devices, Biosens. Bioelectron. 24 (2009) 2810–7.

[43] M.J. Linman, K. Sugerman, Q. Cheng, Detection of low levels of Escherichia coli in fresh spinach by surface plasmon resonance spectroscopy with a TMB-based enzymatic signal enhancement method, Sens. Actuators B 145 (2010) 613–619.

[44] R. Maalouf, C. Fournier-Wirth, J. Coste, H. Chebib, Y. Saïkali, O. Vittori, et al., Label-free detection of bacteria by electrochemical impedance spectroscopy: comparison to surface plasmon resonance, Anal. Chem. 79 (2007) 4879–86.

[45] C.-K. Joung, H.-N. Kim, H.-C. Im, H.-Y. Kim, M.-H. Oh, Y.-R. Kim, Ultra-sensitive detection of pathogenic microorganism using surface-engineered impedimetric immunosensor, Sens. Actuators B 161 (2012) 824–831.

[46] V. Escamilla-Gómez, S. Campuzano, M. Pedrero, J.M. Pingarrón, Gold screen-printed-based impedimetric immunobiosensors for direct and sensitive Escherichia coli quantisation, Biosens. Bioelectron. 24 (2009) 3365–71.

[47] E. Pavlovic, R.Y. Lai, T.T. Wu, B.S. Ferguson, R. Sun, K.W. Plaxco, et al., Microfluidic device architecture for electrochemical patterning and detection of multiple DNA sequences, Langmuir 24 (2008) 1102–7.

[48] X. Yu, R. Lv, Z. Ma, Z. Liu, Y. Hao, Q. Li, et al., An impedance array biosensor for detection of multiple antibody-antigen interactions, Analyst. 131 (2006) 745–50.

[49] F. Farabullini, F. Lucarelli, I. Palchetti, G. Marrazza, M. Mascini, Disposable electrochemical genosensor for the simultaneous analysis of different bacterial food contaminants, Biosens. Bioelectron. 22 (2007) 1544–9.

[50] S. Neugebauer, A. Zimdars, P. Liepold, M. Gebala, W. Schuhmann, G. Hartwich, Optimization of an electrochemical DNA assay by using a 48-electrode array and redox amplification studies by means of scanning electrochemical microscopy, Chembiochem. 10 (2009) 1193–9.

[51] X. Li, J.S. Lee, H.-B. Kraatz, Electrochemical detection of single-nucleotide mismatches using an electrode microarray, Anal. Chem. 78 (2006) 6096–101.

[52] P.M. Levine, P. Gong, R. Levicky, K.L. Shepard, Real-time, multiplexed electrochemical DNA detection using an active complementary metal-oxide-semiconductor biosensor array with integrated sensor electronics, Biosens. Bioelectron. 24 (2009) 1995–2001.

[53] F.-Y. Yu, T.-F. Chi, B.-H. Liu, C.-C. Su, Development of a sensitive enzyme-linked immunosorbent assay for the determination of ochratoxin A, J. Agric. Food Chem. 53 (2005) 6947–53.

[54] V. Hodnik, G. Anderluh, Toxin detection by surface plasmon resonance, Sensors 9 (2009) 1339–54.

[55] B. Prieto-Simón, M. Campàs, J.-L. Marty, T. Noguer, Novel highly-performing immunosensor-based strategy for ochratoxin A detection in wine samples, Biosens. Bioelectron. 23 (2008) 995–1002.

[56] N. Prabhakar, Z. Matharu, B.D. Malhotra, Polyaniline Langmuir-Blodgett film based aptasensor for ochratoxin A detection, Biosens. Bioelectron. 26 (2011) 4006–11.

[57] J.A. Cruz-aguado, G. Penner, Fluorescence polarization based displacement assay for the determination of small molecules with aptamers, Anal. Chem. 80 (2008) 8853–5.

[58] J.A. Cruz-Aguado, G. Penner, Determination of ochratoxin a with a DNA aptamer, J. Agric. Food Chem. 56 (2008) 10456–61.

[59] A. Hayat, A. Sassolas, J.-L. Marty, A.-E. Radi, Highly sensitive ochratoxin A impedimetric aptasensor based on the immobilization of azido-aptamer onto electrografted binary film via click chemistry, Talanta 103 (2013) 14–9.

[60] H. Kuang, W. Chen, D. Xu, L. Xu, Y. Zhu, L. Liu, et al., Fabricated aptamer-based electrochemical “signal-off” sensor of ochratoxin A., Biosens. Bioelectron. 26 (2010) 710–6.

[61] B. Prieto-Simón, J. Samitier, “Signal Off” aptasensor based on enzyme inhibition induced by conformational switch, Anal. Chem. (2014).

[62] Y. Peng, D. Zhang, Y. Li, H. Qi, Q. Gao, C. Zhang, Label-free and sensitive faradic impedance aptasensor for the determination of lysozyme based on target-induced aptamer displacement, Biosens. Bioelectron. 25 (2009) 94–9.

# Publications and conference communications

## *Scientific Publications:*

"Highly sensitive detection of pathogen E.coli O157:H7 by Electrochemical Impedance Spectroscopy" M. Barreiros dos Santos, J. P. Agusil, B. Prieto-Simón, C. Sporer, V. Teixeira, J. Samitier, Biosensors and Bioelectronics 45, 2013, 174–180.

"Properties of bilayer contacts to porous silicon"; D. Gallach, V. Torres-Costa, L. García-Pelayo, A. Climent-Font, R.J. Martín-Palma, M. Barreiros dos Santos, C. Sporer, J. Samitier, M. Manso; Applied Physics A 107, 2012, 293–300.

"Detection of pathogenic Bacteria by Electrochemical Impedance Spectroscopy: Influence of the immobilization strategies on the sensor performance"; M. Barreiros dos Santos, C. Sporer, N. Sanvicens, N. Pascual, A. Errachid, E. Martinez, M.-P. Marco, V. Teixeira, J. Samiter; Procedia Chemistry, Volume 1, Issue 1, 2009,1291-1294.

"Development of a high performance nanobased multianalyte device for detection of pathogens" M. Barreiros Dos Santos, C. Sporer, V. Teixeira, J. Samitier, New Biotechnology, Volume 25, Supplement, 2009, Pages S32-S33

"Label-free ITO-based immunosensor for the detection of very low concentrations of pathogenic bacteria"; M. Barreiros dos Santos, S. Azevedo, J. P. Agusil, B. Prieto-Simón, C. Sporer, E. Torrents, A. Juárez, V. Teixeira, J. Samitier, under review in Bioelectrochemistry journal

## *Participation in Congresses and Conferences:*

Poster presentation, "Electrochemical immunosensor for the detection of E.coli O157:H7 in human plasma"; M. Barreiros dos Santos, J. P. Agusil, B. Prieto-Simón, C.Sporer, V. Teixeira, J. Samitier; Biosensors 2012 (Mexico), 2012.

Poster presentation, “Multi-analyte device for the electrochemical detection of pathogenic bacteria”; M. Barreiros dos Santos, J. P. Agusil, B. Prieto-Simón, S.Martinez-Rodriguez, C.Sporer ,E. Torrents, A. Juárez, V. Teixeira, J. Samitier; Biosensors 2012 (Mexico), 2012.

Poster presentation, “Novel aptamer-based assay for detection of Salmonella typhimurium”; J.L. Sebastián-Avila, M. Barreiros dos Santos, J.P. Agusil, A. Juárez, J. Samitier, B. Prieto-Simón; Biosensors 2012 (Mexico), 2012.

Poster and flash presentation, “Fabrication of a multi sensor for electrochemical detection of pathogenic bacteria”; M. Barreiros dos Santos, J.P.Agusil, S. Martinez-Rodriguez, B. Prieto, C. Sporer, V. Teixeira and J. Samitier; 4th IBEC Symposium on Bioengineering and nanomedicine in Barcelona (Spain), 2011.

Poster presentation, “Development of an immunosensor based on ITO-electrodes for the detection of pathogenic bacteria”; M. Barreiros dos Santos, S. Azevedo, C. Sporer,V. Teixeira and J. Samitier; 5th International Meeting on Developments in Materials, Processes and Applications of Emerging Technologies in Alvor (Portugal), 2011.

Poster presentation, “Development of pathogenic bacteria using an electrochemical multi sensor platform”; M. Barreiros dos Santos, C. Sporer, J. P. Agusil1, B. Prieto, V. Teixeira, J. Samitier; VI International Materials Symposium MATERIAIS 2011 in Guimarães (Portugal), 2011.

Oral presentation, “Detection of pathogenic bacteria using an electrochemical multi sensor platform”; M. Barreiros dos Santos, B. Prieto, J. P. Agusil, V. Teixeira, J. Samitier, C. Sporer; XV Cross-border meeting of sensors and biosensors in Sant Carles de la Ràpita (Spain), 2010.

Oral presentation, “Fabrication of a multi sensor for electrochemical detection of pathogenic bacteria”; M. Barreiros dos Santos, C. Sporer, B.Prieto, V. Teixeira and J. Samitier; 4th International MPA in Braga (Portugal), 2010.

Poster presentation, “Fabrication of Electrodes and Multiprotein arrays with an automatized Microcontact printing tool” J.P. Agusil, M. Barreiros dos Santos, B. Brieto, E. Álvarez de Eulate, C. Sporer, J. Samitier; 3rd IBEC Symposium on Bioengineering and nanomedicine in Barcelona (Spain), 2010.

Poster presentation, “Development of an electrochemical multi sensor platform for the rapid and sensitive detection of pathogenic bacteria”; M. Barreiros dos Santos, B. Prieto, E. Alvarez, C. Sporer, V. Teixeira and J. Samitier ; Biosensors 2010 in Glasgow (United Kingdom), 2010.

Poster presentation, “Development of a high performance nanobased multianalyte device for detection of pathogens”; M. Barreiros dos Santos, C. Sporer, V. Teixeira and J. Samitier; 14th European Congress on Biotechnology in Barcelona (Spain), 2009.

Oral presentation, “Detection of pathogenic bacteria by electrochemical impedance spectroscopy: influence of the immobilization strategies on the sensor performance”; M. Barreiros dos Santos, C. Sporer, N. Sanvicens, N. Pascual, A. Errachid, E. Martinez, P.Marco, V. Teixeira and J. Samitier; Eurosensors XXIII, Lausanne (Switzerland), 2009.

Poster presentation, “Development of nanostructured materials for medical nanobiosensors”; S. Azevedo, L. Diéguez, P.Carvalho, J.Carneiro, V.Teixeira, M. Barreiros dos Santos, E. Martinez, J.Samitier; 6th International Conference-NN09 & 3rd International Summer School- SS-NN09 on Nanosciences & Nanotechnologies, Thessalonii (Greece), 2009.

Poster presentation, “Development of a high performance nanobased multianalyte device for detection of pathogens”; M. Barreiros dos Santos, C. Sporer, V. Teixeira and J. Samitier; 6th International Conference-NN09&3rd International Summer School- SS-NN09 on Nanosciences & Nanotechnologies, Thessalonii (Greece), 2009.

Poster and flash presentation, “Development of a high performance nanobased multianalyte device for detection of pathogens”; M. Barreiros dos Santos, C. Sporer, V. Teixeira and J. Samitier; 2nd EFS/UB European Summer School in Nanomedicine, Cascais (Portugal), 2009.

Poster and flash presentation, “Development of a high performance nanobased multianalyte device for detection of pathogens”; M. Barreiros dos Santos, S. Martinez, M. Kuphal, E. Álvarez de Eulate, C. Sporer, V. Teixeira and J. Samitier; 2nd IBEC Symposium in Barcelona (Spain), 2009.

*Pelo sonho é que vamos,*
*comovidos e mudos.*
*Chegamos? Não chegamos?*
*Haja ou não haja frutos,*
*pelo sonho é que vamos.*
*Basta a fé no que temos.*
*Basta a esperança naquilo*
*que talvez não teremos.*
*Basta que a alma demos,*
*com a mesma alegria,*
*ao que desconhecemos*
*e ao que é do dia a dia.*
*Chegamos? Não chegamos?*
*- Partimos. Vamos. Somos.*

*Sebastião da Gama – "Pelo sonho é que vamos"*